AN ABSTRACT OF THE THESIS OF

JOHN P. COLLINS for the degree of Doctor of Philosophy in Chemical Engineering presented on June 24, 1993.

Title: Catalytic Decomposition of Ammonia in a Membrane Reactor

Redacted for privacy

Abstract approved: _____

Dr. James Douglas Way

The U.S. Department of Energy is investigating technologies for removing trace amounts of ammonia from the high temperature, high pressure synthesis gas produced by advanced coal gasification power systems such as the integrated, gasification combined cycle process (IGCC). Catalytic decomposition of ammonia to hydrogen and nitrogen is a potential method for removing the ammonia. However, use of a conventional packed bed reactor is not feasible because ammonia conversion is limited by chemical equilibrium due to the high concentrations of nitrogen and hydrogen in the synthesis gas. The objective of this project was to investigate the catalytic decomposition of ammonia in a packed bed membrane reactor. The purpose of the membrane reactor was to shift the equilibrium of the ammonia decomposition reaction by selectively removing hydrogen from the feed gas. A hydrogen selective membrane capable of operating at large transmembrane pressure differences and high temperatures was developed in the study.

Composite palladium-ceramic membranes with palladium films ranging from 11.4 to 20 μm were made by depositing palladium on the inside surface of asymmetric tubular ceramic membranes. Electroless plating was used to deposit the palladium film. Membranes were characterized by conducting permeability experiments with hydrogen, nitrogen, and helium at temperatures from 723 to 913 K and feed pressures from 160 to 2445 kPa. The hydrogen permeability for a composite membrane with an 11.4 μm palladium film was $3.23 \cdot 10^{-9}$ moles•m/m^2•s•Pa$^{0.602}$ at 823 K. The hydrogen/nitrogen selectivity for this membrane was 380 at 823 K at a transmembrane pressure difference of 1500 kPa.

Membrane reactor experiments were conducted with a gas stream that simulated the temperatures, pressures, hydrogen, nitrogen, and ammonia concentrations in IGCC

synthesis gas. An ammonia conversion of over 94 percent was achieved in the membrane reactor at 873 K. Since the equilibrium conversion of the feed gas was only 58 percent, a significant equilibrium shift was obtained with the membrane reactor. The equilibrium shift was even higher at lower temperatures.

A membrane reactor model was developed to predict the ammonia conversion in a membrane reactor. The effect of interphase and intraparticle mass transfer was included in the model. Predicted and experimental ammonia conversions generally showed good agreement.

Catalytic Decomposition of Ammonia in a Membrane Reactor

by

John P. Collins

A THESIS

submitted to

Oregon State University

in partial fulfillment of
the requirements for the
degree of

Doctor of Philosophy

Completed June 24, 1993

Commencement June 1994

APPROVED:

Redacted for privacy

Professor of Chemical Engineering in charge of major

Redacted for privacy

Head of department of Chemical Engineering

Redacted for privacy

Dean of Graduate School

Date thesis is presented June 24, 1993

Typed by John P. Collins

ACKNOWLEDGMENTS

This research project was accomplished with the assistance of many people. I am especially grateful to Dr. Doug Way, my major advisor, for his guidance during the project. This project could not have been completed without his technical advice, moral support, and patience. He was a very good mentor. I am also grateful to the members of my graduate committee, Dr. S. Kimura, Dr. John Westall, Dr. William Warnes, and Dr. Michael Lerner. Dr. Kimura was especially generous in allowing me to use some of his equipment. I would like to thank Nick Wannenmacher, Adam King, and Jim Byford for helping me assemble the experimental apparatus. There is no one who provides better advice about equipment and is nicer about giving it than Nick. Nichakorn Kraisuwansarn helped develop the membrane reactor model and did a very good job. I would like to thank my friends Zoran Jovanovic and Milind Kulkarni, Zoran for his advice and encouragement, and Milind for his constant verbal harassment which helped motivate me to complete the project. Milind and Carlos Kokron also helped me with some of the computer code used in the membrane reactor model. I would also like to thank my family for their encouragement and support during my years as a graduate student.

This project received financial support from several sources including grants from the U.S. Department of Energy, and the American Chemical Society Petroleum Research Fund. I also received an Energy Research Fellowship from Battelle Pacific Northwest Laboratories and a Selfridge Graduate Fellowship from Oregon State University. I am very grateful to these sources of financial support.

John P. Collins

TABLE OF CONTENTS

TABLE OF CONTENTS, CONTINUED

TABLE OF CONTENTS, CONTINUED

LIST OF FIGURES

LIST OF FIGURES, CONTINUED

LIST OF FIGURES, CONTINUED

LIST OF TABLES

CHAPTER I
INTRODUCTION

Separation processes are extremely important in the chemical industry and related industries for reactant recovery, product purification and for the removal of environmental toxins prior to the release of waste gas streams into the environment. A relatively new technology gaining increasing importance as a means of separating mixtures is the field of membrane separations. High temperature membranes are an emerging membrane technology with many potential industrial applications. One of their most significant applications is in a new type of chemical reactor called a membrane reactor where chemical conversion and product purification by separation take place in the same device. By selectively separating the reaction products, it is possible to achieve significant enhancement over the equilibrium conversion of the reactor feed stream. Reaction rates are increased in some systems resulting in a decrease in the required reactor size. Product selectivity is also improved in some cases.

The U.S. Department of Energy is seeking to develop advanced power generation systems such as the integrated, gasification combined cycle process (IGCC) using coal or other fossil fuels. Gasification of coal containing organic nitrogen and sulfur compounds produces a synthesis gas stream containing trace amounts of ammonia and other toxic and corrosive impurities such as hydrogen sulfide. The temperature and pressure ranges encountered under reducing conditions are 811 to 1366 K and 1379 to 6895 kPa, respectively (U.S. Department of Energy, 1988). Table 1.1 summarizes typical gas stream compositions found in IGCC processes.

Ammonia formed in the gasification process is converted to nitrogen oxides (NO_X) when the synthesis gas is combusted at high temperatures in gas turbines. It is desirable to remove the ammonia prior to combustion of the synthesis gas to reduce NO_X emissions. Conventional gas separation processes such as absorption and polymeric membranes cannot be used because the synthesis gas temperature is too high. Catalytic decomposition of ammonia to hydrogen and nitrogen in the gas feed to the turbine is a potential method for reducing NO_X emissions. However, ammonia conversion in a conventional packed bed catalytic reactor is limited by chemical

Table 1.1
Composition of Coal Derived Synthesis Gas

Component	Mole %[a]	Mole %[b]
Nitrogen	48.0	36.4
Carbon dioxide	5.0	13.6
Carbon monoxide	21.0	7.5
Hydrogen	20.0	20.5
Water	1.0	20.4
Methane	4.2	0.65
Hydrogen sulfide	0.001 - 0.5[c]	0.311
Argon	-	0.564
Ammonia	0.3	0.075
Temperature (K)	811 - 1366	811
Pressure (kPa)	1379 - 6895	2378

[a] U.S. Department of Energy 1988.

[b] Southern Company Services, Inc. et al., 1990.

c 0.001 mole % or 10 ppm hydrogen sulfide concentration is typical downstream of the high temperature zinc ferrite process, while 0.5 mole % is typical if the hydrogen sulfide is not removed using zinc ferrite or an equivalent process (U.S. Department of Energy, 1988).

equilibrium due to the high concentrations of hydrogen and nitrogen in the synthesis gas. A high-temperature, high-pressure catalytic membrane reactor which can selectively remove hydrogen from the synthesis gas stream is needed to shift the equilibrium of the decomposition reaction.

The objective of this research project is the investigation of catalytic decomposition of ammonia in a high-temperature, high-pressure, packed bed membrane reactor. A schematic diagram of a packed bed membrane reactor for ammonia decomposition is shown in Figure 1.1. The membrane reactor system consists of a shell and tube type configuration similar to a shell and tube heat exchanger. The membranes are on the tube side. Synthesis gas enters the membrane tubes (tube side) which are packed with catalyst. Selective permeation of hydrogen through the membrane walls and into the shell (sweep) side shifts the chemical equilibrium on the tube side resulting in a higher conversion of ammonia to hydrogen and nitrogen. The partial pressure driving force required for hydrogen permeation is obtained by operating the shell side at a lower total pressure than the tube side, or by diluting the permeated gas with a sweep gas. The shell side gas can flow in either a cocurrent or countercurrent direction to the tube side gas.

There are several necessary characteristics for the membrane in a membrane reactor for ammonia decomposition. One of the most important characteristics is the ability to operate at high temperatures. A high selectivity for hydrogen over the other synthesis gas constituents is needed. A high hydrogen permeability is desirable to minimize the required reactor size. To eliminate the need for a sweep gas on the shell side, the membrane should remain hydrogen selective when there is a large total pressure difference (i.e., transmembrane pressure difference) between the tube and shell side. Resistance to chemical attack or corrosion by constituents of the synthesis gas stream is also important. Finally, a tubular membrane design is desirable since membrane tubes can be fabricated into a shell and tube membrane reactor configuration which is amenable to scale-up to an industrial size process. The shell and tube design requires less space than flat plate membranes due to its higher surface area to volume ratio.

Commercial availability of high-temperature membranes is currently limited to porous ceramic membranes. These membranes are highly permeable, resistant to chemical attack by synthesis gas constituents, and are available in tubular design configurations. The smallest available pore size is approximately 4 to 5 nm. At low total pressure differences between the tube and shell side, gases permeate through these

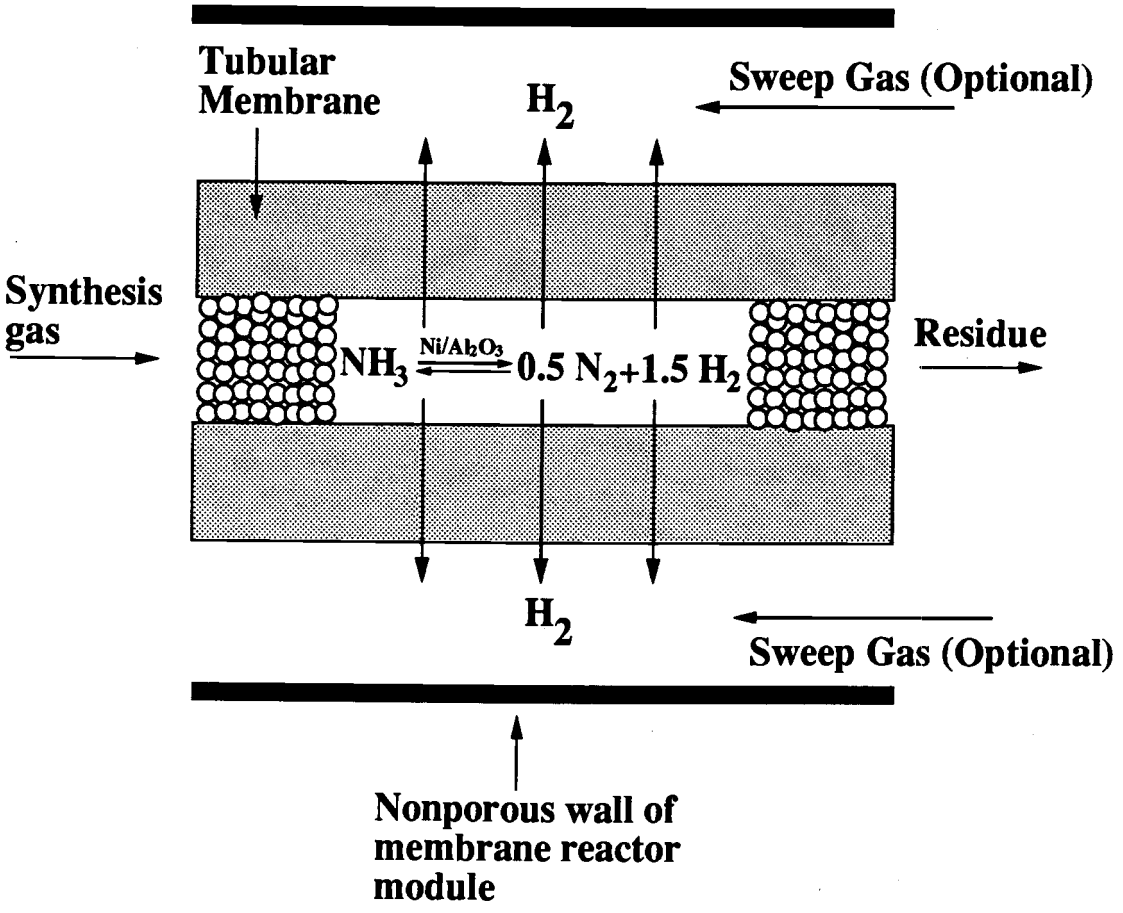

Figure 1.1 Cross-section of a Membrane Reactor for Ammonia Decomposition

membranes by the Knudsen diffusion mechanism. In a membrane with Knudsen diffusion selectivity, the ratio of membrane permeabilities for any two gases is inversely proportional to the square root of the ratio of their molecular weights. Therefore, the maximum hydrogen/nitrogen selectivity in these membranes is 3.74 and the maximum hydrogen/ammonia selectivity is 2.92. At total pressure differences above about 150 kPa, membrane selectivity starts to decrease below the Knudsen diffusion selectivity since permeation by viscous flow becomes significant (Champagnie et al., 1990). It is not feasible to use these membranes in a membrane reactor for ammonia decomposition because the hydrogen selectivity is too low. Ammonia conversion would be limited by permeation of ammonia into the shell side where there is no catalyst and chemical equilibrium does not favor the decomposition reaction. In addition, the synthesis gas pressure is too high to operate these membranes without a sweep gas which dilutes the permeated gas stream and lowers its fuel value.

The objectives of this research project are as follows:

- Develop a high-temperature, high-pressure membrane which improves upon the hydrogen selectivity of ceramic membranes, and improves the efficiency of the ammonia decomposition reaction at temperatures, pressures, nitrogen, hydrogen, and ammonia concentrations within the range of IGCC conditions.
- Develop a membrane that has potential use in other high-temperature membrane separation and membrane reactor applications in addition to ammonia decomposition.
- Characterize the membrane performance by conducting permeability tests with nitrogen and hydrogen over a range of temperatures and pressures.
- Conduct kinetic experiments to determine the kinetic parameters for the ammonia decomposition catalyst used in the membrane reactor.
- Pack a membrane tube with the decomposition catalyst and conduct performance tests on the resulting catalytic membrane reactor with a gas stream that simulates the temperatures, pressures, hydrogen, nitrogen, and ammonia concentrations in IGCC synthesis gas.
- Develop a mathematical model for predicting the performance of a catalytic membrane reactor for ammonia decomposition.

The primary objective is to develop a membrane that has as many of the desirable membrane characteristics discussed above as possible, and to demonstrate that this membrane can significantly improve on the ammonia conversion of a conventional reactor when dilute concentrations of ammonia and high concentrations of hydrogen and nitrogen are in the feed gas.

This document is organized in the following manner. Chapter II presents background and literature survey information. Ammonia decomposition kinetics are addressed in Chapter III. The mathematical model developed to predict the performance of a membrane reactor for ammonia decomposition is described in Chapter IV along with results of preliminary modeling calculations. Chapter V describes the preparation and characterization of a composite palladium-ceramic membrane which was the membrane design chosen for this project. Results of ammonia decomposition experiments performed with the packed bed palladium-ceramic membrane reactor are presented in Chapter VI. Results of modeling calculations used to evaluate the accuracy of the membrane reactor model are also included in Chapter VI. Finally, conclusions and recommendations for future work are discussed in Chapter VII.

The order of presentation approximately coincides with the chronological order in which research was performed on the project. Kinetic experiments and membrane reactor modeling were performed first to help determine an appropriate membrane design. Procedures for preparing the membrane were then developed and the permeability experiments were performed to characterize the membrane. Finally, the membrane was filled with catalyst and membrane reactor experiments were performed.

CHAPTER II
BACKGROUND AND LITERATURE SURVEY

AMMONIA CATALYSIS

The literature pertaining to ammonia catalysis is extensive and has been reviewed by Nielson (Nielson, 1971; Nielson et al., 1964), Satterfield (Satterfield, 1980), and Krishnan (Krishnan et al., 1987). Although several reaction mechanisms have been proposed, the mechanism proposed by Temkin and Pyzhev (Temkin and Pyzhev, 1940) has been found to fit data over a wide range of conditions including conditions that favor ammonia synthesis (Nielson, 1964) and conditions that favor ammonia decomposition (Nandy, 1981). While numerous studies have been conducted with ammonia synthesis under high temperature and pressure conditions, research on ammonia decomposition at high temperatures and pressures has been limited (Nandy, 1981). Nandy (Nandy, 1981) conducted ammonia decomposition experiments with pure ammonia at temperatures from 873 to 1050 K and pressures from 6991 kPa to 9930 kPa using an alumina supported nickel catalyst.

Steam and sulfur can have various deleterious effects on the activity of ammonia decomposition catalysts. Although these effects are not addressed in this research project, some background information is presented below.

Krishnan and coworkers (Krishnan et al., 1988) examined the effect of hydrogen sulfide and steam on various supported nickel, nickel/iridium, and nickel manganese catalysts supported on alumina or $MgAl_2O_4$. The alumina supported nickel/iridium catalyst was the only catalyst that worked when exposed to 7.2 mole percent steam and 0.01 mole percent hydrogen sulfide at 823 K. An ammonia conversion of 55 percent was achieved with the nickel/iridium catalyst for a space time of 0.36 seconds. The catalysts worked better when exposed to steam and hydrogen sulfide at 1073 K but most had physical deterioration problems.

Alumina supported nickel catalyst as well as catalyst based on iron, ruthenium, platinum, and molybdenum were also evaluated in screening tests conducted with simulated synthesis gas (Krishnan et al., 1987). The screening tests were performed at atmospheric pressure and temperatures ranging from 923 to 1033 K. The simulated synthesis gas contained ammonia, hydrogen sulfide, steam, carbon monoxide, carbon dioxide, and methane. The supported nickel catalysts were the only catalysts that survived the screening test. In subsequent 100 hour tests, the supported nickel

catalysts experienced deactivation problems when exposed to various concentrations of hydrogen sulfide and steam. However, 100 percent ammonia conversion was achieved for 80 hours for a gas that contained 0.001 mole percent hydrogen sulfide and 5 mole percent steam at 923 K. Ammonia conversion dropped to 81 percent after 100 hours.

INORGANIC MEMBRANES

A membrane is a semi-permeable barrier between two phases through which differential mass transfer can occur. In a membrane process, separation is a consequence of differences in the transport rates of chemical species through the membrane. The following generalized equation may be used to quantify the permeation rate or flux (J_J) of gas species J through a membrane:

$$J_J = \frac{\bar{P}_J}{t_m}\left(P_{Jt}^{n(J)} - P_{Js}^{n(J)} \right) \qquad (2.1)$$

where P_{Jt} and P_{Js} are the partial pressures of gas species J on the two faces of the membrane. The mass transfer driving force may also be expressed in terms of fugacity or concentration, if desired. As shown in Equation 2.1, the permeation rate (J_J) depends on the membrane permeability for the gas ($\bar{P}_J$) as well as the characteristic thickness of the membrane (t_m). The value of n(J) depends on the mechanism for gas transport through the membrane.

Selectivity is a term often used to compare the permeabilities for different gases in a particular membrane. When the n(J) values for two gases are the same, the following equation may be used to determine membrane selectivity for gas species I over gas species J:

$$\alpha(I/J) = \frac{\bar{P}_I}{\bar{P}_J} \qquad (2.2)$$

When n(J) is not the same for two gases, membrane selectivity may be calculated from the ratio of pure gas permeation rates at the same total pressure, temperature, and transmembrane pressure difference. Increasing the membranes selectivity for a particular gas species, increases the membranes ability to separate that gas species from a mixture of gases.

There is generally a trade off between membrane selectivity and permeability. Membranes with the highest permeabilities tend to have low selectivities. Conversely,

highly selective membranes have low permeabilities. The choice of membrane depends on the requirements for the desired application. In some cases the benefits associated with high permeation rates out weigh the disadvantage of low selectivity. High selectivities are essential in some applications. For this project it is desirable to have a membrane with a very high hydrogen selectivity that can achieve reasonable hydrogen permeation rates.

Membranes are conveniently classified into organic and inorganic membranes. This discussion focuses on inorganic membranes.

The two basic types of inorganic membranes are dense membranes and porous membranes. High-temperature microporous ceramic membranes are commercially available in a variety of design configurations including single tubes and multichannel monolithic membranes (Hsieh, 1991). A high permeability is achieved with an asymmetric design consisting of a thick macroporous (12 μm) support structure and a thin multilayer composite membrane. Pore diameters as low as 4 nm on a 5 μm thick top (selective) layer are commercially available. These membranes are thermally and mechanically stable, chemically resistant, and highly permeable, but their selectivity is low since gas transport through a 4 nm pore layer occurs primarily by Knudsen diffusion at high temperature. Porous Vycor glass membranes with Knudsen diffusion selectivities are also commercially available. Permeation rates achieved with the Vycor glass membranes are much lower than those achieved with asymmetric ceramic membranes because the same pore diameter of roughly 4 nm exists through out the membrane cross sectional thickness of roughly 1.5 mm. Developmental silica microporous membranes with higher gas selectivities were reported by Way and Roberts (1992).

Metal oxide membranes and metal membranes are two types of dense membranes suitable for high temperature applications. One recent development in the field of metal oxide membranes is the deposition of metal oxides in the pores of microporous membranes. Tsapatis et al. (1991) prepared hydrogen selective metal oxide membranes by chemical vapor deposition of SiO_2, TiO_2, Al_2O_3, and B_2O_3 layers within the pores of Vycor tubes. These membranes had hydrogen to nitrogen selectivities of up to 1000 to 5000, but a relatively low hydrogen permeability compared to hydrogen permeable metal membranes and porous membranes.

Palladium and its alloys, nickel, platinum and the metals in Groups 3 to 5 of the Periodic Table are all permeable to hydrogen (Barrer, 1941). Due to the wide spread use of hydrogen in industrial processes, there is great interest in using membranes

constructed of hydrogen permeable metals. Hydrogen permeable metal membranes made of palladium and its alloys are the most widely studied due to their high hydrogen permeability, chemical compatibility with many hydrocarbon containing gas streams, and essentially infinite hydrogen selectivity. Several metals in Groups 3 to 5 of the Periodic Table have a higher hydrogen permeability than palladium but they are not compatible with many feed streams due to their high chemical reactivity (Edlund, 1992). A major problem with palladium and palladium alloy membranes is they are difficult to modularize into compact units with high surface area. Foils as thin as 25 μm are commercially available but membranes constructed from flat foils are less amenable to modularization than those constructed from tubes. For mechanical stability, palladium or palladium alloy tubes need to be well over 0.1 mm when used for applications requiring high transmembrane pressure differences. The palladium tubes are too thick to achieve high hydrogen permeation rates and are not economically feasible for large scale operations. An additional problem is that palladium and palladium alloys are poisoned by hydrogen sulfide resulting in either a reduced permeability (Hurlbert, 1961) or membrane failure (Edlund, 1993).

Recent research efforts are focused on developing composite metal membranes consisting of relatively thin palladium or platinum coatings on hydrogen permeable base metals (Edlund, 1992; Buxbaum, 1992), and composite metal-microporous membranes (Uemiya et al, 1988).

The composite metal membranes consist of thin (2 to 25 μm) metal coatings of palladium or platinum on a hydrogen permeable base metal such as vanadium, niobium, or tantalum (Edlund, 1992; Buxbaum, 1992). The metal coatings are chosen for their chemical compatibility with feed gas constituents, and the base metal for its high hydrogen permeability, mechanical stability, and relatively low cost. Buxbaum (1992) tested membranes with a 2 μm palladium coating on 2 mm thick discs of niobium and tantalum at temperatures up to about 698 K. The hydrogen permeation rates for these membranes were between one and two orders of magnitude higher than those of palladium membranes of the same total thickness. The durability of these membranes at high temperatures is a problem since intermetallic diffusion between the different metal layers reduces membrane permeability. Buxbaum estimates that membrane durability is a manageable issue for membrane operation below about 823 K (Buxbaum, 1992; Hsu and Buxbaum, 1986).

Edlund and coworkers are developing a composite metal membrane suitable for use at higher temperatures. Membrane durability at high temperature is obtained by

placing a barrier to intermetallic diffusion between the metal coatings and the hydrogen permeable base metal. A constant hydrogen flux was obtained over a 7 day thermal stability test at 973 K (Edlund, 1992). In contrast, the flux from a composite metal membrane with no diffusion barrier was essentially eliminated after 2 days at 973 K (Edlund, 1992).

Another way to obtain a membrane with high hydrogen permeability and selectivity is to coat the selective layer of a microporous membrane with a thin film of hydrogen permeable metal. The result is a composite metal-microporous membrane. The microporous membrane provides the mechanical support required for the thin metal film. Uemiya and coworkers used electroless plating to deposit palladium films ranging from 13 to 20 μm on the outside surface of porous glass tubes with 0.3 μm pores (Uemiya et al., 1988, 1991a, 1991b, 1991c). They report an infinite hydrogen selectivity which means a defect free palladium layer was deposited. Uemiya and coworkers (Uemiya et al., 1990) also made a composite palladium-ceramic membrane for use in a membrane reactor for aromatization of propane by depositing an 8.6 μm layer of palladium on the outside surface of a porous alumina cylinder. The hydrogen selectivity for this membrane was not reported.

A Japanese patent was issued to Abe for a composite palladium-ceramic membrane consisting of a 5 to 10 μm layer of palladium supported on an alumina membrane with a 0.3 μm pore size (Abe, 1987). The hydrogen selectivity of Abe's membrane was not discussed. Govind discussed the characteristics of a palladium-ceramic membrane made from a commercially available 0.2 μm alumina membrane from U.S. Filter in Warrendale, Pa (Govind, 1992). He has deposited palladium films of 3 to 9 μm on the selective layer of the ceramic membrane using electroless plating. The film was said to be porous and selectivities of 40 to 120 for hydrogen over argon where obtained at 673 K. The transmembrane pressure difference applicable for the reported selectivities was not discussed. Based on Govind's results, it appears a thickness of over 10 μm is needed to obtain a nonporous palladium film on the support membrane when electroless plating is used for film deposition.

The extent of hydrogen sulfide poisoning on metal membranes appears to depend on the gas composition, temperature, and the composition of the metal. Hurlbert (1961) reported that the hydrogen permeability of a 24 μm palladium foil was reduced to about 15 percent of the original permeability when $5 \cdot 10^{-5}$ mole percent of hydrogen sulfide was added to a 172 kPa hydrogen stream at 623 K. The hydrogen permeation rate rapidly dropped upon exposure to the hydrogen sulfide but eventually leveled off

after about 100 minutes. The poisoning was associated with the formation of a gray surface film on the palladium and was practically irreversible (Hurlbert, 1961). Edlund (1993) reported that a palladium coated composite metal membrane failed by catastrophic rupture within seconds of exposure to 793 kPa of pure hydrogen sulfide at 973 K. In contrast, a membrane with a 25 μm platinum coating showed no degradation in performance after 8 hours exposure to the same conditions. One problem is that the hydrogen permeability of platinum is over two orders of magnitude lower than palladium. Therefore, substantially thinner films than 25 μm are needed to obtain reasonable hydrogen permeation rates through platinum coated membranes.

Palladium-gold alloys showed improved resistance to hydrogen sulfide poisoning compared to pure palladium and other palladium alloys such as palladium-silver (McKinley, 1967). McKinley (1967) studied the effect of hydrogen sulfide poisoning on 20 to 30 μm membrane foils of pure palladium, palladium-gold, palladium-silver, and palladium-copper alloys. The alloy compositions were 40 weight percent gold, 27 weight percent silver, and 40 weight percent copper, respectively. The permeability of the pure palladium and each of the palladium alloy foils dropped after about $4 \cdot 10^{-4}$ mole percent of hydrogen sulfide was added to a hydrogen stream at 623 K and 618 kPa. However, the palladium-gold alloy foil was less effected by the hydrogen sulfide than the other metals. The palladium-gold permeability was only reduced to about 80 percent of the unpoisoned permeability after six days exposure to the hydrogen sulfide. In contrast, the pure palladium foil permeability was reduced to 30 percent of its unpoisoned value after three to four days exposure. The palladium-silver foil permeability was reduced to practically zero within hours of exposure to hydrogen sulfide, and the palladium-copper to five percent of the unpoisoned permeability. The poisoned palladium-gold alloy permeability was about 40 percent of the unpoisoned permeability of the pure palladium foil.

McKinley (1967) found that the original permeabilities for each of the tested metals were completely recovered when the feed was switched to a hydrogen sulfide free gas. He concluded that the hydrogen sulfide poisoning was reversible. He also noted that the pure palladium and palladium-silver alloys were changed in appearance after exposure to the hydrogen sulfide. These foils lost their luster and appeared slightly dull. Although not stated by McKinley, this appears to indicate that a chemical change occurred in the pure palladium and palladium-silver alloy even though the original permeabilities were recovered. In contrast, the palladium-gold alloy retained its original appearance and luster even after exposure to 6.6 mole percent hydrogen

sulfide. McKinley concluded that the palladium-gold alloy poisoning was due to adsorption of hydrogen sulfide on the foil surface rather than to chemical attack or sulfide formation on the metal surface.

Goltsov (1975) also studied the effect of hydrogen sulfide poisoning on pure palladium and palladium alloy membranes. He found that the presence of steam in the gas mixture eliminated the poisoning of metal surfaces by hydrogen sulfide. In one of Goltsov's experiments, a 100 μm thick membrane foil composed of 70 percent palladium and 30 percent silver by weight was exposed to a feed gas composed of 60 mole percent hydrogen, 30 mole percent carbon dioxide, 6 mole percent carbon monoxide, 3 mole percent methane, and 1 mole percent hydrogen sulfide. The feed gas temperature and pressure were 773 K and 1520 kPa, respectively. After exposure to the hydrogen sulfide containing gas stream, the permeability dropped to about 8 percent of the unpoisoned permeability after an unspecified time period. Approximately 60 kPa of steam was then added to the gas mixture. As a result of the steam injection, the initial permeability of the membrane was recovered. In a similar experiment conducted by Goltsov, an 80 μm thick membrane foil composed of 85 percent palladium and 15 percent silver by weight was exposed to feed gas containing 70 mole percent hydrogen, 25 mole percent carbon dioxide and 5 mole percent hydrogen sulfide. The feed gas temperature and pressure were 723 K and 3040 kPa, respectively. The membrane permeability dropped to about 3 percent of the initial permeability after 10 hours of exposure to the hydrogen sulfide containing gas stream. The initial permeability was completely recovered when 101 kPa of steam was added to the feed gas.

Goltsov's findings are significant for this project because IGCC gas contains both steam and hydrogen sulfide. Since IGCC gas contains steam, membranes composed of palladium or palladium alloys are potentially feasible even though IGCC gas contains hydrogen sulfide. Experiments similar to those conducted by Goltsov but at higher temperatures are needed to verify his findings at temperatures greater than 773 K. These experiments were not performed in this project but are a promising area of future research.

MEMBRANE REACTORS

Membrane reactors are one of the most promising applications of high temperature inorganic membranes. A membrane reactor is a device where chemical conversion and product purification by separation take place at the same time. By

selectively separating one or more reaction products through the membrane wall, it is possible to achieve significant enhancement over the equilibrium conversion of the reactor feed stream. Reaction rates are increased in some systems resulting in a decrease in the required reactor size. Product selectivity may also be improved, in some cases. Review articles by Hsieh (1991), Armor (1989), and Shu et al. (1991) discuss basic principles and potential applications for inorganic membrane reactors. Some of the many potential applications include steam reforming of methane, water gas shift, hydrogen sulfide decomposition, and dehydrogenation of various hydrocarbons including cyclohexane, ethylbenzene, ethane, propane, and butane. Since these reactions produce hydrogen, improvements in reactor performance are obtainable when using a membrane with high hydrogen permeability and selectivity.

Wood was one of the first to recognize the potential benefits of combining chemical reaction and product separation processes in one unit (Wood, 1968). Wood used a palladium-silver alloy membrane to dehydrogenate cyclohexane to cyclohexene at 423 K even though cyclohexane is thermodynamically stable with respect to cyclohexene in the presence of hydrogen. Wood was able to dehydrogenate cyclohexane by selectively removing hydrogen through the membrane as it was formed. Membrane reactors have been investigated for numerous high temperature reactions of industrial interest since that time. Most of these reactions involve hydrogen as either a reactant or product. Membranes composed of palladium or palladium alloy foils and tubes have been the most widely used membranes in these studies since palladium is essentially infinitely selective for hydrogen. A comprehensive review of palladium-based membrane reactor studies was recently conducted (Shu et al.,1991). A few of the high temperature reactions studied with these palladium-based membranes are listed in Table 2.1.

Uemiya and coworkers have used their composite palladium-microporous membranes in several membrane reactor studies. These studies provide good examples of the potential benefits associated with using a membrane reactor. A composite palladium-porous glass membrane with a 20 μm palladium film was used for the water gas shift reaction (Uemiya et al., 1991a). The pore diameter of the porous glass tube was 300 nm. The experimental temperature and pressure were 673 K and 101 kPa. Argon was supplied on the sweep side to reduce the partial pressure of the permeated hydrogen. The conversion of carbon monoxide and steam to carbon dioxide and hydrogen was higher than the equilibrium conversion of the feed gas. Therefore, the

Table 2.1

Reactions Investigated Using Palladium-based Membranes

Reaction	Temperature (K)	Reaction Pressure (kPa)
$H_2O \rightleftarrows H_2 + O_2$	673 to 1073	
$2CH_4 \rightleftarrows C_2H_6 + H_2$	623 to 713	8
$2CH_4 + 3H_2O \rightleftarrows CO + CO_2 + 7H_2$	623 to 1000	101 to 1963
$CO + H_2O \rightleftarrows CO_2 + H_2$	673	101
$2C_3H_8 \rightleftarrows C_6H_6 + 5H_2$	823	
butene $\rightleftarrows$ butadiene + H_2	810	108
cyclohexane $\rightleftarrows$ C_6H_6 + H_2	473 to 850	
(di)methylnaphthalenes + $H_2 \rightleftarrows$ CH_4 + naphthalenes	750 to 800	

Information in this table is from Shu et al. (1991).

membrane reactor shifted the equilibrium of the reaction. In addition, the membrane reactor gave the same level of conversion, at equimolar ratio of steam to carbon monoxide, as obtained at a molar ratio of 2 in a conventional reactor. Therefore, the amount of steam needed to achieve a desired conversion was reduced with the membrane reactor. The high level of conversion achieved in the membrane reactor was credited to the thinness and essentially infinite selectivity of the 20 μm palladium film. Computer simulations showed that the level of carbon monoxide conversion is enhanced by decreasing the palladium film thickness as a result of the increased hydrogen permeation rate (Uemiya et al., 1991a).

Uemiya and coworkers studied steam reforming of methane in a composite palladium-porous glass membrane with a 20 μm palladium film (Uemiya et al., 1991b). The pore diameter of the porous glass tube was 300 nm. Experimental temperatures were 623 to 773 K and pressures ranged from about 101 to 900 kPa. Since the permeate gas was at atmospheric pressure, transmembrane pressure differences as high as about 800 kPa were studied. Argon gas was supplied on the sweep side to reduce the partial pressure of the permeated hydrogen. The methane conversion achieved with the composite palladium-porous glass membrane was compared to the equilibrium conversion of the feed gas and the conversions achieved in experiments conducted with a Vycor glass membrane. The pore size of the Vycor glass membrane was not reported but they typically have pore diameters of approximately 4 nm. Methane conversions achieved with the composite palladium-porous glass membrane approximately doubled the equilibrium conversion of the feed gas. In comparison, methane conversions achieved with the Vycor glass membrane were close to the equilibrium conversion of the feed gas. The improved performance of the composite palladium-porous glass membrane was primarily due to its higher hydrogen permeation rates. The hydrogen permeation rates for the composite palladium-porous glass membrane were over 10 times higher than permeation rates measured for the Vycor glass membrane. Methane conversion was also observed to increase with increasing reaction pressure even though thermodynamics favors a decrease in conversion with increasing pressure. This was attributed to the increased rate of hydrogen permeation from the reaction side with the increased pressure.

Aromatization of propane in a composite palladium-porous ceramic membrane was also studied by Uemiya and coworkers (Uemiya et al., 1990). Palladium film thickness was 8.6 μm. Experimental temperature was 773 K with the reaction side at atmospheric pressure and permeate at vacuum pressure. Experiments with a

conventional reactor were also performed to allow direct comparison of membrane reactor and conventional reactor performance. The conversion of propane and yield of aromatics was enhanced by using the membrane reactor. Formation of the undesirable side products methane and ethane was suppressed in the membrane reactor due to the efficient removal of product hydrogen from the reaction zone. The yield of aromatics was also higher than the yield obtained by Clayson (Clayson et al., 1987) where a membrane reactor with a 100 μm palladium film was used. Thus, the high hydrogen permeation rates obtained with the composite palladium-ceramic membrane resulted in improved product selectivity compared to both a conventional reactor and a membrane reactor with lower permeation rates. Therefore, we see that a membrane reactor may be used to improve both the conversion and product selectivity of a reaction.

A composite metal membrane containing a 25 μm platinum coat was used to decompose hydrogen sulfide (Edlund and Pledger, 1993). Experimental temperature and pressure were 973 K and 793 kPa with 1.5 mole percent hydrogen sulfide in the feed. The experimentally measured hydrogen sulfide conversion was 99.4 % compared to the equilibrium conversion of 13 percent for the feed gas.

Microporous membranes have also been used in membrane reactor studies. Microporous glass membranes have been used in membrane reactor studies for dehydrogenation reactions (Sun and Khang, 1988; Shinji et al., 1982; Itoh et al., 1988) and hydrogen sulfide decomposition (Fukuda et al., 1978; Kameyama et al.,1979; Kameyama et al.,1981; Kameyama et al., 1983). Microporous alumina membranes have been used in membrane reactor studies for dehydrogenation reactions (Champagnie et al., 1990) and synthesis of petrochemicals (Govind and Badra, 1992; Sperry et al., 1991).

MEMBRANE REACTOR MODELING

Packed bed membrane reactors contain both a feed (tube) side and permeate (sweep) side. A sweep gas flows through the permeate side or the permeate side is operated at a lower total pressure than the feed side to obtain the driving force needed to permeate reactant or product species. The membrane reactor may also operate with both a sweep gas and a transmembrane pressure difference. Feed and sweep gas can flow in either a cocurrent or a countercurrent flow configuration. Mathematical models of membrane reactors must account for both the consumption and generation of reactant and product species, and the permeation of species through the membrane walls. This

is done by writing differential material balance equations on both the feed side and sweep side for each species. These differential material balance equations are then solved simultaneously using numerical solution methods. The cocurrent flow configuration requires solution of an initial value problem since boundary conditions for the tube and sweep sides are at the same end of the membrane. A boundary value problem is solved for the countercurrent flow configuration since boundary conditions are at opposite ends of the membrane for the tube and sweep sides.

Itoh and coworkers simulated the dehydrogenation of cyclohexane to benzene in a packed bed membrane reactor that utilized a porous Vycor glass membrane with Knudsen diffusion selectivity (Itoh et al., 1985). The model reaction was assumed to occur on a supported palladium ($Pd\text{-}Al_2O_3$) or platinum catalyst ($Pt\text{-}Al_2O_3$). The membrane was assumed to operate in the cocurrent flow configuration with an argon sweep flowing through the permeate side. The following assumptions were used to derive the differential material balance equations for cyclohexane, benzene, hydrogen, and argon:

- Isothermal operation
- Negligible pressure drop along the axial (longitudinal) length of the membrane reactor on both the tube and sweep sides
- Reaction occurs only inside catalyst bed on the reaction (tube) side
- Negligible interphase mass transfer resistance between the bulk gas and outer surface of catalyst particles
- Negligible intraparticle mass transfer resistance within the catalyst particles
- Plug flow on the tube and sweep side
- The mixture permeabilities are the same as the pure gas values
- Steady state operation

The resulting initial value problem was solved using a Runge-Kutta method (RKG method). Itoh and coworkers studied the effect of various parameters on membrane reactor performance including membrane thickness (t_m) and the preexponential factor for the kinetic rate constant (k_o). They concluded that conversions which are higher than the equilibrium conversion of the feed gas were obtainable with a porous Vycor glass membrane reactor. In addition, there was an optimum membrane thickness which depended on the value of k_o. Since permeation rates are inversely proportional to membrane thickness, the optimum conversion depended on the relative rates of reaction and permeation. Itoh used a similar model to simulate the dehydrogenation of

cyclohexane to benzene in a packed bed membrane reactor that utilized a 200 μm thick palladium tube (Itoh, 1987). The simulated results showed good agreement with experimental results.

Mohan and Govind published a series of articles regarding membrane reactor modeling (Mohan and Govind, 1986; Mohan and Govind, 1988a; Mohan and Govind, 1988b; Mohan and Govind, 1988c). They first analyzed the dehydrogenation of cyclohexane to benzene in a cocurrent packed bed membrane reactor (Mohan and Govind, 1986). Model assumptions were the same as those listed above for Itoh and coworkers and the differential material balance equations were solved using Hammings' fourth-order predictor corrector method. Simulated membrane reactor performance depended on several parameters including the relative rates of permeation and reaction, pressure ratio (P_r), membrane selectivity, and inert gas flow rates on the tube and sweep side. Back permeation of reactant and product species from the sweep side to the tube side was predicted to occur at a $P_r = 1$ for long reactor lengths.

In an extension of their previous results, Mohan and Govind (1988a) studied the effect of various design parameters, operating variables, physical properties, and flow patterns on the performance of an isothermal membrane reactor. They simulated both the cocurrent and countercurrent flow configurations as well as a membrane reactor that employed a recycle stream and intermediate feed location. Model assumptions were the same as those listed above. The countercurrent model was solved using either an iterative convergence method or an adaptive random search method. The adaptive random search method was used because the iterative convergence method did not always work. The adaptive random search method was an optimization method where an objective function consisting of the sum of the squares of deviation between calculated values and known boundary conditions was minimized. The recycle case was solved by tearing one or two streams and using the method of successive substitution to iterate on their unknown compositions.

The following generalized reaction was studied in the modeling simulations (Mohan and Govind, 1988a):

$$\nu_A A \rightleftarrows \nu_B B + \nu_C C \tag{2.3}$$

One of the more interesting conclusions from this analysis was that the cocurrent flow configuration is better than the countercurrent flow configuration in some cases. Since most of the reaction occurs near the feed inlet, permeation rates of the reactant and

products in that region govern the choice between cocurrent or countercurrent flow (Mohan and Govind, 1988a). The driving force for product permeation near the feed inlet is lower for the countercurrent flow configuration which reduces conversion in that region. However, more reactant is lost near the feed inlet in the cocurrent case due to the higher permeation driving force which also lowers conversion. Therefore, the optimum configuration depends on physical properties and operating conditions. The cocurrent flow configuration was optimum when the permeabilities of both reaction products were greater than the reactant permeability. When the permeability of the reactant was between the product permeabilities, the optimum configuration depended on the ratio of reactant permeation rate to reaction rate. Countercurrent flow was better than cocurrent flow when this ratio was high because reactant loss near the feed end limits conversion for cocurrent flow.

Mohan and Govind also studied the effect of temperature on membrane reactor performance (Mohan and Govind, 1988b; Mohan and Govind, 1988c). Model assumptions were the same as those listed above except the isothermal operation assumption was dropped.

Membrane reactors may also be used to improve product selectivity in systems where side reactions occur. Wu and Liu included side reactions in a cocurrent flow membrane reactor model for the catalytic dehydrogenation of ethylbenzene to styrene (Wu and Liu, 1992). Model assumptions were the same as those listed above except side reactions were included and the assumption of negligible axial pressure drop on the tube and sweep sides was dropped. The membrane was assumed to have Knudsen diffusion selectivity. A hybrid reactor consisting of a conventional packed bed reactor followed by a membrane reactor was proposed to improve existing processes for ethylbenzene dehydrogenation. The purpose of the hybrid reactor was to minimize the loss of ethylbenzene resulting from permeation to the sweep side in the membrane reactor.

CHAPTER III
CHARACTERIZATION OF AMMONIA DECOMPOSITION CATALYST

INTRODUCTION

Results of experiments performed to determine the kinetics of the ammonia decomposition reaction are presented in this chapter. The objective of the kinetic experiments was to determine the kinetic parameters for the Temkin-Pyzhev rate equation (Temkin and Pyzhev, 1940), and to determine whether the rate equation was valid at the temperatures, pressures, and gas concentrations of this study. This information was needed in the membrane reactor modeling calculations described in Chapter IV. An alumina supported nickel catalyst was chosen for the ammonia decomposition catalyst because of its high catalytic activity and low cost relative to other catalysts. In addition, supported nickel catalysts performed better than catalysts based on other metals in screening tests with simulated synthesis gas (Krishnan et al., 1987).

THEORY

The generally accepted Temkin-Pyzhev mechanism and corresponding rate equation (Temkin and Pyzhev, 1940) was chosen to describe the catalytic ammonia decomposition rate. The rate equation written in terms of ammonia generation is as follows:

$$1.5\,H_2 + 0.5\,N_2 \rightleftarrows NH_3 \tag{3.1}$$

$$r'_A = k' \left[f_N K_{eq}^2 \left(\frac{f_H^3}{f_A^2} \right)^{1-\beta} - \left(\frac{f_A^2}{f_H^3} \right)^{\beta} \right] \tag{3.2}$$

where

$$k' = k'_o e^{-E_a/RT} \tag{3.3}$$

and

$$K_{eq} = \frac{f_{Aeq}}{f_{Neq}^{0.5} f_{Heq}^{1.5}} \tag{3.4}$$

The first term inside the brackets in Equation 3.2 accounts for ammonia synthesis while the second term accounts for ammonia decomposition. Therefore, the value of the ammonia decomposition term is larger than the value of the ammonia synthesis term when conditions favor ammonia decomposition. The rate equation was originally written in terms of partial pressures but fugacities may be substituted to account for deviations from ideal conditions at high pressure. One of the difficulties associated with the Temkin-Pyzhev equation is that the rate constant depends on pressure (Nielson et al., 1964). Nielson (Nielson et al., 1964) pointed out that partial pressures were normally used instead fugacities so deviations from ideal conditions were not always taken into account. A modified form of the Temkin-Pyzhev equation was proposed by Temkin to account for the effect of total pressure on the reaction rate (Nielson et al., 1964). The modification used fugacities instead of partial pressures and an additional parameter was added to the exponential term in Equation 3.3 to account for the effect of total system pressure on the rate constant (k'). Equation 3.2 remains unchanged but the rate constant (k') is determined from the following modified equation:

$$k' = k_0' e^{-(E_a + E_b P)/RT} \tag{3.5}$$

The pre-exponential factor in Equation 3.5 is reportedly independent of the total system pressure (Nielson et al., 1964).

There are three kinetic parameters to measure in the original Temkin-Pyzhev rate equation (Equations 3.2 and 3.3), the pre-exponential factor (k_0'), the activation energy (E_a), and β. The ammonia synthesis term may be neglected if no nitrogen is included in reactor feed stream and the reactor is operated at a low conversion. Combining Equations 3.2 and 3.3, and taking the natural logarithms of both sides of the resulting equation yields the following equation when the ammonia synthesis term is neglected:

$$\log_e(-r_A') = \log_e(k_0') - \frac{E_a}{RT} + \beta \log_e(f_A^2/f_H^3) \tag{3.6}$$

Ammonia decomposition rates for various temperatures, pressures, f_H, and f_A values can be measured for reactor feeds containing no nitrogen. The kinetic parameters in Equation 3.6 can then be determined from multiple linear regression of the collected rate

data. One assumption of this kinetic analysis is that the kinetic parameters are not significantly effected by the nitrogen concentration in the feed gas. This assumption was checked in the membrane reactor experiments discussed in Chapter VI by conducting conventional and membrane reactor experiments with nitrogen feed concentrations ranging from 0 to 48 mole percent.

Combining Equations 3.2 and 3.5 and taking the natural logarithms of both sides of the resulting equation yields the following equation when the ammonia synthesis term is neglected:

$$\log_e(-r'_A) = \log_e(k'_0) - \frac{E_a}{RT} - \frac{E_b P}{RT} + \beta \log_e(f_A^2/f_H^3) \qquad (3.7)$$

The kinetic parameters in Equation 3.7 can be determined in the same manner as those in Equation 3.6.

Direct measurement of the ammonia decomposition rate associated with a particular gas composition is possible if the reactor is operated in the differential mode. A differential reactor is a reactor where the reaction rate is assumed constant at all points in the reactor (Levenspiel, 1972). Since reaction rates depend on concentration, the differential reactor assumption is usually reasonable only for low conversions (Levenspiel, 1972). The ammonia decomposition rate in a differential reactor may be determined from the following equation when no nitrogen is present in the reactor feed:

$$-r'_A = \frac{2 F_{Nout}}{W} \qquad (3.8)$$

The r'_A value from Equation 3.7 is correlated with the average f_{AG}^2/f_{HG}^3 value in the differential reactor, temperature, and pressure.

It is important to minimize the effect of interphase and intraparticle mass transfer when conducting kinetic experiments with supported catalyst. The measured r'_A values must be correlated with the appropriate ammonia and hydrogen fugacities. Correlation of the measured r'_A values with the average f_{AG}^2/f_{HG}^3 value in the differential reactor assumes that ammonia and hydrogen fugacities within the porous catalyst support are constant and equal to the bulk gas values. This assumes there are no concentration gradients between either the bulk gas stream and outer surface of the catalyst particles (interphase mass transfer resistance) or within the catalyst particles (intraparticle mass transfer resistance). Intraparticle mass transfer resistance may be minimized by using small catalyst particles of around 1 mm or less in size. Unfortunately, the small

catalyst particles and low flow rates typically used in laboratory scale reactors often result in significant interphase mass transfer resistance, especially when reactants are present at dilute concentrations (Satterfield, 1980). Interphase mass transfer resistance is readily detected in a differential reactor by varying the gas flow rate at constant inlet gas conditions. It is indicated by an increase in the observed reaction rate with increasing flow rate. It is desirable to operate the differential reactor in the region where the observed reaction rate does not vary with gas flow rate in order to collect rate data that is free from interphase mass transfer effects.

The following procedure was developed to estimate interphase mass transfer coefficients from data regarding the effect of flow rate (Re_p) on the observed reaction rate in the differential reactor experiments. It is assumed that intraparticle mass transfer resistance is negligible and the concentrations of ammonia and hydrogen are constant in the catalyst particles. The observed reaction rate (r'_{Aobs}) is then written in terms of interphase mass transfer equations for ammonia and hydrogen:

$$-r'_{Aobs} = k'_{gA}\, C_t\, (Y_{AG} - Y_A) \tag{3.9}$$

$$-r'_{Aobs} = \frac{2}{3}\, k'_{gA}\, C_t\, (Y_H - Y_{HG}) \tag{3.10}$$

where Y_{AG} and Y_{HG} are the bulk gas mole fractions of ammonia and hydrogen and Y_A and Y_H are the mole fractions in the catalyst particle. The observed reaction rate is then compared to the reaction rate that occurs at high Re_p values where interphase mass transfer resistance is negligible:

$$\frac{-r'_{Aobs}}{-r'_{AG}} = \left[\frac{Y_A^2\, Y_{HG}^3}{Y_{AG}^2\, Y_H^3}\right]\beta \tag{3.11}$$

The ammonia and hydrogen mole fractions are equal to the bulk gas values for r'_{AG} because their concentrations in the catalyst particles are assumed to be equal to the bulk gas values. Equations 3.9 and 3.10 are then combined to give:

$$Y_H = \frac{3}{2}\frac{D_{MA}}{D_{MH}}\left[Y_{AG} - Y_A\right] + Y_{HG} \tag{3.12}$$

Equation 3.12 assumes k'_{gA} and k'_{gH} are proportional to the bulk gas molecular diffusion coefficients (D_{MA} and D_{MH}). Equation 3.11 and 3.12 may be solved using experimental data for r'_{Aobs} and r'_{AG}.

The following correlation is available to estimate interphase mass transfer coefficients at the low Re_p values typically used in laboratory reactors (Satterfield, 1980):

$$Sh = C_1 Re_p \tag{3.13}$$

Equation 3.13 is valid for $0.1<Re_p<10$. There is limited data regarding the value of C_1. Satterfield recommended a value of $C_1 = 0.07$ as a rough estimate (Satterfield, 1980). The k'_{gA} values calculated from the above procedure may be used to estimate Sh (Sherwood number) as a function of Re_p (particle Reynolds number) to determine a C_1 value for the differential reactor experiments. The k'_{gA} (m^3 gas/kg catalyst•s) values are converted to k_{gA} (m^3 gas/m^2 catalyst•s) values to calculate Sh using the following equation:

$$k_{gA} = \frac{k'_{gA}\,\rho_p\,R_p}{3} \tag{3.14}$$

Equation 3.14 assumes the catalyst particles are spherical which is a reasonable approximation for the particles used in the differential reactor experiments.

EXPERIMENTAL

Catalyst Preparation and Pore Size Analysis

The catalyst was prepared at SRI International in Menlo Park, California. The alumina particles were obtained from United Technologies, Inc., Louisville, Kentucky (Product No. CS308). Particles were between 250 μm and 841 μm (20/60 mesh). The catalyst was prepared by dripping an aqueous solution consisting of 21.5 g of nickel nitrate ($Ni(NO_3)_2 \cdot 6H_2O$) in 40 ml of water onto a batch of alumina particles. The nickel solution was slowly added to 50 g of alumina particles with an eye dropper. The particles were dried overnight at room temperature, at 393 K for 24 hours, and then calcined at 673 K for two hours. The particles were then placed in a tube, and exposed to hydrogen at 101 kPa of pressure. The gas temperature was raised at 150 K

per hour to 673 K and held at 673 K for two hours. The oven was then turned off, the system was purged with nitrogen, and the catalyst was stored under nitrogen. The catalyst was sent to Oregon State University for use in the kinetic tests and membrane reactor experiments. After receiving the catalyst from SRI, the particle size distribution was narrowed to 595 μm to 841 μm (20/28 mesh) using a Ro-Tap testing sieve shaker. A description of a Ro-Tap testing sieve shaker is available in Perry's Handbook (Perry and Chilton, 1973).

The surface area and average pore diameter of the catalyst particles were determined by micropore analysis using the Accelerated Surface Area and Porosimetry (ASAP) 2000 system (Micromeretics Company, Norcross, GA). The surface area of the catalyst was 220000 m^2/kg as determined by the Brunauer-Emmett-Teller (BET) method using nitrogen as the analysis gas. The pore volume was approximately 0.0006 m^3/kg and the average pore diameter was about 10 nm.

Experimental Procedures for Kinetic Experiments

Figure 3.1 is a schematic of the experimental system for the kinetic experiments. The flow and composition of the reactor feed stream were controlled by Brooks 5850 Series E mass flow controllers (Brooks Instrument Division of Emerson Electric Company, Hatfield, Pa) with a Tylan General Model RO-28 readout and control box (Tylan General Corporation, Torrance, CA). The mass flow controllers were calibrated for each gas using 100 and 1000 cm^3 bubble flow meters (Supelco, Inc., Bellefonte, PA). The reactor feed gas flow rate and composition were based on the calibrated mass flow controller settings.

The nitrogen concentration in the reactor effluent was determined using a Hewlett Packard (HP) 5890 Series II gas chromatograph (GC). The GC was linked to a Hewlett Packard Vectra QS/16S personal computer with 80386SX microprocessor. HP 3365 ChemStation software was used to control both GC sample collection and analysis of peak areas. The GC was equipped with two thermal conductivity detectors (TCDs) but only one was used in the kinetic experiments. A Molecular Sieve 13X packed column (Alltech Associates, Inc., Deefield, IL) was used in the GC. Gas samples were taken with one of the two 10-port sampling valves connected to the GC. The second 10-port sampling valve was used in another experiment conducted in the laboratory. Two 0.25 cm^3 sample loops (Valco Instruments Co. Inc., Houston, TX) were connected to the 10-port sampling valve. Only one sample loop was needed for

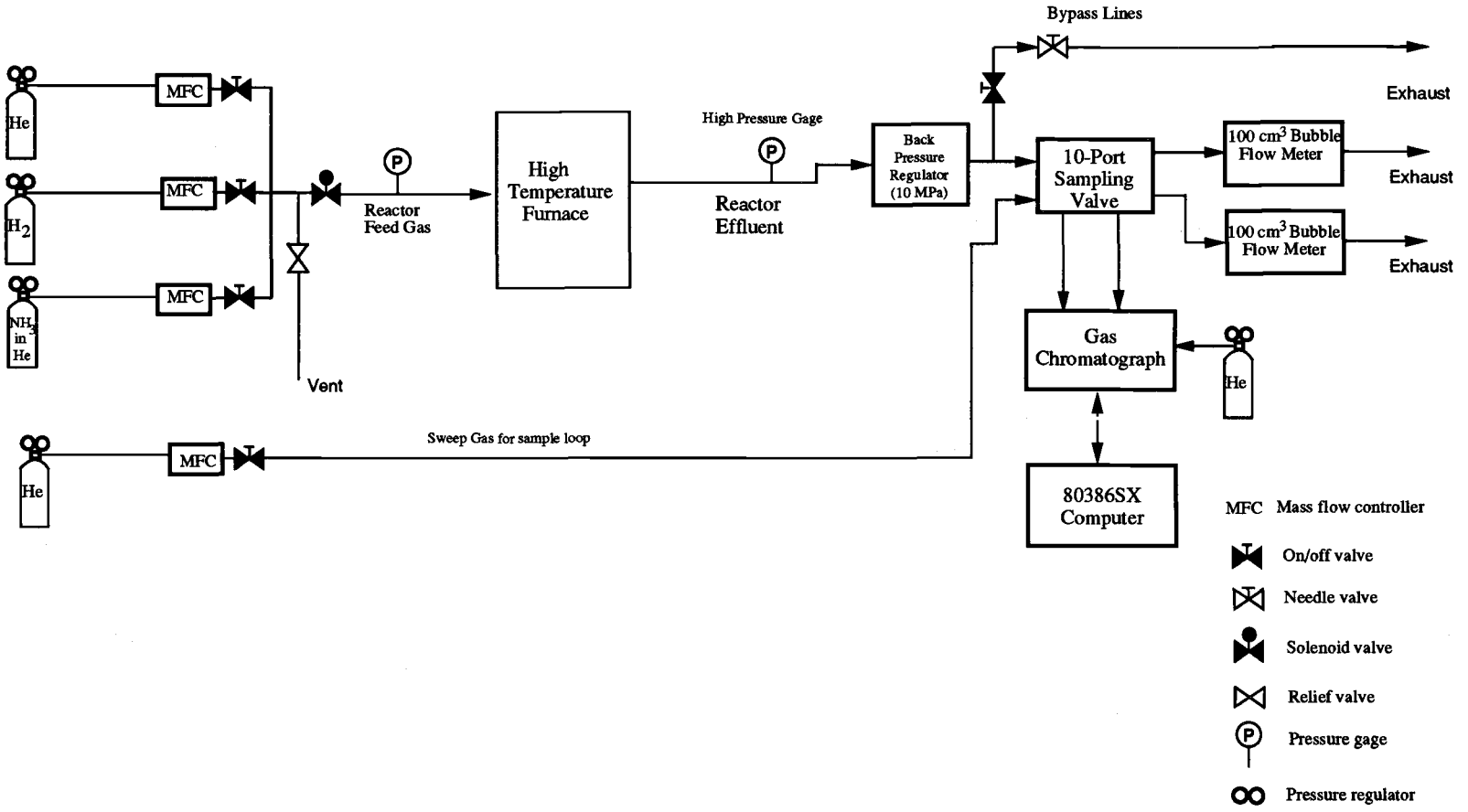

Figure 3.1 Flow System for Kinetic Experiments

the kinetic experiments so a helium sweep gas was flowed through the other sample loop. Gas flow rates for the kinetic experiments ranged from about 150 to 2650 cm^3(STP)/min (sccm). Peak areas for a particular gas composition were found to vary with gas flow rate through the sample loop. Therefore, a constant sample loop flow was maintained by using a bypass line. The flow through the bypass line was controlled with a needle valve. Nitrogen concentrations as low as about 15 ppm (0.0015 mole percent) could be measured on the GC with the system used in the kinetic experiments.

A back pressure regulator (Go Inc., Whittier, CA) was used to control the system pressure. The maximum operating pressure for the back pressure regulator was about 13900 kPa. Pressure measurements were made with liquid filled gages installed on the reactor inlet and outlet lines (Model LFP312, Span Instruments Inc., Plano, TX). The gages had a 8.89 cm face and the pressure scale was divided into increments of 69 kPa. Maximum operating pressure for the gages was 6994 kPa. There was no measurable difference in the pressure readings on the inlet and outlet lines during the kinetic experiments which indicates that the pressure drop through the packed bed was minimal.

Figure 3.2 is a schematic of the reactor which consisted of a catalyst bed inside a quartz U-tube. The inside diameter (ID) of the tube was 6 mm in some experiments and 3 mm in other experiments. The tube was inserted through a hole in the top of a temperature controlled box furnace. The tube was long enough to allow for preheating of the gas to the furnace temperature. The furnace was a Thermolyne Type 30400 (Barnstead/Thermolyne Corporation, Dubuque, IA) equipped with a Eurotherm Type 818 controller/programmer. Maximum furnace temperature was 1273 K. A Type K thermocouple was inserted into the tube directly above the catalyst bed and in some experiments it was inserted into the bed. The thermocouple was connected to a digital thermometer (Model AD2036 from Analog Devices, Inc., Seattle, WA). Thermocouple readings taken from different locations for the same reactor conditions indicate the reactor operated under isothermal conditions. A polysilazane coat was applied to the thermocouple to minimize any catalytic activity it might possess.

Except for the quartz tube reactor, all high pressure gas plumbing lines were constructed from 0.3175 cm OD stainless steel tubing. Stainless steel Swagelok® fittings were used to connect the various plumbing lines and valves. The 6 mm OD quartz tube reactor was connected to inlet and outlet gas plumbing lines in the following manner. Stainless steel tubes were connected to the inlet and outlet sides of the quartz

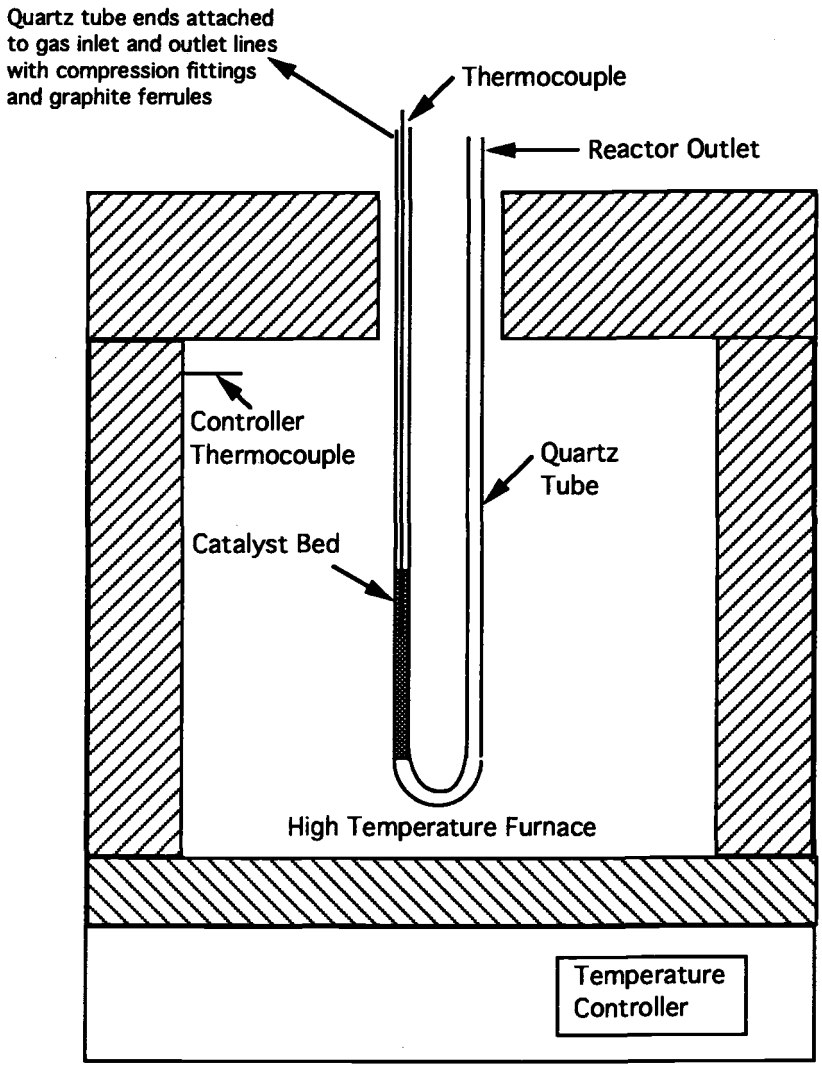

Note: Drawing is not to scale.

Figure 3.2 Catalytic Reaction System for Kinetic Experiments.

tube using quartz to metal joints. Stainless steel Swagelok® fittings were then used to connect the reactor to gas plumbing lines. The stainless steel tubes joined to the quartz U-tube had relatively thin walls so Vespel® graphite ferrules (Alltech Associates, Inc.) were used for seals to avoid deforming the tubes. This design was pressure tested up to 4240 kPa and was used in kinetic experiments up to 3548 kPa. For the 3 mm ID quartz tube reactor, Vespel® graphite ferrules were used directly on the quartz. This design was effective but the reactor ruptured after several sets of experiments were conducted at 823 K and 3548 kPa. The Vespel® graphite ferrules were also used on the thermocouple connections.

Since kinetic experiments were conducted at high pressures and nitrogen was used to determine the ammonia conversion in the differential reactor, it was very important to ensure that there were no leaks in the gas plumbing system. A helium leak detector (Model 21-150, Gow Mac Instrument CO., Bridgewater, NJ) was used to check each fitting for leaks while helium was flowed through the system. In addition, leak checks were made by using the GC to monitor for nitrogen while helium flowed through the system. These leak checking procedures ensured that there were no leaks in the experimental system.

Except for the computer and hydrogen and helium gas cylinders, the entire experimental system was inside a walk-in hood. An AG2002 toxic gas monitor (International Sensor Technology, Irvine, CA) was used check for ammonia leaks. The toxic gas monitor controlled a 2-way solenoid valve (Automatic Switch Co. (ASCO), Florham Park, NJ) which shut off the flow of gas if an ammonia leak was detected. The toxic gas sensor was factory calibrated to shut down the system if the ammonia concentration inside the walk-in hood reached 25 ppm (0.0025 mole percent). Coincidentally, the sensor was also extremely sensitive to hydrogen and was used in the hydrogen permeation experiments discussed in Chapter V. The safety system successfully shut off the gas flow when the 3 mm ID quartz tube ruptured.

The kinetic experiments were conducted in the following manner. Catalyst was first weighed and then placed in the quartz tube reactor. The catalyst bed was held in place with a quartz wool plug. The catalyst weight for experiments conducted with the 6 mm ID reactor was 0.98 g. In experiments conducted with the 3 mm ID reactor, the catalyst weight was 0.202 g. Catalyst particle diameters ranged from 0.595 to 0.841 mm. The reactor was connected to gas plumbing and the catalyst was activated by passing a mixture of hydrogen and helium through the catalyst bed. The hydrogen partial pressure was at 101 kPa. Gas temperature was raised at 180 K per hour to 673

K and held at 673 K for two hours while flowing the hydrogen/helium mixture through the reactor. Ammonia decomposition experiments were then begun. The experiments conducted with each reactor took several days. The catalyst was stored in the reactor under a helium atmosphere overnight. Hydrogen was generally flowed through the reactor each morning for about an hour to ensure the catalyst was activated prior to the start of the ammonia decomposition experiments. Periodic checks of the catalyst activity were made to ensure that catalyst deactivation was not occurring. Kinetic experiments were performed by flowing various mixtures of ammonia, hydrogen, and helium through the reactor and measuring the nitrogen concentration in the reactor effluent stream. Ammonia conversion was held to less than five percent to minimize the error associated with assuming differential reactor operation.

The ammonia source for kinetic experiments was a gas cylinder containing a dilute mixture of ammonia in helium. A total of two gas cylinders were used in the kinetic experiments. Ammonia concentrations in the two cylinders were certified by the gas supplier (Airco) at 0.54 and 1.08 mole percent. The certified concentrations were independently verified using the following procedure. The certified mixture was run through the quartz tube packed with the supported nickel catalyst at temperatures from 773 K to 1173 K. Since no hydrogen or nitrogen was present in the inlet gas the equilibrium ammonia conversion was essentially 100 percent. The nitrogen concentration in the reactor effluent was measured on the GC. The inlet ammonia concentration was then calculated from the effluent nitrogen concentration and reaction stoichiometry. The effluent nitrogen concentration was constant at temperatures above about 873 K indicating that all ammonia had decomposed.

RESULTS AND DISCUSSION

Thermal Decomposition Experiments

Thermal decomposition experiments were conducted by passing a mixture of ammonia in helium through the 6 mm ID quartz tube. The quartz tube was empty. The objective of the thermal decomposition experiments was to determine the temperature that thermal decomposition of ammonia begins. The catalytic rate experiments were conducted below this temperature to ensure that only the activity of the supported catalyst was measured. Thermal decomposition experiments were conducted at pressures of 101 kPa, 1825 kPa, and 3548 kPa over a temperature range

of 773 K to 1023 K. A 300 cm^3(STP)/min (sccm) gas stream containing 0.2745 mole percent ammonia was passed through the quartz tube in all experiments. Thermal decomposition began at about 923 K at pressures of 1825 kPa and 3548 kPa with ammonia conversions of about 0.5 and 0.7 percent, respectively. No thermal decomposition occurred in the atmospheric pressure experiments until the temperature was 1023 K.

A second set of thermal decomposition experiments were conducted with the polysilazane coated thermocouple in the 6 mm ID quartz tube. The objective of these experiments was to determine whether the thermocouple exhibited any catalytic activity to decompose ammonia. Experimental conditions were identical to those in the thermal decomposition experiments conducted without any thermocouple. The thermocouple exhibited some ability to decompose ammonia. Ammonia decomposition began at 873 K as opposed to 923 K when no thermocouple was present. Ammonia conversions of about 0.6 and 0.7 percent were obtained at 1825 and 3458 kPa, respectively. Based on the results of these experiments, experiments with the supported catalyst were not conducted at temperatures above 873 K.

Results of Catalytic Ammonia Decomposition Experiments

Figure 3.3 shows the results of an experiment designed to detect the presence of interphase mass transfer resistance. This particular experiment was conducted at a temperature of 673 K and total pressures of 3548 and 1825 kPa. The ammonia and hydrogen concentrations in the inlet gas were 0.53 and 1.8 percent, respectively. Since the observed reaction rate increases with increasing Re_p, interphase mass transfer resistance is present at the lower flow rates but not in the region where the observed reaction rate is independent of Re_p. Similar experiments were conducted each time inlet gas conditions were changed to ensure that data were collected in the region where the reaction rate was independent of flow rate. It generally took two to three runs to locate the region where interphase mass transfer resistance was not present. As temperature and the resulting reaction rate increased, it was necessary to increase the hydrogen mole fraction to obtain data free from interphase mass transfer effects. The range of hydrogen concentrations tested was from 0.5 to 57 mole percent. Gas flow rates ranged from about 150 to 2650 cm^3(STP)/min (sccm). The 3 mm ID quartz tube was used at the higher temperatures to increase the gas velocity and Re_p in the catalyst bed resulting in a decrease in the interphase mass transfer resistance. All data used to

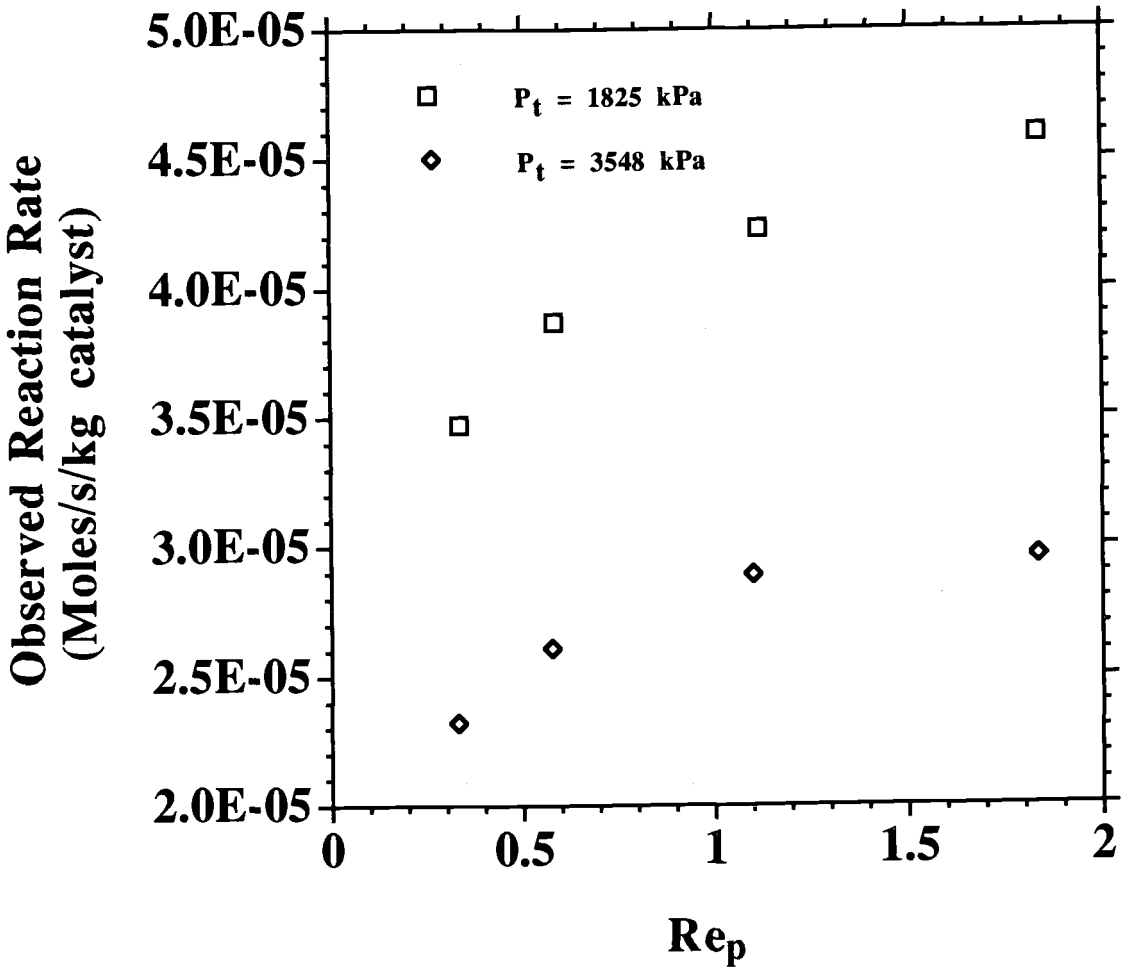

Figure 3.3 Effect of Flow Rate on Ammonia Decomposition Rate. Inlet gas composition was 0.52 mole percent ammonia, 1.8 mole percent hydrogen, and balance helium. Experimental temperature was 673 K.

determine the kinetic parameters were from the region where the observed reaction rate was independent of Re_p. Kinetic experiments were not conducted at temperatures higher than 823 K because data free from interphase mass transfer effects would have been difficult to collect due to the high reaction rate. Simulations performed with the membrane reactor model indicate that intraparticle mass transfer resistance was minimal for the conditions of the differential reactor experiments.

Multiple linear regression was performed on the collected rate data to determine the kinetic parameters for both the Temkin-Pyzhev equation and modified Temkin-Pyzhev equation. Results of this analysis are summarized in Table 3.1. Figure 3.4 presents a plot of the reaction rate predicted from the Temkin-Pyzhev equation using the measured kinetic parameters versus the observed reaction rate. The equation fits the data fairly well (correlation coefficient (r) = 0.989), but the effect of total pressure is not well correlated. Predicted reaction rates for a total pressure of 3548 kPa are generally underestimated while those at 928 kPa are generally overestimated. Figure 3.5 presents a plot of the reaction rate predicted from the modified Temkin-Pyzhev equation using the measure kinetic parameters versus the observed reaction rate. The modified equation does a better job of accounting for the effect of total pressure on the observed reaction rate (correlation coefficient (r) = 0.994). Nandy (Nandy, 1981) reported activation energies ranging from $1.92 \cdot 10^5$ to $2.74 \cdot 10^5$ J/mol for ammonia decomposition experiments conducted with pure ammonia at temperatures ranging from 873 to 1050 K. The activation energies (E_a) listed in Table 3.1 are between the values reported by Nandy.

Reaction rates in the differential reactor experiments were measured in units of mols/kg catalyst•s. The corresponding pre-exponential factor for the rate constant (k_o') has units of mols/kg catalyst•s•$Pa^{-\beta}$. Units for the rate constant in the membrane reactor model (k_o) must be mols/m^3 reactor•s•$Pa^{-\beta}$. The value of k_o was calculated by multiplying the k_o' value by the measured catalyst bed density of 580 kg/m^3. Assuming a catalyst bed voidage of ε=0.4, the estimated bulk density of the catalyst particles is ρ_p = 970 kg/m^3.

The data in Figure 3.3 were used to estimate a value for C_1 in Equation 3.13. Table 3.2 lists the estimated Sh values corresponding to the Re_p values shown in Figure 3.3. The Sh value at 3548 kPa for Re_p=1.10 is significantly higher than the other values. If this value is not included in the calculations, a C_1 value of 0.002 is obtained. This value is significantly lower than the 0.07 value listed by Satterfield (Satterfield, 1980). The C_1 value associated with the outlier data point is 0.006. The

Table 3.1
Results of Kinetic Data Analysis

Parameter Description	Calculated Value
Temkin-Pyzhev Equation Parameters:	
k_o'(mols/kg catalyst•s•Pa$^{-0.674}$)	$1.877 \cdot 10^{17}$
k_o (mol/m^3 reactor•s•Pa$^{-0.674}$)	$1.09 \cdot 10^{20}$
E_a (J/mol)	$2.304 \cdot 10^{5}$
β	0.674
correlation coefficient squared (r^2)	0.978
Modified Temkin-Pyzhev Equation Parameters:	
k_o' (mols/kg catalyst•s•Pa$^{-0.654}$)	$3.008 \cdot 10^{16}$
k_o (mol/m^3 reactor•s•Pa$^{-0.654}$)	$1.745 \cdot 10^{19}$
E_a (J/mol)	$2.187 \cdot 10^{5}$
E_b (J/mol•Pa)	$1.16 \cdot 10^{-3}$
β	0.654
correlation coefficient squared (r^2)	0.989

Table 3.2

Sherwood Numbers (Sh) Calculated From Data in Figure 3.3

Pressure (kPa)	Re_p	Sh
1825	0.335	$6.48 \cdot 10^{-4}$
1825	0.585	$1.16 \cdot 10^{-3}$
1825	1.117	$2.60 \cdot 10^{-3}$
3548	0.331	$5.01 \cdot 10^{-4}$
3548	0.576	$1.06 \cdot 10^{-3}$
3548	1.100	$6.1 \cdot 10^{-3}$

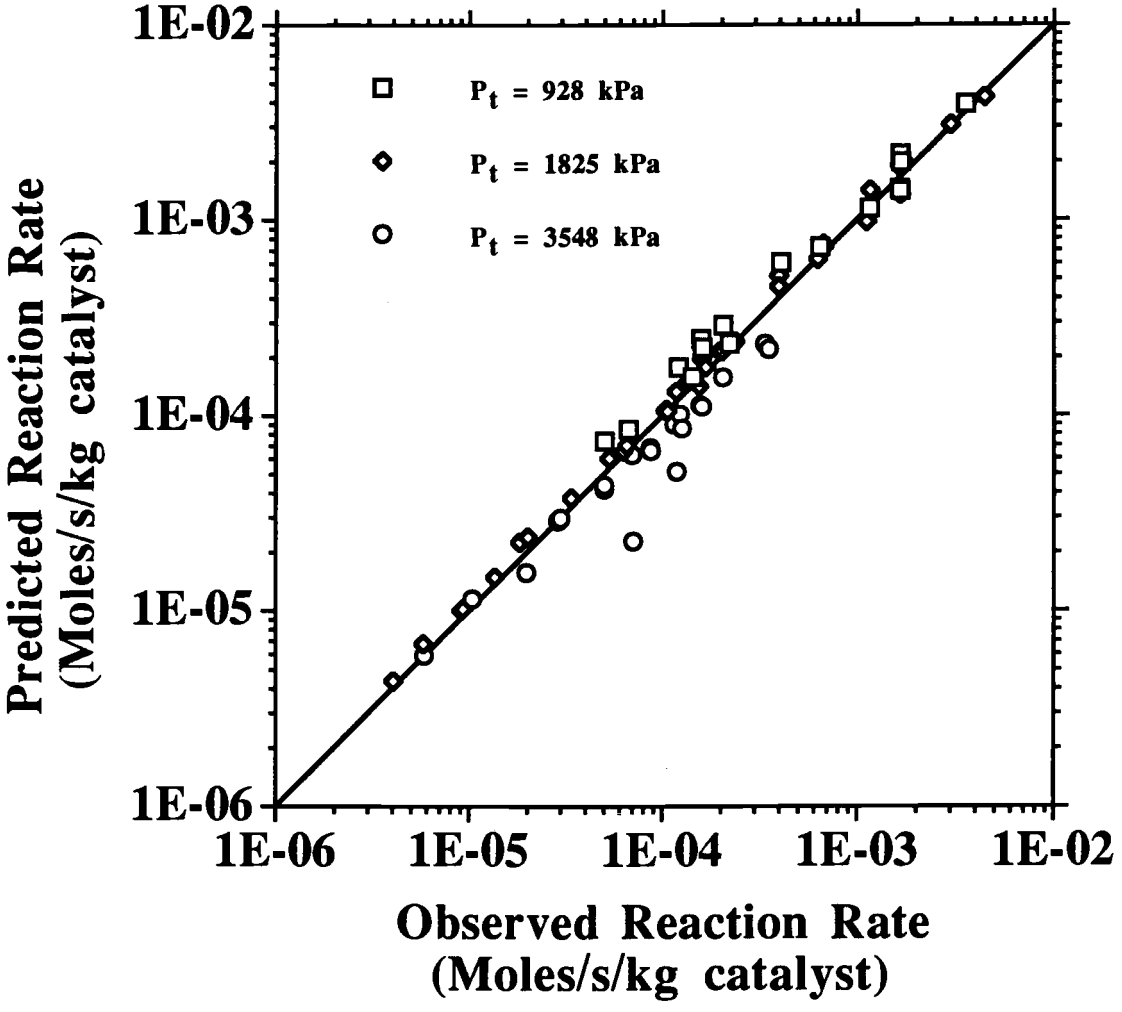

Figure 3.4 Predicted Versus Observed Reaction Rates for Temkin-Pyzhev Equation (Equations 3.2 and 3.3).

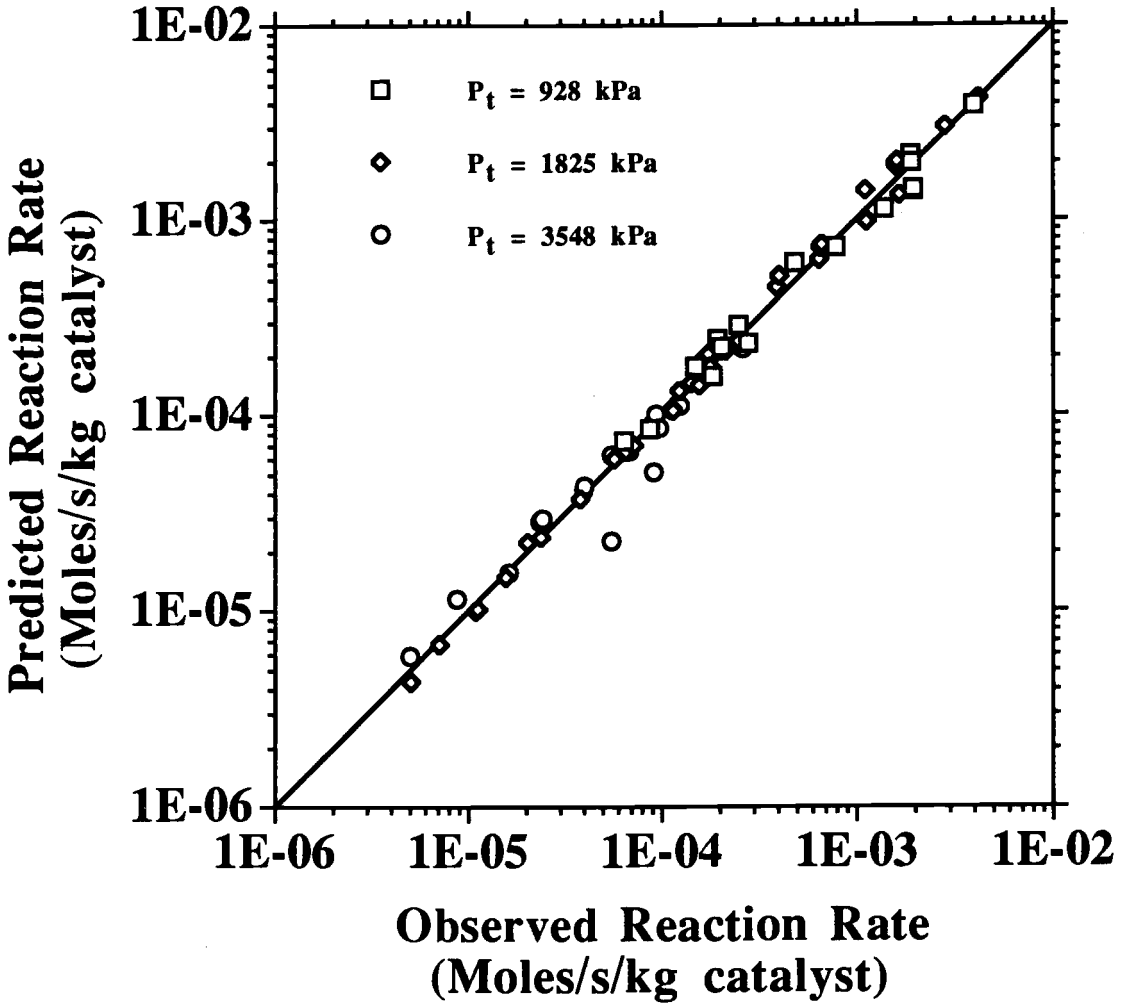

Figure 3.5 Predicted Versus Observed Reaction Rates for Modified Temkin-Pyzhev Equation (Equations 3.2 and 3.5).

accuracy of the C_1 values calculated from the differential reactor experiments is questionable for several reasons. First, they are based on a limited amount of data. Although flow rate effect experiments were conducted each time inlet conditions to the differential reactor changed, it only took two or three runs to locate the region where interphase mass transfer was not present. Therefore, the data in Figure 3.3 and Table 3.2 are the only data that could be used to estimate C_1. Also, the r'_{Aobs} values are only 2 to 25 percent lower than the r'_{AG}. values. Therefore, experimental error could significantly effect the accuracy of the calculated ratios of r'_{Aobs} to r'_{AG}. used in Equation 3.11. Finally, even though the reactor was operated in the differential mode with constant inlet gas composition and less than five percent ammonia conversion, the average $(Y^2_{AG}/Y^3_{HG})^\beta$ value in the reactor increased with increasing Re_p. This is because ammonia conversion is lower for the higher Rep values due to the lower space time. For the 1825 kPa experiments shown in Figure 3.3, the average $(Y^2_{AG}/Y^3_{HG})^\beta$ value was six percent higher at Re_p=1.84 than at Re_p=0.335. Therefore, the effect of Re_p on the observed reaction rates is slightly exaggerated in Figure 3.3 because the increase in r'_{Aobs} values with increasing Re_p was partially due to the higher average $(Y^2_{AG}/Y^3_{HG})^\beta$ values.

CONCLUSIONS

Kinetic parameters for ammonia decomposition on an alumina supported nickel catalyst were determined from experimental measurements made with a differential quartz tube reactor. The experimental data was reasonably well represented by the Temkin-Pyzhev equation. The modified Temkin-Pyzhev equation provided a better fit of the experimental data because it accounts for the effect of total system pressure on the observed reaction rates. Interphase mass transfer resistance was observed in experiments conducted at low Re_p values. Therefore, the membrane reactor model should account for the effect of interphase mass transfer resistance.

CHAPTER IV
MATHEMATICAL MODEL OF AMMONIA DECOMPOSITION IN A MEMBRANE REACTOR

INTRODUCTION

A mathematical model was developed to predict the performance of a membrane reactor for ammonia decomposition. Details of the model are presented in this section as well as results of preliminary modeling calculations. The objective of the preliminary modeling effort was to determine hydrogen selectivity requirements for the membrane and evaluate the potential effectiveness of a membrane reactor for ammonia decomposition. Results of these calculations influenced the membrane design chosen for the project. The accuracy of the membrane reactor model was tested by comparing predicted ammonia conversions to conversions obtained from the membrane reactor experiments. Results of these calculations are discussed in Chapter VI.

The preliminary modeling calculations were performed prior to the first successful testing of the composite palladium-ceramic membranes developed in this project. Membrane design was not firmly established at the time of these calculations and it heavily influences the performance and appropriate operating conditions for a membrane reactor. Therefore, the effects of operating conditions such as cocurrent flow versus countercurrent flow, sweep gas flow rates, and hydrogen selectivity were investigated. The composite palladium-ceramic membranes developed later in the study had a very high hydrogen selectivity and could be operated at a high transmembrane pressure difference. Under these conditions there was no need to use a sweep gas and there was essentially no difference between the cocurrent and countercurrent flow configuration. However, the preliminary modeling calculations provided valuable information regarding the choice of cocurrent or countercurrent flow, and the impact of sweep gas flow on membrane reactor performance.

The differences between the present work and previous modeling studies discussed in Chapter II include modeling a different reaction and reaction rate mechanism and the use of a different numerical method (orthogonal collocation) to solve the countercurrent flow model equations. The effect of interphase mass transfer between the bulk gas and catalyst surface, and intraparticle mass transfer within catalyst

particles was also considered in this study. These mass transfer effects were not considered in the previous modeling studies but are important in this study since ammonia is present at dilute concentrations.

Figure 4.1 shows a longitudinal cross-section of a tubular membrane reactor for ammonia decomposition. The feed gas flows down the inside of the membrane tube where ammonia reacts on the supported nickel catalyst to form nitrogen and hydrogen. The purpose of the membrane is to selectively remove hydrogen present in the inlet gas stream and hydrogen formed in the reaction in order to shift the equilibrium of the ammonia decomposition reaction. A sweep gas may flow down the annulus between the membrane tube and outer shell tube of the membrane module. The purpose of the sweep gas is to dilute the concentration of the permeated hydrogen in order to maintain the concentration driving force required for permeation. An alternative method for obtaining the required driving force is to operate the membrane at a large transmembrane pressure difference to eliminate the need for a sweep gas. The choice of operating mode depends on membrane design and feed gas pressure. The purpose of the membrane reactor model is to determine the molar flow rate of each gas species as a function of axial (longitudinal) position on both the inside (tube side) and outside (sweep or shell side) of the tubular membrane. This requires the simultaneous solution of the differential material balance equations written for each gas species on both the tube side and sweep side.

THEORY

Assumptions

The differential conservation of species equations were derived for membrane reactors with cocurrent and countercurrent flow configurations. The equations were derived subject to the following assumptions:

- Isothermal operation
- Negligible pressure drop along the axial (longitudinal) length of the membrane reactor on both the tube and sweep sides
- Reaction occurs only inside catalyst bed on the reaction (tube) side
- Plug flow on the tube and sweep side
- The mixture permeabilities are the same as the pure gas values
- Steady state operation

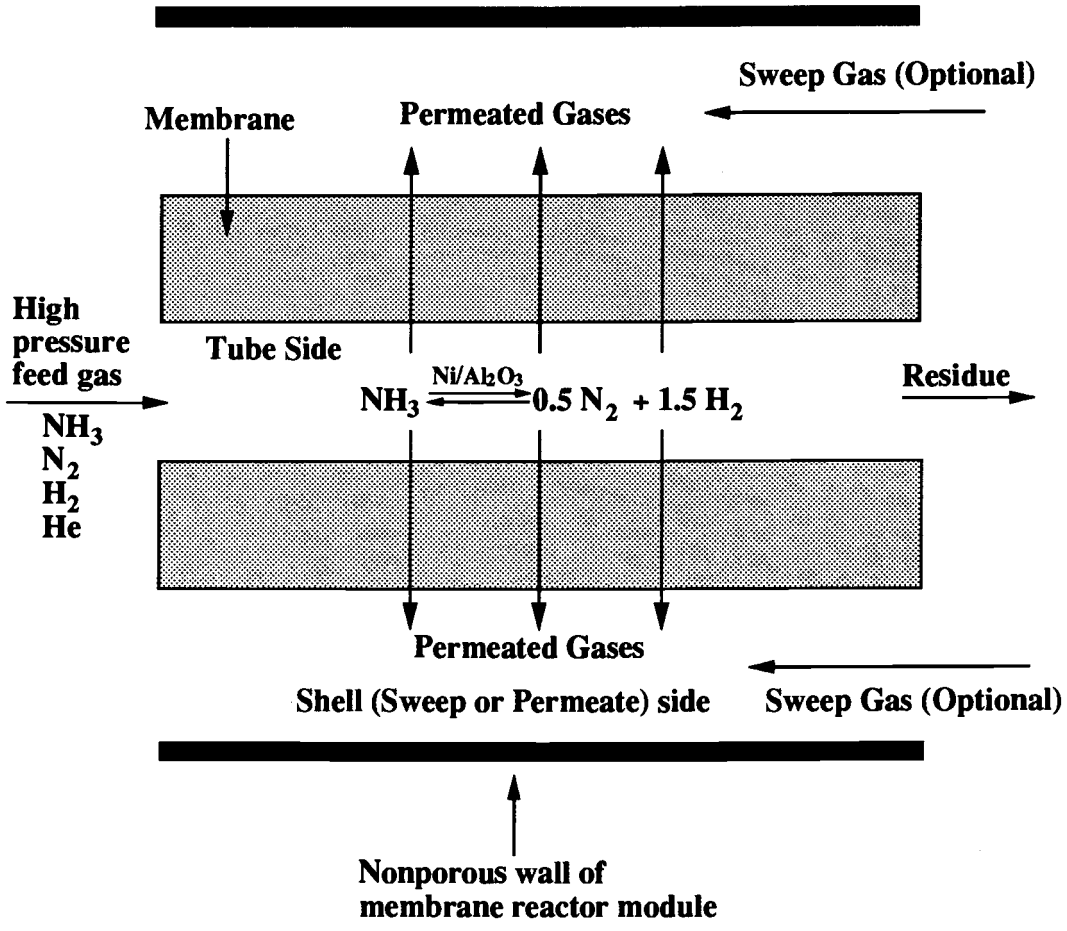

Figure 4.1 Cross-section of a Countercurrent Flow, Packed Bed Membrane Reactor for the Decomposition of Ammonia Present in High Temperature, High Pressure, Synthetic Gas.

Unless otherwise specified, the simulation results presented in this paper are for decomposition at very dilute concentrations of ammonia. Therefore, it is reasonable to assume the reactor operates isothermally. The pressure drop through the catalyst bed was estimated using the Ergun equation for the conditions simulated in this study. A typical pressure drop was approximately 10 kPa. This pressure drop is negligible compared to the operating pressures used in this study so it is reasonable to assume isobaric operation in the catalyst bed. Since no catalyst is packed on the sweep side, the sweep side pressure drop is also assumed insignificant.

Material Balance Equations

The model determines the molar flow rates of all species as a function of axial position in both the tube side and sweep side of the membrane. These molar flow rates are determined by numerical evaluation of the differential material balance equations for the tube and sweep side. The differential material balance equation on species J for the tube side of a cocurrent or countercurrent flow membrane reactor is given below:

$$\frac{d\frac{F_J}{F_{A0}}}{d\frac{L}{L_0}} = \frac{V}{F_{A0}}\left[\nu_J r_{AG}\eta - \frac{2}{R_1} J_J\right] \tag{4.1}$$

The first term within the brackets of Equation 4.1 is the reaction term and the second term accounts for the mass transfer of species J from the tube side to the shell side of the membrane reactor.

A similar differential material balance equation is obtained for the sweep side of the membrane reactor. No reaction term is incorporated into the equation because it is assumed that the reaction is confined to the catalyst bed inside the membrane reactor.

$$\frac{d\frac{Q_J}{F_{A0}}}{d\frac{L}{L_0}} = \pm\frac{V}{F_{A0}}\left[\frac{2}{R_1} J_J\right] \tag{4.2}$$

The sign on the right hand side of Equation 4.2 is positive for cocurrent flow and negative for countercurrent flow. The model accounts for four species, ammonia, nitrogen, hydrogen, and helium. The boundary conditions for Equations 4.1 and 4.2 for species J are:

Cocurrent flow

$$\text{At } L = 0,\ F_J = F_{J0} \tag{4.3}$$

$$\text{At } L = 0,\ Q_J = Q_{J0} \tag{4.4}$$

Countercurrent flow

$$\text{At } L = 0,\ F_J = F_{J0} \tag{4.5}$$

$$\text{At } L = L_0,\ Q_J = Q_{J0} \tag{4.6}$$

The model consists of a system of eight ordinary differential equations and corresponding boundary conditions. An initial value problem is solved for the cocurrent case since all boundary conditions are at the same point. A boundary value problem is solved for the countercurrent model since the tube and shell side boundary conditions are at opposite ends of the reactor.

The following equation is used to calculate the permeation rate through the membrane of species J (J_J) at a particular axial position in the reactor:

$$J_J = \frac{\bar{P}_J P_t^{n(J)}}{t_m}\left(\left(\frac{\frac{F_J}{F_{A0}}}{\frac{F_T}{F_{A0}}} \phi_{Jt} \right)^{n(J)} - \left(\frac{\frac{Q_J}{F_{A0}}}{\frac{Q_T}{F_{A0}}} \phi_{JS} P_r \right)^{n(J)} \right) \tag{4.7}$$

The only difference between Equation 4.7 and 1.1 is that fugacity is used for the permeation driving force instead of partial pressure. Equation 4.7 is written in terms of molar flow rates on the tube and sweep side but it reduces to Equation 1.1 if fugacity coefficients are set equal to one. The value of n(J) depends on the gas species and the type of membrane. The value of n(J) is 1 for all gas species for gas permeation through a porous ceramic membrane in the Knudsen flow regime. When the transmembrane pressure difference between the tube side and sweep side is increased, viscous flow lowers the selectivity of a porous membrane and $n(J) > 1$. For hydrogen permeation through a metal film, $0.5 \leq n(J) \leq 1$. The preliminary modeling calculations were not based on any particular type of membrane, and n(J) was set equal to 1 for all gas species. Experimentally determined values of n(J) were used in the modeling calculations presented in Chapter VI for the composite palladium-ceramic membrane reactor. Also the form of Equation 4.7 was slightly modified for nitrogen, helium, and ammonia in the calculations presented in Chapter VI. These modifications are discussed in Chapters V and VI.

The driving force for permeation through the membrane wall is the chemical potential difference between the tube and sweep side for component J. Fugacity was

used as the chemical potential driving force instead of partial pressure to avoid the assumption of ideal gas behavior in the preliminary modeling calculations. The effect of using fugacity instead of partial pressure for the permeation driving force was minor because the fugacity coefficients of all gas species are between 0.93 and 1.04 at the simulated reaction pressure and temperatures. Fugacities were not used to estimate permeation rates in the modeling calculations presented in Chapter VI.

The effectiveness factor (η) listed in Equation 4.1 accounts for the effect of interphase and intraparticle mass transfer resistance on the reaction rate. Since η is a local value, it is calculated at each axial position that Equation 4.1 is evaluated. This involves solving differential material balance equations in the spherical domain for reacting species to determine their concentration profile within the catalyst particles at a particular axial position in the reactor. These equations are presented below following the discussion of the kinetics of ammonia decomposition.

Reaction Kinetics

Details regarding the kinetics of ammonia decomposition were presented in Chapter III. The Temkin-Pyzhev rate equation was used to estimate reaction rates in the membrane reactor model. This equation has the following form when written in terms of ammonia generation (r_A):

$$1.5\ H_2 + 0.5\ N_2 \rightleftarrows NH_3 \tag{4.8}$$

$$r_A = k \left[f_N\ K_{eq}^2 \left(\frac{f_H^3}{f_A^2} \right)^{1-\beta} - \left(\frac{f_A^2}{f_H^3} \right)^{\beta} \right] \tag{4.9}$$

where

$$k = k_0 e^{-Ea/RT} \tag{4.10}$$

and

$$K_{eq} = \frac{f_{Aeq}}{f_{Neq}^{0.5}\ f_{Heq}^{1.5}} \tag{4.11}$$

The equilibrium constant (K_{eq}) was calculated using the equation developed by Harrison and Kobe (1953). The preexponential factor for the rate constant (k_0) was calculated by multiplying the experimental value of k_0' from Chapter III by the density

of the catalyst bed. A catalyst density of $\rho = 510$ kg/m^3 and bed void fraction of $\varepsilon = 0.4$ were used to estimate the catalyst bed density in the preliminary modeling effort. The catalyst density was based on the 510 kg/m^3 packing density of the alumina support reported by United Technologies, Inc. This packing density is significantly lower than the estimated catalyst density of 970 kg/m^3 because of void space and the nickel content of the catalyst. (See Chapter III for details regarding the estimated catalyst density.) Therefore, the k_0 value used in the preliminary modeling calculations was underestimated. This has no effect on any of the conclusions reached in the preliminary modeling analysis.

Interphase and Intraparticle Mass Transfer Equations

When interphase and/or intraparticle mass transfer resistance is present, the fugacity of ammonia within a catalyst particle is lower than the bulk gas value and may vary with radial position in the particle. Consequently, the actual reaction rate is lower than the reaction rate calculated using the bulk gas fugacity. The ammonia fugacity profile in a catalyst particle is estimated by solving the following dimensionless differential material balance equation in spherical coordinates:

$$\frac{1}{r^2}\frac{d}{dr}\left(r^2\frac{dX_A(r)}{dr}\right) = \frac{k\,R_p^2}{C_t\,Y_{AG}\,De_A\,(1-\varepsilon)}Z(r) \qquad (4.12)$$

where Z(r) is given by:

$$Z(r) = \left(\left(\frac{f_{AG}^2\,X_A^2(r)}{f_{HG}^3\,X_H^3(r)}\right)^{\beta} - f_{NG}\,X_N(r)\,K_{eq}^2\left(\frac{f_{HG}^3\,X_H^3(r)}{f_{AG}^2\,X_A^2(r)}\right)^{1-\beta}\right) \qquad (4.13)$$

The boundary conditions for Equation 4-12 are:

$$\text{At } r = 0,\quad r^2\frac{dX_A(r)}{dr} = 0 \qquad (4.14)$$

$$\text{At } r = 1,\quad -\frac{dX_A(r)}{dr} = Bi_A(X_A(r) - 1) \qquad (4.15)$$

To simplify computations, fugacities were not included in the diffusion term of Equation 4.12.

Similar differential material balance equations and boundary conditions may also be written for nitrogen and hydrogen. The resulting set of three differential material balance equations can be reduced to the differential material balance equation listed above for ammonia (Equation 4.12) and the following two equations:

$$X_H(r) = 1 + \frac{1.5\ De_A\ Y_{AG}}{De_H\ Y_{HG}} \left(X_A(1) + \frac{Bi_A}{Bi_H}(1 - X_A(1)) - X_A(r) \right) \qquad (4.16)$$

$$X_N(r) = 1 + \frac{0.5\ De_A\ Y_{AG}}{De_N\ Y_{NG}} \left(X_A(1) + \frac{Bi_A}{Bi_N}(1 - X_A(1)) - X_A(r) \right) \qquad (4.17)$$

With Equations 4.13 to 4.17, Equation 4.12 can be solved numerically to determine the $X_A(r)$ profile within the catalyst particles at a particular axial position in the membrane reactor. The effectiveness factor (η) at that axial position is then calculated using the following equation:

$$\eta = \frac{\int_0^1 Z(r)\ r^2\ dr}{\left(\left(\frac{f_{AG}^2}{f_{HG}^3} \right)^{\beta} - f_{NG}\ K_{eq}^2 \left(\frac{f_{HG}^3}{f_{AG}^2} \right)^{1-\beta} \right) \int_0^1 r^2\ dr} \qquad (4.18)$$

Thus η is the average reaction rate in the catalyst particle divided by the average reaction rate if the rate of reaction is evaluated using bulk stream conditions. The integrals in Equation 4.18 are evaluated numerically.

Gas Permeabilities and Mass Transfer Coefficients

Permeability data for the composite palladium ceramic membranes eventually used in the project were not available when the preliminary modeling calculations were performed. The permeabilities used in the preliminary modeling effort were based on data obtained in the Knudsen diffusion regime for a porous ceramic membrane. The

hydrogen permeability ($\bar{P}_H$) was experimentally determined for a commercially available U.S. Filter T-170 Al_2O_3 ultrafilter which had a selective layer with 5 nm diameter pores. The objective was to get a hydrogen permeability estimate suitable for use in preliminary calculations. The apparatus and experimental procedure were similar to those described in Chapter V for characterization of the composite palladium-ceramic membrane. The main difference was that metal compression fittings were not used to connect the tubular ceramic membrane to membrane inlet and outlet lines. Instead, a high temperature ceramic adhesive (Aron Ceramics) was used to glue the nonporous alumina inlet and outlet tubes into the ends of the membrane. Since the adhesive was porous, Aremo 617 (Aremco Products, Inc., Ossining, New York) was then used to seal the glued joints.

The conditions of the measurement were 723 K with total pressures of approximately 653 and 632 kPa on the tube and sweep sides, respectively. A sweep gas was used to dilute the permeated hydrogen. The experimental operating conditions were similar to conditions that would be used if a porous ceramic membrane was used for ammonia decomposition. A sweep gas and very low transmembrane pressure difference were used because it would not be feasible to operate the ceramic membrane at a high transmembrane pressure difference in a membrane reactor application. The resulting hydrogen permeability of $1.7 \cdot 10^{-9}$ mols•m/m^2•s•Pa was calculated using the 0.0015 m wall thickness of the ultrafilter. The remaining permeabilities for nitrogen, ammonia, and helium were calculated using the selectivity from Knudsen diffusion theory. Permeabilities were also corrected for temperature using Knudsen diffusion theory. It was assumed that the permeabilities did not vary with total system pressure in the preliminary modeling calculations. The estimated permeabilities were reasonable for the preliminary modeling calculations but should not be used for anything else due to some uncertainty in the experimental transmembrane pressure difference for the hydrogen permeability measurement. This is because 0-1000 psig (101 to 6994 kPa total pressure) pressure gages were used to measure the tube and sweep pressures. Therefore, the reported difference in tube and sweep side pressures is not based on an accurate pressure reading. The transmembrane pressure difference significantly impacts the permeation rate and resulting hydrogen permeability for the conditions under which these permeation experiments were performed.

Permeability measurements for the composite palladium ceramic membranes are discussed in detail in Chapter V.

The effective diffusion coefficients for a catalyst particle were estimated from the following equations (Satterfield, 1980):

$$\frac{1}{De_J} = \frac{1}{Dke_J} + \frac{1}{DMe_J} \tag{4.19}$$

where

$$Dke_J = \frac{194\ \theta^2}{\tau_p\ S_g\ \rho_p} \sqrt{\frac{T}{M_J}} \tag{4.20}$$

$$DMe_J = \frac{D_{M_J}\theta}{\tau_p} \tag{4.21}$$

The Biot number for mass transfer (Bi_J) may be estimated from the equations listed for interphase mass transfer coefficients by Satterfield (1980) . The appropriate equation depends on the particle Reynolds number (Re_p) in the reactor. For the low particle Reynolds numbers typically found in laboratory reactors, data for mass transfer coefficients are limited. As a very rough guide, the following equation was presented for low Re_ps in the range $0.1<Re_p<10$ (Satterfield, 1980):

$$Bi_J = \frac{C_1}{2} \frac{D_{M_J}\ Re_p}{De_J} \tag{4.22}$$

A value of $C_1 = 0.07$ was listed for the proportionality constant (Satterfield, 1980). Data collected from the differential reactor experiments performed in the present study indicate that a significantly lower value for C_1 may be appropriate. For higher Re_ps in the range $3<Re_p<2000$, the following correlation is available (Satterfield, 1980):

$$Bi_J = 0.1785 \frac{D_{M_J}\ Re_p^{0.641}\ Sc^{0.33}}{De_J} \tag{4.23}$$

Equation 4.23 is valid for $0.9\ mm<R_p<4.7\ mm$.

Gas Properties

Empirical correlations were used to calculate the fugacity coefficients for hydrogen, nitrogen, and ammonia (Cooper, 1967; Newton, 1935). The fugacity

coefficient of helium was assumed to be unity. It was found that the cocurrent model obtained equivalent results using either the empirical correlations or a two term virial equation of state with the Pitzer-Curl correction for polar gases (Tsonopoulos, 1978). Since equivalent results were obtained with the empirical correlations, they were used in the countercurrent model to simplify the computations.

Multicomponent molecular diffusion coefficients (D_{Mj}) were estimated using the equation developed by Wilke (1950). Binary molecular diffusion coefficients were calculated using the equation developed by Hirschfelder and coworkers (1949).

Gas mixture viscosities were estimated using the equation recommended by Reid and coworkers (1977) for low-pressure multicomponent gas mixtures. The low pressure equation is valid because the effect of pressure on pure gas viscosity is minimal at the operating pressures considered in this study.

To simplify the computations, the total molar gas density (C_t) in Equation 4.12 was calculated using the ideal gas law.

Numerical Solution of the Model

The system of ODEs that comprise the cocurrent model (Equations 4.1-4.2) were solved using the finite-difference subroutine DIVPAG from the IMSL Math Library (IMSL, 1989) that employs Gear's algorithm. The jacobian matrix was calculated numerically. An IBM-compatible personal computer with an Intel 80486 CPU was used to perform the computations.

The method of orthogonal collocation was used to solve the system of ODEs that comprise the countercurrent model. Details of this method are discussed by Finlayson (1980). Briefly, this technique is based on approximating the solution to the ODEs as a series of polynomials. This converts the system of ODEs into a system of nonlinear algebraic equations. The solution to these algebraic equations contains the values of the dependent variable in the original ODEs at specific values of the independent variable referred to as collocation points. An advantage of using orthogonal collocation instead of a finite difference method to solve boundary value problems is that the algebraic equations are solved simultaneously. Collocation points and matrices were calculated using program code adapted from "Numerical Recipes" (Press et al., 1986). The nonlinear algebraic equations generated by the collocation method were solved using the DNEQNF subroutine from the IMSL Math Library. This subroutine solves a

system of nonlinear equations using the Levenberg-Marquardt algorithm and a finite difference approximation of the jacobian.

The $X_A(r)$ profile in the catalyst particles at a particular axial position in the reactor was determined by solving Equation 4.12 and its boundary condition equations (Equations 4.14 and 4.15) using the orthogonal collocation method described by Finlayson (1980) for diffusion and reaction. The nonlinear algebraic equations generated by this collocation method were solved using the Newton-Raphson method with program code adapted from "Numerical Recipes" (Press et al., 1986). A quadrature formula with weighting parameters generated by the collocation method was used to evaluate the integrals in the equation for the effectiveness factor (Equation 4.18).

RESULTS AND DISCUSSION

Results of the preliminary modeling analysis are discussed below. The model was used to analyze the effect of several parameters on ammonia conversion over a range of temperatures. When the effect of interphase and intraparticle mass transfer was included, the length of reactor needed for a desired conversion level depended strongly on the equation used to calculate the Biot number for mass transfer (Bi_J), and to a lesser extent, the catalyst particle size (R_p). The impact of interphase mass transfer was greatest at low Re_p values typically used in laboratory reactors where data regarding mass transfer coefficients are limited. Since an appropriate value for Bi_J was uncertain, results of simulations performed when interphase and intraparticle mass transfer were not considered in the model are presented first. Figures 4.2 to 4.10 present results calculated using an effectiveness factor of $\eta=1$. In these calculations, the rate of ammonia decomposition was calculated using bulk gas fugacities in Equation 4.9. The effect of interphase and intraparticle mass transfer resistance is considered in Figures 4.11 and 4.12.

Unless otherwise noted, the parameters used in the preliminary modeling calculations are listed in Table 4.1. The composition of the inlet tube stream is based on typical synthesis gas mole fractions of ammonia, nitrogen, and hydrogen. Figures 4.2 to 4.4 are based on membrane reactors with Knudsen diffusion selectivity (SF=1). The performance of a membrane reactor that is more selective for hydrogen is considered in Figures 4.5 to 4.6. The effect of space time on membrane reactor performance is considered in Figures 4.7 to 4.8. Space time was calculated by dividing

Table 4.1

Input Parameters Used in Preliminary Membrane Reactor Modeling Calculations

Reactor size (m)	$R_1 = 0.0035$ $t_m = 0.0015$ $L_o = 0.254$
Gas flow rate at tube inlet (mol/s)	$F_{TO} = 3.7252 \cdot 10^{-3}$
Gas flow rate at sweep inlet (mol/s)	$Q_{TO} = 7.44 \cdot 10^{-3}$
Gas composition at tube inlet (mol %)	
ammonia	0.3
nitrogen	48
hydrogen	20
helium	balance
Gas composition at sweep inlet (mol %)	
helium	100
Reactor pressures	$P_t = 3446$ kPa $P_r = 1$
Kinetic parameters	$k_o = 5.744 \cdot 10^{19}$ (mol/m^3•s•Pa$^{-0.674}$) $E = 2.304 \cdot 10^5$ (J/mol) $\beta = 0.674$
Gas permeabilities (mols•m/m^2•s•Pa)	$\bar{P}_A = \frac{5.93 \cdot 10^{-10}}{SF}\sqrt{\frac{723}{T}}$ $\bar{P}_N = \frac{4.62 \cdot 10^{-10}}{SF}\sqrt{\frac{723}{T}}$ $\bar{P}_H = 1.73 \cdot 10^{-9}\sqrt{\frac{723}{T}}$ $\bar{P}_I = \frac{1.22 \cdot 10^{-9}}{SF}\sqrt{\frac{723}{T}}$ n(A) = 1.0 n(N) = 1.0 n(H) = 1.0 n(I) = 1.0

Note: SF = 1.0 when $\alpha(H_2/N_2) = 3.74$ (Knudsen selectivity); SF = 2.67 when $\alpha(H_2/N_2) = 10$; SF = 13.4 when $\alpha(H_2/N_2) = 50$; SF =10000 when $\alpha(H_2/N_2) = \infty$

the void volume of the catalyst bed by the volumetric flow rate of the inlet tube gas. The void volume was calculated using a void fraction of 0.4. Figure 4.9 shows the effect of the operating pressure ratio (P_r) on the performance of a hydrogen selective membrane. In Figure 4.10, the effect of a membrane reactor on decomposition of a 99 mole % NH_3 gas stream is shown.

Ammonia conversion is defined in terms of its molar flow rates entering and leaving the membrane reactor:

$$\gamma_A = \frac{F_{A0}+Q_{A0}-F_{Aout}-Q_{Aout}}{F_{A0}+Q_{A0}} \cdot 100 \qquad (4.24)$$

Therefore, only ammonia that decomposes to hydrogen and nitrogen is counted when determining conversion in the membrane reactor.

When comparing membrane selectivity for gas I over gas J, the following equation is often used:

$$\alpha(I/J) = \frac{\bar{P}_I}{\bar{P}_J} \qquad (4.25)$$

Equation 4.25 is valid when the units for $\bar{P}_I$ and $\bar{P}_J$ are the same. In some cases, the gas permeation mechanism through a membrane may be different for different gas species and the values of n(I) and n(J) in Equation 4.7 may not be equal. Equation 4.25 is not valid in that case. For the preliminary calculations presented in this Chapter, n(J) was assumed to be 1 for each gas species so Equation 4.25 is used to define the membrane selectivity for hydrogen over the other gas species.

Figure 4.2 compares the ammonia conversion calculated for a membrane reactor with Knudsen diffusion selectivity to the equilibrium ammonia conversion of the tube feed gas. Theoretically, a conventional reactor with impermeable walls could only achieve the equilibrium conversion if it were of infinite length. A significant increase in ammonia conversion is obtained in the membrane reactor. However, the conversion in the membrane reactor is limited because some ammonia permeates to the sweep side before it can decompose. The importance of including a reversible rate expression for the kinetic rate equation is shown on the plot. When the ammonia synthesis term is not included in the kinetic equation, the rate of ammonia decomposition is over predicted, especially at higher temperatures. The synthesis term slows down the reaction rate resulting in a lower conversion since more ammonia permeates through the membrane and exits the reactor with the sweep gas.

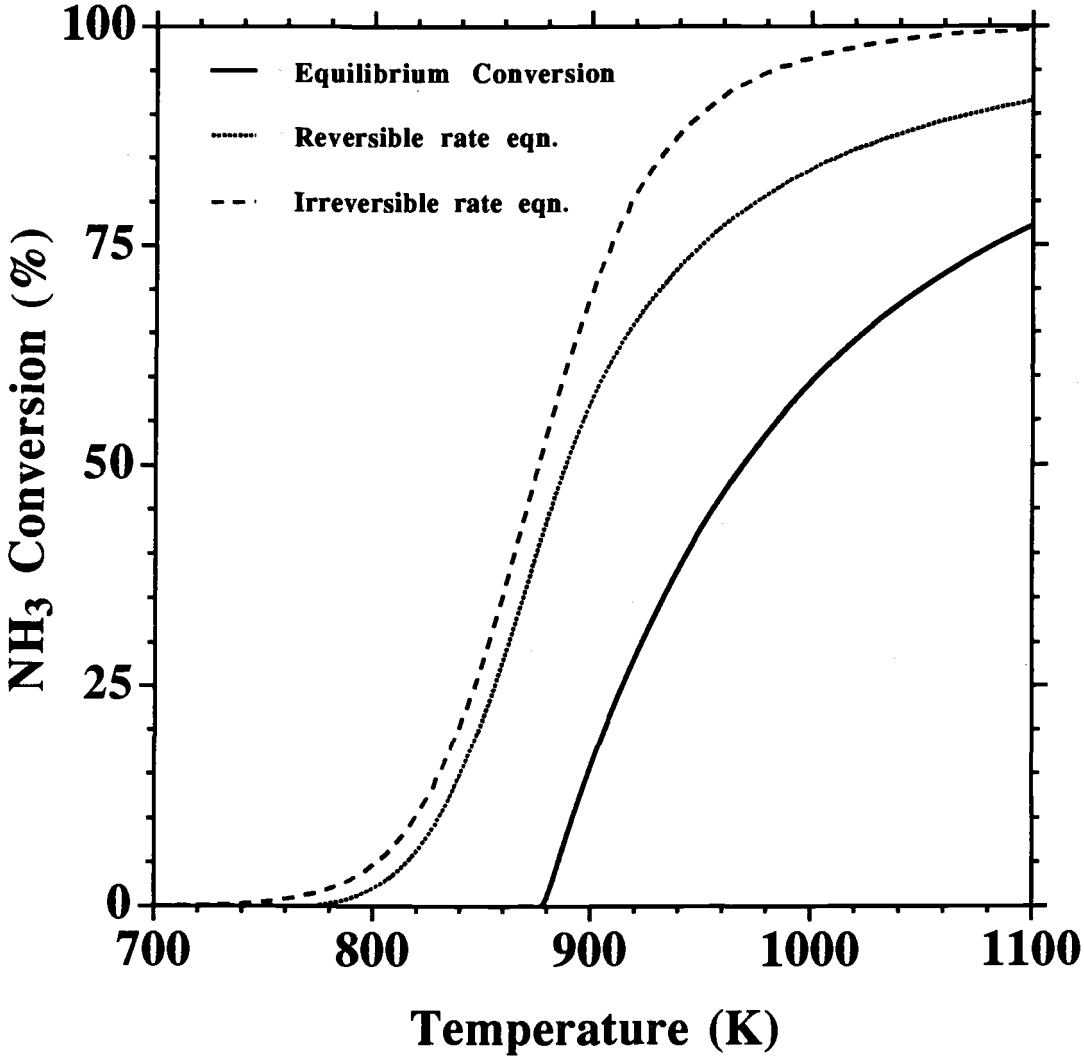

Figure 4.2 The Influence of the Reaction Rate Equation on Predicted Ammonia Conversion for a Cocurrent Process.

Figures 4.3 shows the effect of the sweep to tube side inlet flow rate ratio on ammonia conversion for a countercurrent membrane reactor. Similar results are obtained for a cocurrent reactor. The inlet sweep flow was varied from $3.72 \cdot 10^{-4}$ to $3.72 \cdot 10^{-2}$ mols/s in order to evaluate a range of inlet flow ratios. Ammonia conversion is observed to increase as the sweep flow increases. The driving force for hydrogen permeation is the partial pressure or fugacity difference between the tube and sweep side. With the higher sweep flows, a larger driving force is maintained over the length of the membrane allowing more hydrogen to permeate. Although the ammonia permeation rate is also increased, the rate of decomposition is increased to a greater extent due to the lower hydrogen fugacity.

Figure 4.4 shows the influence of the inlet hydrogen concentration on the ammonia conversion for a countercurrent process. The hydrogen concentration has a large impact on the rate of ammonia decomposition. As expected, ammonia conversion increases as the inlet hydrogen concentration decreases.

The inlet nitrogen concentration does not significantly effect ammonia conversion. This is due to the relatively minor impact of nitrogen on the decomposition rate compared to hydrogen.

The maximum possible conversion is desired in this study since ammonia decomposition is proposed as a pollution reduction technique for NO_x. The modeling results presented above indicate that conversion is limited in a membrane reactor with Knudsen diffusion selectivity. A higher selectivity for hydrogen over the other synthesis gas constituents is desirable to increase the ammonia conversion. Figures 4.5 and 4.6 show the influence of hydrogen selectivity on ammonia conversion for the cocurrent and countercurrent processes. In these graphs, the hydrogen permeability was the same as the Knudsen diffusion permeability, but the permeabilities of ammonia, nitrogen and helium were decreased by a constant defined as the separation factor (SF). The SF values are listed in Table 4.1. Physically, such a decrease in the ammonia, nitrogen, and helium permeabilities could be achieved by depositing a very thin layer (≤ 20 μm) of a hydrogen permeable metal onto the surface of the ceramic membrane. The resulting composite metal-ceramic membrane should have a high hydrogen permeability and be essentially impermeable to other gases. Alternatively, a composite metal membrane could be used. Figures 4.5 and 4.6 merely show the effect of hydrogen selectivity on ammonia conversion. No particular type of membrane is proposed to achieve the higher selectivity although the composite metal-ceramic or composite metal membranes are likely choices. It is recognized that hydrogen

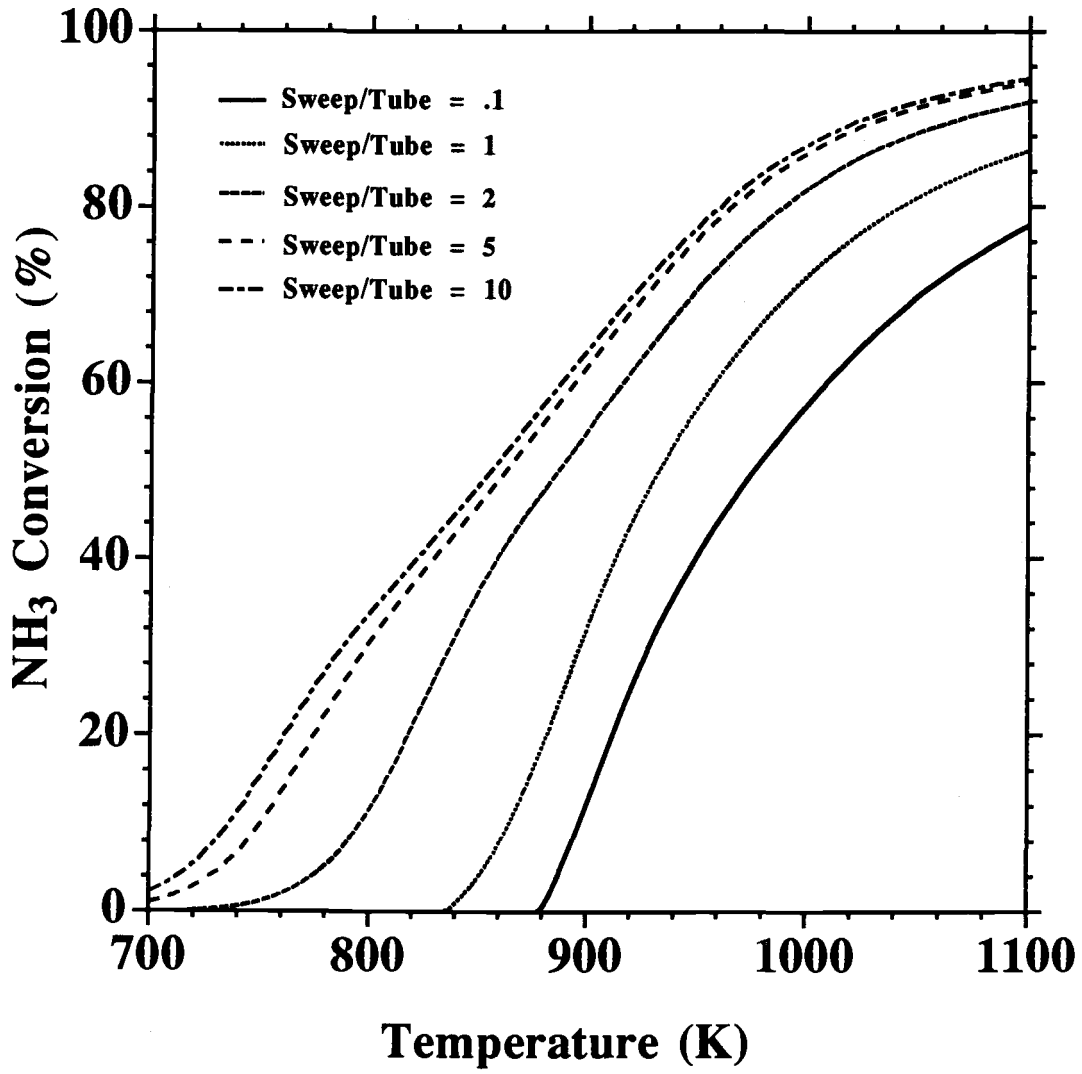

Figure 4.3 The Influence of the Sweep to Tube Flow Rate Ratio on Ammonia Conversion for a Countercurrent Process.

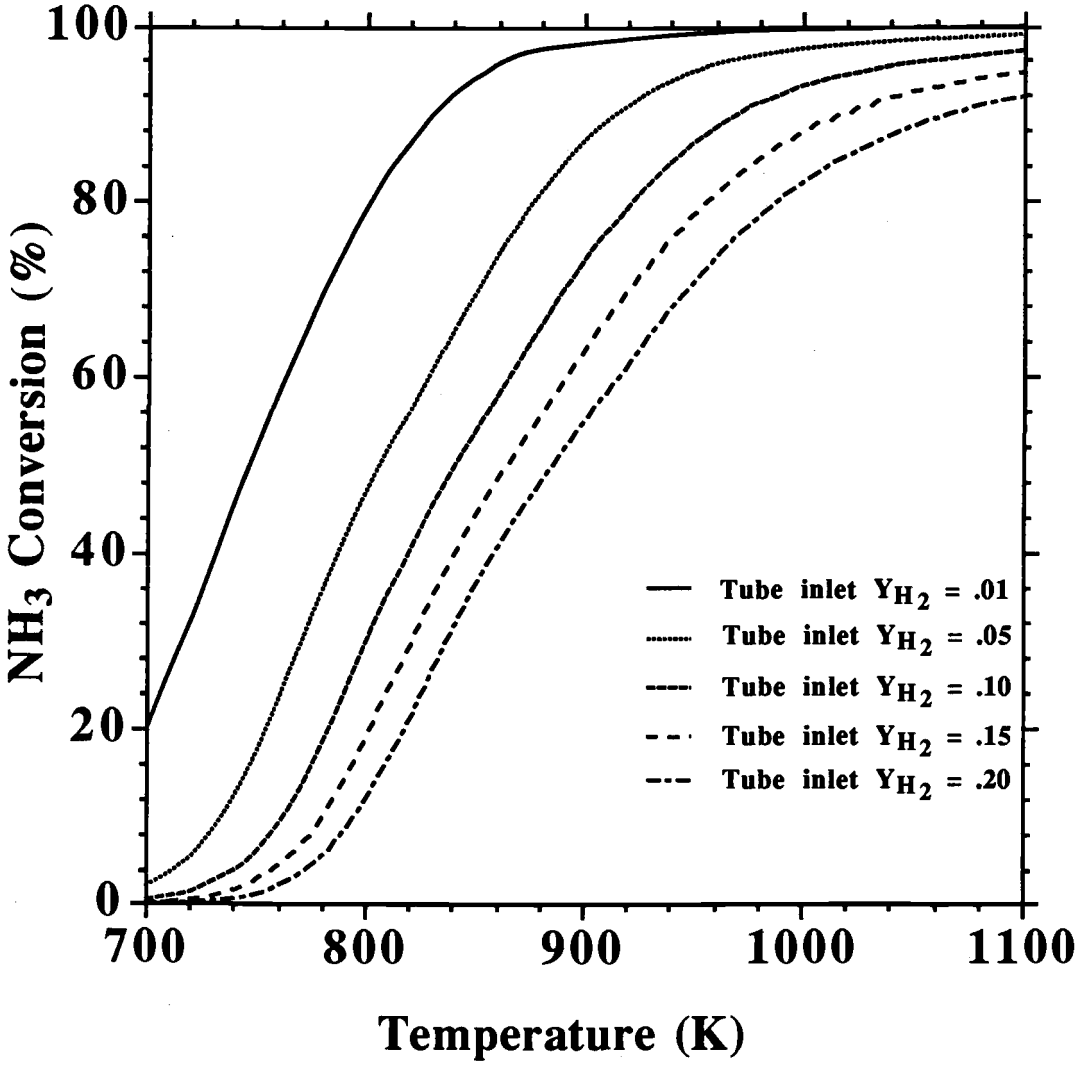

Figure 4.4 The Influence of Inlet Hydrogen Mole Fraction on Ammonia Conversion for a Countercurrent Process.

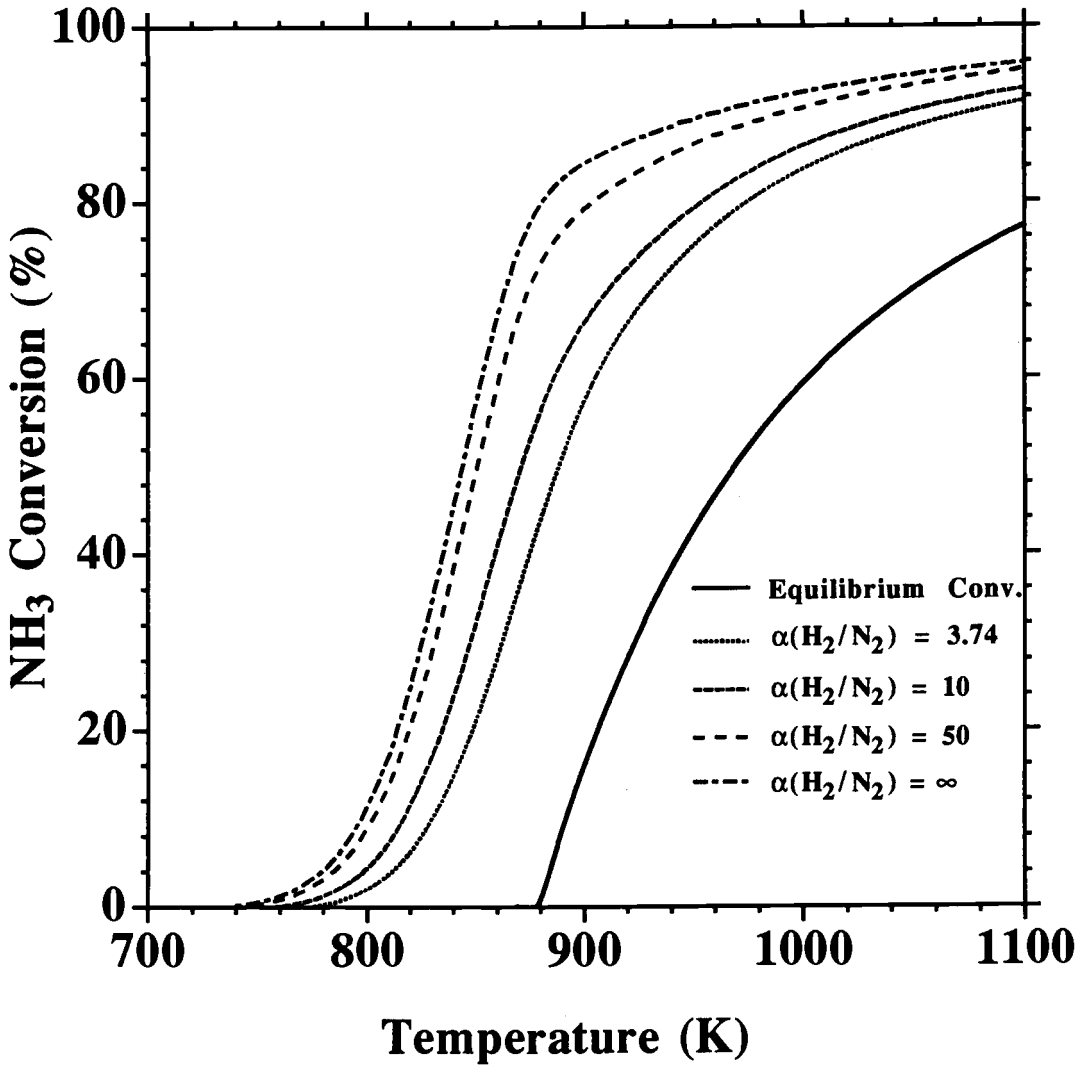

Figure 4.5 The Influence of Selectivity on the Ammonia Conversion for a Cocurrent Process.

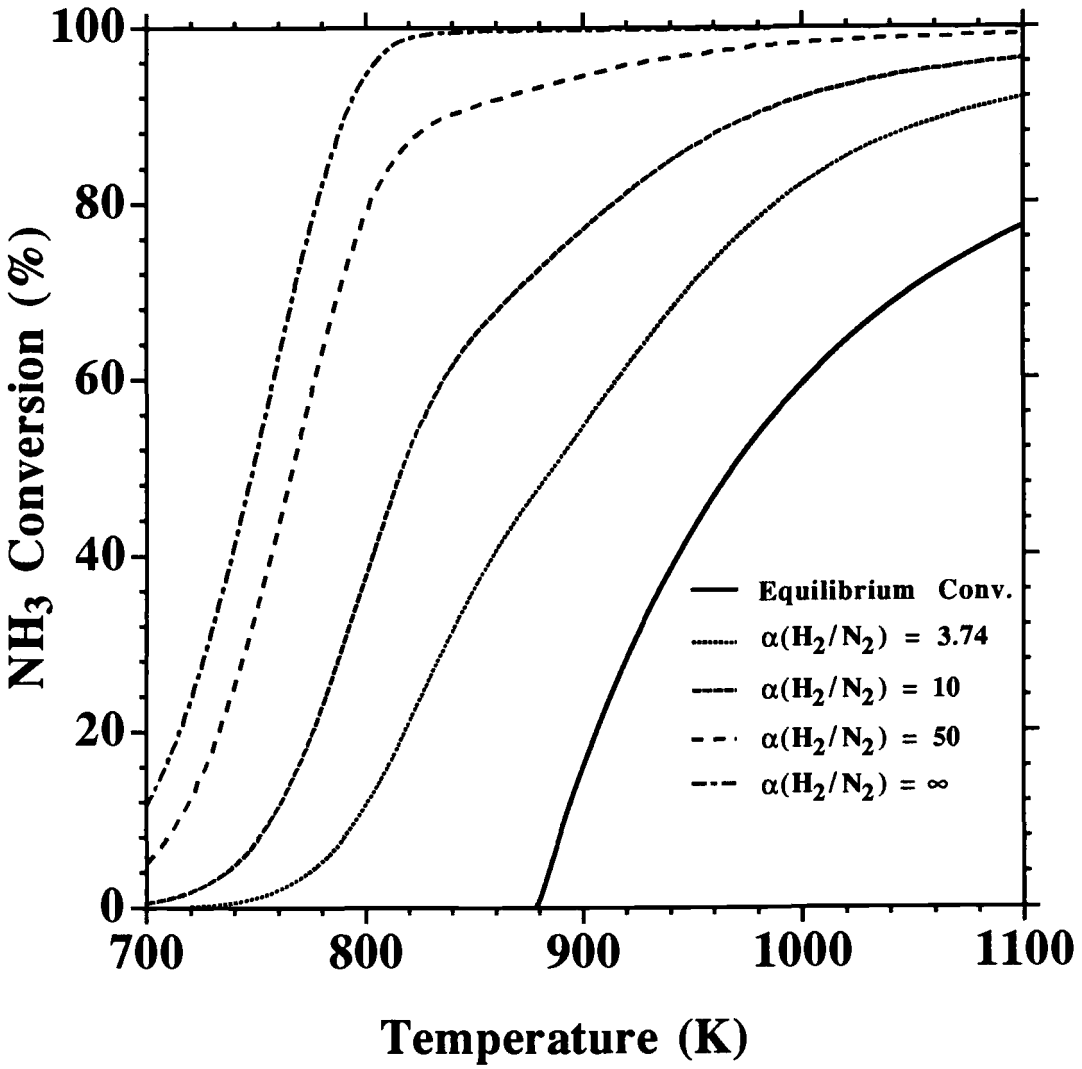

Figure 4.6 The Influence of Selectivity on the Ammonia Conversion for a Countercurrent Process.

permeation through a metal follows a different mechanism than hydrogen permeation through a porous ceramic membrane. Since the objective of the preliminary analysis was to study the effect of hydrogen selectivity rather than design a membrane reactor, no change was made to the Knudsen diffusion permeability estimate for Figures 4.5 and 4.6.

Comparison of Figures 4.5 and 4.6 indicates that the countercurrent process is much more efficient than the cocurrent process when a membrane with increased hydrogen selectivity is operated with a sweep gas stream. The opposing flows of the tube and sweep gas allow more hydrogen to permeate in the countercurrent configuration resulting in a lower hydrogen concentration on the tube side and higher ammonia conversion.

The effect of space time on membrane reactor performance is considered in Figures 4.7 and 4.8. These graphs were generated by varying the tube and sweep side gas flow rates while maintaining a constant inlet sweep to tube flow ratio of 2. Figure 4.7 shows the influence of space time on ammonia conversion for a membrane reactor with Knudsen diffusion selectivity operated at a temperature of 900 K. A limiting conversion is reached at high space times for the cocurrent flow configuration. Further increases in space time have no effect because the component fugacities on the tube and sweep side are equilibrated and the decomposition reaction reaches chemical equilibrium. An optimum space time exists for the countercurrent flow configuration. This optimum countercurrent conversion is significantly lower than the limiting cocurrent conversion.

The additional conversion achieved by cocurrent flow at high space times is due to back permeation of ammonia from the sweep side to the tube side. Near the tube inlet, a significant portion of ammonia permeates to the sweep side before it can decompose due to the large initial fugacity difference. Decomposition of the tube side ammonia decreases the tube side fugacity to a value that is lower than the sweep side fugacity. This allows ammonia to back permeate into the tube gas where additional ammonia decomposition is achieved. Back permeation does not occur in the countercurrent flow configuration because ammonia permeated near the tube inlet immediately flows out of the reactor with the sweep gas. An optimum exists for countercurrent flow because at long space times more ammonia is lost by permeation due to the longer time spent near the tube inlet where the driving force for permeation is highest.

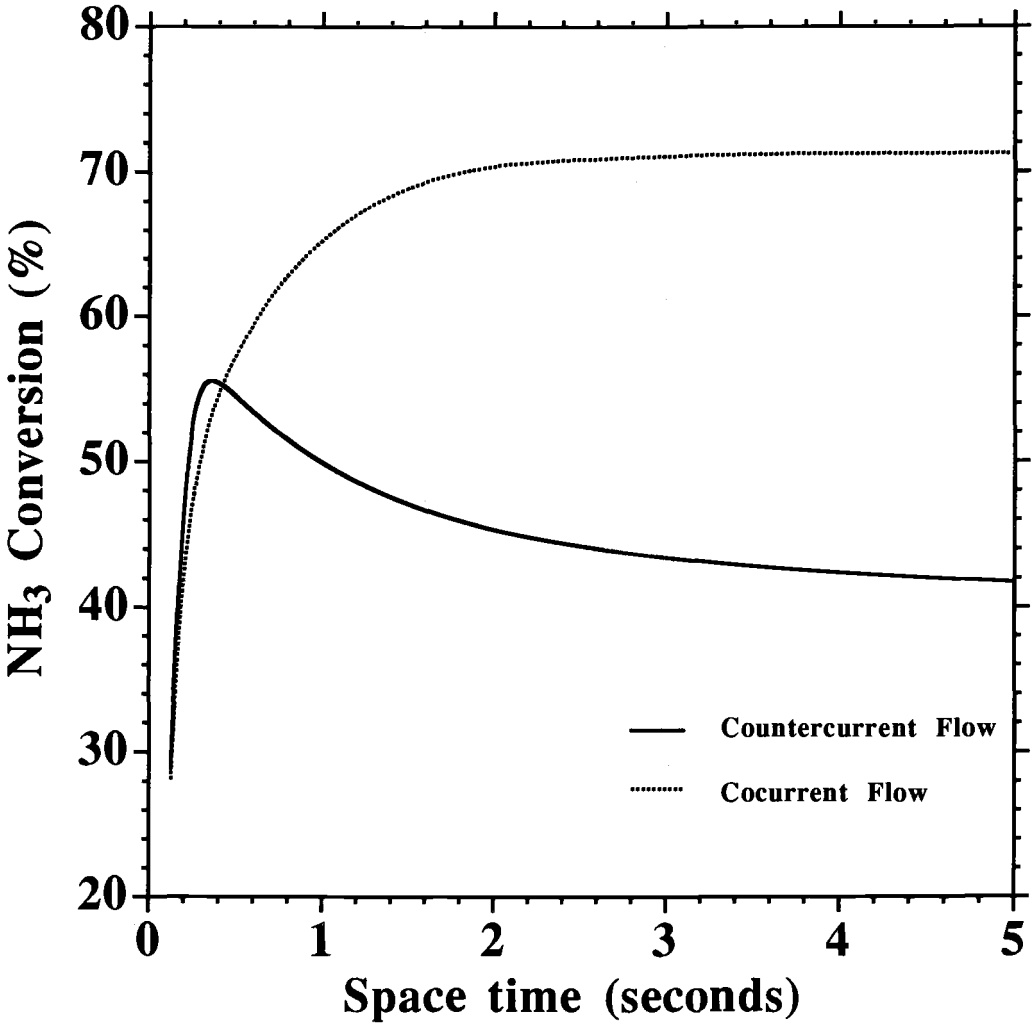

Figure 4.7 Effect of Space Time on Conversion for a Hydrogen Selective Membrane with Knudsen Diffusion Selectivity at 900 K.

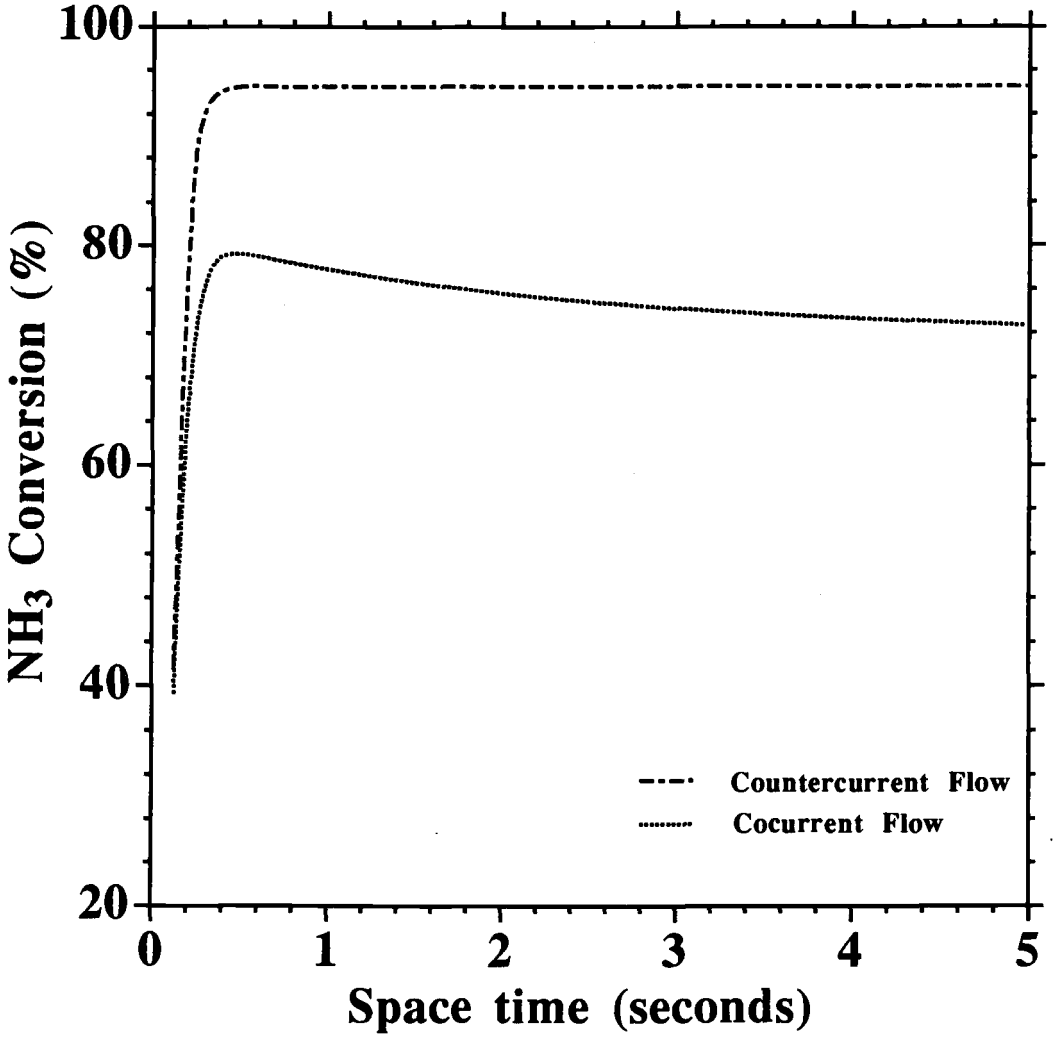

Figure 4.8 Effect of Space Time on Conversion for a Hydrogen Selective Membrane [$\alpha(H_2/N_2) = 50$] at 900 K.

Figure 4.8 shows the influence of space time on ammonia conversion for a more selective membrane reactor ($\alpha(H_2/N_2) = 50$) operated at 900 K. The countercurrent flow configuration is superior for this membrane. The conversion for the countercurrent membrane increases with increasing space time until a limiting value is reached. The limiting conversion is due to ammonia permeation near the tube inlet. There are several reasons why ammonia conversion is lower for the cocurrent configuration. Since the ammonia permeability is relatively low, the sweep side fugacity is never larger than the tube side fugacity so ammonia permeated near the tube inlet cannot back permeate. In addition, less hydrogen is permeated so the equilibrium shift is less, and for long space times, the higher nitrogen fugacity on the tube side shifts chemical equilibrium toward ammonia synthesis near the tube outlet. This is why an optimum space time exists for cocurrent flow.

Figures 4.2 to 4.8 assume there is no difference in total pressure between the tube and sweep side ($P_r = 1$), and a sweep gas is used to maintain the permeation driving force. The dilution of permeated hydrogen by the sweep gas is a potential disadvantage to operating in this manner. Another way to maintain the permeation driving force is to eliminate the need for a sweep gas by operating the sweep side at a lower total pressure than the tube side ($P_r<1$). This type of operation is possible with a composite metal-ceramic membrane or a composite metal membrane. Again no particular type of membrane is proposed for operation at the low P_r values. Therefore, the hydrogen permeability estimate was not changed.

Figure 4.9 shows the effect of P_r on conversion for a countercurrent hydrogen selective membrane reactor ($\alpha(H_2/N_2) = \infty$) operated with a very low inlet sweep gas flow of $7.44 \cdot 10^{-7}$ mols/s. A non zero inlet flow was used to avoid division by zero. The estimated conversions for a cocurrent reactor (not shown) are almost identical to the countercurrent conversions when $P_r < 0.1$. Between a P_r of 0.1 to 0.2 countercurrent is slightly better. Since the hydrogen concentration is constant on the sweep side, there is no advantage to operating the membrane in the countercurrent configuration. At P_r values greater than 0.2, no improvement over the equilibrium conversion of the inlet gas is achieved by the membrane reactor since the sweep side pressure is the same as the partial pressure of hydrogen in the inlet tube gas.

Although the isothermal operation assumption is not valid, the membrane reactor model can also be used to examine the potential of using a membrane reactor to recover hydrogen from relatively pure ammonia. Figure 4.10 compares the predicted ammonia conversion for a membrane reactor to that of a conventional reactor of the same length

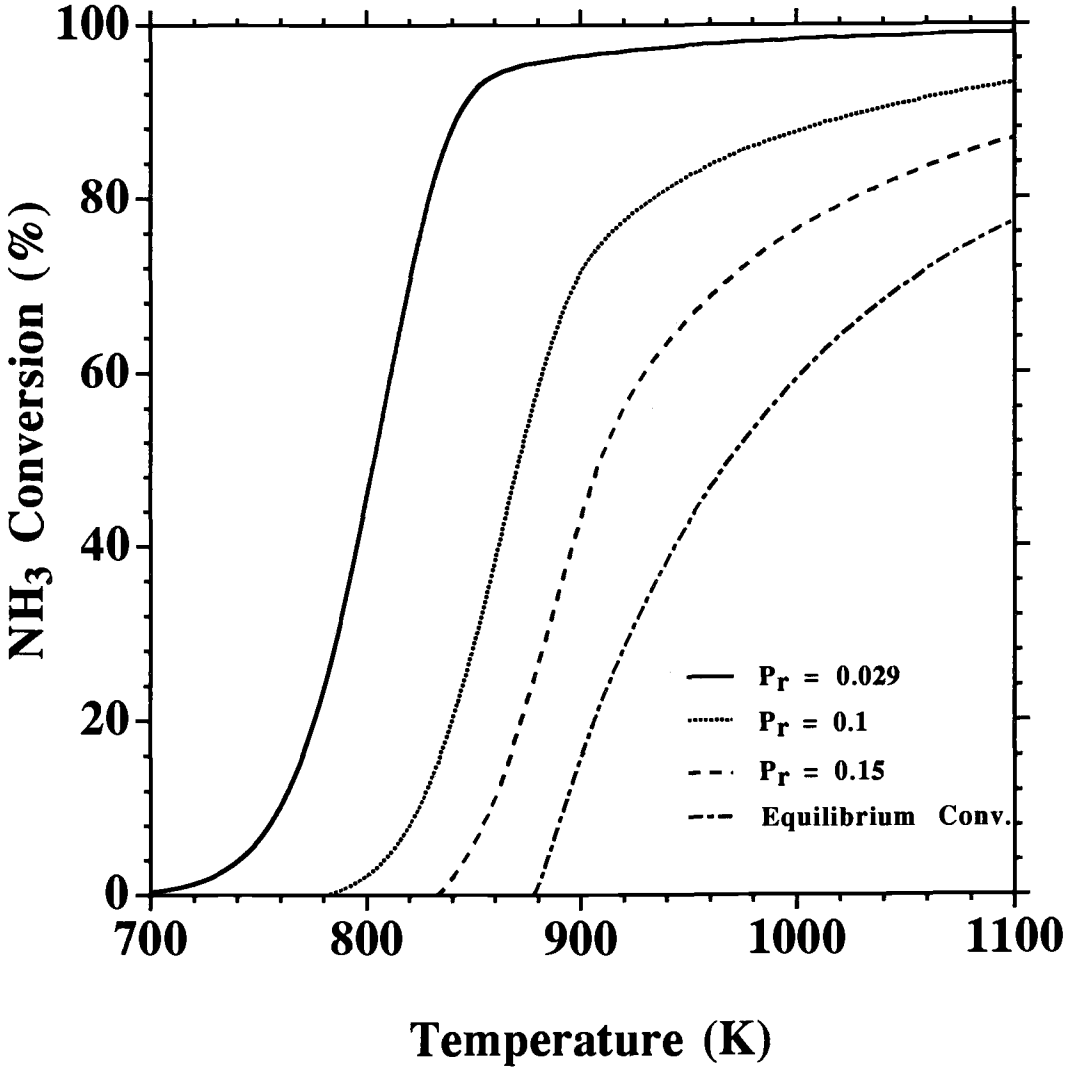

Figure 4.9 The Influence of P_r on Conversion for a Hydrogen Selective Membrane [$\alpha(H_2/N_2) = \infty$] for a Countercurrent Process

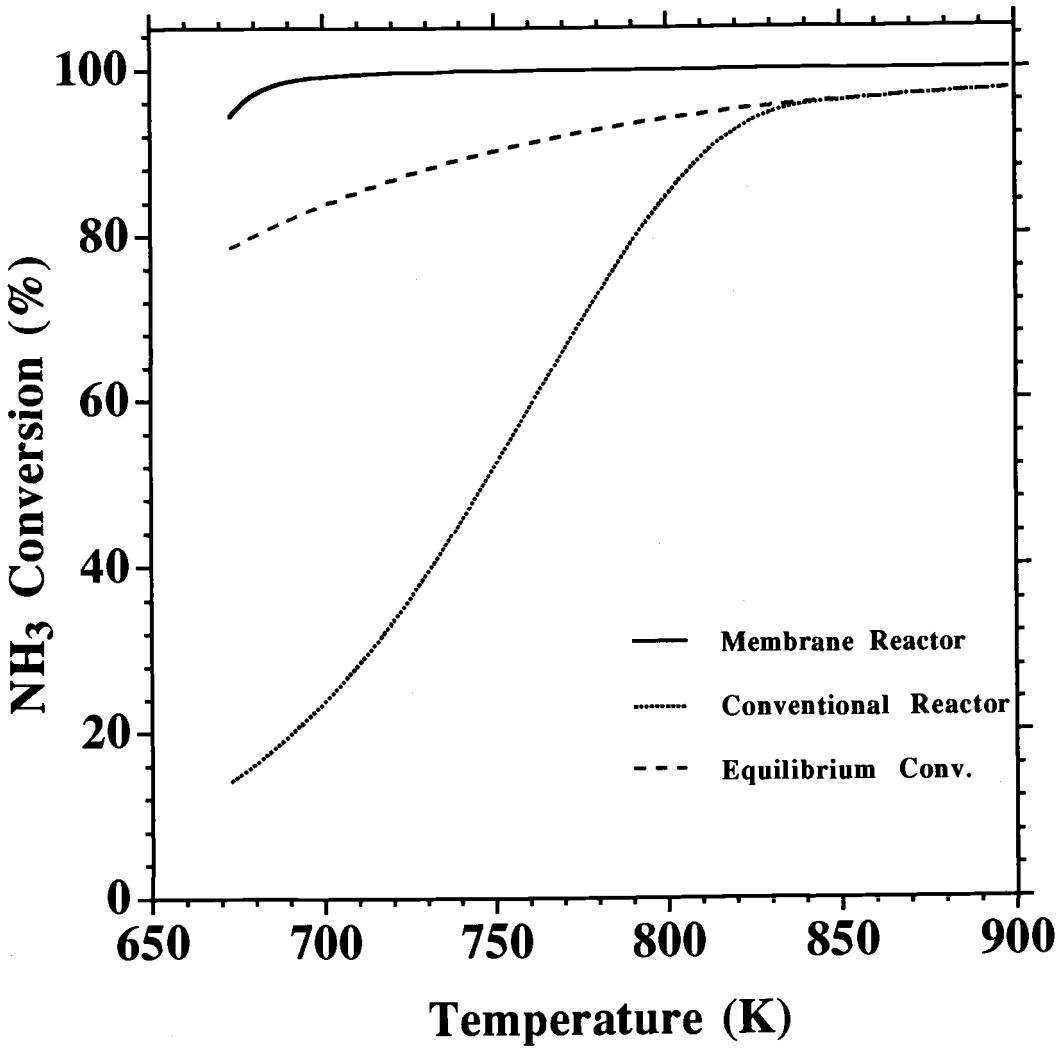

Figure 4.10 Comparison Between Decomposition of 99% Ammonia in a Cocurrent Membrane Reactor Versus a Conventional Reactor of the Same Length

for an inlet gas with 99 mole percent ammonia. The calculations are based on a hydrogen selective membrane reactor ($\alpha(H_2/N_2) = \infty$) with a sweep side at atmospheric pressure and no sweep gas. The inlet ammonia flow is equal to the inlet ammonia flow from Table 4.1 and a Y_{H_2} of 0.01 is included in the gas to avoid numerical instability in the model calculations. Other simulation conditions are the same as those listed in Table 4.1. A significant increase in conversion is achieved in the membrane reactor, especially at low temperatures. This shows that another potential application for membrane reactors is in the efficient use of ammonia as a hydrogen storage material.

The influence of interphase and intraparticle mass transfer on membrane reactor performance is shown in Figure 4.11. Interphase mass transfer resistance is a major concern in this project because ammonia is present in dilute concentrations resulting in a low driving force for mass transfer from the bulk gas to the catalyst surface. As discussed by Satterfield (1980), interphase mass transfer is a potential problem in laboratory reactors where small catalyst particles and low flow rates are often typically used. The small particles reduce intraparticle mass transfer resistance but they also reduce the value of the interphase mass transfer coefficient since Re_p is reduced. The interphase mass transfer coefficient may be so low that interphase resistance becomes more important than intraparticle resistance (Satterfield, 1980). Since interphase mass transfer coefficients associated with low Re_p values are uncertain, a sensitivity analysis was performed by varying the value of C_1 in the equation used to calculate Bi_J (Equation 4.22).

Figure 4.11 presents the results of the sensitivity analysis for a hydrogen selective membrane reactor ($\alpha(H_2/N_2) = \infty$) operated at low P_r ($P_r = 0.03$) with a negligible inlet sweep gas flow. The composition of the inlet gas streams are the same as in Table 4.1, but the flow rates are lower. Additional information regarding the conditions simulated in this figure are presented in Table 4.2. The individual curves in Figure 4.11 were generated using a constant space time. This was done by increasing reactor length as the inlet flow rate increased. Therefore, a constant ammonia conversion would be predicted in the absence of interphase mass transfer resistance. The presence of interphase mass transfer resistance is indicated by an increase in conversion with increasing flow rate or Re_p. This behavior is present to varying degrees in all curves shown in the figure. The influence of C_1 on predicted ammonia conversion is clearly shown. When C_1=0.001, the space time must be over 15 times longer to achieve conversions that are comparable to the predicted conversions for C_1=0.1. This is

Table 4.2
Input Parameters for Figure 4.11

Reactor size (m)	$R_1 = 0.0035$ $t_m = 0.0015$ $L_o = 0.01\text{-}0.75$
Gas flow rate at tube inlet (mol/s)	$F_{TO} = 1.86 \cdot 10^{-4}$ to $9.30 \cdot 10^{-4}$
Gas flow rate at sweep inlet (mol/s)	$Q_{TO} = 1.49 \cdot 10^{-7}$ to $7.4 \cdot 10^{-7}$
Gas composition at tube inlet (mol %)	
ammonia	0.3
nitrogen	48
hydrogen	20
helium	balance
Gas composition at sweep inlet (mol %)	
helium	100
Reactor pressures	$P_t = 3446$ kPa $P_r = 0.03$
Reactor temperature	900 K
Catalyst parameters	$\rho_p = 510$ kg/m^3 $S_g = 190000$ m^2/kg $\tau_p = 4$ $\theta = 0.5$ $\varepsilon = 0.4$ $R_p = 0.0005$ m

Note: Kinetic parameters are the same as those in Table 4.1. Permeabilities calculated using the equations listed in Table 4.1 with SF=10000.

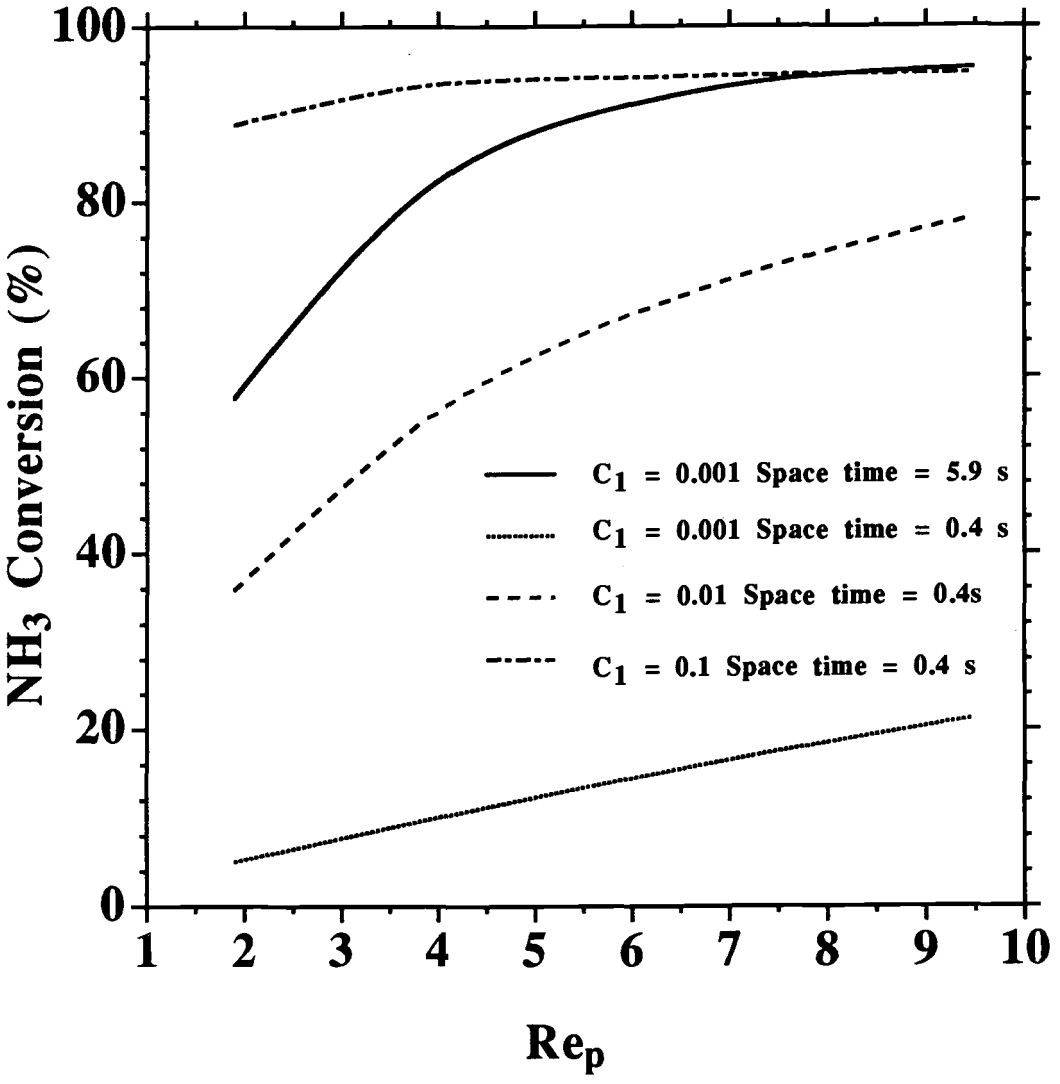

Figure 4.11 Effect of Particle Reynolds Number (Re_p) on the Ammonia Conversion for a Hydrogen Selective Membrane [$\alpha(H_2/N_2) = \infty$] at 900 K.

because the η values for $C_1 = 0.001$ are very low ranging from 0.065-0.24 at the tube inlet down to 0.0017-0.008 at the tube outlet.

Industrial reactors use larger catalyst particles and higher flow rates than laboratory reactors. This reduces interphase mass transfer resistance but increases intraparticle resistance. A sensitivity study was performed to determine the impact of catalyst particle size on ammonia conversion at high Re_p values. A hydrogen selective membrane reactor ($\alpha(H_2/N_2) = \infty$) operated at 900 K and low P_r ($P_r = 0.03$) with a negligible inlet sweep gas flow was simulated. Equation 4.23 was used to estimate Bi_J. The particle size (R_p) was varied between 0.001 and 0.0047 m, and tube side Re_p values ranged from about 4 to 175. Mass transfer resistance had little impact on ammonia conversion for most of the simulated conditions even though η values were significantly less than 1. Conversion was reduced by about 3% compared to conversion calculated with η=1 in a reactor with large particles (0.0047 m) operated at a low flow rate (Re_p=17.5). In this case, η ranged from 0.227 at the tube inlet down to 0.04 at the outlet. Figure 4.12 shows why the low η values had only a minor impact on conversion. When η is not included in the model, a relatively high ammonia decomposition rate is predicted near the tube inlet and the decomposition reaction reaches chemical equilibrium at around $L/L_0 = 0.5$. In the second half of the reactor, the ammonia decomposition rate is controlled by the hydrogen permeation rate which is also relatively low because the hydrogen fugacities on the tube and sweep sides are nearly equilibrated. A more gradual change in the ammonia concentration is predicted when η is included in the model and the decomposition reaction does not approach chemical equilibrium until the tube outlet.

CONCLUSIONS

A mathematical model was used in a preliminary analysis to evaluate the effectiveness of a high temperature membrane reactor for ammonia decomposition in coal derived synthetic gas. Results of this analysis indicate that ammonia conversions greater than the equilibrium conversion of the inlet gas stream are obtainable in a ceramic membrane with Knudsen diffusion selectivity. The cocurrent flow configuration is generally as good or better than the countercurrent configuration for Knudsen diffusion selectivity. This is attributable to a higher initial reaction rate near the tube inlet and decomposition of back permeated ammonia near the tube outlet. The ammonia conversion in a membrane reactor with Knudsen diffusion selectivity is

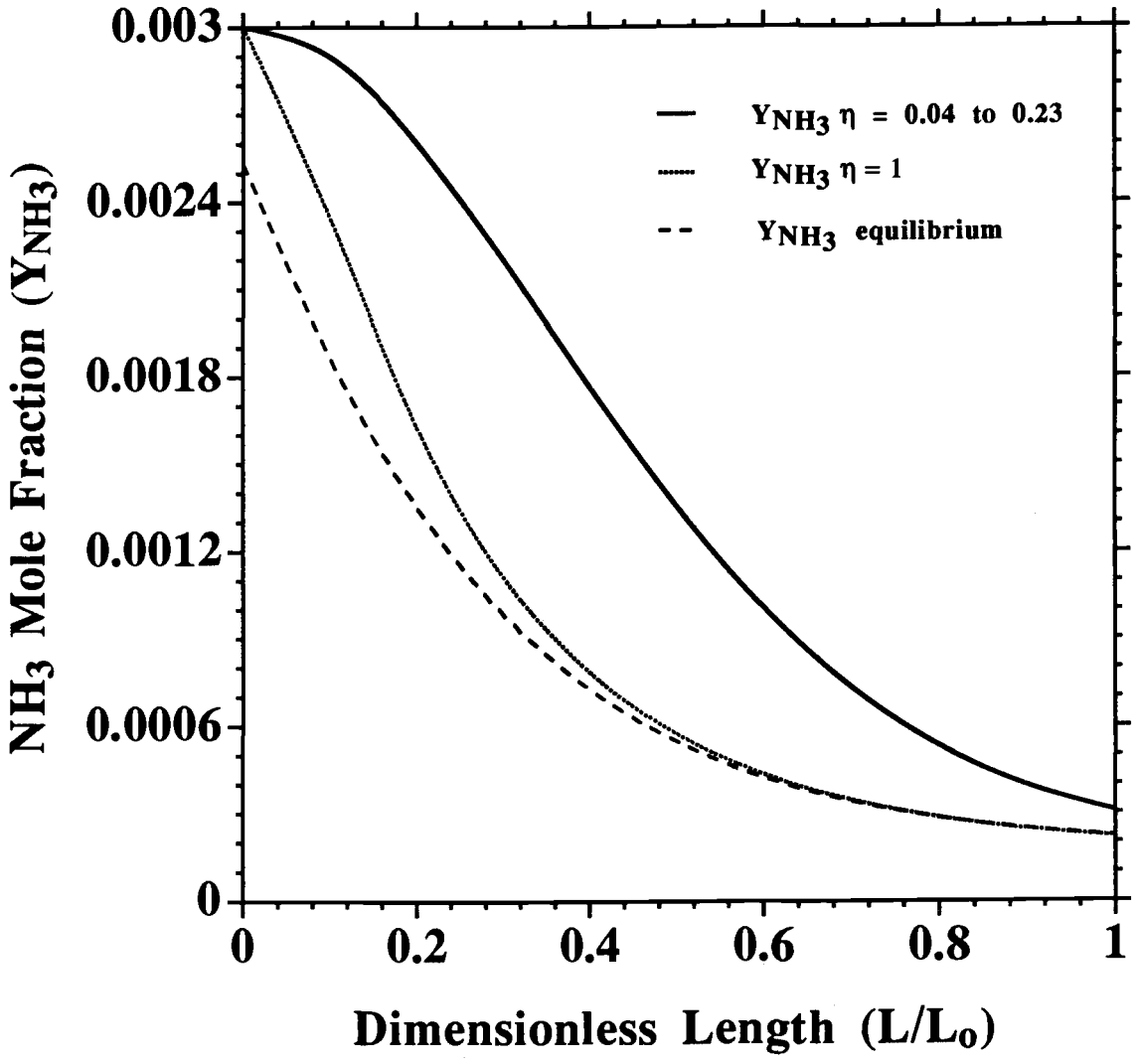

Figure 4.12 Ammonia Mole Fraction Profiles in a Hydrogen Selective Membrane [$\alpha(H_2/N_2) = \infty$] for Large Particles (R_p = 0.0047 m) and Low Inlet Particle Reynolds Number (Re_p = 17.5) at 900 K.

limited due to loss of ammonia to the permeate gas stream. Since the maximum possible conversion is needed for this application, membranes that are more selective for hydrogen are desirable. The more effective flow configuration for membranes with higher hydrogen selectivity depends on the sweep gas flow rate and operating pressure ratio (P_r). The countercurrent flow configuration is better when P_r is 1 and a sweep gas is used. When no sweep gas is used and P_r is low, ammonia conversion is essentially equal for the two flow configurations. To achieve a high ammonia conversion and recover high purity hydrogen on the sweep side, a membrane with a hydrogen selectivity of greater than 50 should be used that is capable of operating with a large transmembrane pressure difference between the tube and sweep side. An additional potential membrane reactor application is in the efficient recovery of hydrogen from pure ammonia. A significantly smaller reactor size and lower operating temperature could be used if a membrane reactor were used for this application in place of a conventional reactor with impermeable walls.

Interphase and intraparticle mass transfer resistance can influence membrane reactor performance when one or more reactants are present in dilute concentrations. Interphase mass transfer resistance may significantly lower conversion in reactors operated at low flow rates with small catalyst particles. Since these conditions are typical of laboratory reactors, the influence of interphase mass transfer resistance should be included in membrane reactor models.

CHAPTER V
PREPARATION AND CHARACTERIZATION OF A COMPOSITE PALLADIUM-CERAMIC MEMBRANE

INTRODUCTION

A composite palladium-ceramic membrane was developed in this project. The composite membrane consists of a palladium film with a thickness of 20 μm or less deposited on the inside surface of an asymmetric tubular ceramic membrane. Figure 5.1 shows a cross-sectional view of the membrane. The palladium film is deposited on the inside surface of the tubular ceramic membrane since the selective membrane layer resides on the inside surface. Whenever the pore diameter of the ceramic membrane is mentioned, I am referring to the pore diameter of the top layer (selective layer). In theory, a composite palladium-ceramic membrane has all of the desirable membrane characteristics previously discussed. However, the resistance of the palladium film to hydrogen sulfide poisoning requires further investigation. An infinite hydrogen selectivity is possible if a defect free palladium film is deposited on the ceramic membrane surface. The combination of a thin metal film and an asymmetric microporous ceramic membrane support results in a membrane that is highly permeable to hydrogen. Microporous ceramic membranes are used for supports instead of the microporous glass membranes used by Uemiya (Uemiya et al., 1988) because of their superior thermal and mechanical properties. This allows for operation at higher temperatures and transmembrane pressure differences. The asymmetric ceramic membranes are also more permeable than microporous glass membranes which have the same pore diameter across the thickness of the membrane. Intermetallic diffusion at high temperatures is not a concern since the metal film is deposited on a ceramic surface. In addition, the microporous ceramic support is more permeable than hydrogen permeable base metals used in composite metal membranes. The tubular membrane design is amenable to scale-up to an industrial size process.

Future research is needed to determine acceptable hydrogen sulfide levels for palladium films at synthesis gas conditions and to determine whether alloying palladium with another metal such as gold or platinum can improve hydrogen sulfide resistance while maintaining a reasonable permeability. Although platinum has shown remarkable resistance to hydrogen sulfide attack at extreme concentrations levels and temperatures (Edlund, 1992), the extremely low hydrogen permeability of platinum makes a

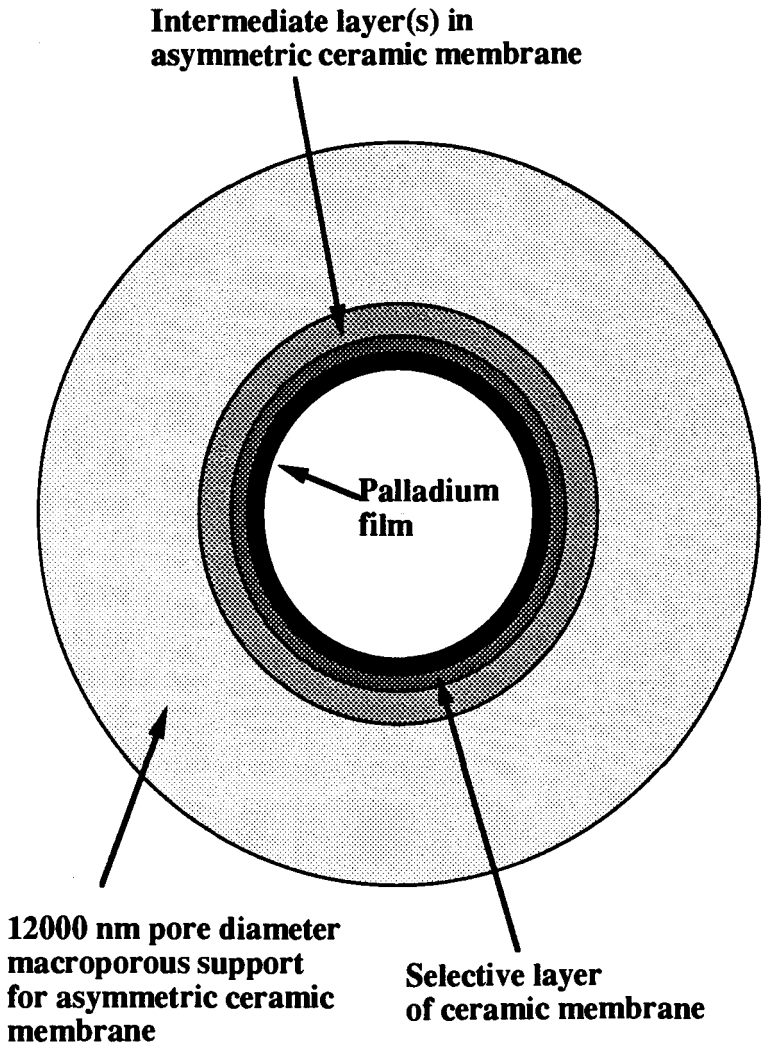

Figure 5.1 Cross-section of Composite Palladium-Ceramic Membrane.

composite platinum-ceramic membrane infeasible for this project. The hydrogen permeability of platinum is over two orders of magnitude lower than palladium. Goltsov (1975) claimed that adding steam to gaseous mixtures eliminated poisoning of palladium and palladium alloy surfaces by hydrogen sulfide. Synthesis gas at IGCC plants already contains steam. Long term membrane durability experiments are needed at temperatures, pressures, steam concentrations, and hydrogen sulfide concentrations typical of synthesis gas conditions to fully address the hydrogen sulfide poisoning issue.

Potential methods for depositing the palladium film include electroless plating and sputtering. The electroless plating method was used for several reasons. Electroless plating does not require a large investment in equipment and materials. All that is needed are some chemicals, glassware, a temperature controlled water bath, and a fume hood. In addition, deposition on the inside surface of tubes is possible with electroless plating. Facilities for sputtering on the inside surface of a tubes were not available at Oregon State University.

The objective of this phase of the project was to make composite palladium-ceramic membranes with high hydrogen selectivities and permeabilities, and to demonstrate that these membranes can operate at high temperatures and transmembrane pressure differences. Permeability experiments with hydrogen, nitrogen, and helium at high temperatures and transmembrane pressure differences were conducted to characterize the membranes. Results of these membrane characterization experiments were used to determine gas permeabilities and hydrogen selectivities. The gas permeabilities were needed to estimate permeation rates in the membrane reactor model. The hydrogen selectivities were needed to evaluate the effectiveness of membrane preparation and sealing procedures.

THEORY

Background information on electroless palladium plating and gas permeation through composite metal-ceramic membranes is presented below.

Electroless Plating Background

The purpose of this discussion is to provide general background information regarding electroless plating of palladium. A general equation for the plating reaction is as follows Rhoda (1959):

$$(\text{Pd complex})^{++} + \underset{\text{agent}}{\text{reducing}} \xrightarrow[\text{surface}]{\text{catalytic}} Pd^0 \text{ (sound and adherent metal)} \qquad (5.1)$$

The two most common reducing agents are hydrazine and sodium hypophosphite. A pure palladium film is deposited when hydrazine is used (Rhoda, 1959). An alloy containing about 2 % phosphorous is deposited when sodium hypophosphite is used (Athavale and Totlani, 1989). Plating bath formulations consist of a palladium-ammine complex in the form of $Pd(NH_3)_4Cl_2$, a stabilizer, and the reducing agent. The purpose of the stabilizer is to minimize the tendency of the bath to decompose (precipitate palladium from solution). The disodium salt of ethylenediaminetetraacetic acid (disodium EDTA) is used as a stabilizer in the hydrazine bath and ammonium chloride stabilizes the sodium hypophosphite bath.

The following reaction is believed to occur when hydrazine is used as the reducing agent (Rhoda, 1959):

$$2Pd(NH_3)_4^{++} + N_2H_4 + 4OH^- \xrightarrow[\text{surface}]{\text{catalytic}} 2Pd^0 + 8NH_3 + N_2 + 4H_2O \qquad (5.2)$$

Nitrogen produced from the plating reaction helps to agitate the bath. Hydrogen is produced when sodium hypophosphite is used as the reducing agent (Athavale and Totlani, 1989).

A catalytic surface is required to initiate the plating reaction. Since ceramic surfaces do not catalyze the reaction, a surface activation step is needed when ceramic substrates are plated. The purpose of the activation step is to seed the ceramic surface with finely divided palladium nuclei which initiate the plating reaction. A common activation procedure consists of a two-step immersion sequence of an acidic stannous chloride solution followed by an acidic palladium chloride solution (Feldstein and Weiner, 1972). The stannous chloride solution is called the sensitizing bath while the palladium chloride solution is called the activation bath. The formation of palladium nuclei is believed to result from a redox reaction taking place between adsorbed Sn^{2+}

ions on the substrate surface and Pd^{2+} ions in the activation solution (Feldstein and Weiner, 1972). The sensitizing bath is the key step. Cohen and West (1972) proposed that a colloidal formation of stannic ion with stannous ions bound onto this colloid is responsible for the sensitizing process.

Gas Permeation in Composite-Metal Microporous Membranes

Hydrogen permeation through composite metal-microporous membranes is discussed below. Theoretically, membranes with an infinite hydrogen selectivity are possible if a defect free palladium film is deposited on the ceramic membrane surface. In practice, imperfections such as tiny leaks in the high temperature seals and defects in the palladium film reduced the measured membrane selectivities. Therefore, permeation of gases through seal leaks or membrane defects is also addressed.

Hydrogen must permeate through both the palladium metal film and the ceramic membrane support. The asymmetric structure of the ceramic membrane support results in a very high hydrogen permeability. Hydrogen permeation rates for an asymmetric ceramic membrane with a 4 nm pore diameter were estimated using permeability data reported by Wu and coworkers (Wu et al., 1993). The estimated permeation rates at transmembrane pressure differences from 100 to 2000 kPa are 23 to 44 times higher than permeation rates measured for the composite-palladium ceramic membranes developed in this study. Pore diameters on the ceramic membrane supports are 10 to 200 nm so these membranes are even more permeable than the 4 nm membranes used by Wu and coworkers. Therefore, the mass transfer resistance of the ceramic support is assumed to be minimal. The following discussion assumes that hydrogen permeation through the palladium film is the rate limiting step in permeation of hydrogen through a composite palladium-ceramic membrane.

Hydrogen permeates through metals by a multistep process, which involves the following steps (Shu et al.,1991):

1) reversible dissociative chemisorption of molecular hydrogen on the membrane surface;
2) reversible dissolution of surface atomic hydrogen in the bulk layers of the metal;
3) diffusion of atomic hydrogen through the bulk metal.

Steps 1 and 2 take place on both surfaces of the metal. The equation for the hydrogen permeation rate (hydrogen flux) is written in terms of Fick's first law as follows (Lewis, 1967; Uemiya et al., 1991a):

$$J_H = \frac{\bar{P}_H}{t_m}\left(P_{Ht}^{n(H)} - P_{Hs}^{n(H)} \right) \qquad (5.3)$$

Equation 5.3 is essentially the same as Equation 4.7 except that the fugacity coefficient is eliminated since it is essentially 1.0 at the pressures and temperatures evaluated in the permeability experiments.

When diffusion through the bulk metal is the rate limiting step and hydrogen atoms form an ideal solution in the metal (Sievert's law hydrogen solubility dependence), n(H) is equal to 0.5 (Hurlbert and Konency, 1961). A value of n(H) greater than 0.5 may result when surface processes influence the permeation rate or when Sievert's law is not followed. Dependence of the hydrogen diffusion coefficient on the concentration of dissolved hydrogen has also been proposed as the reason for n(H) values greater than 0.5 (Uemiya et al., 1991a). Leakage of hydrogen through defects in the metal film or membrane seals would also increase the value of n(H). Hydrogen permeation experiments conducted with palladium have yielded n(H) values of 0.68 (Hurlbert and Konecny, 1961), 0.76 (Uemiya et al., 1991a), and 0.8 (DeRosset, 1960). These experiments were conducted at temperatures ranging from 616 K to 727 K, and hydrogen feed pressures ranging from 101 to 4926 kPa.

The hydrogen permeability ($\bar{P}_H$) depends on temperature in the following manner (Barrer, 1941):

$$\bar{P}_H = \bar{P}_{HO} \exp\left(\frac{-E}{RT}\right) \qquad (5.4)$$

This equation assumes the value of n(H) in Equation 5.3 does not vary with temperature. In fact, n(H) may also depend on temperature since it is influenced by solubility and the relative rates of surface processes and bulk diffusion, which all depend on temperature.

Equation 5.3 is empirical because surface effects, non ideal solution behavior, hydrogen leakage through defects, or diffusion coefficient concentration dependence

are all accounted for by two terms, n(H) and $\bar{P}_H$. No hydrogen solubility data for the temperature and pressure range of interest in this study were found. Therefore, it is not possible to write a more explicit relationship for the hydrogen solubility in Equation 5.3. Some information regarding the rate determining step may be obtained by comparing the hydrogen permeation rates (J_H) for different palladium film thicknesses (t_m). Reducing the film thickness should increase the impact of surface processes on the hydrogen permeation rates. Therefore, the hydrogen permeability ($\bar{P}_H$) should decrease when the palladium film thickness is reduced beyond a certain value and n(H) should increase.

Experimental data are needed to determine the values of $\bar{P}_H$ and n(H) for a membrane at a particular temperature. The data are collected by measuring the hydrogen permeation rate as a function of P_{Ht} and P_{Hs}. The values of $\bar{P}_H$ and n(H) may be obtained by nonlinear regression analysis of the collected permeation data. Pure hydrogen should be used on both the membrane and permeate side to eliminate gas film mass transfer resistance. A convenient method is to vary P_{Ht} while holding P_{Hs} at atmospheric pressure. The values of $\bar{P}_{HO}$ and E (apparent activation energy) are obtained by conducting the permeation experiments over a range of temperatures. Nonlinear regression analysis on the combined data for all temperatures is performed to determine $\bar{P}_{HO}$, E, and an average n(H) value for the temperature range. The values of $\bar{P}_{HO}$, E, and the average n(H) are needed to perform membrane reactor modeling calculations at temperatures where permeability experiments were not conducted.

It is desirable to quantify leak rates through membrane seals or palladium film defects to include the effect of nitrogen, helium, and ammonia leakage in the membrane reactor model. The following empirical equation was chosen to correlate the permeation rate of a gas through a seal leak or membrane defect at high transmembrane pressure differences:

$$J_J = \frac{\bar{P}_J}{t_m}\left(P_t^{n(J)} - P_s^{n(J)}\right) Y_{JG_t} \qquad (5.5)$$

When n(J) is 2 for all gases, Equation 5.5 has the same form as equations for compressible viscous flow of an isothermal ideal gas through porous media or a capillary tube (Bird et al., 1960). Values of n(J) between 1 and 2 indicate that separative flow is occurring through the leaks and both Knudsen diffusion and viscous flow impact the measured permeabilities. Permeabilities would increase with

decreasing molecular weight in this situation. Therefore, helium would have a higher permeability than nitrogen or ammonia. Since the actual length of a seal leak is not known, t_m is used in Equation 5.5 to maintain consistency with Equation 5.3. In addition, the active area for hydrogen permeation is also used to calculate the permeabilities of the other gases since the active area for leaks is not known.

Parameters in Equation 5.5 are determined in the same manner as those in Equation 5.3. Pure nitrogen or helium is flowed through the membrane at various different pressures. A sweep gas may or may not be used on the shell side which is maintained at atmospheric pressure. Nonlinear regression is used to evaluate $\bar{P}_J$ and n(J) for the gas. Although temperature influences the leak rates, no attempt was made to correlate the nitrogen and helium permeation data with an equation similar to Equation 5.4 since leak rates were generally measured at only two temperatures.

EXPERIMENTAL

Experiments are divided into two parts: membrane preparation and membrane characterization by means of permeability studies and scanning electron microscopy (SEM).

Membrane Preparation

The ceramic membrane supports were Membralox® T-170 alumina membranes obtained from U.S. Filter Corporation in Warrendale, Pennsylvania. The alumina membranes consist of a macroporous support tube with an inner surface covered by a thin multiple layer microporous membrane. Membranes with selective layer pore diameters of 10 to 200 nm were used in the study. The inside and outside diameters of the membrane tubes were 0.7 and 1 cm, respectively.

Preparation of the composite palladium-ceramic membranes involved three steps:

- Membrane pretreatment
- Membrane activation
- Electroless plating

Procedures used to make the membrane are discussed in detail below. These procedures were developed by pooling together information from previous studies regarding surface cleaning, surface activation, and electroless plating, with a few additional innovations.

Membrane Pretreatment

Ceramic membrane tubes bought in lengths of 25 and 75 cm were first cut to the desired length of 6 cm using a diamond saw. The 6 cm length was convenient for both the electroless plating operation and permeation experiments. The outside diameter (OD) was reduced by gentle sanding so the membrane would fit into the 1 cm compression fittings used for gas sealing in the permeation experiments. The sanding operation was performed with a drill press to uniformly reduce the outside diameter of the ceramic membrane tube. The 1 cm OD tube was secured in a 1 cm to 0.635 cm Swagelok® reducing union using nylon ferrules. Finger tightening was used to avoid cutting the tube with the nylon ferrules. A 0.635 cm OD stainless steel tube was attached to the other end of the reducing union. The stainless steel tube was then put in the drill chuck. The drill was set to a low speed and the outside diameter of the tube was gently sanded until the OD was about 0.97 to 0.98 cm. After one end was sanded to the desired OD, the sanding procedure was repeated on the other end.

Following sanding, tubes were cleaned by ultrasonic rinsing in an alkaline solution, deionized water, and isopropyl alcohol to remove sanding grit and any contaminants present from the membrane fabrication process. Membrane cleaning was needed to obtain an adherent palladium film even when the sanding step was omitted. The cleaning procedure is summarized in Table 5.1. This procedure is based on a ceramics cleaning procedure discussed by Sasaki (1991). Membranes were handled with rubber gloves after cleaning to avoid contamination.

A high temperature sealant , Aremco 617 (Aremco Products, Inc., Ossining, New York) was used to seal the ends of the membrane after cleaning. These end seals were needed to prevent bypassing of gas through the porous support at the membrane inlet and outlet. The sealant was applied 0.25 to 1.0 cm from the ends on the inside of the tube, around the outer rims, and 1.5 cm from the ends on the outside of the tube using a fine paint brush. The curing schedule was as follows:

- Cure at room temperature for 1 hour
- Heat to 1053 K at a 6 K/minute ramp rate
- Hold oven at 1053 K for 15 minutes
- Allow oven to cool naturally back to around 373 K

Each membrane had two to three coats of sealant applied and went through two to three curing cycles. After the final curing cycle, the length of sealant applied to the inside

Table 5.1
Membrane Cleaning Procedure

Description	Recipe
Membrane cleaning procedure	• ultrasonic rinse in deionized H_2O for five minutes • ultrasonic rinse in alkaline cleaning solution for five minutes • rinse with cold deionized H_2O for one minute • soak in 25 wt. % acetic acid for five minutes • ultrasonic rinse in cold deionized H_2O for three minutes • ultrasonic rinse in 333 K deionized H_2O for one minute • rinse in 333 K deionized H_2O for one minute • ultrasonic rinse in isopropyl alcohol for five minutes
alkaline cleaning solution	• dissolve 0.25 g Alconox detergent in 250 ml of 323 K deionized H_2O • add 10 ml of NH_4OH (28 weight % NH_3) • add 250 ml of cold deionized H_2O

tube was measured using a ruler. The inside length covered with sealant was subtracted from the total membrane length to determine the active area of the membrane.

Membrane Activation

It was essential to properly activate the ceramic membrane surface prior to plating. Defects in the palladium film usually occurred when the membrane surface was not uniformly activated prior to electroless plating. Palladium adhesion was also a problem when the surface was not properly activated.

The sensitizing bath formulation was based on the recipe developed by Feldstein and Weiner (1972). This recipe is shown in Table 5.2. The recipe for the activation bath is shown in Table 5.3. The palladium chloride concentration was between concentrations reported in the literature by Honma and Kanemitsu (1987) and Baudrand (1984).

Membranes were activated in the following manner:

- Soak in sensitizing bath for 5 minutes
- Rinse with deionized water
- Soak in activation bath for 5 minutes
- Rinse with deionized water
- Repeat until membrane is uniformly activated

Both the sensitizing and activation baths were at room temperature. The process was generally repeated 3 to 7 times until the inner membrane surface was uniformly activated. The activated surface had a grayish brown appearance. Teflon® tape was wrapped around the membrane tube to prevent activation of the outside membrane surface. Following activation, the Teflon tape was removed and the membrane was rinsed in deionized water.

Electroless Plating

Both the hydrazine and the sodium hypophosphite baths were tried in this study but good results were only obtained with the hydrazine bath. Adhesion of the palladium film was a problem with the sodium hypophosphite bath. The palladium film peeled away from the ceramic surface and cracked after about 4 to 5 μm were plated. The hydrazine bath was used exclusively in fabrication of membranes tested in permeation experiments and membrane reactor experiments.

Table 5.2
Sensitizing Bath Recipe

Solution Description	Recipe	Comments
Sensitizing bath	• add 96.25 ml of deionized H_2O to bath container • add 8.25 ml of aged 0.1 M $SnCl_4 \cdot 5H_2O$ solution • add 5.5 ml of 2.6 M $SnCl_2 \cdot 2H_2O$ solution	• 110 ml was bath volume used for sensitizing • bath container was a glass jar or beaker • prepare bath one to two hours prior to use • periodically shake bath to keep collodial suspension evenly distributed • fresh sensitizing bath was used each day
0.1 M $SnCl_4 \cdot 5H_2O$ solution	• dissolve 20.9 g of $SnCl_4 \cdot 5H_2O$ in 1000 ml of deionized H_2O • allow solution to age for one week	• colloidal suspension forms after about one week of aging • solution has an indefinite shelf life • purity of $SnCl_4 \cdot 5H_2O$ was 98 % (metals basis)
2.6 M $SnCl_2 \cdot 2H_2O$ solution	• dissolve 587 g of $SnCl_2 \cdot 2H_2O$ in 780 ml of concentrated (37 weight %) HCl	• volume of resulting solution is about 1000 ml with an HCl concentration of about 9.4 M • solution has an indefinite shelf life • $SnCl_2 \cdot 2H_2O$ was reagent grade

Table 5-3
Activation Bath Recipe

Solution Description	Recipe	Comments
Activation Bath	• add 12.5 ml of activation solution to 12.5 ml of deionized H_2O	• bath container was 30 ml glass vial • fresh activation bath was used for each five minute soak period during membrane activation • activation solution can also be used without dilution for membrane activation, if desired
Activation solution	• add 5 ml concentrated (37 weight %) HCl to 995 ml of deionized H_2O • add 0.267 g of $PdCl_2$ in the acidic solution • allow solution to sit for several hours to dissolve the $PdCl_2$	• shelf life of solution is indefinite • purity of $PdCl_2$ was 99.9 % (metals basis)

The hydrazine plating bath used in this study was based on a recipe developed by Rhoda (1959). The recipe was the same as described by Rhoda but the concentration of disodium EDTA was doubled to improve bath stability at the relatively high plating temperatures (343-353 K). The recipes used to prepare the complex solution and plating bath are presented in Table 5.4. The palladium ammine complex is formed by adding ammonium hydroxide to an acidified palladium chloride solution. Table 5.5 shows a typical set of plating bath composition and operating conditions.

The plating procedure was relatively simple. Teflon tape was wrapped several times around the outside of the membrane tube to protect the end seals from the plating bath. The plating bath container was a 30 ml glass vial with a screw-on cap. After addition of the membrane, the cap was loosely screwed back on and the container was placed in a temperature controlled water bath. A constant temperature circulator (VWR Scientific, Model 1120) was used to control the water bath temperature. No agitation other than bubbles produced from the plating reaction and occasional shaking of the bath container was used in the plating bath. After one hour, the membrane was removed from the plating bath, rinsed off, and fresh Teflon tape was applied. It was then added to a fresh bath and the plating process was continued until a desired palladium film thickness was obtained. The one hour plating period was used because the plating rate was significantly reduced after one hour. This is attributed to catalytic decomposition of hydrazine by palladium (Rhoda, 1959). Rinsing the membrane between plating baths as well as adding the EDTA a few hours before each bath was used helped maintain bath stability at the plating temperatures of 343 to 353 K. Palladium was plated at a rate of 2 to 2.5 μm per hour under these conditions.

Membranes were rinsed in deionized water and dried at 383 to 393 K for several hours after plating. The thickness of the palladium film was calculated by dividing the weight difference in the unplated and plated membrane by the plated surface area and the palladium density. Plating thickness for a membrane with a 20 μm palladium film was independently determined by weighing the film after it was removed from the membrane, and by scanning electron microscopy (SEM). The three measurements agreed within five percent.

Hydrazine is very hazardous so special safety procedures were followed when it was used. The hydrazine was always handled under a fume hood while wearing a respirator, face shield, rubber gloves, and lab coat. Pipettes used to dispense hydrazine

Table 5.4
Plating Bath Recipe

Solution Description	Recipe	Comments
Plating bath	• add 1.75 g of disodium EDTA to 25 ml of Pd-ammine complex solution • allow solution to sit for at least two hours • add 0.25 ml of 1.0 M N_2H_4 solution just before membrane is added to plating bath	• plating bath container was a 30 ml glass vial
$PdCl_2$ stock solution	• add 20 ml of concentrated HCl (37 weight %) to 980 ml of deionized H_2O • add 10 g of $PdCl_2$ to the acidic solution • allow solution to sit for several hours to dissolve the $PdCl_2$	• solution has indefinite shelf life • purity of $PdCl_2$ was 99.9 % (metals basis)
Pd-ammine complex solution	• add 120 ml of deionized H_2O to 1000 ml of $PdCl_2$ stock solution • slowly add 715 ml of NH_4OH (28 weight % NH_3) • allow solution to sit for two to three days to redissolve precipitate • filter the clear solution	• solution has indefinite shelf life
1.0 M N_2H_4 (hydrazine) solution	• add 100 g of 35 weight percent hydrazine solution to 995 ml of deionized H_2O	• respirator and protective clothing worn at all times when handling hydrazine

Table 5.5
Typical Electroless Plating Bath Composition

component	concentration
palladium chloride	5.4 g/L
ammonium hydroxide (28 percent)	390 mL/L
disodium EDTA	70 g/L
hydrazine (1 molar solution)	10 mL/L
pH	11
Temperature	343 to 353 K
Plating surface area	527 cm^2/L

were rinsed with a 2 % sodium hypochlorite solution (bleach) to neutralize the hydrazine.

Membrane Characterization

The objectives of the membrane characterization experiments were as follows:

- Develop high temperature seals to connect the membrane to gas plumbing lines for the permeability experiments.
- Determine the hydrogen selectivity of the membrane as a function of the transmembrane pressure difference between the tube and shell side.
- Measure the permeation rate of hydrogen, nitrogen, and helium.

The key objectives were to determine the hydrogen permeability and the hydrogen/nitrogen selectivity of the composite palladium-ceramic membrane.

High Temperature Sealing

Figure 5.2 is a schematic of the shell and tube test apparatus used for the permeation tests. High temperature seals were needed to connect the membrane to the nonporous inlet and outlet tubes. Two methods were developed for this purpose. One involved the use of a ceramic adhesive and high temperature sealant (Aremco 617) and the other used Grafoil seals (graphite based packing material) and compression fittings.

I believe it was more difficult to seal the membranes used in this study than those developed by Uemiya and coworkers. Uemiya and coworkers plated palladium on the outside surface of the porous support membranes. Their membrane sealing procedures were not discussed in detail, but I believe the membranes were sealed with o-rings outside the heated zone of the furnace. In one paper (Uemiya et al.,1991b), they stated that hydrogen permeation was restricted to the section of membrane where catalyst was packed, and the other part of the tube was plated with a nickel film that was scarcely permeable to hydrogen. It appears they used a tube that went all the way through the furnace with permeation restricted to the middle part of the tube where palladium was plated. Therefore, high temperature seals were probably not required.

High temperature seals were required in this project because the total membrane length was only 6 cm. Since palladium was plated on the inside of the ceramic membrane, it was not practical to plate a long membrane and then plate over the ends

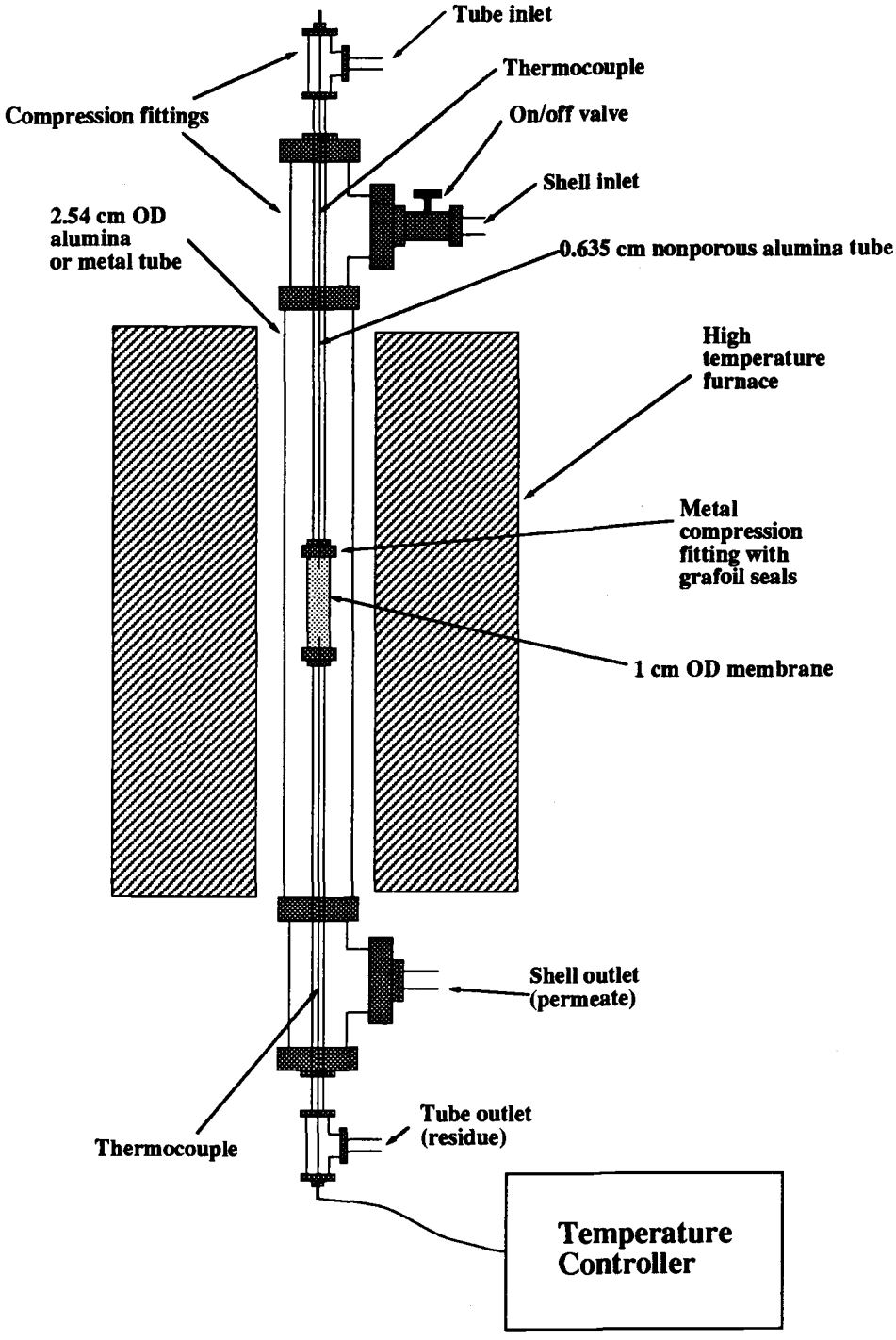

Figure 5.2 Membrane Module for Permeation Experiments.

with nickel. Commercial application of a composite metal-ceramic membrane would undoubtedly require high temperature seals. Therefore, the membrane sealing procedure used in this study was more realistic.

The ceramic adhesive/sealant method involved gluing nonporous alumina tubes into both ends of the membrane and then sealing off the ends with Aremco 617 sealant. This sealing method was successfully tested in blank experiments where the alumina inlet and outlet tubes were glued into a nonporous alumina tube the same size as the membranes. A leak rate of less than 0.05 cm^3(STP)/min was observed when pure nitrogen was run through the tubes at a total pressure difference of 1550 kPa and a temperature of around 873 K. This leak rate was over 10000 times lower than the hydrogen permeation rates through the composite palladium-ceramic membranes at the same temperature and pressure. Unfortunately, the 617 sealant required curing in air at 1053 K. This required application of the sealant prior to plating to avoid oxidation of the palladium film. Since palladium was plated on the inside of the ceramic membrane tubes, it was not practical to use the 617 sealant. Other commercial sealants requiring lower cure temperatures were tried but none worked at temperatures above 673 K.

The second sealing method involved the use of compression fittings and graphite based seals. This procedure was used in all permeation experiments conducted with the composite palladium-ceramic membranes. Graphite based seals were applicable since permeation experiments were conducted in the absence of oxygen. The 1 cm OD membranes were joined to 0.635 cm OD nonporous alumina tubes using stainless steel Swagelok® reducing unions, Grafoil ferrules, and graphite ferrules. The Grafoil ferrules were fabricated using Grafoil tape. The fabricated Grafoil ferrules were used on the membrane because commercial (prefabricated) ferrules for the 1 cm OD membranes were not available. Commercial graphite ferrules obtained from Alltech were used on the 0.635 cm OD nonporous alumina tubes.

Fabrication of the Grafoil ferrules required extreme care to avoid breaking the membrane and to insure a straight connection was made between the membrane and compression fittings. The membrane would either get stuck inside the shell side tube or the 0.635 cm OD nonporous alumina tubes would not fit through the tee compression fittings at the ends of the shell and tube test apparatus if a crooked connection was made.

The first step in fabricating a Grafoil ferrule was to wrap a 15 to 16 cm long piece of Grafoil tape counterclockwise around one end of a membrane. The tape was fit into the nut for the compression fitting, and a rubber o-ring was placed on the seat of the

compression fitting. The nut was then tightened down on the compression fitting to form the ferrule. The Grafoil tape molded around the nut and membrane when the nut was tightened to form a seal. The o-ring was needed to avoid breaking the membrane when the nut was tightened. It cushioned the membrane from being crushed against the metal seat during the tightening process. After the ferrule was formed, the nut was untightened to remove the rubber o-ring. The fitting was then retightened until the nut would no longer turn. The membrane did not break during retightening because there was clearance between the metal seat and membrane due to the presence of the o-ring during the initial tightening process.

A straight connection between the compression fitting and membrane was made by conducting the Grafoil ferrule fabrication process in a lathe. The compression fitting used to form the ferrule was secured in one end of the lathe. A second compression fitting with nylon ferrules was secured on the opposite end of the membrane. Finger tightening was used to avoid cutting the membrane with the nylon ferrules. A short (8 to 10 cm long) 0.635 cm OD metal tube was attached to the other end of the second compression fitting. The metal tube was loosely fit into the lathe's guide drill so it could turn during the tightening process. This kept the membrane straight when the nut was tightened over the compression fitting to form the Grafoil ferrule. The result was a straight connection between the membrane and compression fitting. When the second ferrule was formed on the membrane, the compression fitting with the first Grafoil ferrule replaced the fitting with the nylon ferrules.

The edges of the metal compression fittings had to be ground down to fit inside the alumina tube used for the shell of the permeation apparatus. It was very difficult to form the grafoil ferrules with the ground down fittings. To avoid grinding down the fittings, a stainless steel tube with a larger ID was used for the shell on permeation experiments conducted for two of the five membranes tested in this study. These two membranes had significantly lower hydrogen permeabilities. Therefore, use of the metal tube was discontinued.

Procedures For Permeability Experiments

Membranes were characterized by conducting permeability experiments with hydrogen, nitrogen, and helium. Figures 5.2 and 5.3 show schematics of the experimental apparatus. The experimental system was similar to the system used in the kinetics experiments except plumbing for the permeate gas stream was added. Feed gas

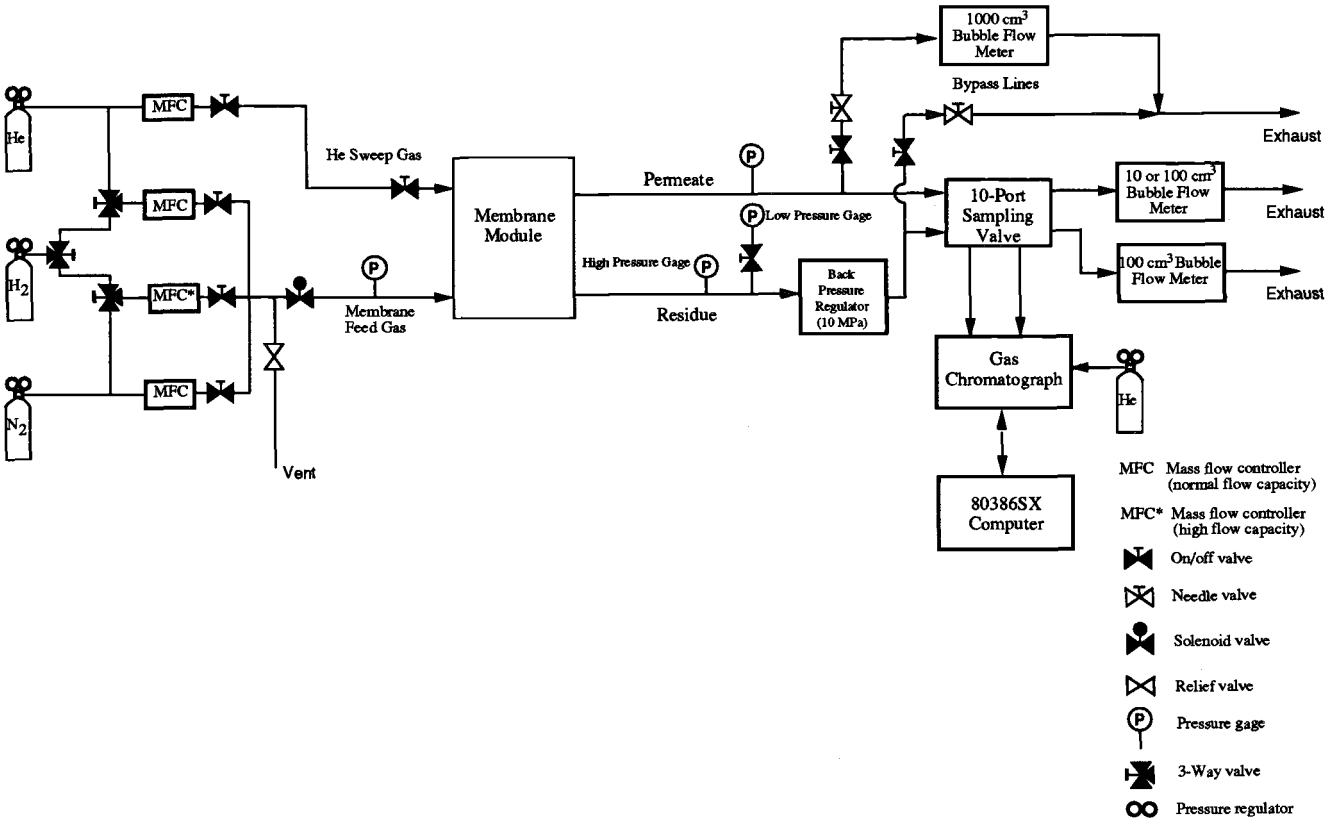

Figure 5.3 Experimental System for Membrane Characterization Experiments

flowed down the inside of the membrane tube (tube side) and permeated gases were collected on the shell side. A sweep gas was also used on the shell side, in some experiments.

The purpose of the three-way valves was to switch the mass flow controller used for a particular gas without breaking any plumbing connections. Each mass flow controller was calibrated with all gases for which it was used. The high flow capacity controller was sized for a maximum flow of 5000 cm^3(STP)/minute of nitrogen. The other flow controllers were sized for maximum flows of 500 cm^3(STP)/minute of nitrogen or helium. The mass flow controller settings determined the inlet gas flows and compositions.

The furnace was a Type MK-70 tube furnace from Hevi-Duty Electric Co. in Milwaukee, Wisconsin. An Omega CN9000 temperature controller was used to regulate membrane temperature. Type K thermocouples placed at the membrane inlet and outlet measured the temperature. The inlet temperature was higher than the outlet temperature due to a non-uniform temperature profile in the furnace. The maximum temperature difference was 20 K. Membrane temperature was taken as the average of the inlet and outlet temperature.

Membrane pressure was controlled by a back pressure regulator installed on the reject line. The permeate side was at atmospheric pressure or slightly above. Pressure measurements were made with pressure gages. Two gages were installed on the reject line to increase the accuracy of membrane pressure measurements over the relatively wide range of pressures evaluated in the permeability experiments. Measurements at absolute pressures less than 791 kPa were made with a liquid-filled Wika gage (Model L4625-4L-100). The pressure scale on this gage was divided into increments of 13.8 kPa, and the pressure could be read with a resolution of about 7 kPa. Higher pressures were measured with a liquid-filled gage from Span Instruments (Model LFP412). The pressure scale on this gage was divided into increments of 34.5 kPa, and it could be read with a resolution of about 17 kPa. The pressure scale on the gage installed on the membrane feed line (Span Instruments, Model LFP312) was divided into increments of 69 kPa, and it could be read with a resolution of about 35 kPa. A Wika gage with pressure increments of 3.4 kPa measured the permeate pressure. Pressure could be read with a resolution of about 1.7 kPa on this gage.

Reject and permeate stream flows were measured with bubble flow meters. Bubble flow meter sizes ranged from 10 cm^3 to 1000 cm^3 to increase the accuracy of

the flow measurements over the wide range of flows encountered in the permeability experiments.

The gas chromatograph measured nitrogen and hydrogen concentrations in reject and permeate gas streams for experiments involving gas mixtures. Sample loop volume was 0.25 cm^3 for both the reject and permeate lines. A Molecular Sieve 13X packed column (Alltech Associates, Inc., Deerfield, Illinois) was used in the gas chromatograph. As in the kinetics experiments, bypass lines were used to maintain constant flow rates through the sample loops.

Permeability experiments were conducted over a range of temperatures and pressures. Experimental temperatures ranged from 723 to 913 K. The upper temperature limit was set by the maximum operating temperature of the Aremco 617 end seals. Feed pressures ranged from 156 to 2445 kPa, and permeate pressures from 101 to 140 kPa. Transmembrane pressure differences ranged from about 40 to 2330 kPa. Operation at even higher transmembrane pressure differences appears possible with the ceramic membrane used to support the palladium film. Wu and coworkers (1993) reported using a 4 nm Membralox® membrane at transmembrane pressure differences up to 3575 kPa.

Hydrogen and helium permeabilities were determined by flowing pure gas through the membrane at various pressures and measuring the volumetric flow rate of the permeate stream with the bubble flow meters. No inlet sweep gas was used in the hydrogen and helium permeation experiments or in experiments conducted with gas mixtures of hydrogen, nitrogen and helium. A helium sweep gas was generally used in the nitrogen permeability experiments. Nitrogen permeabilities were determined by measuring the effluent sweep gas flow rate with the bubble flow meters and composition on the gas chromatograph. The measured volumetric flow rates were converted to molar flows and normalized by dividing by the active membrane area to determine permeation rates (i.e., gas fluxes). As previously discussed, nitrogen and helium flow rates were normalized using the active membrane area even though they result from localized leaks in the membrane seals or defects in the palladium film.

During startup, membranes were slowly heated to 723 K over a three to four hour period under a helium atmosphere. This was done to avoid hydrogen embrittlement and possible pin hole formation in the palladium film due to heating in a hydrogen atmosphere at temperatures below the critical temperature of the palladium-hydrogen system (about 573 K). Hydrogen was introduced into the system after the membrane reached 723 K. The permeate flow for a set membrane pressure was monitored until a

constant flow rate was reached prior to beginning the permeation experiments. This generally took about 12 hours or more. When permeation experiments were not being conducted, hydrogen flowed through the membrane at a pressure of about 310 kPa. The idea was to keep the membrane pressure well above the permeate pressure to reduce the possibility of palladium film delamination. Hydrogen was degassed from the palladium film by flowing helium through the membrane for 12 hours before cooling the membrane down below 573 K.

RESULTS AND DISCUSSION

Figure 5.4 is an SEM micrograph of a composite palladium-ceramic membrane. The ceramic membrane had a 10 nm pore top layer. The palladium film is shown on the lower horizontal band of the SEM micrograph. The slight delamination of the palladium film occurred when the membrane was cut with a jewelers saw to take the SEM micrograph. Palladium film thickness on this membrane was about 1.5 μm. Figure 5.5 is an SEM micrograph of a 20 μm palladium film removed from a composite palladium-ceramic membrane. Thickness measurements taken with a micrometer at various positions along the length of the membrane indicate the film thickness is uniform. Visual inspection of the palladium film revealed no apparent film defects. The SEM micrographs and visual inspection of broken membranes indicate that penetration of palladium into the pores of the ceramic membrane support was minimal.

Membranes with palladium films ranging from 11.4 to 20 μm were tested in the high temperature permeability tests. Ambient temperature leak tests were conducted by immersing membranes pressurized with nitrogen to about 240 kPa in water. Membranes with palladium films less than 10 μm leaked nitrogen between the seals so they were not tested in the high temperature experiments. Tiny leaks from the grafoil seals were observed on all membranes. Seal leakage was reduced but not eliminated with practice and experience. Based on visual observations from the ambient temperature leak tests, a significant portion of the measured nitrogen and helium permeabilities are due to leaks in the grafoil seals rather than defects in the palladium film. Therefore, even higher hydrogen selectivities than those measured in this work are possible with improvements in membrane sealing.

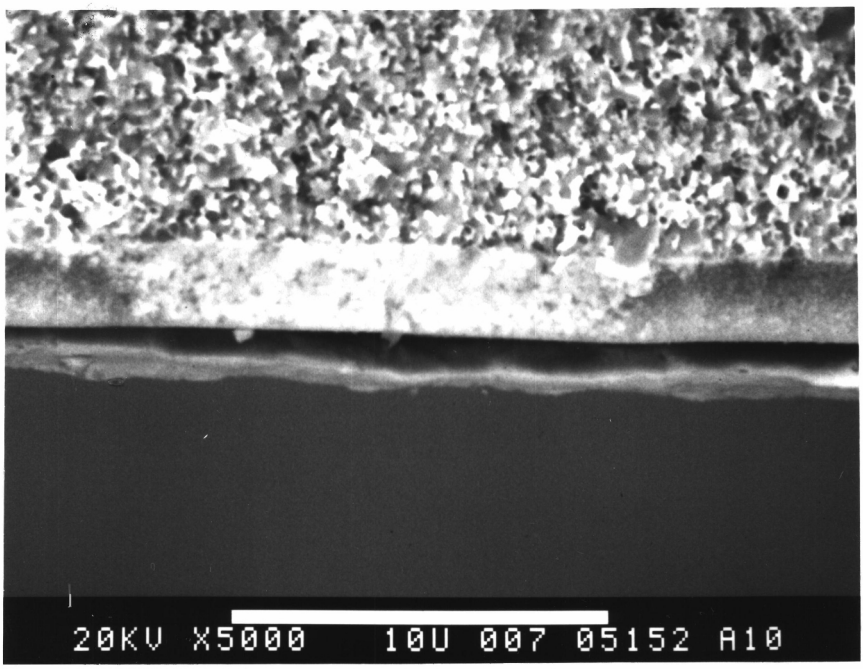

Figure 5.4 SEM Micrograph of a Composite Palladium-Ceramic Membrane. The third horizontal band from the top of the image is the palladium film.

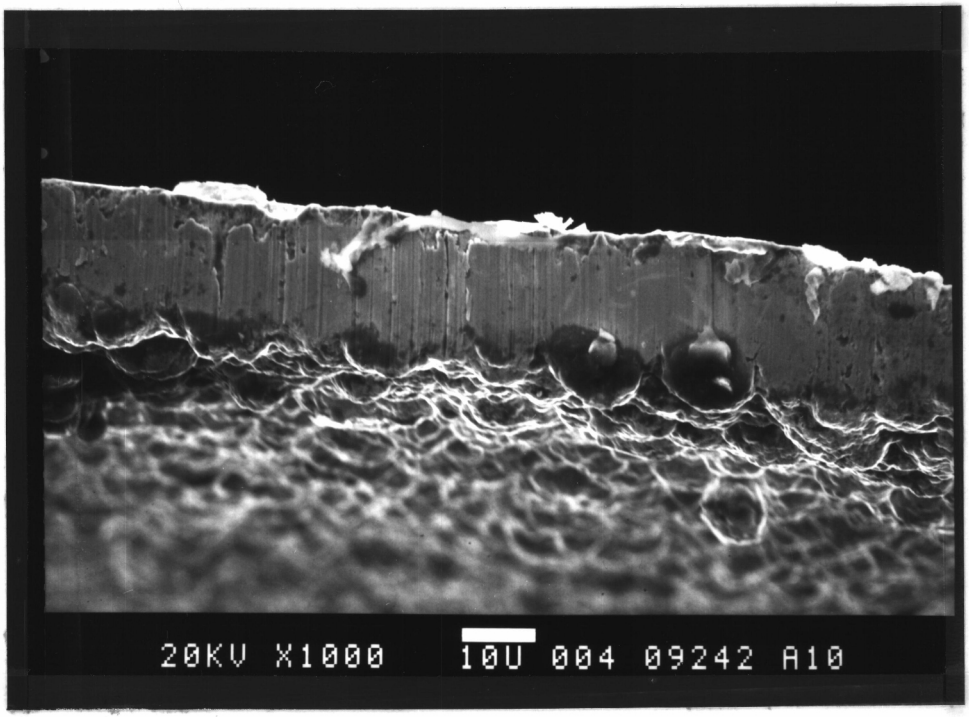

Figure 5.5 SEM Micrograph of a 20 μm Palladium Film Removed from a Composite Palladium-Ceramic Membrane.

Hydrogen Permeabilities of Composite Palladium-Ceramic Membranes

A total of five membranes were tested in the high temperature hydrogen permeability experiments. The collected permeation data for each membrane are summarized in Figures 5.6 to 5.10. These figures show the range of temperatures and pressures evaluated in the permeability experiments. The solid lines represent permeation rates estimated from Equations 5.3 and 5.4 using $\bar{P}_{HO}$, E, and the n(H) value calculated from nonlinear regression analysis of the combined temperature data. The STATGRAPHICS® statistical graphics system (Statistical Graphics Corporation) was used in the nonlinear regression calculations. Table 5.6 summarizes the $\bar{P}_{HO}$, E, and n(H) values obtained for four of the five membranes. Better agreement between actual and predicted values was obtained when nonlinear regression was used to calculate $\bar{P}_H$ and n(H) in Equation 5.3 for a particular temperature. This is due to the variation of n(H) with temperature. Table 5.7 summarizes the $\bar{P}_H$ and n(H) values obtained for the membranes at individual temperatures.

A stainless steel tube was used on the shell side for the two membranes with 12.2 and 19 μm palladium films. A nonporous alumina tube was used on the shell side for the other three membranes. Hydrogen permeabilities were significantly lower for the two membranes that used the metal tube. The lower permeabilities may be attributable to surface contamination from the metal tube. The higher n(H) values for the two membranes are also symptoms of surface contamination. The outside surface of the ceramic membrane support was black from carbon deposition when the two membranes were removed from the membrane module. In comparison, the outside ceramic surfaces of the other three membranes were relatively clean with only minor carbon deposits near the ends of the membrane where metal compression fittings were located. The following discussion focuses on results obtained for the three membranes where the nonporous alumina tube was used for the shell side, because hydrogen permeabilities for the other two membranes were apparently significantly influenced by contamination introduced by the metal tube.

Table 5.7 summarizes values of $\bar{P}_H$ and n(H) obtained for the three membranes where the nonporous alumina tube was used on the shell side. The n(H) values decreased with increasing temperature. The membrane with the 17 μm palladium film had significantly higher nitrogen permeation rates than the other two membranes which means that significantly more hydrogen permeated through leaks in the grafoil seals or defects in the palladium film. The hydrogen leakage increased the values of n(H)

Table 5.6

Hydrogen Permeability Parameters from Combined Temperature Analysis for Composite Palladium-Ceramic Membranes

Membrane Description	T (K)	$\bar{P}_{HO}$ (moles·m/m²·s·Pa$^{n(H)}$)	n(H)	E (J/mole)	r^2
17 μm palladium film on ceramic membrane with 200 nm pore layer[a]	723 to 873	$5.29 \cdot 10^{-8}$ ($4.85 \cdot 10^{-9}$)	0.573 (0.005)	14450 (191)	0.9994
11.4 μm palladium film on ceramic membrane with 200 nm pore layer[a]	823 to 873	$1.62 \cdot 10^{-8}$ ($3.27 \cdot 10^{-9}$)	0.580 (0.008)	8880 (576)	0.9994
19 μm palladium film on ceramic membrane with 200 nm pore layer[b]	723 to 873	$1.98 \cdot 10^{-8}$ ($7.56 \cdot 10^{-9}$)	0.634 (0.023)	15790 (1041)	0.9918
12.2 μm palladium film on ceramic membrane with 200 nm pore layer[b]	723 to 913	$5.28 \cdot 10^{-8}$ ($1.25 \cdot 10^{-8}$)	0.596 (0.015)	20435 (475)	0.9957

[a] Nonporous alumina tube used for shell in hydrogen permeation experiments.

[b] Stainless steel tube used for shell in hydrogen permeation experiments.

( ) Values in parantheses represent the standard errors of the calculated parameters.

Table 5.7

Hydrogen Permeability Parameters at Specific Temperatures for Composite Palladium-Ceramic Membranes

Membrane Description	Temperature (K)	$\bar{P}_H$ (moles·m/m²·s·Pa$^{n(H)}$)	n(H)	r^2
20 μm palladium film on ceramic membrane with 10 nm pore layer[a]	823	$1.43 \cdot 10^{-8}$ ($2.55 \cdot 10^{-8}$)	0.526 (0.119)	0.9938
17 μm palladium film on ceramic membrane with 200 nm pore layer[a]	723	$2.34 \cdot 10^{-9}$ ($2.79 \cdot 10^{-10}$)	0.622 (0.008)	0.9998
	773	$4.04 \cdot 10^{-9}$ ($4.89 \cdot 10^{-10}$)	0.595 (0.008)	0.9998
	823	$6.82 \cdot 10^{-9}$ ($6.30 \cdot 10^{-10}$)	0.568 (0.006)	0.9998
	873	$9.96 \cdot 10^{-9}$ ($6.53 \cdot 10^{-10}$)	0.552 (0.004)	0.9999
11.4 μm palladium film on ceramic membrane with 200 nm pore layer[a]	823	$3.23 \cdot 10^{-9}$ ($4.85 \cdot 10^{-10}$)	0.602 (0.010)	0.9996
	873	$5.84 \cdot 10^{-9}$ ($6.90 \cdot 10^{-10}$)	0.566 (0.008)	0.9997
19 μm palladium film on ceramic membrane with 200 nm pore layer[b]	723	$1.04 \cdot 10^{-9}$ ($1.25 \cdot 10^{-10}$)	0.659 (0.008)	0.9998
	823	$6.97 \cdot 10^{-10}$ ($1.14 \cdot 10^{-10}$)	0.701 (0.011)	0.9994
	873	$9.19 \cdot 10^{-10}$ ($8.85 \cdot 10^{-11}$)	0.698 (0.006)	0.9999
12.2 μm palladium film on ceramic membrane with 200 nm pore layer[b]	723	$8.63 \cdot 10^{-10}$ ($5.53 \cdot 10^{-11}$)	0.647 (0.004)	1.0000
	823	$2.32 \cdot 10^{-9}$ ($1.49 \cdot 10^{-10}$)	0.604 (0.004)	1.0000
	873	$2.65 \cdot 10^{-9}$ ($2.88 \cdot 10^{-10}$)	0.605 (0.007)	0.9997
	913	$7.70 \cdot 10^{-9}$ ($8.50 \cdot 10^{-10}$)	0.546 (0.007)	0.9997

[a] Nonporous alumina tube used for shell in hydrogen permeation experiments.

[b] Stainless steel tube used for shell in hydrogen permeation experiments.

( ) Values in parantheses are the standard errors of the calculated parameters.

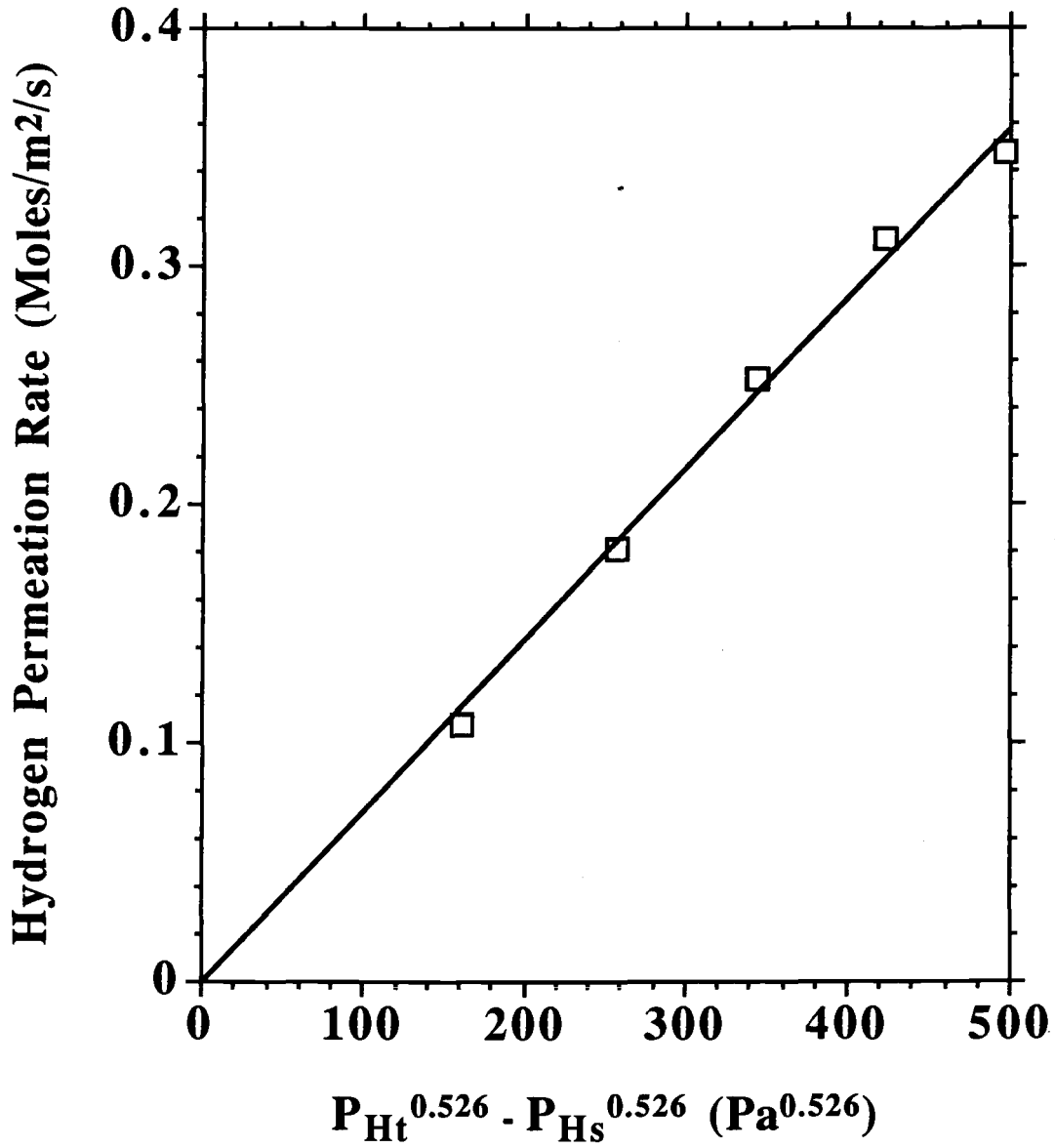

Figure 5.6 Hydrogen Permeation Data at 823 K for Composite Palladium-Ceramic Membrane with 20 μm Palladium Film. The solid line represents predicted permeation rates calculated using parameters in Table 5.7. Nonporous alumina tube was used on shell side.

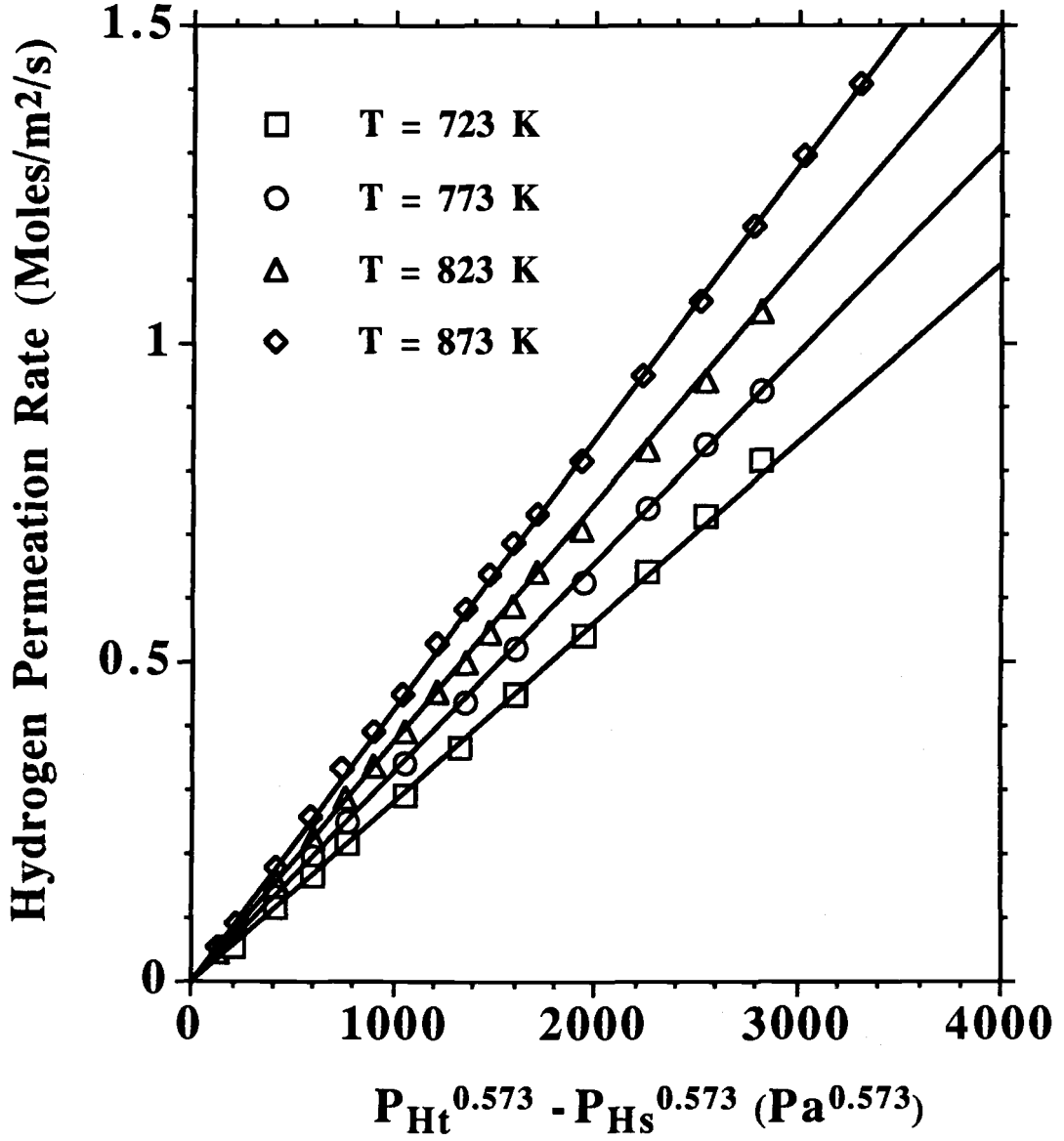

Figure 5.7 Hydrogen Permeation Data for Composite Palladium-Ceramic Membrane with 17 μm Palladium Film.
The solid lines represent predicted permeation rates calculated using the parameters in Table 5.6. Nonporous alumina tube used on shell side.

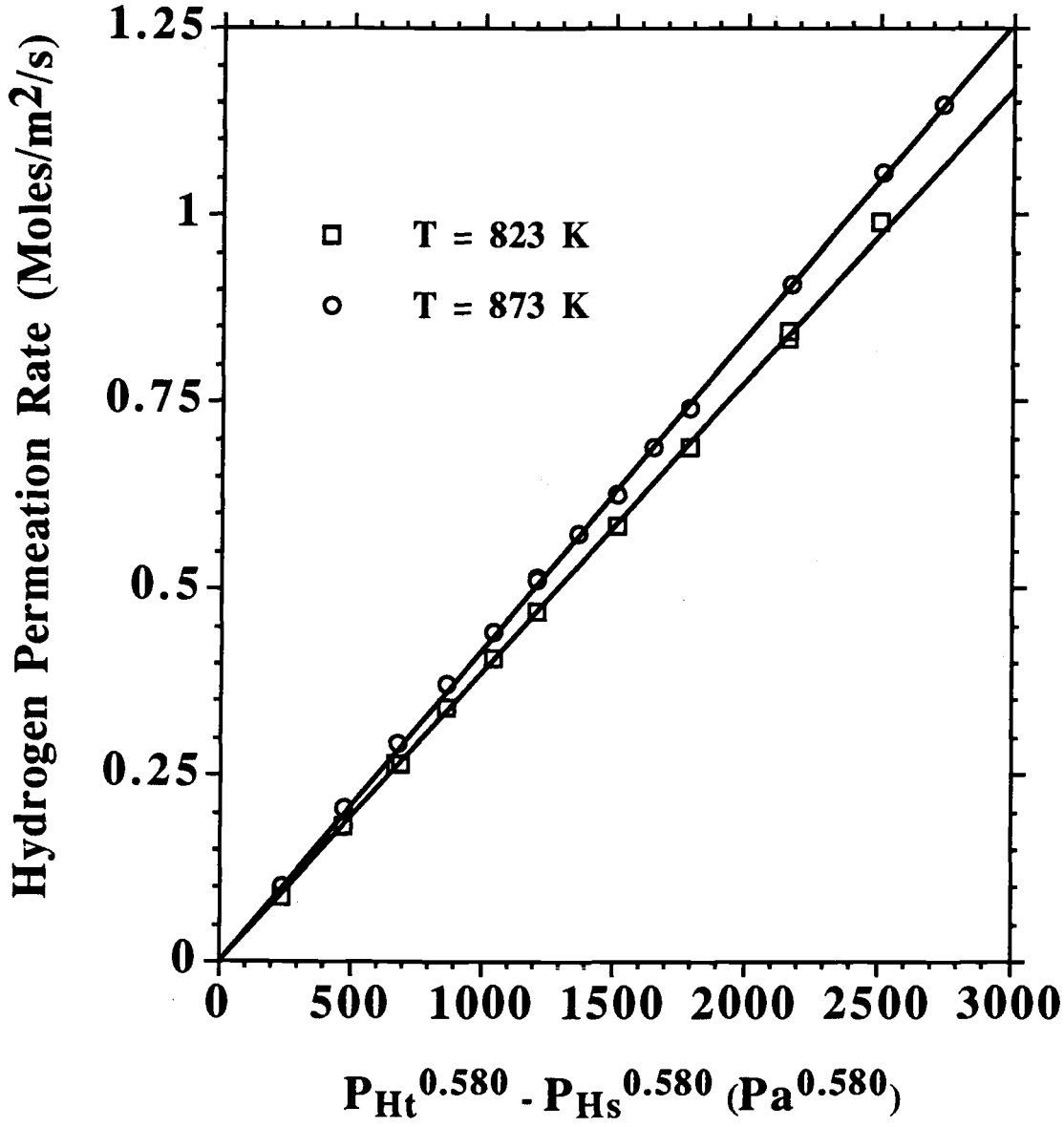

Figure 5.8 Hydrogen Permeation Data for Composite Palladium-Ceramic Membrane with 11.4 μm Palladium Film.
The solid lines represent predicted permeation rates calculated using the parameters in Table 5.6. Nonporous alumina tube used on shell side.

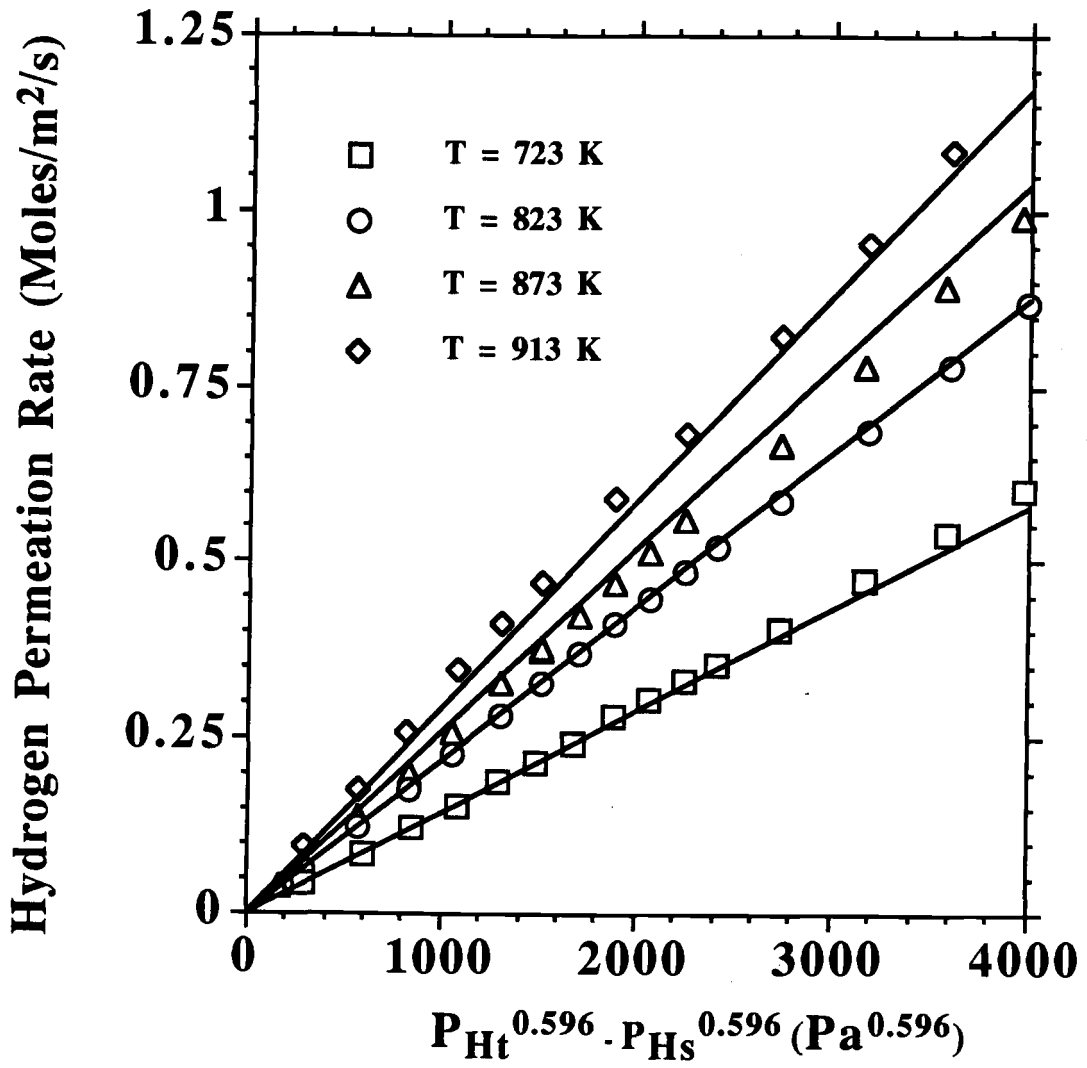

Figure 5.9 Hydrogen Permeation Data for Composite Palladium-Ceramic Membrane with 12.2 μm Palladium Film.
The solid lines represent predicted permeation rates calculated using the parameters in Table 5.6. Stainless steel tube used on shell side.

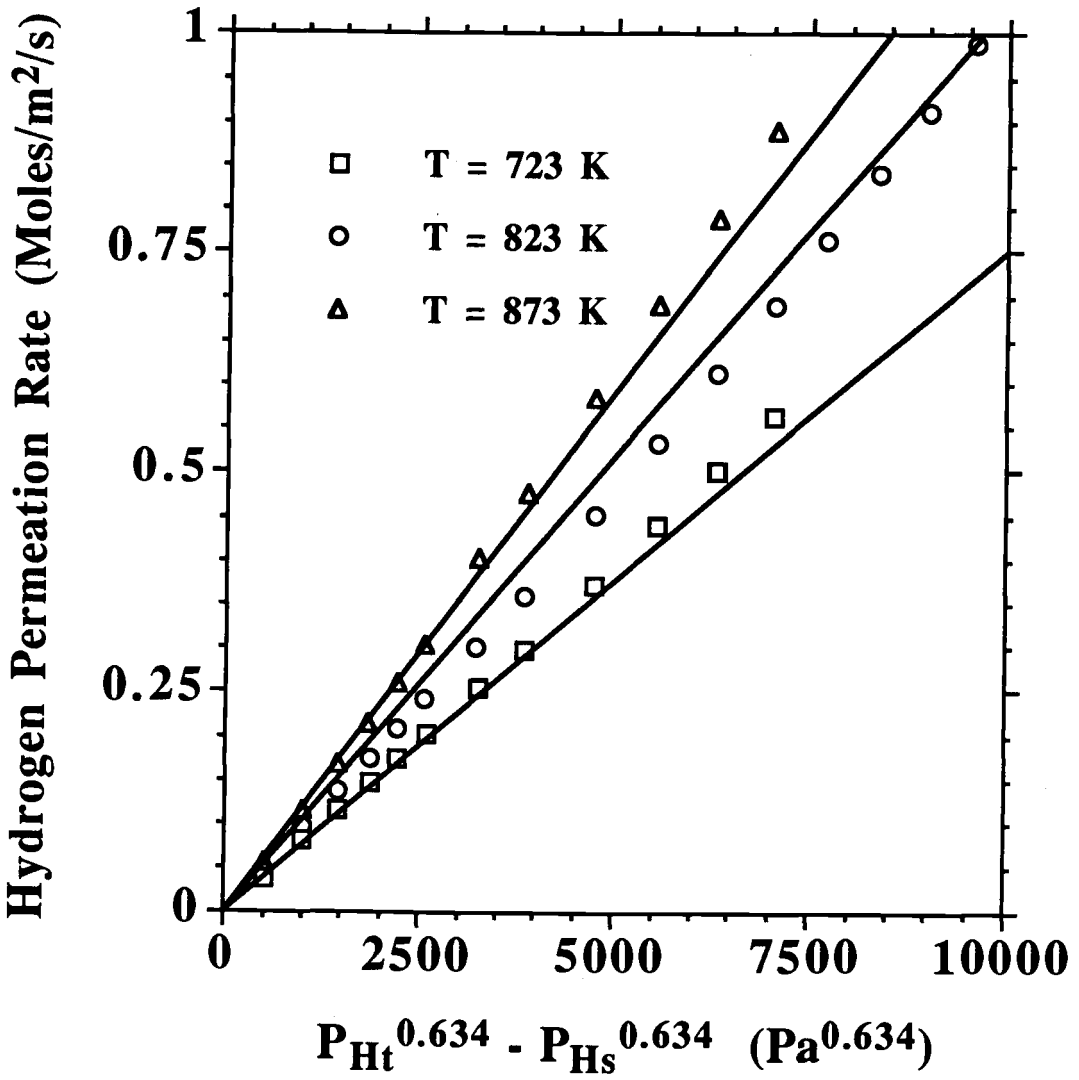

Figure 5.10 Hydrogen Permeation Data for Composite Palladium-Ceramic Membrane with 19 μm Palladium Film.
The solid lines represent predicted permeation rates calculated using the parameters in Table 5.6. Stainless steel tube used on shell side.

obtained for this membrane. The membrane with the 20 μm palladium film delaminated before hydrogen permeability experiments could be conducted at other temperatures. This was probably caused by a pressure surge on the sweep side which pushed the palladium film away from the ceramic membrane surface. The ceramic membrane pore diameter for this composite membrane was 10 nm. In general, composite membranes made using ceramic membranes with 200 nm pores were more durable than those made using 10 nm pores. The surface of a 200 nm pore layer is rougher than the surface of a 10 nm pore layer due to the larger particle size. This makes it easier to deposit the palladium film by electroless plating and improves adhesion of the resulting film.

Figure 5.7 summarizes results of hydrogen permeability experiments performed with the membrane with the 17 μm palladium film. It is important to note the temperature history of the membrane. The chronological temperature history was 723, 773, 823, 873, 773, and 723 K. Hydrogen permeability experiments were conducted at each of these temperatures. A significant increase in membrane permeability occurred when the membrane was heated from 773 to 823 K. When the membrane was cooled back down to 773 and 723 K, the hydrogen permeabilities were significantly higher than the initial permeabilities and the n(H) values obtained from nonlinear regression were lower. At 723 K, the n(H) value decreased from 0.73 to 0.62, and hydrogen permeation rates increased by 20 to 40 percent, depending on the transmembrane pressure difference. A possible explanation is that surface contaminants initially present on the membrane surface were removed after it was heated to 823 K. Operation at the higher temperatures may also have had an annealing effect on the palladium surface. The initial data from 723 and 773 K were not used to determine the parameters in Tables 5.6 and 5.7, and are not included in Figure 5.7. The membrane was operated for over 200 hours at temperatures of 723 K and above. The estimated apparent activation energy was 14450 J/mole. Hurlbert and Konecny (1961) reported an apparent activation energy of 11925 J/mole for hydrogen permeation through palladium films ranging from 27 to 154 μm in thickness while Uemiya and coworkers (1988) reported an activation energy of 10700 J/mole for a composite palladium-porous glass membrane with a 13 μm palladium film.

A comparison of hydrogen permeabilities for the three membranes tested with the nonporous alumina shell was made by dividing hydrogen permeation rates by the palladium film thickness (t_m). Normalized permeation rates should be equal if diffusion through the palladium film is the rate determining step. Normalized permeation rates at 823 K are plotted as a function of transmembrane pressure

difference in Figure 5.11. Normalized permeation rates for the membrane with the 11.4 μm palladium film are significantly less than those for the membranes with 17 and 20 μm palladium films. This indicates that the hydrogen permeability of the 11.4 μm palladium film is lower than the permeability of the 17 and 20 μm palladium films. This observation is consistent with the data of Hurlbert and Konecny (1961) who also reported that the hydrogen permeability of an 11.4 μm palladium film was significantly lower than the permeability of films of 24 μm and above. Their conclusion was that hydrogen permeation rates through palladium films approach a limiting value when the film thickness is reduced below 20 μm. On the other hand, Uemiya and coworkers (1991c) reported hydrogen permeation rates for their composite palladium-porous glass membranes were inversely proportional to the palladium film thickness down to a film thickness of 13 μm. They concluded that diffusion of atomic hydrogen through the palladium film was still the rate limiting step at this film thickness and that the hydrogen permeability of the 13 μm film was the same as for thicker films.

Examination of the n(H) values listed in Table 5.7 provides support for the theory that surface processes impact the hydrogen permeability of the membrane with the 11.4 μm palladium film. The n(H) values for 823 K should be equal for all membranes if diffusion of atomic hydrogen through the palladium film is rate limiting. The higher n(H) value for the membrane with the 11.4 μm palladium film indicates that surface processes have a more significant impact on the hydrogen permeability of this membrane. In addition, a significantly lower n(H) value for the membrane with the 17 μm palladium film is obtained when the comparatively high hydrogen leakage through grafoil seals or membrane defects is estimated and subtracted from the measured hydrogen permeation rates. Assuming a hydrogen leakage equal to twice the nitrogen permeation rate for a given transmembrane pressure difference results in an n(H) value of 0.538. The n(H) value barely changes from 0.602 to 0.599 when the same analysis is applied to the membrane with the 11.4 μm palladium film due to the much lower hydrogen leakage rate through seals or membrane defects.

The apparent activation energy of 8880 J/mole for the membrane with the 11.4 μm palladium film is significantly lower than the 14450 J/mole value obtained for the membrane with the 17 μm palladium film. Surface processes are believed to have a more significant impact on the hydrogen permeability for the membrane with the 11.4 μm palladium film so the difference in the apparent activation energies is not surprising.

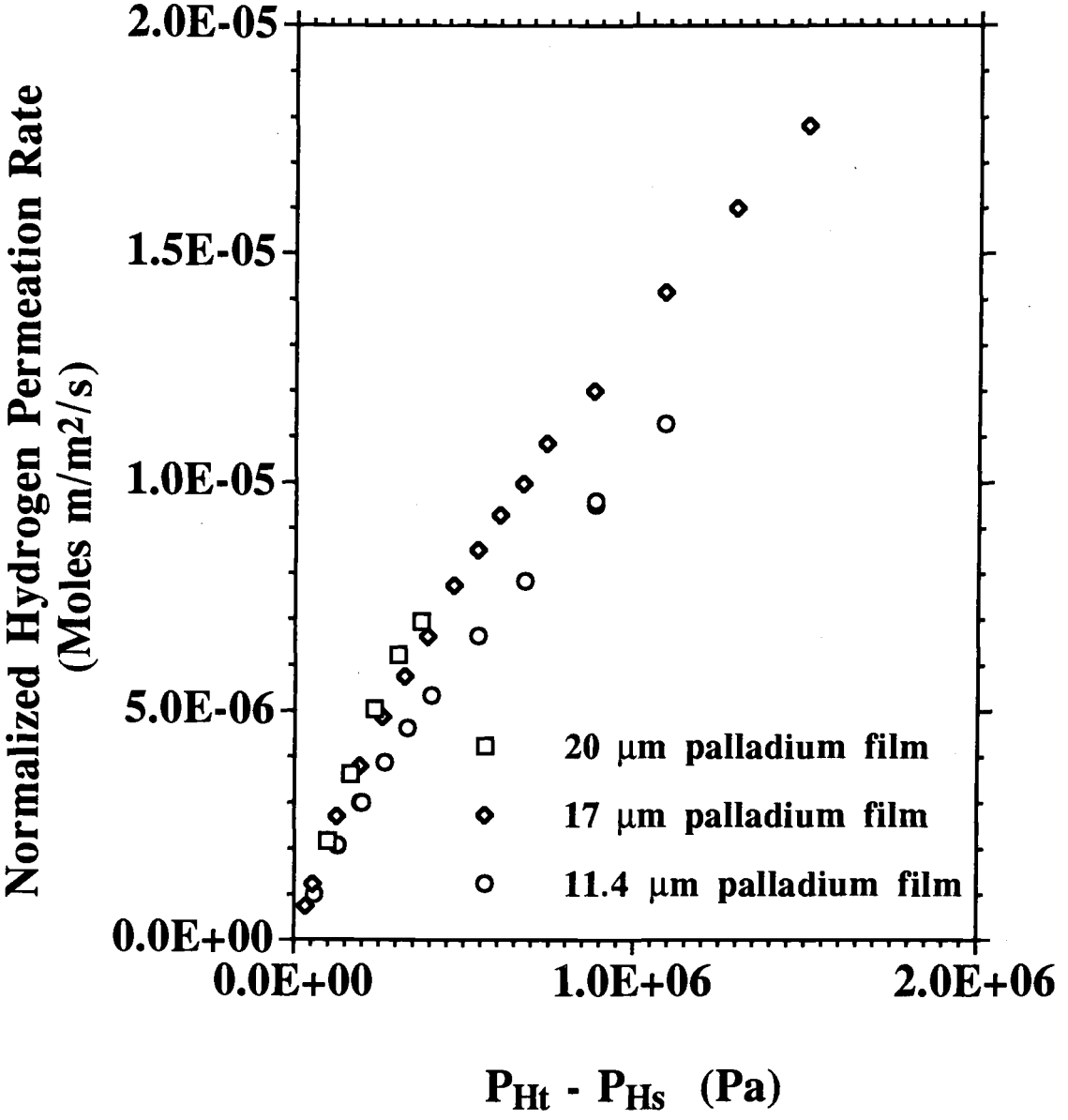

Figure 5.11 Comparison of Normalized Hydrogen Permeation Rates at 823 K for Composite Palladium-Ceramic Membranes.
Permeation rates normalized by dividing by palladium film thickness. Only membranes tested using nonporous alumina shell tube are included in the figure.

Hydrogen Selectivities of Composite Palladium-Ceramic Membranes

Hydrogen/nitrogen and hydrogen/helium selectivities for four of the five tested membranes are summarized in Figure 5.12 to 5.15. The selectivities are defined as the ratio of the hydrogen permeation rate to the nitrogen or helium permeation rate at the same transmembrane pressure difference. The hydrogen selectivity decreases with increasing transmembrane pressure difference because the permeation rate through membrane seals or palladium film defects is proportional to a higher power of pressure than permeation of hydrogen through the palladium film. Correlation of the helium and nitrogen permeability data with Equation 5.5 resulted in n(J) values ranging from 1.26 to 1.78. This indicates that both Knudsen diffusion and viscous flow were significant in permeation through leaks at the transmembrane pressure differences evaluated in this study. Helium permeation rates were higher than nitrogen permeation rates which indicates that separative flow was occurring through the leaks. This indicates that microporous defects in the membrane seals and possibly the palladium film were present. Table 5.8 summarizes the $\bar{P}_J$ and n(J) values obtained from nonlinear regression analysis of Equation 5.5.

The membrane with the 11.4 μm palladium film had the highest hydrogen selectivities. This was also the last membrane tested. Preparation of the composite palladium ceramic membranes as well as the grafoil seals required quite a bit of skill. The practice and experience gained from previous membranes helped improve the selectivity of the last membrane. A hydrogen/nitrogen selectivity of 380 was obtained at 823 K and a transmembrane pressure difference of 1500 kPa. This is well above the hydrogen/nitrogen selectivity of 50 targeted in the membrane reactor modeling analysis. The temperature and transmembrane pressure difference are also within the range of IGCC conditions. Higher transmembrane pressure differences were not evaluated for this particular membrane because the hydrogen permeation rates were too high to measure with the bubble flow meters. (The bubbles kept breaking due to the high hydrogen flow rate when the transmembrane pressure difference was raised above a certain value.) A smaller active area would be needed to evaluate permeation rates at high transmembrane pressure differences.

Nitrogen permeability experiments for the membrane with the 20 μm film were only conducted at one pressure. Both the membrane and permeate side were held at the same pressure (140 kPa) so the experiments were conducted at a transmembrane pressure difference of zero. Pure nitrogen flowed through the tube side and a helium

Table 5.8

Nitrogen and Helium Permeability Parameters at Specific Temperatures for Composite Palladium-Ceramic Membranes

Membrane Description	Temperature (K)	Gas	$\bar{P}_J$ (moles·m/m²·s·Pa$^{n(J)}$)	n(J)	r^2
17 μm palladium film on ceramic membrane with 200 nm pore layer	823	N_2	$6.07 \cdot 10^{-16}$ ($2.68 \cdot 10^{-16}$)	1.419 (0.028)	0.9986
	873	N_2	$6.86 \cdot 10^{-15}$ ($1.20 \cdot 10^{-15}$)	1.258 (0.011)	0.9998
11.4 μm palladium film on ceramic membrane with 200 nm pore layer	823	N_2	$1.53 \cdot 10^{-17}$ ($8.20 \cdot 10^{-18}$)	1.513 (0.034)	0.9994
		He	$1.71 \cdot 10^{-16}$ ($3.18 \cdot 10^{-17}$)	1.374 (0.012)	0.9999
	873	N_2	$2.28 \cdot 10^{-17}$ ($1.48 \cdot 10^{-17}$)	1.488 (0.041)	0.9979
		He	$3.12 \cdot 10^{-17}$ ($1.90 \cdot 10^{-17}$)	1.510 (0.038)	0.9980
19 μm palladium film on ceramic membrane with 200 nm pore layer	723	N_2	$5.92 \cdot 10^{-18}$ ($6.53 \cdot 10^{-18}$)	1.685 (0.068)	0.9972
	823	N_2	$1.92 \cdot 10^{-17}$ ($5.11 \cdot 10^{-18}$)	1.648 (0.016)	0.9996
	873	N_2	$6.12 \cdot 10^{-18}$ ($3.80 \cdot 10^{-18}$)	1.777 (0.039)	0.9983
12.2 μm palladium film on ceramic membrane with 200 nm pore layer	723	N_2	$4.01 \cdot 10^{-17}$ ($9.56 \cdot 10^{-18}$)	1.463(0.015)	0.9998
	823	N_2	$1.60 \cdot 10^{-17}$ ($5.36 \cdot 10^{-18}$)	1.582 (0.021)	0.9996
	823	He	$5.42 \cdot 10^{-17}$ ($2.15 \cdot 10^{-17}$)	1.531 (0.025)	0.9988

( ) Values in parantheses are the standard errors of the calculated parameters.

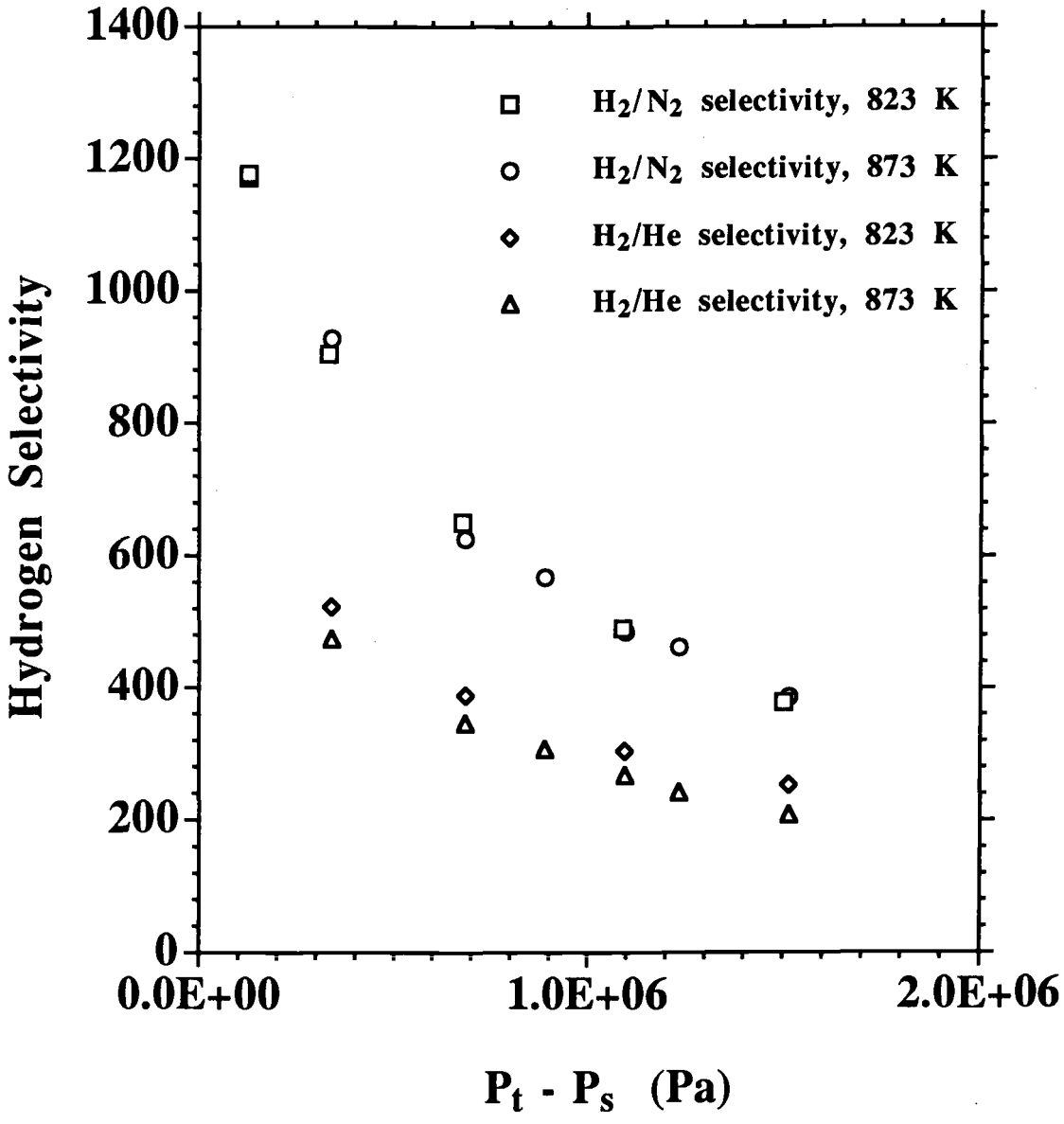

Figure 5.12 Hydrogen Selectivity Data for Composite Palladium-Ceramic Membrane with 11.4 μm Palladium Film.
Hydrogen selectivity defined as ratio of hydrogen permeation rate to nitrogen or helium permeation rate at the same transmembrane pressure difference.

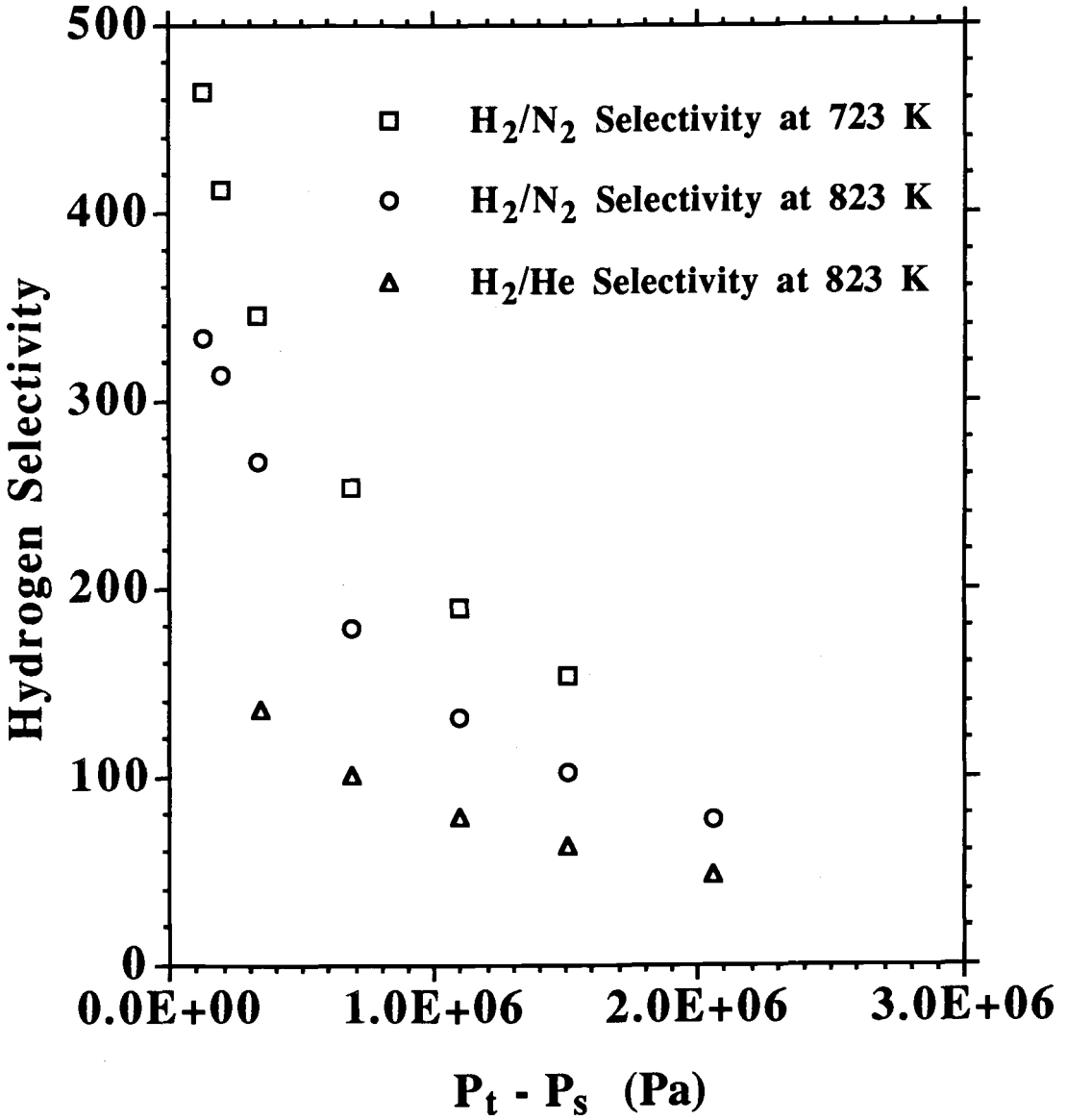

Figure 5.13 Hydrogen Selectivity Data for Composite Palladium-Ceramic Membrane with 12.2 μm Palladium Film.
Hydrogen selectivity defined as ratio of hydrogen permeation rate to nitrogen or helium permeation rate at the same transmembrane pressure difference.

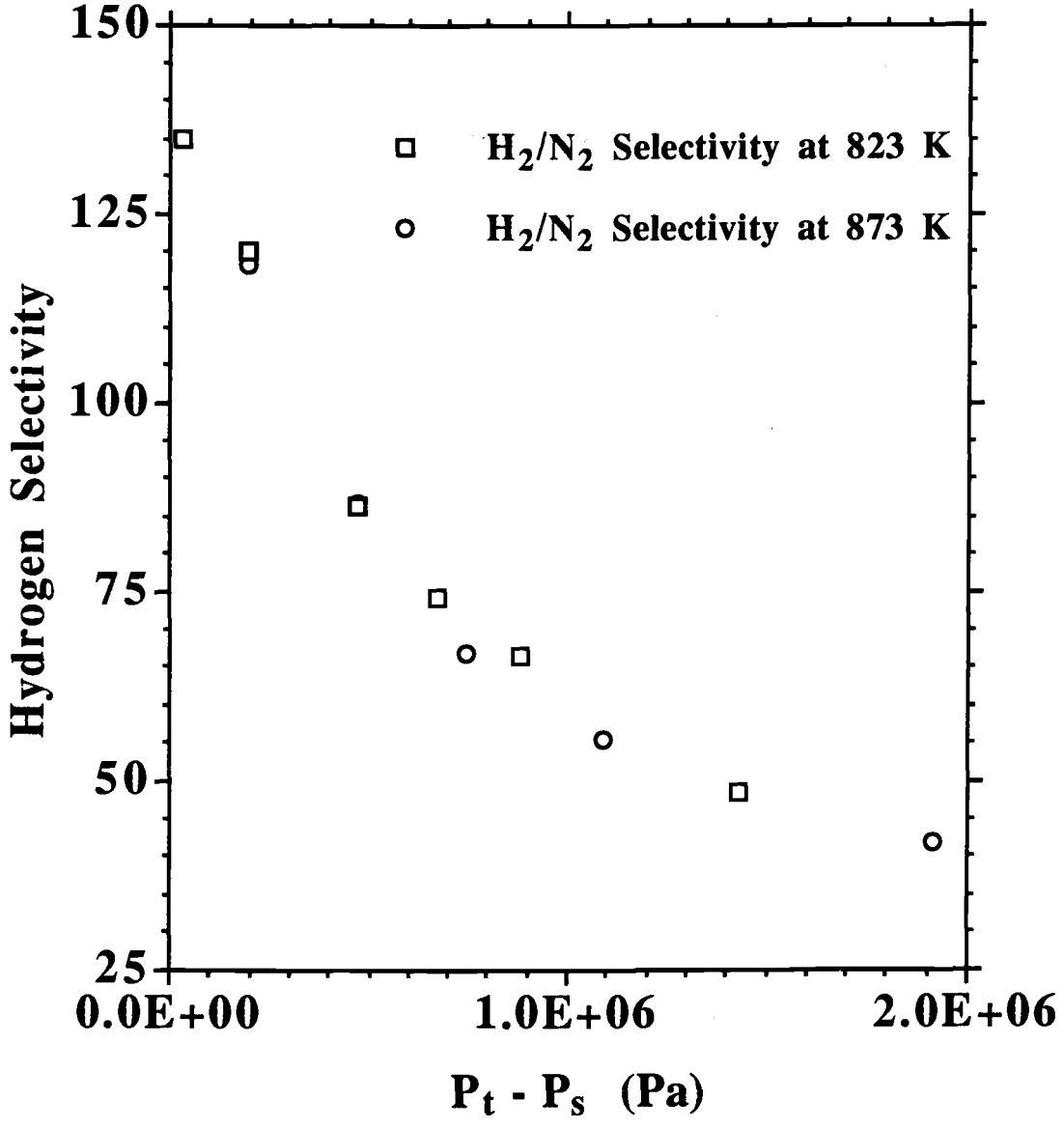

Figure 5.14 Hydrogen Selectivity Data for Composite Palladium-Ceramic Membrane with 17 μm Palladium Film. Hydrogen selectivity defined as ratio of hydrogen permeation rate to nitrogen permeation rate at the same transmembrane pressure difference.

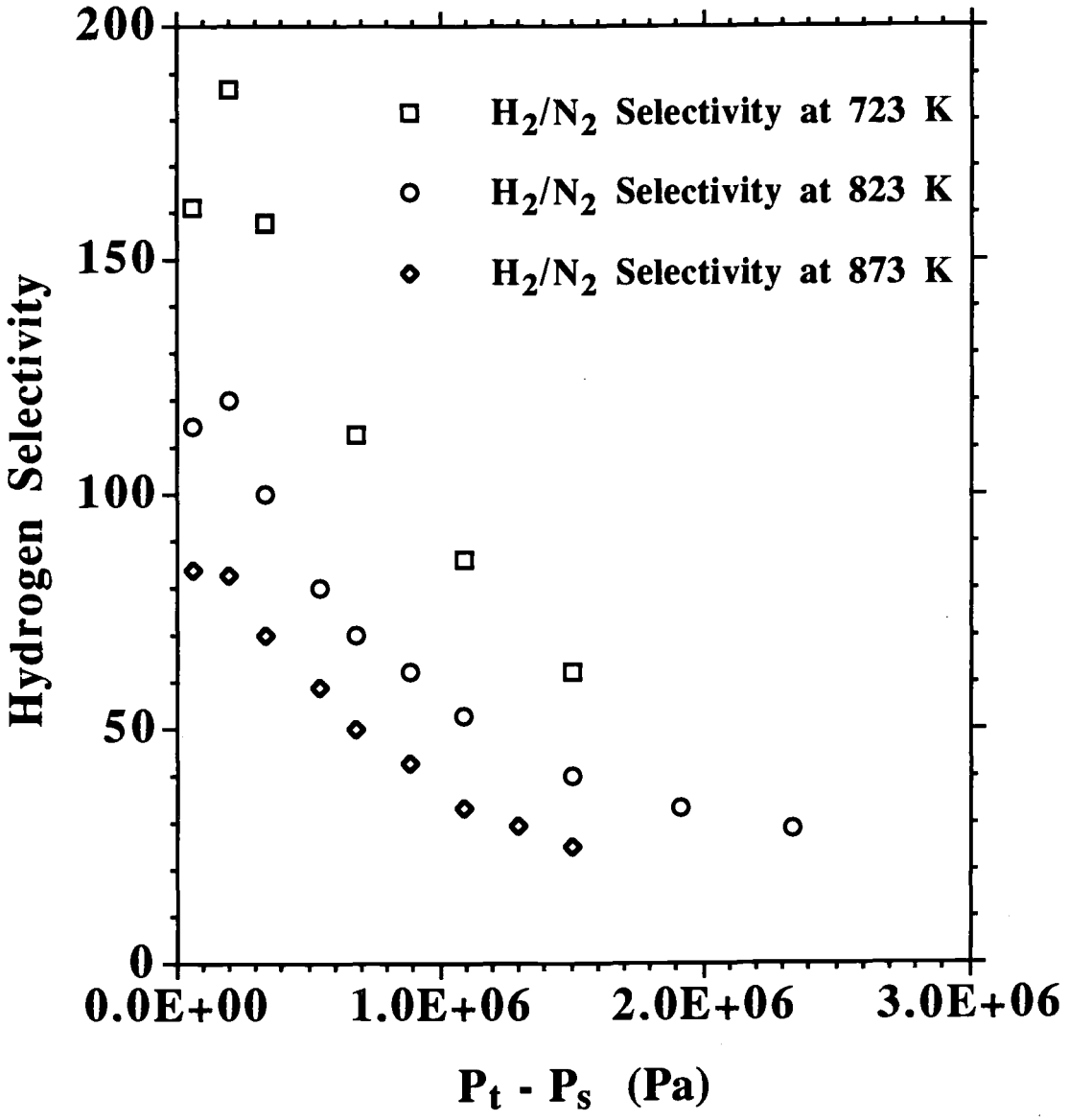

Figure 5.15 Hydrogen Selectivity Data for Composite Palladium-Ceramic Membrane with 19 μm Palladium Film. Hydrogen selectivity defined as ratio of hydrogen permeation rate to nitrogen permeation rate at the same transmembrane pressure difference.

sweep gas flowed through the shell side. The nitrogen flow rate in the permeate stream was compared to the hydrogen flow rate when pure hydrogen was flowed through the membrane under the same experimental conditions. The calculated hydrogen/nitrogen selectivities were greater than 1300 over the temperature range of 723 to 823 K. Therefore, the hydrogen selectivity of this membrane was similar to the selectivity of the membrane with the 11.4 μm palladium film.

Results of Experiments with Gas Mixtures

Experiments with feed gas mixtures of hydrogen, nitrogen, and helium were also performed to test for the presence of gas phase mass transfer resistance in the membrane tube. No sweep gas was used so the permeate gas had a high hydrogen concentration. Therefore, gas film resistance on the permeate side is assumed to be minimal. The $\bar{P}_H$ and n(H) values listed in Table 5.7, and $\bar{P}_J$ and n(J) listed in Table 5.8 were used in a membrane separator model to predict the hydrogen flow rate in the permeate stream. The model was the membrane reactor simulation model operated without the chemical reaction terms. The predicted hydrogen permeate flow should match the experimental flow if gas film mass transfer resistance in the membrane tube is insignificant. Results of the gas mixture experiments are summarized in Table 5.9.

Predicted flows were generally higher with the percent difference between predicted and actual flows generally less than 20 percent. Some of the difference is due to experimental error in the measured hydrogen concentration of the permeate stream. There appears to be some mass transfer resistance but simulations performed with pure gas permeabilities provide a reasonable estimate of the hydrogen permeation rate.

A more definitive conclusion regarding gas film resistance cannot be made for the following reasons. The ratios of predicted to actual permeate hydrogen flows do not follow a set pattern. The ratio decreased with increasing flow rate for the membrane with the 19 μm palladium film. Conversely, the ratio increased with increasing flow rate for the membrane with the 12.2 μm palladium film. This is opposite of the expected trend of a decreasing ratio with increasing flow rate. Gas film mass transfer coefficients increase as the flow rate increases so the ratios should have decreased with increasing flow rate. A possible explanation for the observed results is that hydrogen pressures in the reject and permeate stream were almost equal at the lower flow rates. This means that the membrane length was close to the length needed to achieve the maximum hydrogen flow in the permeate stream. Therefore, predicted and actual flows

Table 5.9

Comparison of Predicted and Actual Hydrogen Permeate Flows for Gas Mixture Study

Membrane	T (K)	P_t (kPa)	P_s (kPa)	Tube Inlet (sccm)[a]	Y_{H_2tin}	Y_{N_2tin}	Y_{Hetin}	Actual H_2 Permeate Flow (sccm)[a]	Ratio[b]
11.4 μm palladium film on ceramic membrane with 200 nm pore layer	823	1618	110	408	0.20	0.48	0.32	63	0.97
	823	1618	110	574	0.20	0.48	0.32	85	0.99
	823	1618	110	812	0.20	0.48	0.32	109	1.06
	823	1618	110	819	0.20	0.26	0.54	121	1.00
	823	1618	110	814	0.21	0.00	0.79	121	1.07
	823	1618	117	1018	0.21	0.48	0.31	135	1.10
	823	1618	110	820	0.30	0.00	0.70	206	1.01
	873	1618	110	816	0.20	0.48	0.32	120	0.97
	873	1618	112	1017	0.20	0.48	0.32	153	0.99
12.2 μm palladium film on ceramic membrane with 200 nm pore layer	823	1480	112	401	0.50	0.50	0.00	185	1.00
	823	1480	117	800	0.50	0.50	0.00	332	1.08
	823	1480	119	1214	0.50	0.50	0.00	414	1.17
	823	1480	115	1201	0.35	0.65	0.00	259	1.20
	823	1480	110	410	0.20	0.80	0.00	61	0.98
	823	1480	112	801	0.20	0.80	0.00	98	1.11
	823	1480	115	1207	0.20	0.80	0.00	120	1.21
	823	1480	112	1596	0.20	0.80	0.00	128	1.35
	823	2169	117	685	0.50	0.50	0.00	323	1.01
	823	2169	119	798	0.50	0.50	0.00	369	1.02
	823	2169	122	999	0.50	0.50	0.00	439	1.06
	823	2169	124	1200	0.50	0.50	0.00	491	1.11
19 μm palladium film on ceramic membrane with 200 nm pore layer	823	997	110	484	0.20	0.80	0.00	51	0.96
	823	997	110	1003	0.20	0.80	0.00	61	1.07
	823	997	110	1497	0.20	0.80	0.00	67	1.07
	823	997	110	2081	0.20	0.80	0.00	72	1.05
	823	997	110	2500	0.20	0.80	0.00	79	0.98

[a] sccm equal cm^3(STP)/minute

[b] Ratio defined as predicted hydrogen permeate flow divided by actual flow.

should agree at the lower flow rates even if gas film mass transfer resistance was present. As the flow rate increased, the membrane with the 12.2 μm palladium film was not long enough to achieve the maximum hydrogen removal. The increase in the ratio of predicted to actual hydrogen flow rates with increasing flow rate is a symptom of gas film mass transfer resistance. The ratios should eventually have started to decrease if experiments were conducted at higher flow rates.

Ratios of actual to predicted hydrogen permeate flows for the membrane with the 11.4 μm palladium film were all within 10 percent but also tended to increase with increasing flow rate. Experimental flow rates were lower for this membrane and hydrogen pressures in the reject and permeate streams were close to equilibrated at all flow rates. Therefore, the predicted and actual hydrogen permeate flows should show better agreement than those for the membrane with the 12.2 μm palladium film. In addition, the membrane with the 11.4 μm palladium film was packed with catalyst since it was used in membrane reactor experiments for ammonia decomposition. The packing material increases the gas velocity which increases the gas film mass transfer coefficient. The plug flow assumption used in the membrane separator model is also more valid for tubes packed with catalyst than empty tubes.

Ratios of actual to predicted hydrogen permeate flows for the membrane with the 19 μm palladium film generally followed the expected trend of a decreasing ratio with increasing flow rate. This membrane was less permeable to hydrogen than the membranes with 11.4 and 12.2 μm palladium films and also was shorter in length. The active length of the membrane was only 3.8 cm compared to 5.5 cm for the other two membranes. Therefore, it was not long enough to achieve the maximum hydrogen removal, except at the lowest flow rate. Since the membrane was the least permeable to hydrogen, gas film resistance at the higher flow rates had less impact than for the other two membranes.

No attempt was made to estimate gas film mass transfer coefficients from experimental results obtained with gas mixtures.

Comparison of Hydrogen Permeation Rates for Inorganic Membranes

Table 5.10 compares the hydrogen permeation rate at a transmembrane pressure difference of 690 kPa for the membrane with the 11.4 μm palladium film to hydrogen permeation rates estimated for inorganic membranes from other studies. With the exception of the ceramic membrane, composite palladium-microporous membranes

Table 5.10

Comparison of Hydrogen Permeation Rates for Inorganic Membranes[a]

Membrane Description	T (K)	Hydrogen Permeation Rate (moles/m^2·s)	Reference
composite palladium-ceramic membrane (11.4 μm palladium film)	823	0.71	this work
composite palladium-porous glass membrane (13 μm palladium film)	773	0.56[b]	Uemiya et al. (1988)
composite metal membrane (25 μm palladium film on 30 μm vanadium foil with 1 μm intermetallic diffusion barrier between palladium and vanadium)	973	0.30[c]	Edlund (1992)
composite metal membrane (2 μm palladium film on 0.2 cm thick niobium disk)	698	0.09[b]	Buxbaum (1992)
metal oxide membrane (SiO_2 deposited in pores of 4 nm Vycor glass membrane)	723	0.015[b]	Tsapatis et al. (1991)
ceramic membrane (asymmetric membrane with 4 nm pore top layer)	811	23[b]	Wu et al. (1993)

a Permeation rates are based on a feed pressure of pure hydrogen equal to 790610 Pa and a permeate pressure of 101325 Pa.

b Permeation rates estimated from hydrogen permeability data reported in cited references.

c Permeation rate taken directly from cited reference.

have the highest hydrogen permeation rates. The hydrogen permeation rate for the membrane from this work is very close to the permeation rate estimated for the composite palladium-microporous glass membrane of Uemiya and coworkers when the effect of temperature is included.

CONCLUSIONS

The composite palladium ceramic membranes prepared in this study have both a high hydrogen permeability and selectivity. Improvements in membrane sealing should further increase the hydrogen selectivity. Experiments conducted at temperatures to 913 K and transmembrane pressure differences to 2330 kPa show that composite metal-ceramic membranes can operate at high temperatures and pressures. Results of this study demonstrate the potential for using composite metal-ceramic membranes in membrane reactors including applications that require operation at relatively high temperatures and transmembrane pressure differences.

CHAPTER VI
MEMBRANE AND CONVENTIONAL REACTOR STUDIES

INTRODUCTION

Results of membrane reactor and conventional reactor experiments are presented in this chapter. The main objective of the membrane reactor experiments was to perform an experimental evaluation of a composite palladium-ceramic membrane reactor for ammonia decomposition. A second objective of the membrane reactor experiments was to test the accuracy of the membrane reactor model discussed in Chapter IV. The experimental pressure, temperatures and feed gas composition were within the range of conditions found in IGCC processes. Experimental conditions were similar to those that would be used in an industrial application since no inlet sweep gas was used and the membrane was operated at a high transmembrane pressure difference. The membrane was the composite palladium-ceramic membrane with 11.4 μm palladium film discussed in Chapter V. Conventional reactor experiments were performed to make a direct comparison of ammonia conversions from a membrane reactor to those from a conventional reactor operated under identical conditions. This shows the advantage of using the membranes developed in this study. Another objective of the conventional reactor experiments was to collect data to estimate interphase mass transfer coefficients because results of the membrane reactor experiments indicated that the C_1 value estimated in Chapter III was too low.

EXPERIMENTAL

Experimental procedures for the conventional and membrane reactor experiments were similar to procedures for the membrane characterization experiments. The membrane was the composite palladium-ceramic membrane with 11.4 μm palladium film discussed in Chapter V. Membrane characterization experiments were performed for this membrane during the same time period as the membrane reactor experiments. Hydrogen, nitrogen, and helium permeation experiments at 823 and 873 K were performed right after the membrane reactor experiments for those temperatures were completed. Hydrogen and nitrogen concentrations measured in the residue and permeate streams during the membrane reactor experiments were used in the gas mixture analysis discussed in Chapter V.

Figure 6.1 shows a cross section of the experimental packed bed membrane reactor. The membrane was packed with the supported nickel catalyst discussed in Chapter III. Catalyst was packed inside the membrane tube along the entire 5.5 cm active length. The catalyst was held in place with quartz wool plugs inserted at both ends. The conventional reactor was similar to the membrane reactor except a nonporous alumina tube with 0.6 cm ID and 1 cm OD replaced the membrane. The same mass of catalyst was used in both the membrane and conventional reactors to allow direct comparison of the experimental ammonia conversions.

Table 6.1 summarizes experimental conditions for the membrane and conventional reactor studies. Gas compositions, temperatures, and pressures were within the range of conditions found in IGCC processes. The experimental procedure consisted of running gas mixtures through the reactors at various temperatures. The main objective of the experimental measurements was to determine the ammonia conversion. The effluent ammonia flow rate was determined by measuring effluent gas compositions with the GC and effluent flow rates with bubble flow meters. Ammonia conversions were then calculated from Equation 4.24. Hydrogen, nitrogen, and helium effluent flows were determined from GC analysis and mass balance calculations when desired.

The membrane module shown in Figure 5.2 was used for both the conventional and membrane reactor experiments. A nonporous alumina tube was used for the shell side of the membrane module. The cocurrent flow configuration was used in the membrane reactor experiments. As discussed in Chapter IV, there is no advantage associated with either the cocurrent or countercurrent flow configuration when a membrane with infinite hydrogen selectivity is operated at a low pressure ratio ($P_r<0.1$). The membrane used in the membrane reactor had a very high hydrogen selectivity and was operated at a P_r value of approximately 0.07 so there was no or little advantage associated with either flow configuration. The flow system was similar to the system used in membrane characterization experiments except a minor modification was made to allow for GC analysis of ammonia in addition to hydrogen and nitrogen in effluent gas streams. GC analysis procedures are discussed later in this section. Figure 6.2 shows a schematic of the experimental flow system. Sealing procedures were identical to those discussed for the membrane characterization experiments. Grafoil seals and metal compression fittings were used to connect both the membrane and conventional reactor to gas plumbing lines. The membrane reactor experiments were conducted with the shell side at close to atmospheric pressure and no inlet sweep

Table 6.1
Experimental Conditions for Membrane Reactor Studies

	Membrane Reactor	Conventional Reactor
Feed composition (mol %)		
ammonia	0.33 to 0.34	0.33 to 0.34
nitrogen	0 to 48	0 to 48
hydrogen	10 to 30	5 to 30
helium	balance	balance
Feed flow rate:		
(mol/s)	$2.2 \cdot 10^{-4}$ to $7.6 \cdot 10^{-4}$	$2.2 \cdot 10^{-4}$ to $7.7 \cdot 10^{-4}$
(sccm)[a]	300 to 1020	300 to 1040
Shell-side inlet flow rate	0	—
Feed (tube) pressure (kPa)	1618	1618
Shell-side pressure (kPa)	108 to 117	—
Temperature (K)	723 to 873	723 to 873
Reactor tube ID (m)[b]	0.007	0.006
Reactor length (m)	0.055	0.075
Catalyst weight (kg)	$1.2263 \cdot 10^{-3}$	$1.2263 \cdot 10^{-3}$
Reactor description	Composite palladium-ceramic membrane (11.4 μm palladium film on inside surface of 200 nm asymmetric ceramic membrane) packed with catalyst.	Nonporous alumina tube packed with catalyst.

[a] sccm = cm^3 (STP)/min

[b] ID = inside diameter

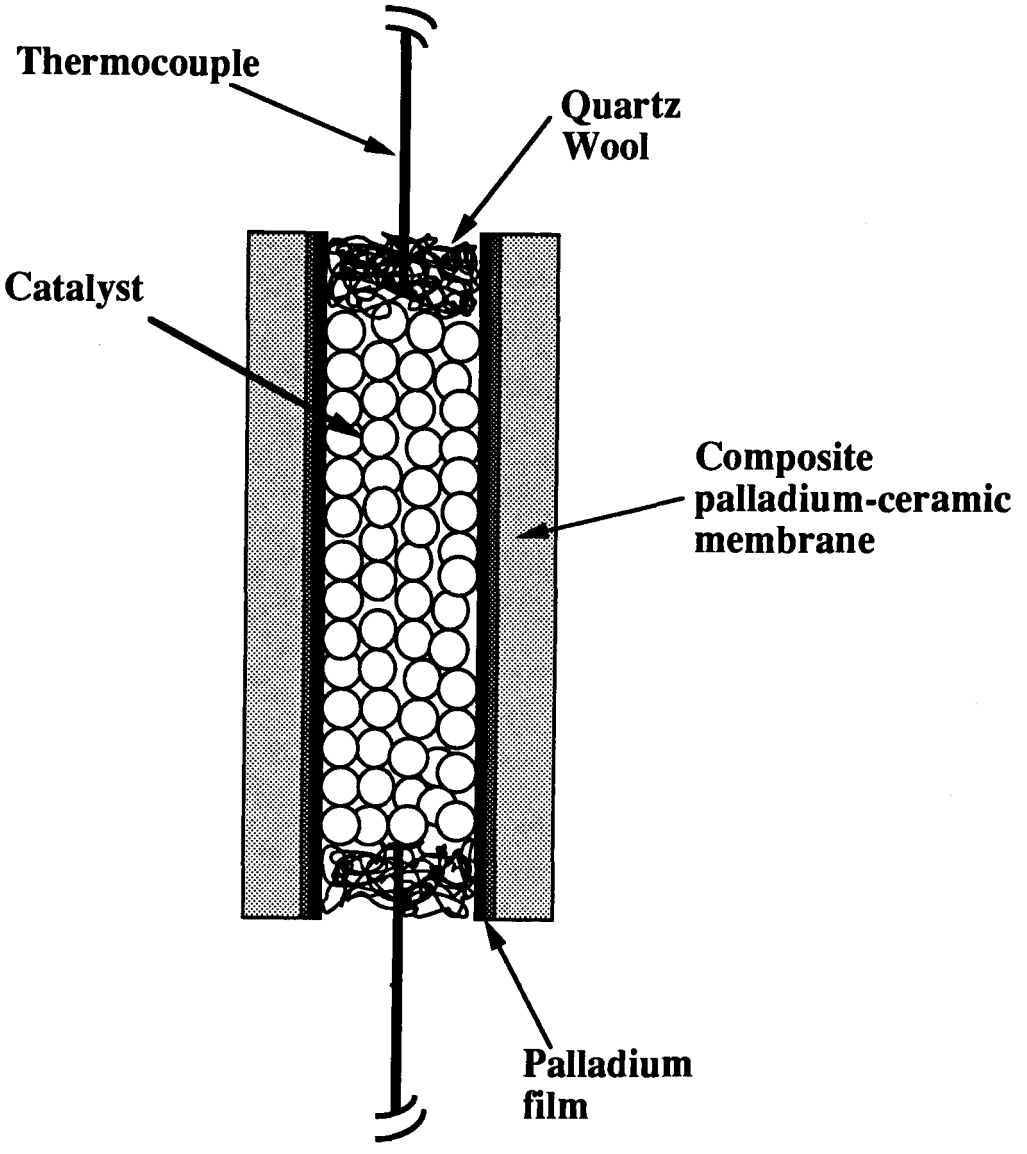

Figure 6.1 Cross-section of Packed Bed Membrane Reactor.

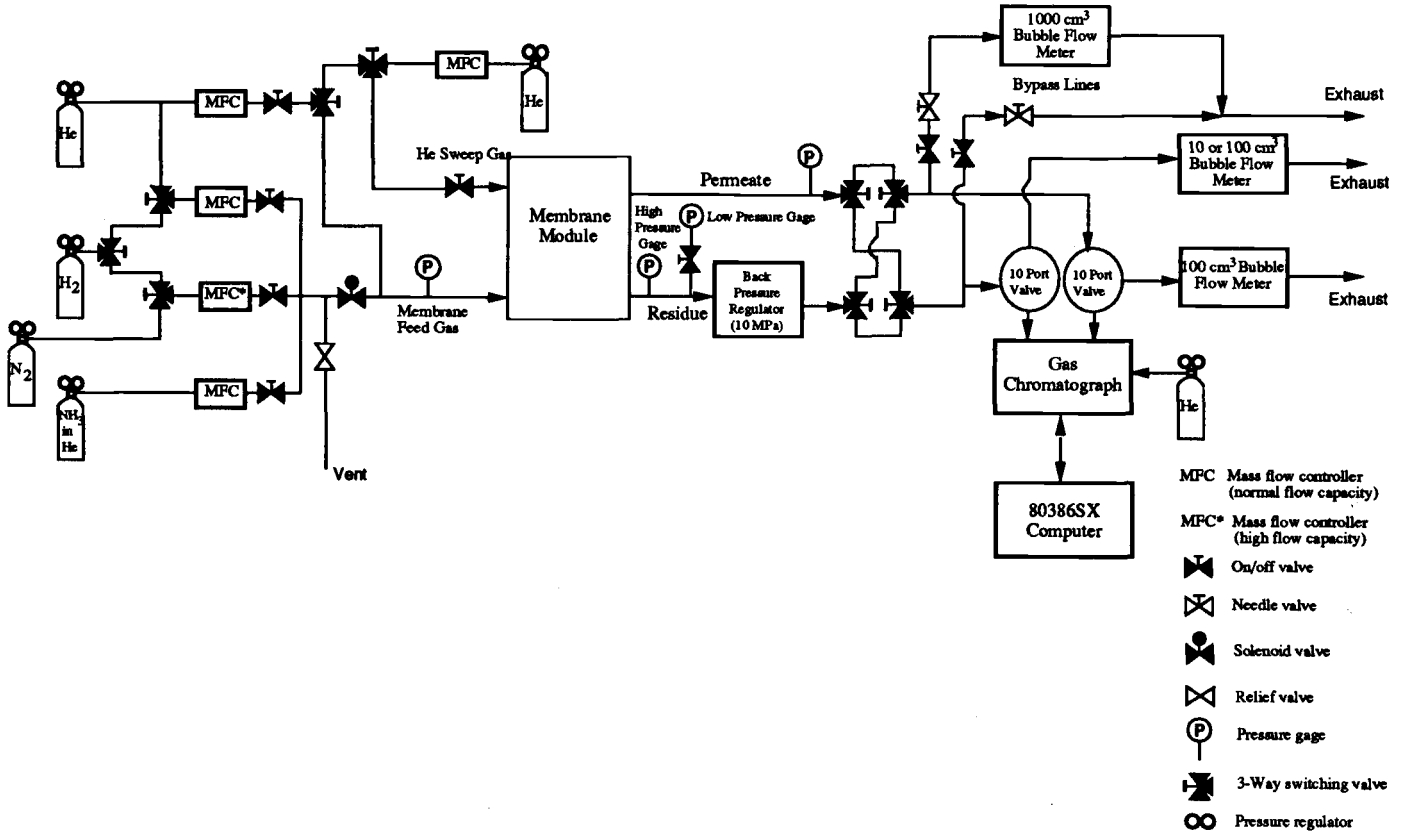

Figure 6.2 Experimental System for Membrane and Conventional Reactor Experiments

gas. A helium sweep gas flowed through the shell side during the conventional reactor experiments to prevent oxidation of the seals. The leak rate through the Grafoil seals in the conventional reactor experiments was approximately 2 cm^3(STP)/minute at 873 K. This leak rate is minimal compared to the total gas flow rates. Startup procedures were the same as those used in the membrane characterization experiments.

Membrane reactor and conventional reactor temperatures were monitored with Type K thermocouples inserted at both the reactor inlet and outlet, as shown in Figures 5.2 and 6.1. The inlet thermocouple was connected to the CN9000 Omega temperature controller to control the reactor temperature. The reactor inlet temperature was generally higher than the outlet temperature. Reactor temperature was taken as the average of the inlet and outlet temperatures. During runs performed for a particular average temperature, the inlet temperature was either raised or lowered to keep the average reactor temperature constant. The temperature difference is attributable to a non uniform temperature profile in the furnace rather than heat of reaction since it was also present in permeability experiments. The average temperature difference in the membrane reactor experiments was 7 K, and the maximum temperature difference was 14 K. The temperature difference was 7 K or less in 15 of the 22 membrane reactor experiments, and 12 K or less in 21 of the 22 experiments. The average temperature difference in the conventional reactor experiments was only 2 K, and the maximum temperature difference was 8 K. The lower temperature differences associated with the conventional reactor experiments are attributable to more optimum positioning of the membrane module in the furnace.

The ammonia source for the membrane and conventional reactor experiments was a gas cylinder containing 1.4 mole percent ammonia in helium. The ammonia content was determined by GC analysis of the gas. The calibration curve for this analysis was developed using a certified mixture of ammonia in helium. The ammonia concentration in the certified mixture was independently verified using the procedure described in Chapter III. The certified mixture was run through a quartz tube packed with the supported nickel catalyst at temperatures from 773 K to 1173 K. Since no hydrogen was present in the inlet gas the equilibrium ammonia conversion was essentially 100 percent. The nitrogen concentration in the reactor effluent was measured by GC analysis of the gas. The inlet ammonia concentration was then calculated from the effluent nitrogen concentration and reaction stoichiometry. The effluent nitrogen concentration was constant at temperatures above about 873 K indicating that all ammonia had decomposed.

Calibrated mass flow controller settings were used to determine inlet gas compositions. The sum of the measured residue and permeate flow rates were used to determine the total inlet gas flow rate for the membrane reactor experiments while only the measured residue flow was used for the conventional reactor inlet flow since no gas was permeated. The effect of ammonia decomposition on the measured outlet flows was not considered since the inlet ammonia concentration was very dilute. Measured outlet flows and flows predicted from the mass flow controller settings showed good agreement. The percent difference between the total measured outlet flow and flow predicted from mass flow controller settings was less than 2 percent on 11 of the 22 membrane reactor experiments, less than 3 percent on 18 of 22 experiments, and less than 4 percent on 21 of the 22 experiments. The percent difference was about 5 percent on the remaining membrane reactor experiment. For the conventional reactor experiments, the percent difference was less than 2 percent on 27 of 38 experiments, less than 3 percent on 34 of 38 experiments, and less than 4 percent on all experiments.

The majority of any difference between measured flows and flows predicted from the mass flow controller settings is attributable to errors in the predicted nitrogen flow. This is due to the high flow capacity mass flow controller used for nitrogen during reactor experiments as opposed to the other gases. The nitrogen mass flow controller was sized for 5000 cm^3(STP)/minute of nitrogen while the other controllers were sized for 500 cm^3(STP)/minute of helium or nitrogen. Therefore, predicted nitrogen flows were less accurate than predicted flows for the other gases. The high capacity flow controller was needed when hydrogen permeation experiments were conducted for the membrane to avoid breaking gas plumbing connections during the experiments. Hydrogen was switched to the high flow capacity flow controller when the hydrogen permeation experiments were performed to allow for experimental measurements at high pressures. Another possible explanation for the slight differences between measured and predicted flows is gas leakage out of the high pressure connections used on the membrane feed and residue. As shown in Figure 5.2, several connections were needed for thermocouples etc. and it is possible that a few cm^3/minute leak rate was associated with the combined high pressure connections.

The GC was used to determine ammonia and hydrogen concentrations in the residue and permeate streams from the membrane reactor experiments, and the nitrogen concentration in the permeate stream. The nitrogen concentration in the residue stream was too high to measure with the 0.25 cm^3 sample loop volume used to measure the hydrogen concentration. Reducing the sample loop size was not an option because the

hydrogen peaks would be too small to measure with a sample loop less than 0.25 cm^3. Therefore, the residue nitrogen concentration was estimated from mass balance calculations. Mass balance calculations were also used to estimate effluent helium concentrations since helium was the carrier gas in the GC. Only the effluent ammonia concentrations were needed to determine the ammonia conversion in the membrane reactor. Effluent nitrogen and hydrogen concentrations were used for the gas mixture experiments discussed in Chapter V. Effluent hydrogen and nitrogen concentrations were measured for most but not all of the membrane reactor experiments. Only the effluent ammonia concentration was measured in the conventional reactor experiments.

GC procedures were somewhat different than those previously discussed in Chapters III and V for the differential reactor and membrane characterization experiments. Effluent nitrogen concentrations could not be used to determine ammonia conversions since nitrogen was present at high concentrations in the feed gas and ammonia was present at dilute concentrations. In addition, one column which would allow simultaneous analysis of ammonia, nitrogen, and hydrogen for the desired experimental conditions was not found. The reason is that there was severe tailing in the ammonia peak for columns long enough to separate hydrogen, nitrogen, and ammonia. Based on recommendations from Alltech, columns using the Hayesep Q, P, and D packing material were tried but none could separate the gases and give a reasonable ammonia peak. An additional problem was that a 2 cm^3 sample loop was needed to obtain ammonia peaks large enough to quantify accurately at low ammonia concentrations. It was desirable to analyze ammonia concentrations as low as about 0.015 mole percent in the membrane reactor experiments. It was not possible to measure nitrogen concentrations greater than 1 mole percent with the 2 cm^3 sample loop since the column was overloaded with nitrogen and could not produce a good peak at higher concentrations.

The ammonia concentration measurement problem was solved by using one column to measure the ammonia concentration and another to measure nitrogen and hydrogen concentrations. A 2.44 m Hayesep Q column and 2 cm^3 sample loop was used to determine the ammonia concentration. The GC oven was temperature programmed from 413 K to 483 K at a 70 K/minute ramp rate to reduce tailing of the ammonia peak. Under these conditions, baseline to baseline separation of the nitrogen and ammonia peaks was not achieved when the nitrogen concentration was above about 5 mole percent. Therefore, three different sets of ammonia calibrations were performed

with nitrogen concentrations that were typical of nitrogen concentrations in residue and permeate streams from the membrane and conventional reactor experiments.

One set of ammonia calibrations was performed with no nitrogen in the calibration gas. These calibration data were used to determine ammonia concentrations in the permeate gas where the nitrogen concentration was relatively low, and in the residue stream from experiments conducted with no nitrogen in the inlet gas. A second set of ammonia calibrations was performed with a nitrogen concentration of 29 mole percent. These data were used to measure ammonia concentrations in residue streams from membrane reactor experiments conducted with an inlet nitrogen concentration of 25 mole percent. The 29 mole percent concentration is approximately the effluent nitrogen concentration from these experiments. A third set of ammonia calibrations was performed with a nitrogen concentration of 56 mole percent. These data were used to determine ammonia concentrations in the residue streams from experiments conducted with inlet nitrogen concentrations of 48 mole percent. There were only minor differences in the calibration curves for the three nitrogen concentrations but calibrating at three different concentrations improved the accuracy of the ammonia concentration measurement. There was minimal loss in accuracy when for example the 56 mole percent nitrogen calibration data were used to determine effluent concentrations from conventional reactor experiments with 48 mole percent nitrogen. The calibration curves were all linear with correlation coefficients (r^2) greater than 0.999.

A Molecular Sieve 13X column was used to separate the hydrogen and nitrogen peaks. The GC was operated at an oven temperature of 308 K during these measurements.

Ammonia, and hydrogen and nitrogen concentrations were measured at separate times because the GC was operated under different conditions for the ammonia measurement. The general procedure was to monitor the ammonia concentration in the residue stream until a steady value was achieved. The GC oven temperature was then reduced and nitrogen and hydrogen concentrations were evaluated in the residue and permeate streams. The ammonia concentration in the permeate stream was then measured. The ammonia concentration in the residue stream was then generally analyzed again to make sure it had not changed from the initial measurement. Since the sample loops for the two columns were located on separate 10 port sampling valves, three-way switching valves were used to direct residue and permeate streams to the desired sample loop. The valve configuration is shown in Figure 6.2. One 10 port valve was connected to the 2 cm^3 sample loop and Hayesep Q column for ammonia

analysis and the other was connected to the 0.25 cm^3 sample loop and Molecular Sieve 13X column for analysis of nitrogen and hydrogen. Constant sample loop flows of about 50 cm^3/minute were maintained by directing most of the residue and permeate gas streams through the bypass lines.

MODELING PROCEDURES

The membrane reactor model discussed in Chapter IV was used to predict conversions from the membrane reactor experiments. Reaction rates were estimated using the Temkin-Pyzhev Equation (Equation 4.9). There was little difference in reaction rates calculated from the Temkin-Pyzhev Equation and Modified Temkin-Pyzhev Equation at the pressure used in the membrane reactor experiments. Effectiveness factors (η) were estimated using the equations presented in Chapter IV. Hydrogen permeation rates were calculated using Equations 5.3 and 5.4. Permeation rates for nitrogen, helium, and ammonia were calculated from Equation 5.5. The assumptions made in the derivation of Equation 5.5 were that nitrogen, helium, and ammonia permeation occurs throughout the membrane even though it actually occurs through localized leaks in the membrane seals or defects in the palladium film. The error associated with this assumption is small since the hydrogen selectivity of the membrane was very high. The membrane reactor model was converted to a conventional reactor model by setting the gas permeabilities to zero.

Tables 6.2 and 6.3 summarize the input parameters used in the membrane reactor and conventional reactor modeling calculations. Input flow rates, gas compositions, temperatures, pressures, and reactor characteristics matched the experimental conditions. With the exception of the ammonia permeability, gas permeabilities were calculated from experimental data obtained for the membrane. The ammonia permeability was calculated by dividing the helium permeability by 1.25. As discussed in Chapter V, gas permeation through seals or defects is believed to be impacted by both Knudsen diffusion and viscous flow. The ratio of pure nitrogen to pure helium permeation rates at the experimental pressure was about 1.5. The ratio of ammonia to helium permeation rates should be between 1.0 and 1.5 so a value of 1.25 was chosen. Helium, nitrogen, and ammonia permeabilities were assumed to be independent of temperature. The permeabilities at 823 K were used at all temperatures. With the exception of the proportionality constant (C_1) in the correlation for Bi_j (Equation 4.22), values for kinetic and catalyst parameters were experimentally determined as discussed

Table 6.2

Input Parameters Used in Membrane Reactor Modeling Calculations

Reactor size (m)	$R_1 = 0.0035$ $t_m = 11.4 \cdot 10^{-6}$ $L_o = 0.055$
Gas flow rate at tube inlet (mol/s)	$F_{TO} = 2.2 \cdot 10^{-4}$ to $7.6 \cdot 10^{-4}$
Gas flow rate at sweep inlet (mol/s)	$Q_{TO} = 1.0 \cdot 10^{-8}$ of hydrogen
Gas composition at tube inlet (mol %)	
ammonia	0.335
nitrogen	0 to 48
hydrogen	10 to 30
helium	balance
Reactor pressures	$P_t = 1618$ kPa $P_r = 0.07$
Kinetic parameters	$k_o = 1.09 \cdot 10^{20}$ (mol/m^3•s•Pa$^{-0.674}$)
	$E = 2.304 \cdot 10^5$ (J/mol)
	$\beta = 0.674$
	$C_1 = 0.015$
Catalyst parameters	$\rho_p = 970$ kg/m^3
	$Sg = 220000$ m^2/kg
	$\tau_p = 4$
	$\theta = 0.5$
	$\varepsilon = 0.4$
	$R_p = 0.36 \cdot 10^{-3}$ (m)
Gas permeabilities	$\bar{P}_A = 1.40 \cdot 10^{-16}$ (mol•m/m^2•s•Pa$^{1.374}$)
	$\bar{P}_N = 1.53 \cdot 10^{-17}$ (mol•m/m^2•s•Pa$^{1.513}$)
	$\bar{P}_{HO} = 1.62 \cdot 10^{-8}$ (mol•m/m^2•s•Pa$^{0.580}$)
	$\bar{P}_I = 1.71 \cdot 10^{-16}$ (mol•m/m^2•s•Pa$^{1.374}$)
	$E = 8880$ J/mol
	$n(A) = 1.374$
	$n(N) = 1.513$
	$n(H) = 0.580$
	$n(I) = 1.374$

Table 6.3

Input Parameters Used in Conventional Reactor Modeling Calculations

Reactor size (m)	$R_1 = 0.003$ $L_o = 0.075$
Gas flow rate at tube inlet (mol/s)	$F_{TO} = 2.2 \cdot 10^{-4}$ to $7.7 \cdot 10^{-4}$
Gas composition at tube inlet (mol %)	
ammonia	0.33 to 0.34
nitrogen	0 to 48
hydrogen	5.4 to 30
helium	balance
Reactor pressures	$P_t = 1618$ kPa
Kinetic parameters	$k_o = 1.09 \cdot 10^{20}$ (mol/m^3•s•Pa$^{-0.674}$)
	$E = 2.304 \cdot 10^5$ (J/mol)
	$\beta = 0.674$
	$C_1 = 0.015$[a]
Catalyst parameters	$\rho_p = 970$ kg/m^3
	$Sg = 220000$ m^2/kg
	$\tau_p = 4$
	$\theta = 0.5$
	$\varepsilon = 0.4$
	$R_p = 0.36 \cdot 10^{-3}$ (m)

[a] Initially, C_1 was varied to determine the value which best fit the experimental results. The optimum value of $C_1 = 0.015$ was then used in subsequent modeling calculations.

in Chapters III and IV. Calculation procedures and the results of calculations used to estimate the value of C_1 are described below.

Evaluation of Interphase Mass Transfer Effect

Reaction rates from the differential reactor experiments discussed in Chapter III increased with increasing Re_p until a constant value was reached. As the temperature increased, it was necessary to decrease the reactor ID down to 0.3 cm to obtain data free from interphase mass transfer effects. The diameter of the membrane reactor was fixed at 0.7 cm so interphase mass transfer impacted the ammonia conversion in these experiments. The effect of interphase mass transfer was included in the membrane reactor model but an estimate for the proportionality constant (C_1) in Equation 4.22 was needed. A preliminary estimate of $C_1 = 0.002$ was made using four data points obtained during the differential reactor experiments. Results of the membrane reactor experiments indicate that this value is much too low. Conversions from the membrane reactor experiments were significantly higher than those predicted using the C_1 value of 0.002. Therefore, one objective of the conventional reactor experiments was to collect data that could be used to recalculate C_1 under conditions similar to those in the membrane reactor experiments.

An optimization calculation was used to estimate the C_1 value which best fit the experimental results obtained in the conventional reactor experiments. The procedure for this calculation was as follows:

1) A C_1 value was assumed.
2) The membrane reactor model was then run to predict the ammonia conversion for each conventional reactor experiment. Gas permeabilities were set to zero to convert the membrane reactor model to a model applicable for a conventional reactor operated in the integral mode.
3) For each experimental run, the predicted effluent ammonia flow was subtracted from the actual effluent ammonia flow and the difference was squared to determine the residual squared error.
4) The residual squared errors were then summed to obtain the total residual squared error associated with the C_1 value.

A range of C_1 values were evaluated by repeating the above calculations. The C_1 with the lowest total residual squared error is the value which best fits the experimental data.

A C_1 value of 0.03 was obtained when all 38 conventional reactor data points were included in the calculations. However, the predicted ammonia conversions were greater than the experimental conversions for a large portion of the data points. The reason is that 2 of the 38 data points accounted for nearly 25 percent of the total residual error. The two data points were obtained from experiments at 823 K with no nitrogen in the feed and feed hydrogen concentrations of 5.4 and 7.5 mole percent, respectively. These two data points drove the optimum C_1 to a higher value since their experimental conversions were significantly higher than the predicted conversions. A possible explanation is that the kinetic parameters obtained from the differential reactor experiments may be less accurate at low hydrogen concentrations at this temperature. A C_1 value of 0.05 was needed for agreement between experimental and predicted values for the 7.5 mole percent hydrogen concentration. Experimental conversion was always higher than the predicted conversion regardless of the C_1 value used for the 5.4 mole percent hydrogen concentration. An optimum C_1 value of 0.015 was obtained when the two data points were not included in the analysis. This C_1 value was used in the membrane reactor modeling calculations because it provided a better fit to the majority of the conventional reactor experimental results. In comparison, Satterfield (1980) recommended using a C_1 value of 0.07 as a rough approximation.

RESULTS AND DISCUSSION

Results of the membrane reactor and conventional reactor experiments are discussed below. This discussion summarizes the experimental results and also compares experimental results to those predicted by the membrane reactor model.

Conventional Reactor Results

Results of the conventional reactor experiments are summarized in Figures 6.3 to 6.5. Predicted ammonia conversions using a C_1 value of 0.015 are included in the figures. Figure 6.3 shows the influence of space time on ammonia conversion at 823, 848, and 873 K. The ammonia, hydrogen, and nitrogen concentrations in the gas feed were kept constant at approximately 0.335, 20, and 48 mole percent, respectively, and the feed flow rate was varied to obtain a range of space times. Ammonia decomposition was both kinetically and thermodynamically limited by the high

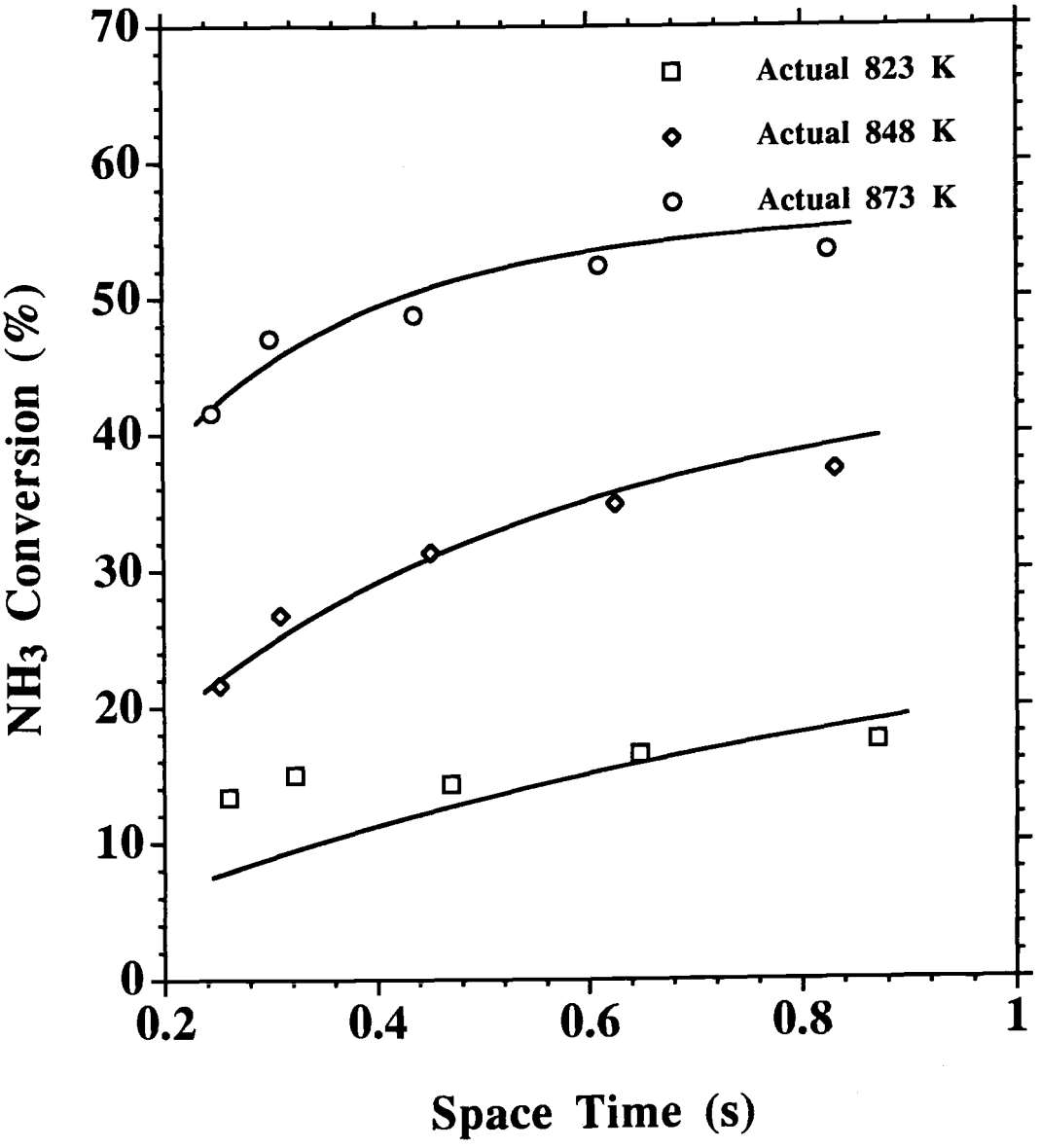

Figure 6.3 Effect of Space Time on Ammonia Conversion for Conventional Reactor. Feed gas concentrations were approximetely 0.335, 48, 20, and 31.665 mole percent for ammonia, nitrogen, hydrogen, and helium, respectively. Total feed gas flows were varied from approximately $2.2 \cdot 10^{-4}$ mol/s to $7.7 \cdot 10^{-4}$ mol/s (300 to 1040 sccm). The solid lines represent the predicted ammonia conversions.

hydrogen concentrations. Agreement between the model and experimental results is good under these experimental conditions.

Figure 6.4 shows the effect of the hydrogen concentration on ammonia conversion at 823 and 873 K for a constant feed gas flow rate of approximately $6.2 \cdot 10^{-4}$ mols/s. The inlet ammonia and nitrogen concentrations were approximately 0.335 and 48 percent, respectively. The inlet hydrogen concentration has a large impact on ammonia conversion, as expected. At 823 K, the ammonia conversion was only about 10 percent when the inlet hydrogen concentration was 20 mole percent. The ammonia conversion increased to 78 percent when the inlet hydrogen concentration was reduced to 5.4 mole percent. Agreement between the model and experimental results is good under these experimental conditions.

Figure 6.5 shows the effect of both the hydrogen and nitrogen concentrations on ammonia conversion for a constant feed gas flow rate of approximately $6.2 \cdot 10^{-4}$ mols/s. The inlet ammonia concentration was the same as in Figures 6.3 and 6.4. Ammonia conversion decreased as the nitrogen concentration increased but the impact of nitrogen is much less than for hydrogen. The observed experimental results are consistent with both the kinetic rate equation and thermodynamics. Increasing the nitrogen concentration decreases the ammonia decomposition rate and the equilibrium conversion. Agreement between model and experimental results is good except at hydrogen concentrations of 5.4 and 7.5 mole percent for the case of no nitrogen in the inlet gas. The disagreement between experimental and predicted conversions for these two data points was previously discussed.

Membrane Reactor Results

Figure 6.6 shows the effect of temperature on ammonia conversion for the membrane reactor. The experimental results shown in this figure were for a feed gas flow rate of $3.05 \cdot 10^{-4}$ mols/s with ammonia, hydrogen, and nitrogen feed concentrations of 0.335, 20, and 48 mole percent, respectively. The equilibrium conversion of the feed gas as well as conversions achieved in conventional reactor experiments operated under the same conditions are also shown in Figure 6.6. The significant advantage of the membrane reactor is clearly shown. An ammonia conversion of over 94 percent was achieved in the membrane reactor at 873 K. This was over 1.6 times higher than the 58 percent equilibrium conversion of the feed gas. The advantage of the membrane reactor is even more pronounced at lower

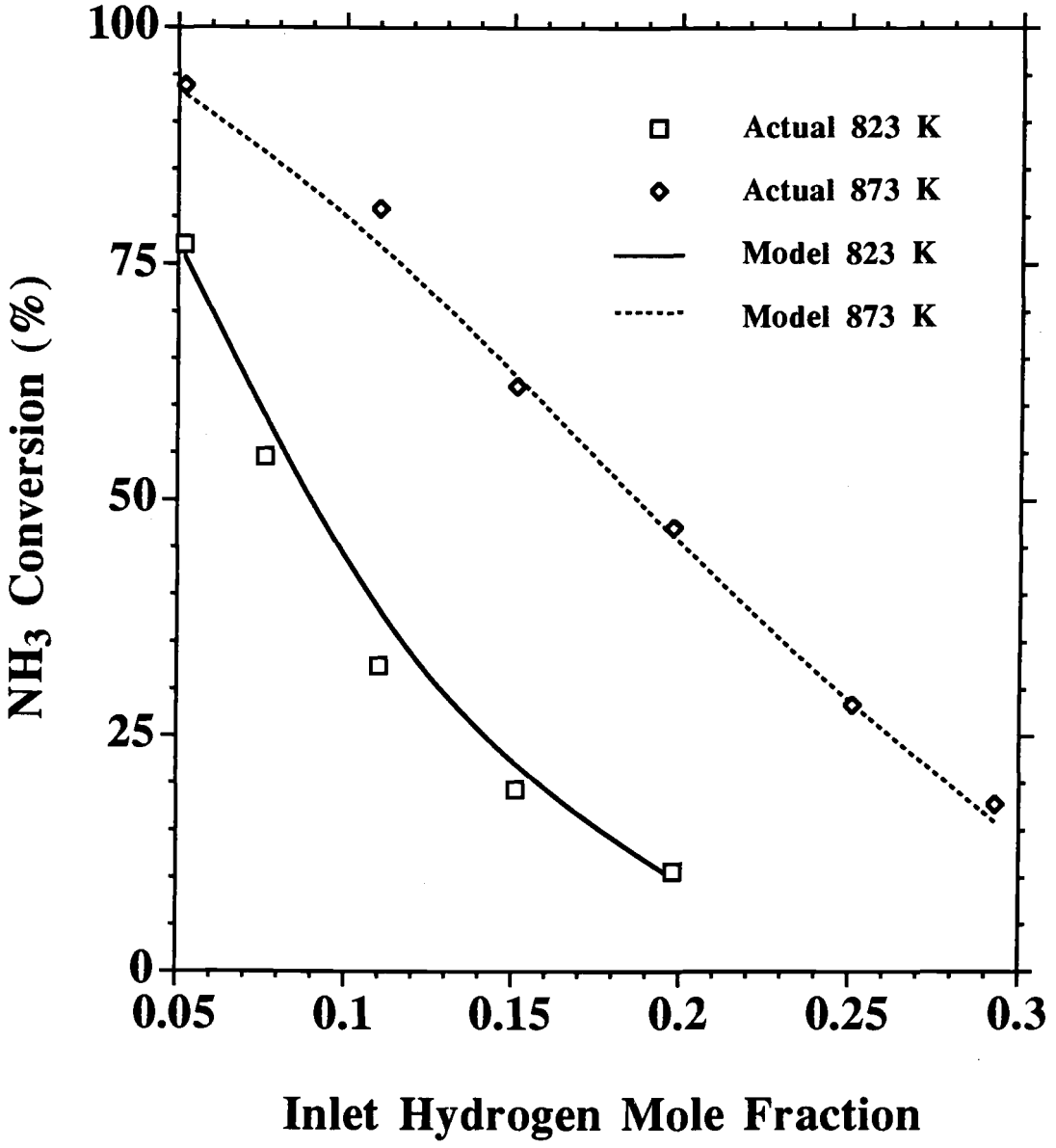

Figure 6.4 Effect of Hydrogen Concentration in Conventional Reactor Feed Gas on Ammonia Conversion. Feed gas concentrations were approximately 0.335 and 48 mole percent for ammonia and nitrogen, respectively. Helium made up the balance. Total feed gas flows were approximately $6.2 \cdot 10^{-4}$ mol/s (840 sccm).

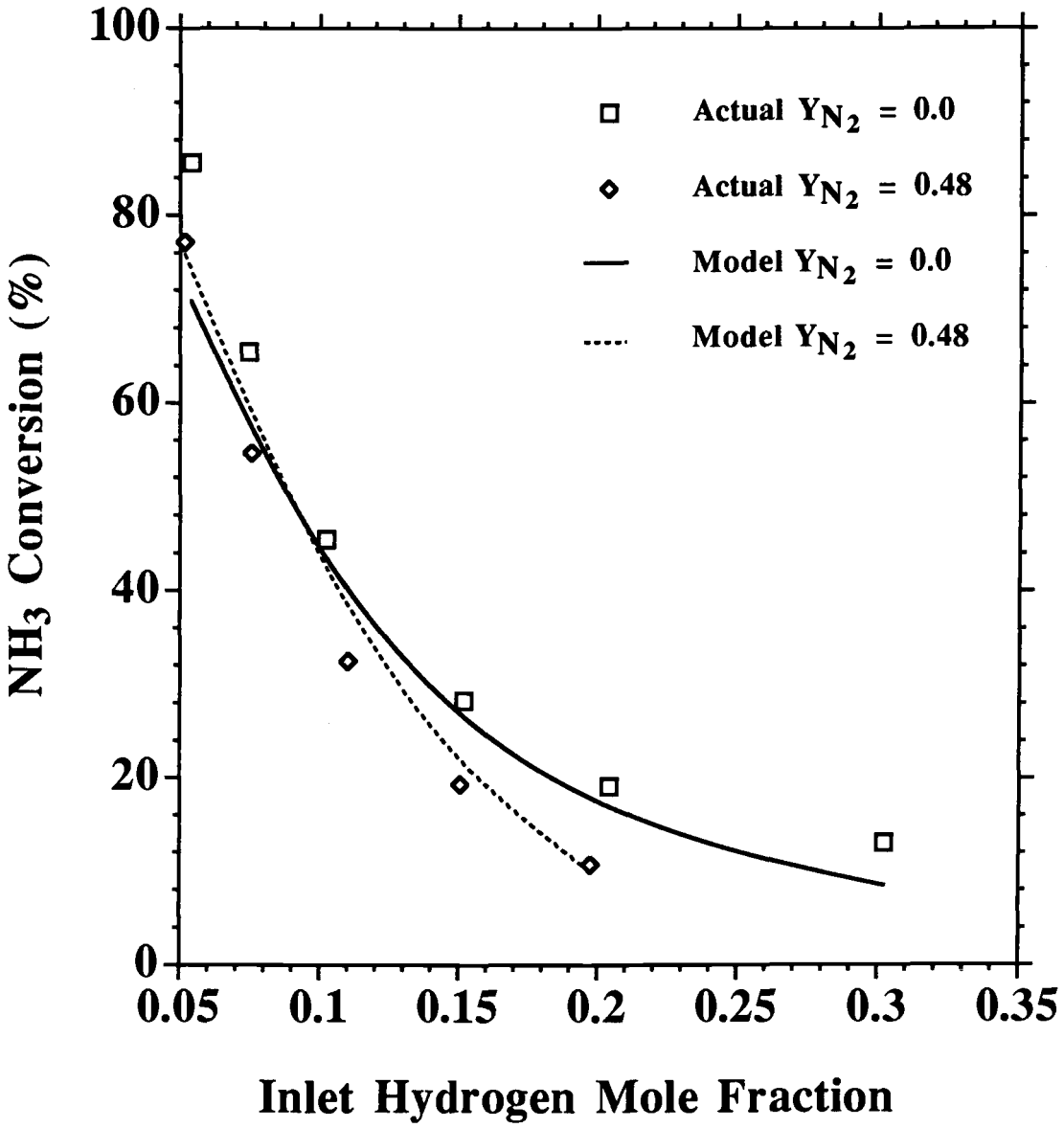

Figure 6.5 Effect of Nitrogen and Hydrogen Concentrations in Conventional Reactor Feed Gas on Ammonia Conversion at 823 K. Feed gas ammonia concentrations were approximately 0.335 mole percent. Helium made up the balance. Total feed gas flows were approximately $6.2 \cdot 10^{-4}$ mol/s (840 sccm).

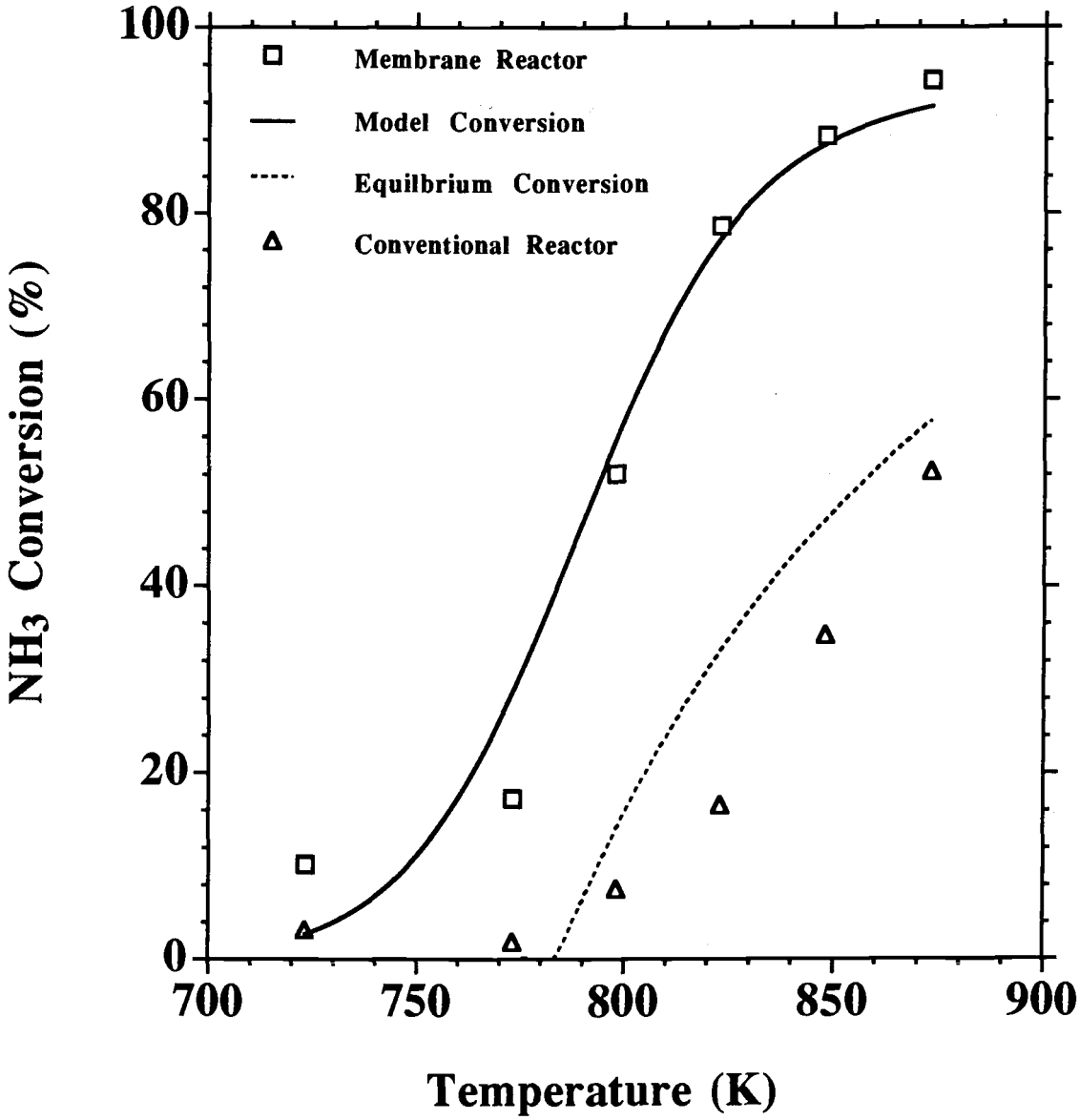

Figure 6.6 Effect of Temperature on Ammonia Conversion for Membrane and Conventional Reactors. Feed gas concentrations were approximately 0.335, 48, 20, and 31.665 mole percent for ammonia, nitrogen, hydrogen, and helium, respectively. Total feed gas flows were approximately $3.05 \cdot 10^{-4}$ mol/s (410 sccm).

temperatures. The ammonia conversion at 823 K was 79 percent compared to an equilibrium conversion of 33 percent for the feed gas, and a conversion of only 17 percent in the conventional reactor. Predicted and experimental conversions show good agreement at temperatures of 798 K and above. In addition, the shape of the predicted curve follows the trend in experimental values.

Figure 6.7 shows the effect of space time on ammonia conversion in the membrane reactor at 823, 848, and 873 K. Experiments were concentrated in the 823 to 873 K temperature region since the highest conversions were obtained in this temperature range. Feed concentrations were the same as those in Figure 6.6 and the feed gas flow rate was varied to obtain a range of space times. These experiments were conducted primarily to evaluate the accuracy of the membrane reactor model. All things considered, the model fits the experimental data quite well. Differences in the predicted and experimental results are attributable to several factors. The model assumes isothermal operation but there was actually a temperature gradient in the reactor. The ammonia decomposition rate is strongly dependent on temperature. The strong temperature dependence also means that errors associated with estimation of the preexponential factor (k_0) and activation energy (E_a) for the decomposition reaction impact modeling accuracy. The reaction rate also depends strongly on the hydrogen concentration which in turn depends on the hydrogen permeation rate. Hydrogen permeation rates were calculated using the hydrogen permeability measured in experiments conducted with pure hydrogen. It was assumed that there was no mass transfer resistance between the bulk gas and the palladium surface. With gas mixtures, mass transfer resistance between the bulk gas and palladium surface may impact the hydrogen permeation rate which in turn would impact the ammonia decomposition rate and conversion. Hydrogen concentrations measured in the residue and permeate stream were used to try to evaluate the accuracy of using pure gas permeabilities. Results of this analysis were discussed in Chapter V. It was difficult to draw a solid conclusion from the analysis because both experimental and predicted hydrogen partial pressures were close to equilibrated at the end of the membrane. Hydrogen partial pressures were also close to equilibrated when the hydrogen permeability was reduced by 25 percent in the modeling calculations. Therefore, the experiment was not sensitive enough to accurately indicate the presence of mass transfer resistance because the membrane was too long.

Effectiveness factors (η) calculated in the modeling calculations for Figure 6.7 depended on temperature and the feed gas flow rate. At 823 K, η ranged from 0.87 at

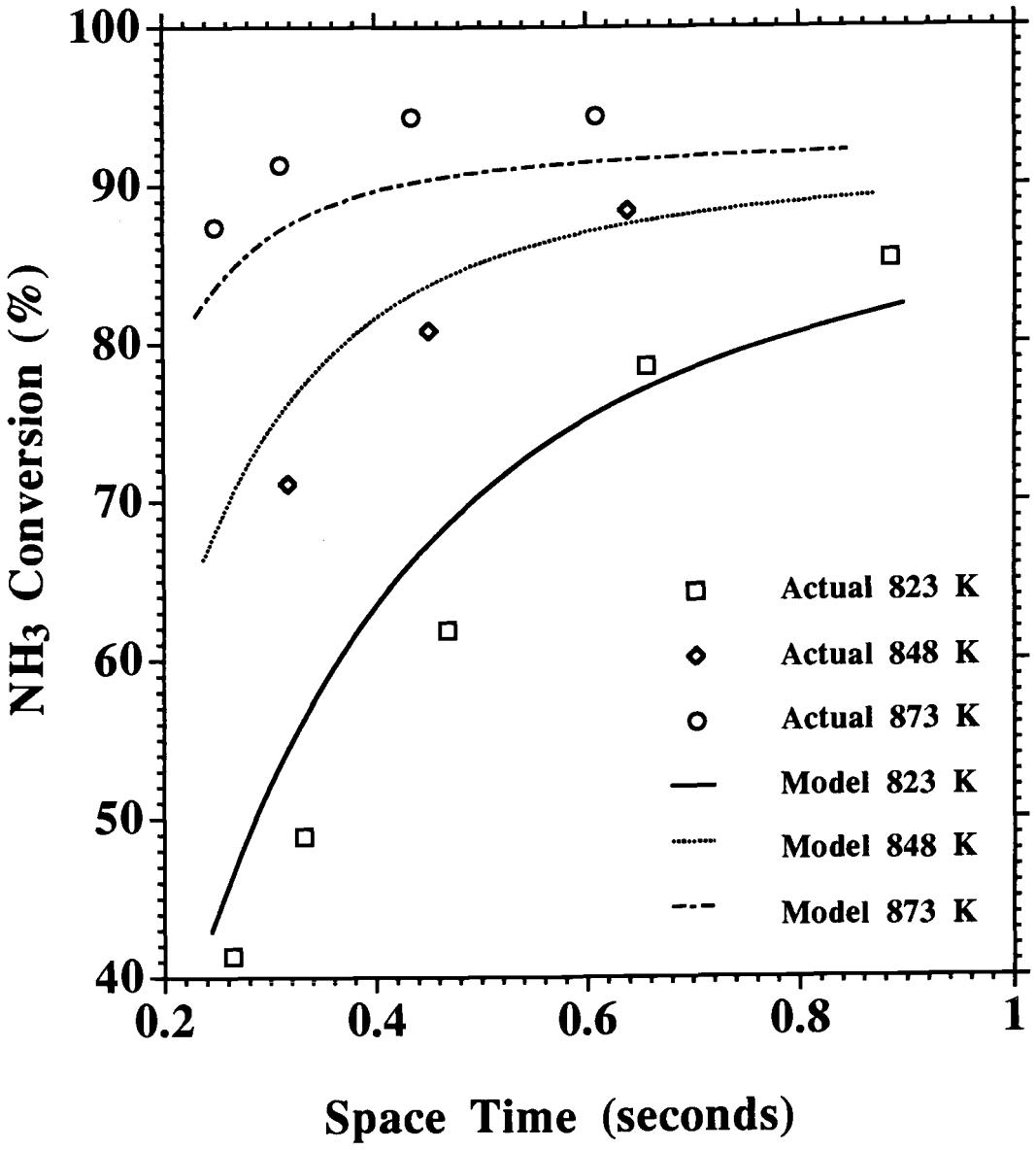

Figure 6.7 Effect of Space Time on Ammonia Conversion for Membrane Reactor. Feed gas concentrations were approximately 0.335, 48, 20, and 31.665 mole percent for ammonia, nitrogen, hydrogen, and helium, respectively. Total feed gas flows were varied from approximately $2.23 \cdot 10^{-4}$ mol/s to $7.58 \cdot 10^{-4}$ mol/s (300 to 1020 sccm).

the reactor inlet to 0.50 at the reactor outlet for an inlet flow rate of $2.2 \cdot 10^{-4}$ mols/s (space time = 0.90 s). The range of η values was from 0.946 at the reactor inlet to 0.71 at the reactor outlet for an inlet flow rate of $7.6 \cdot 10^{-4}$ mols/s (space time = 0.26 s) at 823 K. At 873 K, η ranged from 0.50 to 0.18 for an inlet flow rate of $2.2 \cdot 10^{-4}$ mols/s (space time = 0.84 s). The range of η values was from 0.73 to 0.36 for an inlet flow of $7.6 \cdot 10^{-4}$ mols/s (space time = 0.25 s) at 873 K. The η values increase with increasing flow rate because the Bi_A values calculated by Equation 4.22. for interphase mass transfer increase with increasing flow rate or Re_p. The η values decrease with increasing temperature because the ammonia decomposition rate on the catalyst surface increases at a much faster rate than the interphase mass transfer rate.

Figure 6.8 shows the effect of feed hydrogen concentration on ammonia conversion at 823 K for a feed gas flow rate of $6.1 \cdot 10^{-4}$ mols/s. Ammonia and nitrogen feed concentrations were 0.335 and 0.0 mole percent, respectively. As in the conventional reactor experiments, the feed hydrogen concentration had a large impact on ammonia conversion. A comparison of Figures 6.5 and 6.8 shows advantage of the using the membrane reactor. The increased conversion of the membrane reactor was due to the efficient removal of hydrogen by the composite palladium-ceramic membrane. The partial pressures of hydrogen in the residue and permeate stream were close to equilibrated at even the highest tested hydrogen feed concentration of 30 mole percent. The predicted ammonia conversion was significantly lower than the experimental conversion for the 10 mole percent hydrogen feed. Predicted conversions for conventional reactor experiments were also significantly lower than experimental conversions when no nitrogen was included in the feed and the hydrogen concentration was less than 10 mole percent. Therefore, the model is less accurate for these conditions.

Figure 6.9 shows the impact of the feed nitrogen concentration on ammonia conversion at 823 K for a feed gas flow rate of $6.1 \cdot 10^{-4}$ mols/s (space time = 0.33 seconds). Ammonia and hydrogen feed concentrations were 0.335 and 20 mole percent, respectively. As with the conventional reactor experiments, the nitrogen concentration had only a minor impact on ammonia conversion. Experimental ammonia conversions ranged from 49 percent when there was no nitrogen in the feed to 53 percent for a nitrogen feed concentration of 48 mole percent. Predicted conversions agree fairly well but there is a minor inconsistency in the effect of nitrogen concentration on ammonia conversion between the model and experimental results. As shown in Figure 6.9, predicted conversions increased slightly with increasing nitrogen

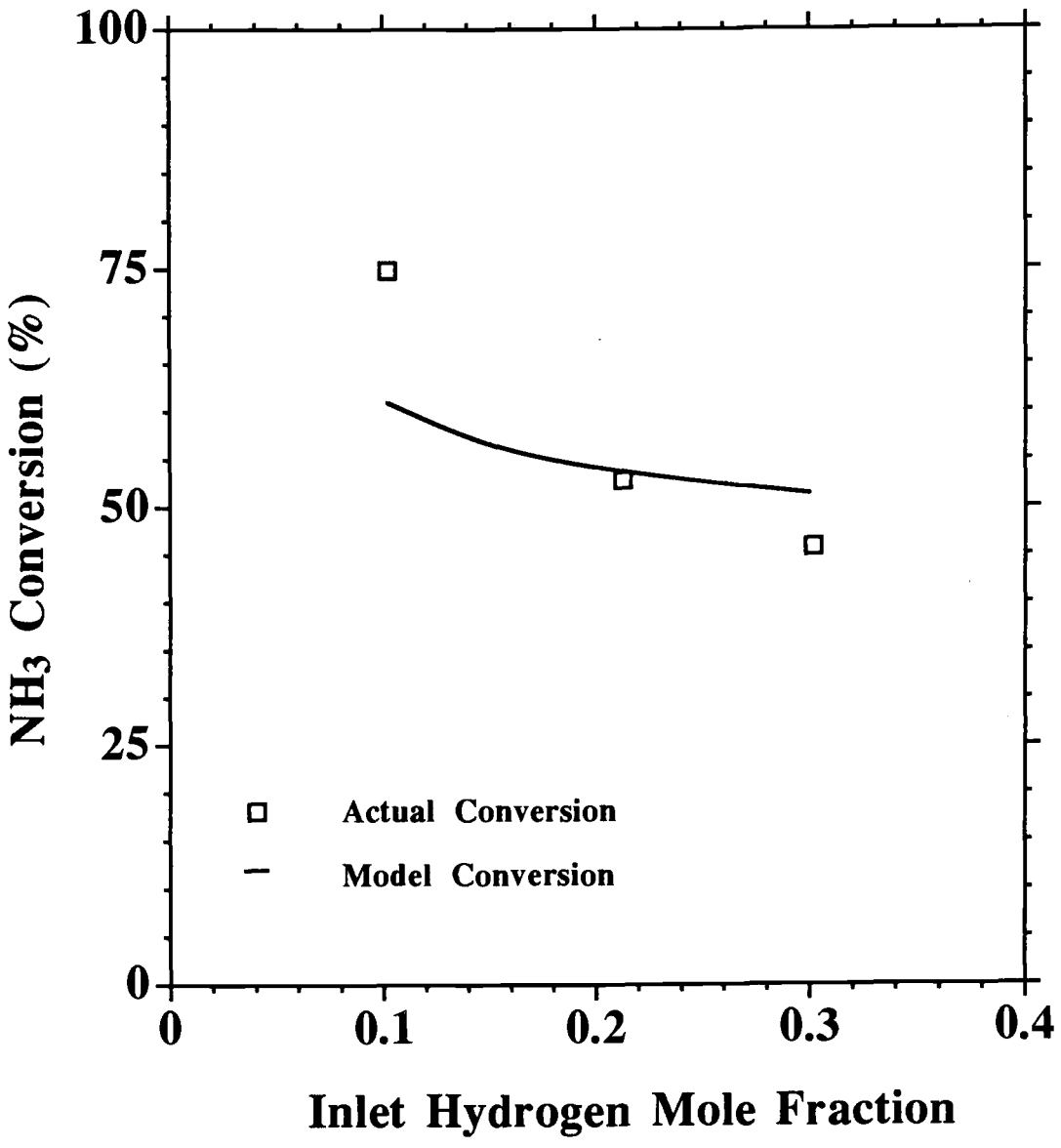

Figure 6.8 Effect of Hydrogen Concentration in Membrane Reactor Feed Gas on Ammonia Conversion at 823 K. Feed gas concentrations were approximately 0.335 and 0.0 mole percent for ammonia and nitrogen, respectively. Helium made up the balance. Total feed gas flows were approximately $6.1 \cdot 10^{-4}$ mol/s (820 sccm).

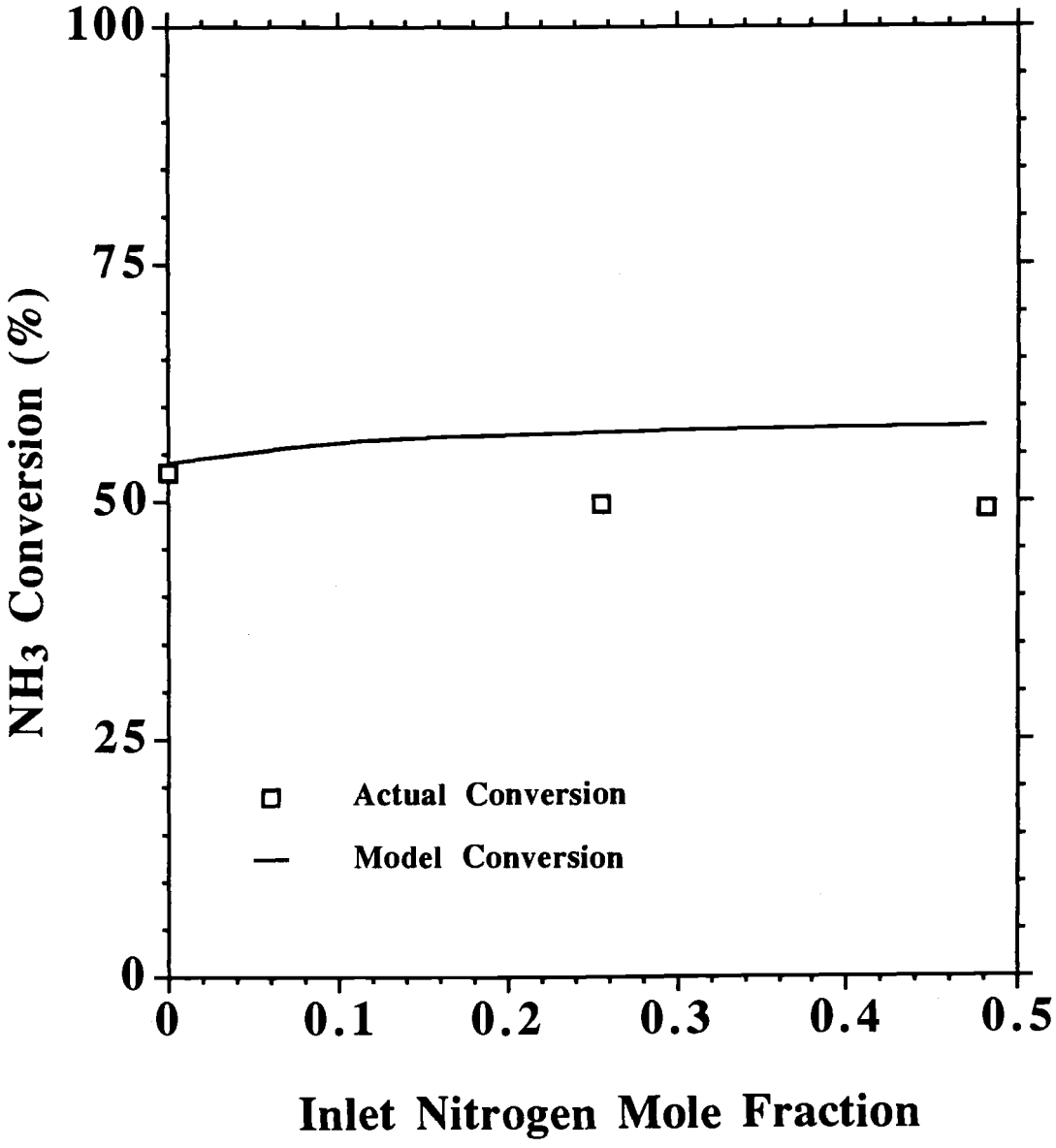

Figure 6.9 Effect of Nitrogen Concentration in Membrane Reactor Feed Gas on Ammonia Conversion at 823 K. Feed gas concentrations were approximately 0.335 and 20.0 mole percent for ammonia and hydrogen, respectively. Helium made up the balance. Total feed gas flows were approximately $6.1 \cdot 10^{-4}$ mol/s (820 sccm).

concentration but experimental conversions decreased slightly. Predicted conversions increase with increasing nitrogen concentration because the Re_p increases with increasing nitrogen concentration resulting in a higher predicted value for the Bi_A in Equation 4.22. This increases the predicted rate of interphase mass transfer of ammonia from the bulk gas to the exterior catalyst surface resulting in an increase in the average predicted ammonia decomposition rate for the higher nitrogen concentrations. Predicted ammonia conversions for the conventional reactor followed the experimental trend of decreasing conversion with increasing feed nitrogen concentration. Thus, it is the combination of hydrogen removal and higher interphase mass transfer rates that caused the increase in predicted ammonia conversion with increasing nitrogen concentration for the membrane reactor simulations.

As discussed in Chapter III, kinetic parameters for the ammonia decomposition catalyst were determined by conducting experiments with a differential reactor. No nitrogen was included in the reactor feed stream in these experiments. A potential concern is that the nitrogen concentration in the gas stream impacts the kinetic parameters k, E_a, and β. The data in Figure 6.9 show that the nitrogen concentration did not significantly impact the ammonia conversion in the membrane reactor at 823 K. Therefore, the nitrogen concentration does not appear to have had a significant impact on the kinetic parameters for these experimental conditions. It should be noted that the space time for the data in Figure 6.9 was only 0.33 seconds. The 0.33 second space time was significantly lower than the 0.88 second space time needed to obtain the highest observed ammonia conversion of about 85 percent at 823 K (see Figure 6.7). Therefore, the data in Figure 6.9 are useful for evaluating the effect of the nitrogen concentration on the kinetic parameters since ammonia conversion with the 0.33 second space time was much lower than the 0.88 second space time needed to obtain the highest observed ammonia conversion.

CONCLUSIONS

The catalytic decomposition of ammonia was investigated in experiments conducted with a packed bed palladium-ceramic membrane reactor. Experimental conditions were similar to those that would be used in an industrial application since no inlet sweep gas was used and the membrane was operated at a high transmembrane pressure difference. Results of these experiments demonstrate that a membrane reactor can significantly improve on the ammonia conversion of a conventional reactor when

dilute concentrations of ammonia and high concentrations of hydrogen and nitrogen are in the feed gas. An ammonia conversion of over 94 percent was achieved in the membrane reactor at 873 K. Since the equilibrium conversion of the feed gas was only 58 percent, a significant equilibrium shift was obtained with the membrane reactor. The equilibrium shift was even higher at lower temperatures. The maximum observed ammonia conversion at 823 K was approximately 85 percent in the membrane reactor compared to an equilibrium conversion of 33 percent for the feed gas, and a conversion of only 17.5 percent in a conventional packed bed reactor operated under the same conditions as the membrane reactor. The high conversions achieved with the membrane reactor are due to the membrane's ability to selectively remove hydrogen from the feed gas at a high transmembrane pressure difference.

Experimental conversions and conversions predicted with the membrane reactor model generally showed good agreement . The shape of predicted curves for ammonia conversion versus temperature and ammonia conversion versus space time followed the trend of experimental values. The percent difference between predicted and experimental conversions was less generally less than 10 percent. Membrane reactor modeling accuracy was not as good when the feed concentration of hydrogen was reduced from 20 to 10 mole percent at 823 K. Modeling accuracy may be improved if a more detailed kinetic study is performed to address the impact of interphase mass transfer on the ammonia decomposition rate.

CHAPTER VII
CONCLUSIONS AND RECOMMENDATIONS

CONCLUSIONS

The following conclusions are drawn from this work:

1) The hydrogen selectivity of a commercial ceramic membrane was dramatically increased by depositing 11.4 to 20 μm palladium films on the selective layer of the ceramic membrane tubes.
2) The composite palladium-ceramic membrane remained hydrogen selective when operated at a large transmembrane pressure difference. A composite palladium ceramic membrane with an 11.4 μm palladium film had a hydrogen to nitrogen selectivity of 380 at 873 K and a transmembrane pressure difference of 1500 kPa. In comparison, the maximum hydrogen to nitrogen selectivity of 3.74 for commercially available ceramic membranes is only achieved when these membranes are operated at a much lower transmembrane pressure difference. Even higher selectivities are possible with the composite palladium-ceramic membrane design if improvements in membrane sealing procedures are made.
3) Experiments conducted at temperatures from 723 to 913 K, and transmembrane pressure differences up to 2330 kPa demonstrate that composite palladium-ceramic membranes can operate at high temperatures and transmembrane pressure differences. Since the membrane can operate at a high transmembrane pressure difference and remain hydrogen selective, it can be operated without a sweep gas.
4) Hydrogen permeation rates for the composite palladium-ceramic membrane were higher than permeation rates reported for both metal oxide membranes and composite metal membranes. The relatively high permeation rates for the composite palladium-ceramic membrane are a result of using a thin metal film on top of a highly permeable ceramic support tube.
5) The composite palladium-ceramic membrane was very effective when used in a packed bed membrane reactor for ammonia decomposition. The membrane reactor significantly shifted the equilibrium ammonia conversion of a high temperature, high pressure feed gas containing dilute concentrations of ammonia and high concentrations of nitrogen and

hydrogen. At 873 K, the membrane reactor conversion was over 94 percent compared to an equilibrium conversion of only 58 percent for the feed gas. An ammonia conversion of 85 percent was obtained at 823 K in the membrane reactor compared to an equilibrium conversion of 33 percent for the feed gas, and a conversion of only 17.5 percent in a conventional packed bed reactor operated under the same conditions as the membrane reactor. In addition, experimental conditions were similar to those desirable for commercial applications such as the IGCC process since the membrane reactor was operated at a high transmembrane pressure difference with no sweep gas.

6) Composite palladium-ceramic membranes have potential use in several high temperature membrane reactor applications due their high hydrogen selectivity, high hydrogen permeation rates, and ability to remain hydrogen selective at high transmembrane pressure differences. Steam reforming of methane and the water gas shift reaction are two industrially important reactions which could benefit from using a composite metal-ceramic membrane reactor.
7) Agreement between experimental conversions and conversions predicted using the membrane reactor model developed in this study was generally good. The shape of predicted curves for ammonia conversion versus temperature and ammonia conversion versus space time followed the trend of experimental values. The percent difference between predicted and experimental conversions was generally less than 10 percent. Membrane reactor modeling accuracy was not as good when the feed concentration of hydrogen was reduced from 20 to 10 mole percent.
8) Palladium films of over 10 μm are needed to obtain a defect free palladium film when electroless plating is used to deposit the palladium film.

RECOMMENDATIONS

The following recommendations are made for future research in the area of high temperature membrane reactors for ammonia decomposition:

1) Experiments similar to those conducted by Goltzov (Goltzov, 1975) but at higher temperatures and gas compositions typical of IGCC conditions are

needed to determine whether composite metal-ceramic membranes made from palladium or palladium alloys are poisoned by hydrogen sulfide at IGCC conditions. The experiments could be conducted by passing a mixture of hydrogen and steam through the membrane until the hydrogen permeation rate reaches steady state. Hydrogen sulfide would then be added and the hydrogen permeation rate would be monitored for several days to determine whether the membrane is poisoned by the hydrogen sulfide. Several different temperatures and gas compositions should be evaluated to establish a range of acceptable conditions. Composite metal-ceramic membranes made from pure palladium or palladium alloys such as palladium-gold could be tested. A potential method for preparing a composite palladium-gold ceramic membrane is to plate a film of gold over the palladium metal and then heat the membrane to a high enough temperature to allow intermetallic diffusion to occur in a reasonable period of time.

2) Only ammonia, nitrogen, hydrogen, and helium were included in the membrane reactor experiments conducted in this study. Other synthesis gas constituents such as steam, hydrogen sulfide, and carbon monoxide may impact the membrane permeability or catalyst activity. Experiments with simulated synthesis gas containing all of the synthesis gas components at typical concentrations are needed to address concerns regarding coking and poisoning.
3) The ceramic membranes used in this study were cut to the desired length after they were purchased. Resealing the ends was a problem because the outside diameter had to be sanded down and then resealed with a high temperature sealant. The resulting end seals were not perfectly smooth or round. This made it very difficult to achieve a perfect seal with the metal compression fittings and Grafoil seals used in the permeation and membrane reactor experiments. If ceramic membranes of the desired length can be obtained with high temperature end seals, the metal compression fittings and Grafoil seals may be more effective. This would improve the hydrogen selectivity of the membranes. Another suggestion is to use ceramic membranes with a 0.933 cm OD instead of a 1 cm OD. Commercial graphite ferrules are available from Alltech for this tube size. It may be easier to seal the membrane with the commercial ferrules rather than those

fabricated from the Grafoil tape. In addition, the Swaglok® fittings for the 0.933 cm OD tubes do not have to be ground down as much as those for the 1 cm OD tubes in order to fit inside the nonporous alumina tube used for the shell side of the membrane module. Therefore, it would be much easier to assemble the permeation apparatus if 0.933 cm OD tubes were used.

4) Accounting for interphase mass transfer in the membrane reactor model was a difficult problem because there was limited data available regarding interphase mass transfer coefficients for the low flow rates and small catalyst particle sizes typically used in laboratory reactors. A more detailed kinetic study than the one used in this project covering a wider range of Re_p values is needed to more accurately estimate interphase mass transfer coefficients. The accuracy of the kinetic parameters for the ammonia decomposition reaction could also be improved by conducting experiments over a wider range of gas conditions than those used in this study.
5) The membrane reactor model was written to simulate results of experiments performed with gas mixtures of ammonia, nitrogen, hydrogen, and helium. Synthesis gas also contains methane, carbon monoxide, carbon dioxide, and steam. Side reactions such as steam reforming of methane, the water gas shift reaction, or their reverse reactions are possible when the synthesis gas is passed through the membrane reactor. Depending on gas conditions, hydrogen may be either consumed or generated by these reactions. Therefore, the membrane reactor model should be extended to include these potential side reactions since the hydrogen concentration has a large impact on the ammonia decomposition rate and ammonia conversion.
6) Electroless plating was used to make the composite palladium-ceramic membranes used in this study. A palladium film thickness of over 10 μm was needed to eliminate defects in the palladium film. It may be possible to deposit a defect free film thinner than 10 μm if another film deposition technique is used. Use of a thinner film would decrease the cost of the composite membrane since less palladium would be needed. Therefore, other film deposition techniques such as sputtering should be investigated to try to reduce the thickness of the palladium film.

BIBLIOGRAPHY

Abe, F. Jpn. Pat., 62 - 121616, as referred to by J.N. Armor, *Catalysis with Permselective Inorganic Membranes*. Applied Catalysis 1989, 49, 17.

Armor, J.N. *Catalysis with Permselective Inorganic Membranes*. Applied Catalysis 1989, 49, 1.

Athavale, S.N.; Totlani, M.K. *Electroless Plating of Palladium*. Met. Fin. 1989, 87(1), 23.

Barrer, R.M. *Diffusion in and Through Solids*. Cambridge University Press: London, 1941.

Baudrand, D.W. *Cleaning and Preparation of Ceramic and Metallized Ceramic Materials for Plating*. Plat. and Surf. Fin. 1984, 71(10), 72.

Bird, R.B.; Stewart, W.E.; Lightfoot, E.N. *Transport Phenomena*. John Wiley & Sons: New York, NY, 1960.

Buxbaum, R.E. *Hydrogen Extraction Via Non-Porous Coated-Metal Membranes*. Preprint for paper presented at AIChE Annual Meeting, Miami Beach, Florida, 1992.

Carnahan, B.; Luther, H.A.; Wilkes, J.O. *Applied Numerical Methods*. John Wiley & Sons: New York, NY, 1969.

Champagnie, A.M.; Tsotsis, T.T.; Minet, R.G.; Webster, I.A. *A High Temperature Catalytic Membrane Reactor for Ethane Dehydrogenation*. Chem. Eng. Sci. 1990, 45(8), 2423.

Clayson, D.M.; Howard, P. UK Patent Application, GB 2190397A, 1987.

Cohen, K.L.; West, K.W. *Solution Chemistry and Colloid Formation in the Tin Chloride Sensitizing Process*. J. Electrochem. Soc.: Electrochemical Science and Technology 1972, 119(4), 433.

Cooper, H.W. *Fugacities for High P and T*. Hydrocarbon Process 1967, 46(2), 159.

Cussler, E.L. *Diffusion Mass Transfer in Fluid Systems*. Cambridge University Press: New York, NY, 1984.

DeRosset, A.J. *Diffusion of Hydrogen through Palladium Membranes*. Ind. Eng. Chem. 1960, 52, 525.

Dokiya, M.; Kameyama, T.; Fukuda, K. *Study of Thermochemical Hydrogen Preparation. Part 4. Application of Effusion on the Thermochemically Limited Reaction*. Denki Kagaku 1977, 45(11), 701.

Edlund, D.J. *A Membrane Process for Hot-Gas Cleanup and Decomposition of H_2S to Elemental Sulfur*. Phase I Final Report to the U.S. Department of Energy on Contract No. DE-FG03-91ER81228 from Bend Research, Inc.: Bend, Oregon, 1992.

Edlund, D.J.; Pledger, W.A. *Thermolysis of Hydrogen Sulfide in a Metal-Membrane Reactor.* J. Membrane Sci. 1993, 77(2&3), 255.

Feldstein, N.; Weiner, J.A. *The Effectiveness of Tin Sensitizer Solutions.* Plating 1972, February, 140.

Finlayson, B.A. *Nonlinear Analysis in Chemical Engineering.* McGraw-Hill: New York, NY, 1980.

Fukuda, K.; Dokiya, M.; Kameyama, T.; Kotera, Y. *Catalytic Decomposition of Hydrogen Sulfide.* Ind. Eng. Chem. Fundam. 1978, 17(4), 243.

Goltsov, V.A.; Vladimirovich, G.; Kagan, G.E.; Timofeev, N.I. *Method for Preparation of Super-High Purity Hydrogen.* U.S. Patent No. 3881891, May, 1975.

Govind, R.; Badra, C. *Studies on the Oxidation of Ethylene to Ethylene Oxide in a Membrane Reactor.* Paper #13D presented at the Fifth Annual Meeting of the North American Membrane Society, Lexington, Kentucky, (May, 1992).

Govind, R.; Atnoor, D. *Surface Modification of Ceramic Membranes for Selective Separation of Gases at High Temperature.* Paper #8C presented at the Fifth Annual Meeting of the North American Membrane Society, Lexington, Kentucky, May, 1992.

Harrison, R.H.; Kobe, K.A. *Thermodynamics of Ammonia Synthesis and Oxidation.* Chem. Eng. Prog. 1953, 49(7), 349.

Hirschfelder, J.O.; Bird, R.B.; Spotz, E.L. *The Transport Properties of Gases and Gaseous Mixtures.* Chem. Rev. 1949, 44, 205.

Honma, H.; Kanemitsu, K. *Electroless Nickel Plating on Alumina Ceramics.* Plat. and Surf. Fin. 1987, 74(9), 62.

Hsieh, H.P. *Inorganic Membrane Reactors.* Catal. Rev. Sci. Eng. 1991, 33(1&2), 1.

Hsieh, H.P. *Microporous Alumina Membranes.* J. Membrane Sci. 1988, 39(3), 221.

Hsu, C.Z.; Buxbaum, R.E. *Palladium Catalyzed Oxidative Diffusion for Tritium Extraction.* J. Nucl. Met. 1986, 141-143, 238.

Hurlbert, R.C.; Konecny, J.O. *Diffusion of Hydrogen through Palladium.* J. Chem. Phys. 1961, 34(2), 655.

IMSL Math/Library , 1.1 ed., IMSL, Houston, Texas, 1989.

Itoh, N.; Shindo, Y.; Haraya, K.; Obata, K; Hakuta,T.; Yoshitome, H. *Simulation of a Reaction Accompanied by Separation.* Int. Chem. Eng. 1985, 25(1), 138.

Itoh, N. *A Membrane Reactor Using Palladium.* AIChE J. 1987, 33(9), 1576.

Itoh, N.; Shindo, Y.; Haraya, K.; Hakuta, T. *A Membrane Reactor Using Microporous Glass for Shifting Equilibrium of Cyclohexane Dehydrogenation.* J. Chem. Eng. Jpn. 1988, 21(4), 399.

Kameyama, T.; Dokiya, M.; Fukuda, K. *Differential Permeation of Hydrogen Sulfide through a Microporous Vycor-Type Glass Membrane in the Separation System of Hydrogen and Hydrogen Sulfide.* Sep. Sci. Technol. 1979, 14(10), 953.

Kameyama, T.; Dokiya, M.; Fujishige, M.; Yokokawa, H.; Fukuda, K. *Possibility for Effective Production of Hydrogen from Hydrogen Sulfide by means of a Porous Vycor Glass Membrane.* Ind. Eng. Chem. Fundam. 1981, 20, 97.

Kameyama, T.; Dokiya, M.; Fujishige, M.; Yokokawa, H.; Fukuda, K. *Production of Hydrogen from Hydrogen Sulfide by Means of Selective Diffusion Membranes.* Int. J. Hydrogen Energy 1983, 8(1), 5.

Krishnan, G.N.; Wood, B.J.; Sanjurjo, A. *Study of Ammonia Removal in Coal Gasification Processes,Topical Report: Literature Review.* Prepared for: U.S. Department of Energy/Morgantown Energy Technology Center on Contract No. DE-AC21-86MC23087 from SRI International: Menlo Park, California, 1987.

Krishnan, G.N.; Wood, B.J.; Tong, G.T.; McCarty, J.G. *Study of Ammonia Removal in Coal Gasification Processes, Final Report.* Prepared for: U.S. Department of Energy/Morgantown Energy Technology Center on Contract No. DE-AC21-86MC23087 from SRI International: Menlo Park, California, 1988.

Kraisuwansarn, N. *Simulation of a Membrane Reactor for Ammonia Decomposition.* M.S. Thesis, Oregon State University, 1991.

Levenspiel, O. *Chemical Reaction Engineering.* 2ND Edition, John Wiley & Sons: New York, NY, 1972.

Lewis, F.A. *The Palladium Hydrogen System.* Academic Press: London, 1967.

McKinley, D.L.; Nitro, W.V. *Metal Alloy for Hydrogen Separation and Purification.* U.S. Patent No. 3350845, Nov. 1967.

Mohan, K.; Govind, R. *Analysis of a Cocurrent Membrane Reactor.* AIChE J. 1986, 32(12), 2083.

Mohan, K.; Govind, R. *Analysis of Equilibrium Shift in Isothermal Reactors with a Permselective Wall.* AIChE J. 1988a, 34(9), 1493.

Mohan, K.; Govind, R. *Effect of Temperature on Equilibrium Shift in Reactors with a Permselective Wall.* Ind. Eng. Chem. Res. 1988b, 27, 2064.

Mohan, K.; Govind, R. *Studies on a Membrane Reactor.* Sep. Sci. Technol. 1988c, 23(12&13), 1715.

Nandy, S. *Observations on Catalytic Dissociation of Ammonia at High Pressures.* M.S. Thesis, Colorado State University, 1981.

Newton, R.H. *Activity Coefficients of Gases.* Ind. Eng. Chem. 1935, 27(3), 302.

Nielsen, A. *Review of Ammonia Catalysis, in: H. Heinemann (Ed.), Catalysis Reviews Volume 4.* Marcel Dekker, Inc., New York, NY, (1971), 1-25.

Nielsen, A.; Kjaer, J.; Hansen, B.L. *Rate Equation and Mechanism of Ammonia Synthesis at Industrial Conditions.* J. Catal. 1964, 3, 68.

Perry, R.H.; Chilton, C.H. *Chemical Engineers' Handbook.* Fifth Edition, McGraw-Hill: New York, NY, 1973.

Press, W.H.; Flannery, B.P.; Teukolsky, S.A.; Vetterling, W.T. *Numerical Recipes.* Cambridge University Press: New York, NY, 1986.

Raymont, M.E.D. *Make Hydrogen from Hydrogen Sulfide.* Hydrocarbon Process. 1975, 54, 139.

Reid, R.C.; Prausnitz, J.M.; Sherwood, T.K. *The Properties of Gases and Liquids.* McGraw-Hill: New York, NY, 1977.

Rhoda, R.N. *Electroless Palladium Plating.* Trans. Inst. Met. Fin. 1959, 36, 82.

Sasaki, Y.T. *Survey of Vacuum Material Cleaning Procedures: A Subcommittee Report of the American Vacuum Society Recommended Practices Committee.* J. Vac. Sci. Technol. A. 1991, 9(3), 2025.

Satterfield, C.N. *Heterogeneous Catalysis in Practice.* McGraw-Hill: New York, NY, 1980.

Shinji, O.; Misonou, M.; Yoneda, Y. *The Dehydrogenation of Cyclohexane by the Use of a Porous-Glass Reactor.* Bull. Chem. Soc. Jpn. 1982, 55, 2760.

Shu J.; Grandjean, B.P.A.; Van Neste, A.; Kaliaguine, S. *Catalytic Palladium-based Membrane Reactors: A Review.* Can. J. Chem. Eng. 1991, 69, 1036.

Southern Company Services, Inc.; The M.W. Kellogg Company; Tennessee Technological University; General Electric Company *Assessment of Coal Gasification/Hot Gas Cleanup Based Advanced Gas Turbine Systems.* Final Report, Prepared for: U.S. Department of Energy/Morgantown Energy Technology Center on Contract No. DE-FC21-89MC26019, 1990.

Sperry, D.P.; Falconer, J.L.; Noble, R.D. *Methanol-Hydrogen Separation By Capillary Condensation in Inorganic Membranes.* J. Membrane Sci. 1991, 60, 185.

Sun, Y.M.; Khang, S.J. *Catalytic Membrane for Simultaneous Chemical Reaction and Separation Applied to a Dehydrogenation Reaction.* Ind. Eng. Chem. Res. 1988, 27, 1136.

Temkin, M.; Pyzhev, V. *Kinetics of the Synthesis of Ammonia on Promoted Iron Catalysts.* Acta Physicochim. URRS. 1940, 12(3), 327, as referred to by Nielsen (1964).

Tsapatsis, M.; Soojin, K; Nam, S.W.; Gavalas, G. *Synthesis of Hydrogen Permselective SiO_2, TiO_2, Al_2O_3, and B_2O_3 Membranes from the Chloride Precursors.* Ind. Eng. Chem. Res. 1991, 30(9), 2152.

Tsonopoulos, C. *Second Virial Coefficients of Water Pollutants.* AIChE J. 1978, 24(6), 1112.

Uemiya, S.; Kude, Y.; Sugino, K.; Sato, N.; Matsuda, T; Kikuchi, E. *A Palladium/Porous-Glass Composite Membrane for Hydrogen Separation.* Chem. Lett. 1988, 1687.

Uemiya, S.; Matsuda, T.; Kikuchi, E. *Aromatization of Propane Assisted by Palladium Membrane Reactor.* Chem. Lett. 1990, 1335.

Uemiya, S.; Sato, N.; Ando, H.; Kikuchi, E. *The Water Gas Shift Reaction Assisted by a Palladium Membrane Reactor.* Ind. Eng. Chem. Res. 1991a, 30(3), 585.

Uemiya, S; Sato, N.; Ando, H.; Matsuda, T.; Kikuchi, E. *Steam Reforming of Methane in a Hydrogen-Permeable Membrane Reactor.* Applied Catalysis 1991b, 67, 223.

Uemiya, S; Sato, N.; Ando, H.; Kude, Y; Matsuda, T.; Kikuchi, E. *Separation of Hydrogen through Palladium Thin Film Supported on a Porous Glass Tube.* J. Membrane Sci. 1991c, 56, 303.

U.S. Department of Energy/Morgantown Energy Technology Center, Program Research and Development Announcement for: Advanced Concepts in Ceramic Membranes for High Temperature Gas Separations, RFP No. DE-RA21-89MC26038, December, 1988.

Way, J.D.; Roberts, D. L. *Hollow Fiber Inorganic Membranes for Gas Separations.* Sep. Sci. Technol. 1992, 27(1), 29.

Wilke, C.R. *Diffusional Properties of Multicomponent Gases.* Chem. Eng. Prog. 1950, 46(2), 95.

Wood, B.J. *Dehydrogenation of Cyclohexane on a Hydrogen-Porous Membrane.* J. Catalysis 1968, 11, 30.

Wu, J.C.S.; Liu, P.K.T. *Mathematical Analysis on Catalytic Dehydrogenation of Ethylbenzene Using Ceramic Membranes.* Ind. Eng. Chem. Res. 1992, 31, 322.

Wu, J.C.S.; Flowers, D.F.; Liu, P.K.T. *High-Temperature Separation of Binary Gas Mixtures Using Microporous Ceramic Membranes.* J. Membrane Sci. 1993, 77(2&3), 85.

APPENDICES

APPENDIX A

NOMENCLATURE

Symbols List

Bi_J Biot number for intraparticle mass transfer for component J $\left[\frac{k_{gJ} R_p}{De_J} \right]$

C_t total molar density of reaction side (tube) gas (mol/m^3)

C_1 proportionality constant in correlation for Sh

De_J effective diffusion coefficient for component J in catalyst (m^2/s)

D_{keJ} effective Knudsen diffusion coefficient for component J in catalyst (m^2/s)

D_{MeJ} effective molecular diffusion coefficient for component J in catalyst (m^2/s)

D_{MJ} molecular diffusion coefficient for component J in bulk gas (m^2/s)

E_a activation energy for rate constant for ammonia decomposition reaction (J/mol)

E_b pressure term for rate constant for ammonia decomposition reaction (J/mol•Pa)

E apparent activation energy for hydrogen permeation throught composite palladium-ceramic membrane, (J/mole)

F_J molar flow rate of component J in reaction side (mol/s)

F_{J0} inlet molar flow rate of component J in reaction side (mol/s)

F_{Jout} outlet molar flow rate of component J in reaction side (mol/s)

F_T total molar flow rate in reaction side (mol/s)

f_J fugacity of component J (Pa)

f_{JG} fugacity of component J in bulk gas (Pa)

f_{Jeq} fugacity of component J at equilibrium (Pa)

G mass flux of gas in reaction side ($kg/m^2 \cdot s$)

J_J permeation rate of component J through membrane, ($mols/m^2 \cdot s$)

k reaction rate constant (mol/m^3 reactor$\cdot s \cdot Pa^{-\beta}$)

k' reaction rate constant (mol/kg catalyst$\cdot s \cdot Pa^{-\beta}$)

k_{gJ} intraphase mass transfer coefficient for component J(m3 gas/m^2 catalyst$\cdot s$)

k'_{gJ} intraphase mass transfer coefficient for component J(m3 gas/kg catalyst$\cdot s$)

k_o pre-exponential factor for reaction rate constant (mol/m^3 reactor$\cdot s \cdot Pa^{-\beta}$)

k'_o pre-exponential factor for reaction rate constant (mol/kg catalyst$\cdot s \cdot Pa^{-\beta}$)

K_{eq} equilibrium constant (Pa^{-1})

L axial position in reactor (m)

L_o reactor length (m)

M_J molecular weight of component J (g/mol)

$n(J)$ pressure dependence term for component J in permeation rate equation

$\bar{P}_J$ permeability of component J ($mol \cdot m/m^2 \cdot s \cdot Pa^{n(J)}$)

$\bar{P}_{HO}$ pre-exponential factor in the Arrhenius relationship for hydrogen permeability, ($moles \cdot m/m^2 \cdot s \cdot Pa^{n(H)}$)

P_t total pressure on reaction side (Pa)

P_S total pressure on sweep side (Pa)

P_r pressure ratio (P_S/P_T)

P_{Jt} partial pressure of component J on tube side (Pa)

P_{Js} partial pressure of component J on sweep side (Pa)

Q_J molar flow rate of component J in sweep side (mol/s)

Q_{J0} initial molar flow rate of component J in sweep side (mol/s)

Q_T total molar flow rate in sweep side (mol/s)

Re_p Reynolds number $\left[\frac{2\ G\ R_p}{\mu}\right]$

R_p radius of catalyst particle (m)

r dimensionless radius (r'/R_p)

r' radial position in catalyst (m)

r correlation coefficient for linear or nonlinear regression analysis of data

r_A rate of generation for component A in reaction (mol/m^3 reactor•s)

r_{AG} rate of generation for component A calculated with bulk gas fugacities (mol/m^3 reactor•s)

r'_A rate of generation for component A in reaction (mol/kg catalyst•s)

r'_{AG} rate of generation for component A calculated with bulk gas fugacities (mol/kg catalyst•s)

r'_{Aobs} observed rate of generation for component A (mol/kg catalyst•s)

R universal gas constant

R_1 inside radius of membrane tube (m)

S_g surface area of catalyst (m^2/kg)

Sc Schmidt number $\left[\frac{\mu}{\rho_g D_{M_J}}\right]$

Sh Sherwood number $\left[\frac{2\ k_{gJ}\ R_p}{D_{M_J}}\right]$

SF separation factor

t_m membrane thickness (m)

T	temperature of the system (K)
W	weight of catalyst in reactor (kg catalyst)
$X_J(r)$	normalized mole fraction of component J in catalyst (Y_J/Y_{JG})
V	volume of catalyst bed in reaction side (m^3)
Y_J	mole fraction of component J in catalyst
Y_{JG}	mole fraction of component J in bulk gas
ϕ_{Jt}	fugacity coefficient of component J in tube gas
ϕ_{JS}	fugacity coefficient of component J in sweep gas
ε	void fraction in catalyst bed
η	effectiveness factor
β	exponential constant in rate law
ν_J	stoichiometric coefficient for component J in reaction
μ	viscosity of gas ($kg/m^2 \cdot s$)
τ_p	tortuosity factor for catalyst
θ	void fraction of catalyst particle
ρ_p	bulk density of catalyst (kg/m^3)
ρ_g	density of tube gas (kg/m^3)
γ_A	% ammonia conversion in membrane reactor
$\alpha(i/j)$	membrane selectivity for component I with respect to component J

Subscript

A	ammonia

N	nitrogen
H	hydrogen
I	inert (helium)
0	inlet or initial
out	outlet

APPENDIX B

DOCUMENTATION FOR MEMBRANE REACTOR MODEL

Background Information

Documentation for the membrane reactor model is presented in this appendix. Input data files, example output, and FORTRAN code for the cocurrent membrane reactor model used in the calculations discussed in Chapter VI are listed. A countercurrent model was also used for some of the calculations presented in Chapter IV. With the exception of a couple of subroutines, the countercurrent model is similar to the cocurrent model. Therefore, a listing of the FORTRAN code for the countercurrent model has not been included in this appendix. As previously discussed in Chapter IV, there is essentially no advantage associated with either the cocurrent or countercurrent flow configuration when a membrane with high hydrogen selectivity is operated at a low pressure ratio (P_r<0.1).

The cocurrent model was first written by Nichakorn Kraisuwansarn (Kraisuwansarn, 1991) for his M.S. Thesis at Oregon State University. The original cocurrent model was modified in the present study by adding subroutines to calculate the effectiveness factor (η) using the orthogonal collocation method. Some other minor modifications to the original program code were also made to the equations that calculate permeation rates to reflect the permeation characteristics of the composite palladium-ceramic membrane developed in the present study. Input data files have also been modified. The model can be run as a membrane reactor model, a conventional reactor model, or a membrane separator model. Procedures for running the model are discussed below.

Data Entry Procedure

Data is entered into the program through two input data files, NH3.DAT and DATA. General information regarding the desired operating mode, membrane characteristics, feed gas characteristics, kinetic data, permeability data, and some thermodynamic data are included in NH3.DAT. Information needed to calculate effectiveness factors by the orthogonal collocation procedure is included in DATA.

Table A.1 summarizes the input parameters included in NH3.DAT. The nomenclature used in the data files and FORTRAN code is somewhat different than that used in the text of this thesis. When appropriate, input parameters are defined using both sets of nomenclature in Table A.1. Table A.2 presents a listing of NH3.DAT.

The integer variable MODE in NH3.DAT is used to select the desired operating mode for the model. When MODE=0, membrane reactor modeling calculations are performed. Conventional reactor calculations are performed when MODE=1. Membrane separator calculations are performed when MODE=2. The membrane separator model is just the membrane reactor model without chemical reaction. The conventional reactor model is just the membrane reactor model without permeation. The value of MODE is the only thing that needs to be changed to select the desired operating mode. There is no need to change the kinetic parameters or permeation parameters in NH3.DAT because the model makes the required adjustments automatically.

The integer variable DREAL is used to select the procedure for calculating fugacity coefficients. When DREAL=0, all fugacity coefficients are set equal to one (ideal gas assumption). Fugacity coefficients are calculated by empirical correlations (Cooper, 1967; Newton, 1935) when DREAL=1. Virial equations for gas mixtures are used to calculate fugacity coefficients when DREAL=2. See Kraisuwansarn (1991) for background information regarding the virial equation procedure. Fugacity coefficients were calculated using the empirical correlations (DREAL=1) in the present study.

Inlet flows are input into the model in units of cm^3(STP)/min (sccm). The membrane reactor simulations performed for Chapter VI were for a membrane reactor operated at low pressure ratio (P_r=0.07) with no inlet sweep gas stream. To avoid division by zero in the permeation equations for the membrane reactor model, it is necessary to include a very low inlet sweep flow of around 0.01 sccm in NH3.DAT for the variable DSCCMIS. It was assumed that this sweep gas was pure hydrogen by setting DMOLSFRAC(7) equal to 1.0.

Table A.3 summarizes the input parameters included in the data file named DATA. Table A.4 presents a listing of DATA. Collocation points, matrices for estimating first and second derivatives in Equations 4.12 and 4.14, and weighting parameters for numerical integration of Equation 4.18 must all be included in DATA. These parameters were determined using the FORTRAN program named OCRXN listed in the appendix of Finlayson's book (Finlayson, 1980). The OCRXN program was available on the Chemical Engineering Computer Network at Oregon State

Table A.1
Summary of Input Parameters For NH3.DAT

Variable Name in NH3.DAT	Variable Name in Thesis Text	Description
MODE	-	Integer variable used to determine operating mode of model (MODE = 0, 1, or 2)
DR1	R_1	Inside radius of catalyst tube (m)
DRLO	L_o	reactor length (m)
DTHICK	t_m	membrane thickness equals palladium film thickness for composite palladium-ceramic membrane (m)
DTEMP	T	Temperature (K)
DPSIG	-	Tube feed gas pressure (psig)
DPR	P_r	pressure ratio = Sweep pressure/Tube pressure
DREAL	-	Integer variable used to determine fugacity calculation procedure (DREAL = 0, 1, or 2)
DSCCMIT	-	Inlet tube side flow (sccm)
DSCCMIS	-	Inlet sweep side flow (sccm)
DMOLSFRAC(J)	-	Mole fractions in tube and sweep inlet gas (J=1 to 4 for ammonia, nitrogen, hydrogen and helium, respectively, in tube side; J=5 to 8 for sweep side mole fractions)

Table A.1
Summary of Input Parameters For NH3.DAT (continued)

Variable Name in NH3.DAT	Variable Name in Thesis Text	Description
DBETA	β	Exponential constant in rate law
DRKO	k_o	pre-exponential factor for reaction rate constant (mol/m^3 reactor•s•$Pa^{-\beta}$)
DE	E_a	activation energy for ammonia decomposition (J/mol)
DPA, DPN, DPI	$\bar{P}_J$	permeabilities of ammonia, nitrogen, and helium, respectively (mol•m/m^2•s•$Pa^{n(J)}$)
DPH	$\bar{P}_{HO}$	pre-exponential factor in the Arrhenius relationship for hydrogen permeability, (mol•m/m^2•s•$Pa^{n(H)}$)
EACT	E	apparent activation energy for hydrogen permeation throught composite palladium-ceramic membrane, (J/mol)
ANA, ANN, ANH, ANI	n(J)	pressure dependence terms for ammonia, nitrogen, hydrogen, and helium, respectively, in permeation rate equations

Note: The remaining parameters in NH3.DAT are only used if fugacity coefficients are calculated using the virial equations. See Kraisuwansarn (1991) for information about these parameters. Fugacities in the present project were calculated using empirical correlations rather than the virial equations by setting DREAL equal to 1.

Table A.2

Listing of Data File NH3.DAT

```
 0
 0.0035      0.055    11.4D-6
873.15      220.     .07      1

800.         .01

0.00335
0.48
0.2
0.31665

0
0
1.0
0

.674        10.9D19        2.304D05
1.40D-16    1.53d-17       1.62D-08    1.71D-16    8880.
1.374       1.513          .580        1.374

405.5  113.5   72.5  0.244  0.250  1.47  17.031
126.2   33.9   89.8  0.290  0.039  0.0   28.013
 33.2   13     65.1  0.306 -0.218  0.0    2.016
  5.19   2.27  57.4  0.302 -0.365  0.0    4.003

 0.0     0.25  -0.45  0.0
 0.25    0.0    0.0   0.16
-0.45    0.0    0.0   0.0
 0.0     0.16   0.0   0.0

-----------------------------------------------------
MODE (MODE=0 for memb. reac.,=1 for conv reac.,=2 for memb. sep.)
DR1(m.)    DRLO(m.)    DTHICK(m.)
DTEMP(K)  DPSIG(psig) DPR   DREAL(0,1,2)
DSCCMIT(sccm)   DSCCMIS(sccm)

DMOLSFRAC(j)

DBETA      DRKO(mol/(m^3 reactor s Pa^-DBETA)   DE(J/mol)
DPA  DPN  DPH  DPI(mol m/m^2 s Pa^n(J))  EACT(J/mol)
ANA  ANN   ANH   ANI (n(J) values)

DTC(i)  DPC(i)  DVC(i)  DZC(i)  DW(i)  DMU(i)  DMW(i)

DK(i,1)  DK(i,2)  DK(i,3)  DK(I,4)
  i= NH3,N2,H2,He
```

Table A.3
Summary of Input Parameters For DATA

Variable Name in DATA	Variable Name in Thesis Text	Description
NP1	-	Total number of collocation points including collocation point at the catalyst surface
XCOLL(I)	r	Array for collocation points (radial positions in catalyst particles where gas concentrations are calculated by orthogonal collocation)
DP	$2R_p$	Diameter of catalyst particle (m)
XGUESS	-	Initial guess for normalized ammonia concentration in catalyst particle (XGUESS assumes ammonia concentration is constant in the particles, just set it equal to 1.0)
A(I,J)	-	Collocation matrix for first derivative terms
B(I,J)	-	Collocation matrix for second derivative terms
W(J)	-	Weighting parameters used in numerical integration to calculate effectiveness factor
ERRREL	-	Convergence criteria for Newton-Raphson method in collocation calculations
BEDVOID	ε	Void fraction in catalyst bed
TORTFAC	τ_p	tortuosity factor for catalyst

Table A.3
Summary of Input Parameters For DATA (continued)

Variable Name in DATA	Variable Name in Thesis Text	Description
CATVOID	θ	Void fraction of catalyst particle
SURFA	S_g	Surface area of catalyst particle (m^2/kg)
CATBDEN	ρ_p	Bulk density of catalyst particle (kg/m^3)
AMASS	C_1	Proportionality constant in equation used to calculate the Sherwood number

Table A.4

Listing of Data File DATA

```
5

.29576  .56524  .78448  .934  1.0

.0007225  1.0

-5.0717   8.6586  -6.3671    4.6458   -1.8656
-1.4346  -2.6538   6.392    -3.7114    1.4077
  .523   -3.1687  -1.9121    6.6239   -2.0661
 -.3861   1.8615  -6.7019   -1.606     6.8325
  .7615  -3.4682  10.2684  -33.5618   26.000

-34.4654   44.1493  -14.2677    7.0025    -2.4186
 13.9798  -52.3162   48.837   -15.1776     4.6771
 -3.1083   33.6001  -94.5282   80.8944   -16.8579
  1.8377  -12.579    97.4469  -286.6901   199.9845
38.5462 -170.365   457.9635  -794.1446   468.000

.0251  .0792  .1152  .0956  .0182

.0000001

0.4  4.0  0.5  220000.  970.

0.015
```

```
NP1

XCOLL(I)  (I=1,NP1)

DP(m)  XGUESS

A(I,J)  ((J=1,NP1),I=1,NP1)

B(I,J)  ((J=1,NP1),I=1,NP1)

W(J)  J=1,NP1

ERRREL

BEDVOID  TORTFAC  CATVOID  SURFA(m2/kg)  CATBDEN(kg/m3)

AMASS
```

University. The collocation parameters are based on the symmetrical polynomials discussed by Finlayson (Section 4-7 of Finlayson, 1980) for orthogonal collocation for diffusion and reaction. Spherical geometry and a weighting function of $W=1-X^2$ were used in OCRXN to determine collocation points, matrices for first and second derivatives, and weighting parameters for numerical integration. See Finlayson (1980) for more information regarding the theory and procedures for orthogonal collocation for diffusion and reaction. The variable NP1 indicates the number of collocation points used in the calculations. Five collocation points (four interior collocation points) were used in the calculations performed in the present study.

Example Output From Membrane Reactor Model

The membrane reactor model was run using the data listed in Tables A.2 and A.4 for NH3.DAT and DATA. Table A.5 shows the program output. Program output includes the mole fractions, molar flow rates, and volumetric flows (sccm) for gas species as a function of dimensionless axial position. In addition, the effectiveness factor (ETA) and equilibrium ammonia mole fraction (YNH3EQ) are also listed as a function of dimensionless axial position. The equilibrium ammonia mole fraction is the ammonia concentration in equilibrium with the nitrogen and hydrogen concentrations at a particular axial position in the membrane reactor.

FORTRAN Code For Cocurrent Membrane Reactor Model

A listing of the FORTRAN code for the cocurrent membrane reactor model is presented on pages 171 to 196.

Table A.5

Example Output From Membrane Reactor Model

********* RESULTS OF CALCULATION *********

MOLE FRACTION		REACTION ZONE			PERMEATION ZONE		
L/Lo	CONV	NH3	N2	H2	NH3	N2	H2
.00	.000000	.003350	.480000	.200000	.000000	.000000	1.000000
.10	.105671	.003159	.506484	.156477	.000051	.006192	.987553
.20	.238871	.002793	.526552	.123836	.000058	.007480	.984970
.30	.380278	.002331	.540427	.101598	.000064	.009013	.981900
.40	.510891	.001867	.549336	.087597	.000070	.010766	.978389
.50	.620046	.001461	.554795	.079238	.000075	.012697	.974527
.60	.705522	.001136	.558085	.074367	.000080	.014753	.970414
.70	.769801	.000888	.560095	.071517	.000083	.016890	.966143
.80	.816866	.000705	.561372	.069795	.000086	.019072	.961785
.90	.850611	.000573	.562234	.068693	.000088	.021273	.957391
1.00	.874330	.000480	.562859	.067931	.000090	.023475	.952994

L/Lo	CONV	YNH3	YNH3EQ	ETA
.00	.000000	.003350	.001418	.689411
.10	.105671	.003159	.001008	.578061
.20	.238871	.002793	.000722	.472059
.30	.380278	.002331	.000544	.391835
.40	.510891	.001867	.000439	.341854
.50	.620046	.001461	.000380	.316398
.60	.705522	.001136	.000346	.307233
.70	.769801	.000888	.000327	.307832
.80	.816866	.000705	.000316	.313437
.90	.850611	.000573	.000309	.320905
1.00	.874330	.000480	.000304	.328356

MOLE/S		REACTION ZONE			PERMEATION ZONE		
L/Lo	CONV	NH3	N2	H2	NH3	N2	H2
.00	.000000	.199E-05	.286E-03	.119E-03	.00E+00	.000E+00	.744E-08
.10	.105671	.178E-05	.285E-03	.882E-04	.161E-08	.195E-06	.311E-04
.20	.238871	.151E-05	.285E-03	.671E-04	.308E-08	.399E-06	.526E-04
.30	.380278	.123E-05	.285E-03	.536E-04	.434E-08	.610E-06	.665E-04
.40	.510891	.969E-06	.285E-03	.455E-04	.537E-08	.826E-06	.750E-04
.50	.620046	.751E-06	.285E-03	.407E-04	.618E-08	.104E-05	.801E-04
.60	.705522	.580E-06	.285E-03	.380E-04	.682E-08	.126E-05	.831E-04
.70	.769801	.451E-06	.285E-03	.364E-04	.731E-08	.148E-05	.849E-04
.80	.816866	.357E-06	.285E-03	.354E-04	.770E-08	.171E-05	.860E-04
.90	.850611	.290E-06	.284E-03	.348E-04	.801E-08	.193E-05	.868E-04
1.00	.874330	.242E-06	.284E-03	.343E-04	.827E-08	.215E-05	.873E-04

Table A.5

Example Output From Membrane Reactor Model (Continued)

SCCM L/Lo	CONV	REACTION ZONE NH3	N2	H2	PERMEATION ZONE NH3	N2	H2
.00	.000000	2.680	384.000	160.000	.000	.000	.010
.10	.105671	2.395	383.879	118.598	.002	.262	41.837
.20	.238871	2.036	383.783	90.259	.004	.537	70.711
.30	.380278	1.655	383.689	72.132	.006	.821	89.407
.40	.510891	1.304	383.574	61.165	.007	1.110	100.899
.50	.620046	1.010	383.427	54.763	.008	1.404	107.740
.60	.705522	.780	383.246	51.069	.009	1.699	111.777
.70	.769801	.607	383.035	48.908	.010	1.996	114.196
.80	.816866	.480	382.800	47.593	.010	2.294	115.701
.90	.850611	.390	382.547	46.739	.011	2.593	116.691
1.00	.874330	.326	382.280	46.137	.011	2.892	117.388

TEMP(K),PRESS(in),PRESS(out) (Psig)= 873.15 220.00 1.73
Total SCCM and MOL/S input for Tube and Shell =
800.00000 .01000 .59490E-03 .74363E-08
Total SCCM and MOL/S output for Tube and Shell =
679.17534 123.17786 .50505E-03 .91598E-04

```
      PROGRAM MRR
C
C          BY: Nichakorn Kraisuwansarn and John Collins
C
C       This program solves for a decompositon of ammonia
C       in a conventional plug flow reactor or a cocurrent
C       membrane reactor including the reverse reaction.
C
C               NH3 = 0.5 N2 + 1.5 H2
C
C
C       Ammonia is converted to nitrogen and hydrogen in the
C       reaction zone. Helium may be used as a dilution gas in the
C       tube side and as a sweep gas in the shell side.  The shell
C       side may also be operated at a much lower total pressure
C       than the tube side which eliminates the need for a sweep
C       gas.
C
C       In the membrane reactor,each component may permeate through
C       the membrane, increasing the conversion above the
C       equilibrium value.
C       (No permeation for conventional reactor.)
C
C       Dimensionless molar flow rates of NH3, N2, N2, and He
C       are calculated as a function of axial position on both
C       the tube side and sweep side by solving a system of eight
C       ordinary differential equations.  Since the flow
C       configuration is cocurrent flow, an initial value problem is
C       solved.
C
C       The eight simultaneous equations are solved using IMSL math
C       libraries. The results of this program are the mole
C       fraction,molar flow rates, and volumetric flow rates (sccm)
C       of each component and ammonia conversion as a function of
C       dimensionless length.
C
C       This program also calculated effectiveness factors (ETA1) at
C       each axial position in the reactor.  The subroutine EFFECT
C       gives more information on how this is done.
C
C       --------------------------------
C       Defining variables and parameters
C       --------------------------------
C
C       **** Membrane configuration.****
C
C       DR1 = Inner radius-inner tube (m.)
C       DTHICK = Thickness of membrane (m) (Note: DTHICK = thickness
C                of Palladium film for Composite Metal Ceramic
C                Membranes)
C       DRLO   = Total length of reactor (m.)
C          DPj = Permeability of component(j) (mol/(m.s.Pa^n(J)))
C                   where j = A, N, H,I
C                   Note: DPH is the preexponential factor for
C                   calculating the hydrogen permeability (DPC) at a
C                   given temperature.
C           EACT  = Activation energy for hydrogen permeability
C                   (J/mol)
C       ANA,ANN  =  n(J) for ammonia, nitrogen, hydrogen and helium.
C       ANH,ANI      (ANA=ammonia, ANN=nitrogen,ANH=hydrogen,
C                     ANI=helium)
```

```
C
C       **** Kinetis and thermodynamics parameters.****
C
C       DTEMP = Temperature of the reactor (K)
C       DPTOT = Pressure of the reactor (Pa)
C       DPR   = Pressure ratio (Pt/Ps)
C       DDDEQ = Equilibrium constant (Pa)
C       DDKP  = Equilibrium constant (atm)
C            DRKO  = Pre-exponential factor for rate constant
C                    (mol/(m^3.s.Pa^(-DBETA)))
C            DRX   = Reaction rate constant
C                    (mol/(m^3.s.Pa^(-DBETA)))
C            DE    = Activation energy for reaction (J/mol)
C            DBETA = Constant for the reaction rate law
C            DREAL = Parameter setting for ideal or real gas
C
C
C             DFAT  = Fugacity coefficient for NH3 in tube
C             DFNT  = Fugacity coefficient for N2  in tube
C             DFHT  = Fugacity coefficient for H2  in tube
C             DFIT  = Fugacity coefficient for He  in tube
C             DFAS  = Fugacity coefficient for NH3 in shell
C             DFNS  = Fugacity coefficient for N2  in shell
C             DFHS  = Fugacity coefficient for H2  in shell
C             DFIS  = Fugacity coefficient for N2  in shell
C
C       **** IMSL parameters.****
C
C       PARAM(1) = HINT  = Initial value of step size.
C       PARAM(4) = MXSTEP= Maximum number of step.
C       PARAM(10)= INORM = Error estimate method.
C       PARAM(12)= IMETH = Numerical method.
C       PARAM(13)= MITER = Type of iteration.
C       PARAM(14)= MTYPE = Matrix type of jacobian.
C       PARAM(19)= IATYPE= Matrix type for A.
C                NEQ = Number of equation.
C                X   = Dimensionless length.
C                XEND= Value of X where solution is desired.
C                TOL = Error tolerance.
C       Y(NEQ) = Dimensionless molar flow rate of each component
C       Inner tube, Y(1) for NH3
C                   Y(2) for N2
C                   Y(3) for H2
C                   Y(4) for Inert gas(He)
C       Outer tube, Y(5) for NH3
C                   Y(6) for N2
C                   Y(7) for H2
C                   Y(8) for Inert gas(He)
C       YPRIME(NEQ).....dY(NEQ)/dX
C
C     **** OUTPUT PARAMETERS. ****
C     DLENGTH  = Dimensionless length
C     DCONVER  = Conversion of reaction
C     DFTOT    = Dimensionless total molar flowrate in tube
C     DQTOT    = Dimensionless total molar flowrate in shell
C     DAIN     = Dimensionless molar flowrate of NH3 in tube
C     DNIN     = Dimensionless molar flowrate of N2  in tube
C     DHIN     = Dimensionless molar flowrate of H2  in tube
C     DIIN     = Dimensionless molar flowrate of He  in tube
C     DAOUT    = Dimensionless molar flowrate of NH3 in shell
C     DNOUT    = Dimensionless molar flowrate of N2  in shell
C     DHOUT    = Dimensionless molar flowrate of H2  in shell
```

```
C     DIOUT    = Dimensionless molar flowrate of He  in shell
C     YAEQ     = Mole fraction of NH3 in equilibrium with
C                H2 and N2 mole fractions at a particular
C                position (DLENGTH) in the membrane reactor
C     ETA      = Effectiveness factor at a particular
C                position (DLENGTH) in the membrane reactor.
C
C     ******* MAIN PROGRAM *********************************
C
      IMPLICIT DOUBLE PRECISION(A-H,O-Z)
      DOUBLE PRECISION DRKO,DE,DTEMP,DPTOT,DFAO,DEQ
     *                ,DR1,DRLO,DPA,DPN,DPH,DPI,DPR
      DOUBLE PRECISION X,Y,A,PARAM,HINIT,XEND,TOL
      DOUBLE PRECISION DCONV,DFAIN
      DOUBLE PRECISION DLENGTH,DCONVER,DFTOT,DQTOT,
     *                 DAIN,DNIN,DHIN,DIIN,DAOUT,DNOUT,DHOUT,DIOUT
      DOUBLE PRECISION DMOLSFEED
      DOUBLE PRECISION DFAT,DFNT,DFHT,DFIT,DFAS,DFNS,DFHS,DFIS
      INTEGER NEQ,NPARAM,MXSTEP,INORM,IMETH,MITER,MTYPE,
     *        IATYPE,IDO,IEND,ISET,I,II,MODE,DREAL
      COMMON/SET1/DRKO,DE,DTEMP,DPTOT,DFAO,DEQ
     *           ,DR1,DRLO,DPA,DPN,DPH,DPI,DPR
      COMMON/FUGA/DFAT,DFNT,DFHT,DFIT,DFAS,DFNS,DFHS,DFIS
      COMMON/FEED/YM(8)
      COMMON/EFFT2/ETA1,YNH3EQ
      COMMON/REAL/DREAL,MODE
      COMMON/PERMCOEF/ANH,ANN,ANI,ANA,EACT
      COMMON/MOLES/DMOLSFRAC(8)
      COMMON/SCCM/DFEEDIT,DFEEDIS,DSCCMIT,DSCCMIS
      DIMENSION A(8,8),PARAM(50),Y(8),ETA(101),YAEQ(101)
      DIMENSION DLENGTH(101),DCONVER(101),DFTOT(101),DQTOT(101),
     *          DAIN(101)   ,DNIN(101)   ,DHIN(101) ,DIIN(101),
     *          DAOUT(101)  ,DNOUT(101)  ,DHOUT(101),DIOUT(101)
      DIMENSION DMOLSFEED(8)
      EXTERNAL FCN,FCNJ,DIVPAG,SSET,UMACH
C
C     ***** READ DATA FROM FILES NH3.DAT AND DATA *************
C
      OPEN(UNIT=1,FILE='NH3.DAT',STATUS='OLD')
      OPEN(UNIT=10,FILE='DATA',STATUS='OLD')
      CALL AREAD(DRKO,DE,DTEMP,DPTOT,DR1,DRLO,
     1           DPA,DPN,DPH,DPI,DPR,DMOLSFEED)
      CLOSE(1)
      CLOSE(10)
C
C     ***** SET INITIAL VALUES OF THE SYSTEM ***
C
      IF(DMOLSFEED(1).GT.0.0)THEN
       IP=1
      ELSEIF(DMOLSFEED(2).GT.0.0)THEN
       IP=2
      ELSE
       IP=3
      ENDIF
      Y(1) = DMOLSFEED(1)/DMOLSFEED(IP)
      Y(2) = DMOLSFEED(2)/DMOLSFEED(IP)
      Y(3) = DMOLSFEED(3)/DMOLSFEED(IP)
      Y(4) = DMOLSFEED(4)/DMOLSFEED(IP)
      Y(5) = DMOLSFEED(5)/DMOLSFEED(IP)
      Y(6) = DMOLSFEED(6)/DMOLSFEED(IP)
      Y(7) = DMOLSFEED(7)/DMOLSFEED(IP)
      Y(8) = DMOLSFEED(8)/DMOLSFEED(IP)
```

```
      DO 69 II2=1,8
      YM(II2)=Y(II2)
 69   CONTINUE
         DFAIN=Y(IP)
         DFAO=DMOLSFEED(IP)

C     ***** CALL FUGACITY SUBROUTINE ***************************
C
      CALL FUGACITY(DFAT,DFNT,DFHT,DFIT,
     *             DFAS,DFNS,DFHS,DFIS,DTEMP,DPTOT,DPR,DREAL)
C
      DLOGKB=2250.322/DTEMP-0.85340-1.51049*DLOG10(DTEMP)
     *         -25.898D-5*DTEMP+14.8961D-8*DTEMP**2
      DDKB=10.0**DLOGKB
      YTOT=Y(1)+Y(2)+Y(3)+Y(4)
      ISET=1
      YAEQ(ISET)=DDKB*(Y(2)/YTOT*DFNT)**0.5*(Y(3)/YTOT*DFHT)**1.5
     *          *DPTOT/DFAT/1.0132D5
               IF(MODE.NE.2) THEN
               CALL EFFECT(ETA1)
                ENDIF
            ETA(ISET)=ETA1
            X=0.0
            DCONV=0.0
            DLENGTH(ISET)=X
            DCONVER(ISET)=DCONV
            DFTOT(ISET)  =(Y(1)+Y(2)+Y(3)+Y(4))
            DQTOT(ISET)  =(Y(5)+Y(6)+Y(7)+Y(8))
            DAIN(ISET)   =Y(1)
            DNIN(ISET)   =Y(2)
            DHIN(ISET)   =Y(3)
            DIIN(ISET)   =Y(4)
            DAOUT(ISET)  =Y(5)
            DNOUT(ISET)  =Y(6)
            DHOUT(ISET)  =Y(7)
            DIOUT(ISET)  =Y(8)
C
C     ***** SET IMSL PARAMETERS ****************************
C
          NPARAM=50
          NEQ=8
          HINIT=1.0D-8
          MXSTEP=10000
          INORM=2
          IMETH=2
          MITER=0
          MTYPE=0
          IATYPE=0
C
C   CALL SSET SUBROUTINE ON IMSL
C
       CALL SSET(50,0.0,PARAM,1)
       PARAM(1)=HINIT
       PARAM(4)=MXSTEP
       PARAM(10)=INORM
       PARAM(12)=IMETH
       PARAM(13)=MITER
       PARAM(14)=MTYPE
       PARAM(19)=IATYPE
        IDO=1
        TOL=1.0D-6
C
```

```
C     ------------------------------------------------------
C     NOW SOLVE THE PROBLEM USING IMSL
C
      DO 10 IEND=1,100
        XEND=FLOAT(IEND)/100.
        IDO=1
        CALL FUGACITY(DFAT,DFNT,DFHT,DFIT,
     *                DFAS,DFNS,DFHS,DFIS,
     *                DTEMP,DPTOT,DPR,DREAL)
C
C     ***** CALL GEARS METHOD ON IMSL VIA DIVPAG IMSL SUBROUTINE
C
      CALL DIVPAG(IDO,NEQ,FCN,FCNJ,A,X,XEND,TOL,PARAM,Y)
C
C     ***** DISPLAY RESULTS *********************************
C
          DCONV=1.-Y(1)/DFAIN-Y(5)/DFAIN
C     STORING RESULT
          I=IEND+1
          ETA(I)=ETA1
          DLENGTH(I)=X
          YAEQ(I)=YNH3EQ
          DCONVER(I)=DCONV
          DFTOT(I)  =(Y(1)+Y(2)+Y(3)+Y(4))
          DQTOT(I)  =(Y(5)+Y(6)+Y(7)+Y(8))
          DAIN(I)   =Y(1)
          DNIN(I)   =Y(2)
          DHIN(I)   =Y(3)
          DIIN(I)   =Y(4)
          DAOUT(I)  =Y(5)
          DNOUT(I)  =Y(6)
          DHOUT(I)  =Y(7)
          DIOUT(I)  =Y(8)
        IDO=3
        CALL DIVPAG(IDO,NEQ,FCN,FCNJ,A,X,XEND,TOL,PARAM,Y)
   10 CONTINUE
C
C-------------------------------------------------------------
C
C     ***** OUTPUT PRINTING *********************************
      CALL WRITE(DLENGTH,DCONVER,DFTOT,DQTOT
     *          ,DAIN,DNIN,DHIN,DIIN,DAOUT,DNOUT,DHOUT,DIOUT,DFAO
     *          ,DTEMP,DPTOT,DPR,ETA,YAEQ)
      END
C
C     ------------------------------------------------------------
C     SUBROUTINES
C
C     This subroutine provides the differential equations to IMSL.
C
      SUBROUTINE FCN (NEQ,X,Y,YPRIME)
      IMPLICIT DOUBLE PRECISION(A-H,O-Z)
      DOUBLE PRECISION DRKO,DE,DTEMP,DPTOT,DFAO,DEQ
     *                ,DR1,DRLO,DPA,DPN,DPH,DPI,DPR
      DOUBLE PRECISION YPRIME,Y,X,DVTFAO,DRX,DRRATE
      DOUBLE PRECISION DBETA,DTHICK
      DOUBLE PRECISION DFAT,DFNT,DFHT,DFIT,
     *                 DFAS,DFNS,DFHS,DFIS
      DOUBLE PRECISION DDEQ,DRR1,DRR2,DDDEQ
      DOUBLE PRECISION DLOGKB,DDKB
      INTEGER NEQ,DREAL,MODE
```

```
      COMMON/SET1/DRKO,DE,DTEMP,DPTOT,DFAO,DEQ,
     *            DR1,DRLO,DPA,DPN,DPH,DPI,DPR
      COMMON/BET/DBETA
      COMMON/FUGA/DFAT,DFNT,DFHT,DFIT,DFAS,DFNS,DFHS,DFIS
      COMMON/THICK/DTHICK
      COMMON/REAL/DREAL,MODE
      COMMON/EFFT2/ETA1,YNH3EQ
      COMMON/PERMCOEF/ANH,ANN,ANI,ANA,EACT
      COMMON/FEED/YM(8)
      DIMENSION Y(8),YPRIME(8)
      DO 5 II1=1,8
         YM(II1)=Y(II1)
5     CONTINUE
      DRX=DRKO*DEXP(-DE/8.314/DTEMP)
      DVTFAO=3.141592654*(DR1)**2.*(DRLO)/DFAO
      DLOGKB=2250.322/DTEMP-0.85340-1.51049*DLOG10(DTEMP)
     *       -25.898D-5*DTEMP+14.8961D-8*DTEMP**2
      DDKB=10.0**DLOGKB
      DDDEQ=1./DDKB*1.0132D5
      DRR1=-DRX *((DPTOT*DFAT*Y(1)/(Y(1)+Y(2)+Y(3)+Y(4)))**2/
     *                (DPTOT*DFHT*Y(3)/(Y(1)+Y(2)+Y(3)+Y(4)))**3
     *               )**DBETA
      DRR2=+DRX     *(DPTOT*DFNT*Y(2)/(Y(1)+Y(2)+Y(3)+Y(4)))
     *                *((DPTOT*DFHT*Y(3)/(Y(1)+Y(2)+Y(3)+Y(4)))**3/
     *                  (DPTOT*DFAT*Y(1)/(Y(1)+Y(2)+Y(3)+Y(4)))**2
     *                 )**(1-DBETA)/DDDEQ**2
      IF(MODE.NE.2) THEN
         CALL EFFECT(ETA1)
      ENDIF
      DRRATE= ETA1*(DRR1+DRR2)
      DPC=DPH*DEXP(-EACT/8.314/DTEMP)
      YTOT=Y(1)+Y(2)+Y(3)+Y(4)
      YNH3EQ=DDKB*(Y(2)/YTOT*DFNT)**0.5*(Y(3)/YTOT*DFHT)**1.5
     *       *DPTOT/DFAT/1.0132D5
      YPRIME(1)=    ( 1.* DRRATE- 2./DR1*DPA/(DTHICK)*(DPTOT**(ANA)-
     *                  (DPTOT*DPR)**ANA)*
     *                      ( Y(1)/(Y(1)+Y(2)+Y(3)+Y(4)))
     *              )
     *               *DVTFAO
      YPRIME(2)=    (- 0.5*DRRATE-2./DR1*DPN/(DTHICK)*(DPTOT**(ANN)-
     *                (DPTOT*DPR)**ANN)*
     *                       ( Y(2)/(Y(1)+Y(2)+Y(3)+Y(4)))
     *               )
     *               *DVTFAO
      YPRIME(3)=    (- 1.5*DRRATE-2./DR1*DPC/(DTHICK)*DPTOT**(ANH)*
     *                         (( Y(3)/(Y(1)+Y(2)+Y(3)+Y(4)))**(ANH)
     *                          -(Y(7)/(Y(5)+Y(6)+Y(7)+Y(8))
     *                *DPR)**(ANH) )
     *               )
     *                *DVTFAO
      YPRIME(4)=    (            -2./DR1*DPI/(DTHICK)*(DPTOT**(ANI)-
     *                     (DPTOT*DPR)**ANI)*
     *                        (  Y(4)/(Y(1)+Y(2)+Y(3)+Y(4)))
     *                 )
     *                 *DVTFAO
      YPRIME(5)=     (             2./DR1*DPA/(DTHICK)*(DPTOT**(ANA)-
     *                           (DPTOT*DPR)**ANA)*
     *                           ( Y(1)/(Y(1)+Y(2)+Y(3)+Y(4)))
     *                 )
     *                  *DVTFAO
      YPRIME(6)=     (             2./DR1*DPN/(DTHICK)*(DPTOT**(ANN)-
     *                           (DPTOT*DPR)**ANN)*
```

```
*                          ( Y(2)/(Y(1)+Y(2)+Y(3)+Y(4)))
*                    )
*                     *DVTFAO
      YPRIME(7)=     (            2./DR1*DPC/(DTHICK)*DPTOT**(ANH)*
*                          (( Y(3)/(Y(1)+Y(2)+Y(3)+Y(4)))**(ANH)
*                           -(Y(7)/(Y(5)+Y(6)+Y(7)+Y(8))
*                     *DPR)**(ANH)     )
*                    )
*                     *DVTFAO
      YPRIME(8)=     (            2./DR1*DPI/(DTHICK)*(DPTOT**(ANI)-
*                          (DPTOT*DPR)**ANI)*
*                          ( Y(4)/(Y(1)+Y(2)+Y(3)+Y(4)))
*                    )
*                     *DVTFAO
      RETURN
      END
C
C
C     ------------------------------------------------------------
C
C     This subroutine provides jacobian matrix to IMSL.
C
      SUBROUTINE FCNJ(NEQ,X,Y,DYPDY)
C
C     This subroutine in not used because the option where
C     IMSL calculates the jacobian numerically was chosen.
C
      RETURN
      END
C
C
C     ------------------------------------------------------------
C
C     This subroutine provides input data to the program.
C
      SUBROUTINE AREAD(DRKO,DE,DTEMP,DPTOT,DR1,DRLO,
     *                 DPA,DPN,DPH,DPI,DPR,DMOLSFEED)
      IMPLICIT DOUBLE PRECISION(A-H,O-Z)
      DOUBLE PRECISION DRKO,DE,DEQ,DR1,DRLO
     *                 ,DPA,DPN,DPH,DPI,DMOLSFEED,DMOLSFRAC
      DOUBLE PRECISION DDEQ
      DOUBLE PRECISION DBETA,DTHICK
      DOUBLE PRECISION DTEMP,DPTOT,DPR,DPSIG
      DOUBLE PRECISION DTC,DPC,DVC,DZC,DW,DMUR,DMW,DK
      DOUBLE PRECISION DFEEDIT,DFEEDIS,DSCCMIT,DSCCMIS
      INTEGER I,NP1,MODE,DREAL
      COMMON/BET/DBETA
      COMMON/CRIT/DTC,DPC,DVC,DZC,DW,DMUR,DMW
      COMMON/INTERAC/DK
      COMMON/THICK/DTHICK
      COMMON/REAL/DREAL,MODE
      COMMON/SCCM/DFEEDIT,DFEEDIS,DSCCMIT,DSCCMIS
      COMMON/PERMCOEF/ANH,ANN,ANI,ANA,EACT
      COMMON/MOLES/DMOLSFRAC(8)
      COMMON/CRXN/A1(7,7),B1(7,7),NP1,W(7),XCOLL(7)
      COMMON/MASSTX/AMASS,DP,GUESS,ERRREL,BEDVOID,TORTFAC,CATVOID,
     *              SURFA,CATBDEN
      DIMENSION DMOLSFEED(8)
      DIMENSION DTC(4),DPC(4),DVC(4),DZC(4),DW(4),DMUR(4),DMW(4),
     *          DK(4,4)
C
      READ(1,*) MODE
```

```
      READ(1,*) DR1,DRLO,DTHICK
      READ(1,*) DTEMP,DPSIG,DPR,DREAL
      READ(1,*) DSCCMIT,DSCCMIS
      DO 90 I=1,8
      READ(1,*) DMOLSFRAC(I)
   90 CONTINUE
      READ(1,*) DBETA,DRKO,DE
      IF(MODE.EQ.2)DRKO=0.0
      READ(1,*) DPA,DPN,DPH,DPI,EACT
      IF(MODE.EQ.1) THEN
       DPA=0.0
       DPN=0.0
       DPH=0.0
       DPI=0.0
      ENDIF
      READ(1,*)ANA,ANN,ANH,ANI
      DO 80 I=1,4
      READ(1,*)DTC(I),DPC(I),DVC(I),DZC(I),DW(I),DMUR(I),DMW(I)
   80 CONTINUE
      DO 70 I=1,4
      READ(1,*)DK(I,1),DK(I,2),DK(I,3),DK(I,4)
   70 CONTINUE
      READ(10,*) NP1
      READ(10,*)(XCOLL(I),I=1,NP1)
      READ(10,*)DP,GUESS
      DO 10 I=1,NP1
      READ(10,*) (A1(I,J), J=1,NP1)
 10   CONTINUE
      DO 20 I=1,NP1
      READ(10,*) (B1(I,J), J=1,NP1)
 20   CONTINUE
      READ(10,*) (W(J),J=1,NP1)
      READ(10,*)ERRREL
      READ(10,*)BEDVOID,TORTFAC,CATVOID,SURFA,CATBDEN
      READ(10,*)AMASS
C     ***CHANGE UNIT***
      DPTOT=(DPSIG+14.7)/14.7*101325.
C     CHANGE SCCM TO MOL/S BASIS
C
      DFEEDIT=DSCCMIT*1.01325/273.15/83.14/60.0
      DFEEDIS=DSCCMIS*1.01325/273.15/83.14/60.0
      DO 60 I=1,4
      DMOLSFEED(I)=DMOLSFRAC(I)*DFEEDIT
   60 CONTINUE
      DO 50 I=5,8
      DMOLSFEED(I)=DMOLSFRAC(I)*DFEEDIS
   50 CONTINUE
C     ******************
      WRITE(*,*)
      WRITE(*,1000)
 1000 FORMAT( ' ********** CALCULATING  WAIT! **********')
      RETURN
      END
C
C
C     ------------------------------------------------------------
C
C     This subroutine gives output result to printer and/or monitor.
C
      SUBROUTINE WRITE(DLENGTH,DCONVER,DFTOT,DQTOT,DAIN,DNIN,DHIN,
     *                 DIIN,DAOUT,DNOUT,DHOUT,DIOUT,DFAO
     *                ,DTEMP,DPTOT,DPR,ETA,YAEQ)
```

```
      IMPLICIT DOUBLE PRECISION(A-H,O-Z)
      DOUBLE PRECISION DLENGTH,DCONVER,DFTOT,DQTOT,
     *     DAIN,DNIN,DHIN,DIIN,DAOUT,DNOUT,DHOUT,DIOUT
      DOUBLE PRECISION DFAO
      DOUBLE PRECISION DFEEDIT,DFEEDIS,DSCCMIT,DSCCMIS
      DOUBLE PRECISION DFEEDOT,DFEEDOS,DSCCMOT,DSCCMOS
      DOUBLE PRECISION DTEMP,DPTOT,DPR
      REAL OUTPUT
      INTEGER I,II
      COMMON/SCCM/DFEEDIT,DFEEDIS,DSCCMIT,DSCCMIS
      DIMENSION DLENGTH(101),DCONVER(101),DFTOT(101),DQTOT(101),
     *          DAIN(101)   ,DNIN(101)   ,DHIN(101)  ,DIIN(101),
     *          DAOUT(101)  ,DNOUT(101)  ,DHOUT(101) ,DIOUT(101)
      DIMENSION ETA(101),YAEQ(101)
      DFEEDOT=(DAIN(101)+DNIN(101)+DHIN(101)+DIIN(101))*DFAO
      DFEEDOS=(DAOUT(101)+DNOUT(101)+DHOUT(101)+DIOUT(101))*DFAO
      DSCCMOT=DFEEDOT*273.15*83.14*60.0/1.01325
      DSCCMOS=DFEEDOS*273.15*83.14*60.0/1.01325
      WRITE(*,*)
      WRITE(*,800)
      WRITE(*,*)
   50 WRITE(*,*)
      WRITE(*,900)
      WRITE(*,1000)
      READ(*,*) OUTPUT
      IF (OUTPUT.EQ.1.0) THEN
       GOTO 10
                  ELSE
                 IF (OUTPUT.EQ.0.0) THEN
                  GOTO 40
                            ELSE
                           IF (OUTPUT.EQ.2.0) THEN
                              GOTO 40
                                        ELSE
                              GOTO 50
                                        ENDIF
                            ENDIF
                   ENDIF
   40 WRITE(*,*)
      WRITE(*,100)
      WRITE(*,*)
      WRITE(*,*)
      WRITE(*,250)
      WRITE(*,350)
      WRITE(*,*)
      DO 25 I=1,101,10
      WRITE(*,450) DLENGTH(I),DCONVER(I),
     *             DAIN(I)/DFTOT(I), DNIN(I)/DFTOT(I),
     *             DHIN(I)/DFTOT(I), DAOUT(I)/DQTOT(I),
     *             DNOUT(I)/DQTOT(I), DHOUT(I)/DQTOT(I)
   25   CONTINUE
      WRITE(*,*)
      WRITE(*,351)
      DO 5 I=1,101,10
      WRITE(*,950) DLENGTH(I),DCONVER(I), DAIN(I)/DFTOT(I), YAEQ(I),
     *             ETA(I)
   5  CONTINUE
      READ(*,*) II
C
C
      WRITE(*,*)
      WRITE(*,360)
```

```
      WRITE(*,350)
      WRITE(*,*)
      DO 26 I=1,101,10
      WRITE(*,460) DLENGTH(I),DCONVER(I),
     *             DAIN(I)*DFAO ,DNIN(I)*DFAO ,DHIN(I)*DFAO,
     *             DAOUT(I)*DFAO,DNOUT(I)*DFAO,DHOUT(I)*DFAO
   26 CONTINUE
      READ(*,*) II
C
      WRITE(*,*)
      WRITE(*,355)
      WRITE(*,350)
      WRITE(*,*)
       DO 27 I=1,101,10
      WRITE(*,465) DLENGTH(I),DCONVER(I),
     *             DAIN(I)*DFAO*273.15*83.14*60./1.01325,
     *             DNIN(I)*DFAO*273.15*83.14*60./1.01325,
     *             DHIN(I)*DFAO*273.15*83.14*60./1.01325,
     *             DAOUT(I)*DFAO*273.15*83.14*60./1.01325,
     *             DNOUT(I)*DFAO*273.15*83.14*60./1.01325,
     *             DHOUT(I)*DFAO*273.15*83.14*60./1.01325
   27    CONTINUE
      WRITE(*,*)
      WRITE(*,440)DTEMP,DPTOT/101325.*14.7-14.7,
     1        DPTOT*DPR/101325.*14.7-14.7
      WRITE(*,480) DSCCMIT,DSCCMIS,DFEEDIT,DFEEDIS
      WRITE(*,470) DSCCMOT,DSCCMOS,DFEEDOT,DFEEDOS
      IF (OUTPUT.EQ.2.0) THEN
       GOTO 10
                   ELSE
       GOTO 60
                   ENDIF
C
   10 OPEN(UNIT=2,FILE='A:NH3R.RES',STATUS='NEW')
      WRITE(2,*)
      WRITE(2,100)
      WRITE(2,*)
      WRITE(2,*)
      WRITE(2,200)
      WRITE(2,300)
      WRITE(2,*)
      DO 20 I=1,101
      WRITE(2,400) DLENGTH(I),DCONVER(I),
     *             DAIN(I)/DFTOT(I), DNIN(I)/DFTOT(I),
     *             DHIN(I)/DFTOT(I), DIIN(I)/DFTOT(I),
     *             DAOUT(I)/DQTOT(I),DNOUT(I)/DQTOT(I),
     *             DHOUT(I)/DQTOT(I), DIOUT(I)/DQTOT(I)
   20   CONTINUE
      WRITE(2,*)
      WRITE(2,*)
      WRITE(2,500)
      WRITE(2,300)
      WRITE(2,*)
      DO 30 I=1,101
      WRITE(2,600) DLENGTH(I),DCONVER(I),
     *             DAIN(I)*DFAO ,DNIN(I)*DFAO ,DHIN(I)*DFAO
     *            ,DIIN(I)*DFAO,
     *             DAOUT(I)*DFAO,DNOUT(I)*DFAO,DHOUT(I)*DFAO
     *            ,DIOUT(I)*DFAO
   30   CONTINUE
      WRITE(2,*)
      WRITE(2,*)
```

```
      WRITE(2,550)
      WRITE(2,300)
      WRITE(2,*)
      DO 35 I=1,101
      WRITE(2,650) DLENGTH(I),DCONVER(I),
     *             DAIN(I)*DFAO*273.15*83.14*60./1.01325,
     *             DNIN(I)*DFAO*273.15*83.14*60./1.01325,
     *             DHIN(I)*DFAO*273.15*83.14*60./1.01325,
     *             DIIN(I)*DFAO*273.15*83.14*60./1.01325,
     *             DAOUT(I)*DFAO*273.15*83.14*60./1.01325,
     *             DNOUT(I)*DFAO*273.15*83.14*60./1.01325,
     *             DHOUT(I)*DFAO*273.15*83.14*60./1.01325,
     *             DIOUT(I)*DFAO*273.15*83.14*60./1.01325
   35 CONTINUE
      WRITE(2,*)
      WRITE(2,440)DTEMP,DPTOT/101325*14.7-14.7,
     1       DPTOT*DPR/101325.*14.7-14.7
      WRITE(2,480) DSCCMIT,DSCCMIS,DFEEDIT,DFEEDIS
      WRITE(2,470) DSCCMOT,DSCCMOS,DFEEDOT,DFEEDOS
      CLOSE(2)
  100 FORMAT('       ********* RESULTS OF CALCULATION *********')
  200 FORMAT(' MOLE FRACTION           REACTION ZONE
     *         PERMEATION ZONE')
  300 FORMAT('   L/Lo       CONV       NH3       N2          H2
     *INERT          NH3       N2         H2       INERT')
  400 FORMAT(2X,F4.2,4X,F8.6,3X,4(F10.6),2X,4(F10.6))
  500 FORMAT(' MOLE/S                  REACTION ZONE
     *       PERMEATION ZONE')
  550 FORMAT(' SCCM                    REACTION ZONE
     *       PERMEATION ZONE')
  600 FORMAT(2X,F4.2,4X,F8.6,3X,4(E10.4),2X,4(E10.4))
  650 FORMAT(2X,F4.2,4X,F8.6,3X,4(F10.3),2X,4(E10.3))
  250 FORMAT(' MOLE FRACTION           REACTION ZONE
     *PERMEATION ZONE')
  360 FORMAT(' MOLE/S                  REACTION ZONE
     *PERMEATION ZONE')
  355 FORMAT(' SCCM                    REACTION ZONE
     *PERMEATION ZONE')
  350 FORMAT('   L/Lo    CONV       NH3       N2       H2         NH3
     *  N2       H2')
  351 FORMAT('   L/Lo    CONV      YNH3    YNH3EQ    ETA')
  440 FORMAT(' TEMP(K),PRESS(in),PRESS(out) (Psig)= ',3(F8.2))
  450 FORMAT(2X,F4.2,2X,F8.6,2X,3(F9.6),1X,3(F9.6))
  950 FORMAT(2X,F4.2,2X,F8.6,2X,3(F9.6))
  460 FORMAT(2X,F4.2,2X,F8.6,2X,3(E9.3),1X,3(E9.3))
  465 FORMAT(2X,F4.2,2X,F8.6,2X,3(F9.3),1X,3(F9.3))
  470 FORMAT(2X,'Total SCCM  and  MOL/S output for Tube    and
     *SHELL='/2X,F13.5,1X,F13.5,3X,E13.5,1X,E13.5)
  480 FORMAT(2X,'Total SCCM  and  MOL/S  input for Tube    and
     *SHELL='/2X,F13.5,1X,F13.5,3X,E13.5,1X,E13.5)
  800 FORMAT(' **** THE CALCULATION IS NOW COMPLETED ****')
  900 FORMAT(' DO YOU WANT THE RESULTS ON MONITOR OR COMPUTER FILE)
 1000 FORMAT(' PRESS <0> FOR MONITOR OR <1> FOR COMPUTER FILE OR <2>
     * FOR BOTH DEVICES ')
   60 RETURN
      END
C
C     ---------------------------------------------------------
C
C     This subroutine calculates fugacity coefficients.
C
      SUBROUTINE FUGACITY(DFAT,DFNT,DFHT,DFIT,
```

```
*                    DFAS,DFNS,DFHS,DFIS,DTEMP,DPTOT,DPR,DREAL)
      IMPLICIT DOUBLE PRECISION(A-H,O-Z)
      DOUBLE PRECISION DFAT,DFNT,DFHT,DFIT,
     *                 DFAS,DFNS,DFHS,DFIS
      DOUBLE PRECISION DTEMP,DPTOT,DPT,DPR
      INTEGER DREAL
      IF (DREAL.EQ.0)THEN
        DFAT= 1.0
        DFNT= 1.0
        DFHT= 1.0
        DFIT= 1.0
        DFAS= 1.0
        DFNS= 1.0
        DFHS= 1.0
        DFIS= 1.0
        GOTO 100
                ELSE
                     IF(DREAL.EQ.1)THEN
      DPT=DPTOT/1.013E5
      DFAT=0.1438996+0.2028538D-2*DTEMP-0.4487672D-3*DPT
     *     -0.1142945D-5*DTEMP**2+0.2761216D-6*DPT**2
      DFNT=0.93431737+0.3101804D-3*DTEMP+0.295896D-3*DPT
     *     -0.2707279D-6*DTEMP**2+0.4775207D-6*DPT**2
      DFHT=DEXP(DEXP(-3.8402*DTEMP**0.125+0.541)*DPT
     *     -DEXP(-0.1263*DTEMP**0.5-15.980)*DPT**2
     *     +300*DEXP(-0.011901*DTEMP-5.941)*(DEXP(-DPT/300)
     *                                                -1))
      DFIT=1.0
      DFAS=0.1438996+0.2028538D-2*DTEMP-0.4487672D-3*DPT*DPR
     *     -0.1142945D-5*DTEMP**2+0.2761216D-6*(DPT*DPR)**2
      DFNS=0.93431737+0.3101804D-3*DTEMP+0.295896D-3*DPT*DPR
     *     -0.2707279D-6*DTEMP**2+0.4775207D-6*(DPT*DPR)**2
      DFHS=DEXP(DEXP(-3.8402*DTEMP**0.125+0.541)*DPT*DPR
     *     -DEXP(-0.1263*DTEMP**0.5-15.980)*(DPT*DPR)**2
     *     +300*DEXP(-0.011901*DTEMP-5.941)*(DEXP(-DPT*DPR/300)
     *                                                -1))
      DFIS=1.0
                          GOTO 100
                          ELSE
                          IF (DREAL.EQ.2)THEN
                          CALL VIRIAL(DFAT,DFNT,DFHT,DFIT,
     *                                DFAS,DFNS,DFHS,DFIS,
     *                                DTEMP,DPTOT,DPR)
                                   ELSE
                          WRITE(*,120)
                          STOP
                                   ENDIF
                     ENDIF
                ENDIF
  100 RETURN
  120 FORMAT(' ERROR IN STATE OF CALCULATION !  PROGRAM STOP!')
      END
C
C
C     ---------------------------------------------------------------
C
C
C     This subroutine calculates fugacity coefficient by virial
      equation.
C
      SUBROUTINE VIRIAL(DFAT,DFNT,DFHT,DFIT,DFAS,DFNS,DFHS,DFIS,
     *                  DTEMP,DPTOT,DPR)
```

```
      IMPLICIT DOUBLE PRECISION(A-H,O-Z)
      INTEGER I,J
      DOUBLE PRECISION DFAT,DFNT,DFHT,DFIT,DFAS,DFNS,DFHS,DFIS
      DOUBLE PRECISION V,DPR,DTEMP,DPTOT
      DOUBLE PRECISION Y,Z
      DOUBLE PRECISION DFO ,DF1 ,DF2 ,D2COEF,
     *                 DFOM,DF1M,DF2M,D2COEFM,
     *                 DTC,DPC,DVC,DZC,DW,DMUR,DMW,DK,
     *                 DTR,FRAC,DPRESS,DZMIX,D2MIX,
     *                 DTCM,DVCM,DZCM,DWM,DPCM,DTRM
      DIMENSION DFO(4),DF1(4),DF2(4),D2COEF(4),
     *          DFOM(4,4),DF1M(4,4),DF2M(4,4),D2COEFM(4,4),
     *          DTC(4),DPC(4),DVC(4),DZC(4),DW(4),DMUR(4),DMW(4),
     *          DTR(4),FRAC(8),DK(4,4),
     *          DTCM(4,4),DVCM(4,4),DZCM(4,4),DWM(4,4),DPCM(4,4),
     *          DTRM(4,4)
      DIMENSION Y(8)
      COMMON/CRIT/DTC,DPC,DVC,DZC,DW,DMUR,DMW
      COMMON/FEED/Y
      COMMON/INTERAC/DK
C
      DO 30 I=1,4
      DTR(I)=DTEMP/DTC(I)
      DFO(I)=0.1445-0.330/DTR(I)-0.1385/DTR(I)**2
     *      -0.0121/DTR(I)**3-0.000607/DTR(I)**8
      DF1(I)=0.0637+0.331/DTR(I)**2-0.423/DTR(I)**3-0.008/DTR(I)**8
      DF2(I)=(-2.112D-4*DMUR(I)-3.877D-21*DMUR(I)**8)/DTR(I)**6
      D2COEF(I)=(DFO(I)+DW(I)*DF1(I)+DF2(I))*83.1439*DTC(I)/DPC(I)
      Z=1.+D2COEF(I)*(DPTOT/1.0D5)/(83.14*DTEMP)
   30 CONTINUE
C
      DO 10 I=1,4
          DO 20 J=1,4
      DTCM(I,J)=(DTC(I)*DTC(J))**0.5*(1-DK(I,J))
      DVCM(I,J)=((DVC(I)**(0.33333)+DVC(J)**(0.33333))/2.0)**3
      DZCM(I,J)=(DZC(I)+DZC(J))/2.0
      DWM(I,J)=(DW(I)+DW(J))/2.0
      DPCM(I,J)=(DZCM(I,J)*83.1439*DTCM(I,J))/DVCM(I,J)
      DTRM(I,J)=DTEMP/DTCM(I,J)
   20       CONTINUE
   10 CONTINUE
C
      DO 40 I=1,4
          DO 50 J=1,4
      DFOM(I,J)=0.1445-0.330/DTRM(I,J)-0.1385/DTRM(I,J)**2
     *         -0.0121/DTRM(I,J)**3-0.000607/DTRM(I,J)**8
      DF1M(I,J)=0.0637+0.331/DTRM(I,J)**2-0.423/DTRM(I,J)**3
     *         -0.008/DTRM(I,J)**8
      DF2M(I,J)=(-2.112D-4*DMUR(I)-3.877D-21*DMUR(I)**8)/
     *          DTRM(I,J)**6
      D2COEFM(I,J)=(DFOM(I,J)+DWM(I,J)*DF1M(I,J)+DF2M(I,J))
     *             *83.1439*DTCM(I,J)/DPCM(I,J)
   50       CONTINUE
   40 CONTINUE
C
C
       FRAC(1)=Y(1)/(Y(1)+Y(2)+Y(3)+Y(4))
       FRAC(2)=Y(2)/(Y(1)+Y(2)+Y(3)+Y(4))
       FRAC(3)=Y(3)/(Y(1)+Y(2)+Y(3)+Y(4))
       FRAC(4)=Y(4)/(Y(1)+Y(2)+Y(3)+Y(4))
      D2MIX  =FRAC(1)**2*D2COEF(1)+
     *        FRAC(2)**2*D2COEF(2)+
```

```
*         FRAC(3)**2*D2COEF(3)+
*         FRAC(4)**2*D2COEF(4)+
*         2.0*FRAC(1)*FRAC(2)*D2COEFM(1,2)+
*         2.0*FRAC(1)*FRAC(3)*D2COEFM(1,3)+
*         2.0*FRAC(1)*FRAC(4)*D2COEFM(1,4)+
*         2.0*FRAC(2)*FRAC(3)*D2COEFM(2,3)+
*         2.0*FRAC(2)*FRAC(4)*D2COEFM(2,4)+
*         2.0*FRAC(3)*FRAC(4)*D2COEFM(3,4)
      DPRESS=DPTOT/1.0E5
      V=83.1439*DTEMP/DPRESS
      DZMIX=1.0+D2MIX/V
      DFAT=DEXP(2.0/V*(FRAC(4)*D2COEFM(1,4)+FRAC(3)*D2COEFM(1,3)+
     *                 FRAC(2)*D2COEFM(1,2)+FRAC(1)*D2COEFM(1,1))
     *                -DLOG(DZMIX))
      DFNT=DEXP(2.0/V*(FRAC(4)*D2COEFM(2,4)+FRAC(3)*D2COEFM(2,3)+
     *                 FRAC(2)*D2COEFM(2,2)+FRAC(1)*D2COEFM(2,1))
     *                -DLOG(DZMIX))
      DFHT=DEXP(2.0/V*(FRAC(4)*D2COEFM(3,4)+FRAC(3)*D2COEFM(3,3)+
     *                 FRAC(2)*D2COEFM(3,2)+FRAC(1)*D2COEFM(3,1))
     *                -DLOG(DZMIX))
      DFIT=DEXP(2.0/V*(FRAC(4)*D2COEFM(4,4)+FRAC(3)*D2COEFM(4,3)+
     *                 FRAC(2)*D2COEFM(4,2)+FRAC(1)*D2COEFM(4,1))
     *                -DLOG(DZMIX))
C
      DPRESS=DPTOT/1.0E5*DPR
      FRAC(5)=Y(5)/(Y(5)+Y(6)+Y(7)+Y(8))
      FRAC(6)=Y(6)/(Y(5)+Y(6)+Y(7)+Y(8))
      FRAC(7)=Y(7)/(Y(5)+Y(6)+Y(7)+Y(8))
      FRAC(8)=Y(8)/(Y(5)+Y(6)+Y(7)+Y(8))
      D2MIX =FRAC(5)**2*D2COEF(1)+
     *       FRAC(6)**2*D2COEF(2)+
     *       FRAC(7)**2*D2COEF(3)+
     *       FRAC(8)**2*D2COEF(4)+
     *       2.0*FRAC(5)*FRAC(6)*D2COEFM(1,2)+
     *       2.0*FRAC(5)*FRAC(7)*D2COEFM(1,3)+
     *       2.0*FRAC(5)*FRAC(8)*D2COEFM(1,4)+
     *       2.0*FRAC(6)*FRAC(7)*D2COEFM(2,3)+
     *       2.0*FRAC(6)*FRAC(8)*D2COEFM(2,4)+
     *       2.0*FRAC(7)*FRAC(8)*D2COEFM(3,4)
      V=83.1439*DTEMP/DPRESS
      DZMIX=1.0+D2MIX/V
      DFAS=DEXP(2.0/V*(FRAC(8)*D2COEFM(1,4)+FRAC(7)*D2COEFM(1,3)+
     *                 FRAC(6)*D2COEFM(1,2)+FRAC(5)*D2COEFM(1,1))
     *                -DLOG(DZMIX))
      DFNS=DEXP(2.0/V*(FRAC(8)*D2COEFM(2,4)+FRAC(7)*D2COEFM(2,3)+
     *                 FRAC(6)*D2COEFM(2,2)+FRAC(5)*D2COEFM(2,1))
     *                -DLOG(DZMIX))
      DFHS=DEXP(2.0/V*(FRAC(8)*D2COEFM(3,4)+FRAC(7)*D2COEFM(3,3)+
     *                 FRAC(6)*D2COEFM(3,2)+FRAC(5)*D2COEFM(3,1))
     *                -DLOG(DZMIX))
      DFIS=DEXP(2.0/V*(FRAC(8)*D2COEFM(4,4)+FRAC(7)*D2COEFM(4,3)+
     *                 FRAC(6)*D2COEFM(4,2)+FRAC(5)*D2COEFM(4,1))
     *                -DLOG(DZMIX))
      RETURN
      END

*-----------------------------------------------------------------
*-----------------------------------------------------------------
*-----------------------------------------------------------------
*  THE FOLLOWING SUBROUTINES DETERMINE THE EFFECTIVENESS FACTOR
*  (ETA1) AT EACH AXIAL POSITION IN THE REACTOR WHERE THE
*  DIFFERENTIAL MATERIAL BALANCE EQUATIONS IN SUBROUTINE FCN ARE
```

```
*  EVALUATED.
*
*-----------------------------------------------------------------------
*
      SUBROUTINE EFFECT(ETA1)
************************************************************************
*
*
*     ORTHOGANAL COLLOCATION PROGRAM FOR NH3 DECOMPOSITION
*
*                 BY: JOHN COLLINS
*
*     THIS SUBROUTINE DETERMINES THE NH3, N2 AND H2 CONCENTRATION
*     PROFILES IN A POROUS NH3 DECOMPOSITION CATALYST PARTICLE.
*     THE PROGRAM SOLVES THE FOLLOWING DIFFERENTIAL MATERIAL
*     BALANCE EQUATION AND BCs FOR NH3 USING ORTHOGANAL COLLOCATION.
*
*
*     DEL^2(Y(r))-C3(C1(Y(r)^2/YH2(r)^3)^DBETA-
*                       C2(YN2(r))*(YH2(r)^3/Y(r)^2)^(1-DBETA)=0
*
*               BC#1:-dY(1)/dr = BiNH3(Y(1)-1)
*               BC#2: dY(0)/dr = 0
*
*     THE CONCENTRATIONS OF H2 AND N2 ARE DETERMINED FROM THE NH3
*     CONCENTRATION AND MASS BALANCE EQUATIONS (SEE CHAPTER 4 OF
*     THIS THESIS FOR MORE INFORMATION.)
*
*     THE DIFFERENTIAL EQUATIONS ARE DIMENSIONLESS AND Y(r),YN2(r)
*     AND YH2(r) REFER TO NORMALIZED MOLE FRACTIONS OF NH3, N2,
*     AND H2 IN THE CATALYST PARTICLES AT A PARTICULAR AXIAL
*     POSITION IN THE TUBE SIDE OF THE MEMBRANE REACTOR.  THE
*     NORMALIZED MOLE FRACTIONS VARY WITH RADIAL POSITION (r) IN THE
*     CATALYST PARTICLES.  Y(1) REFERS TO THE NORMALIZED NH3 MOLE
*     FRACTION AT THE SURFACE OF THE CATALYST PARTICLE AND Y(0) TO
*     THE NORMALIZED MOLE FRACTION AT THE CENTER OF THE PARTICLE.
*     HERE r IS THE DIMENSIONLESS RADIUS WHICH VARIES FROM 0 TO 1.
*
*     THE NORMALIZED MOLE FRACTION REFERS TO AN ACTUAL MOLE FRACTION
*     AT A PARTICULAR RADIAL POSITION IN THE CATALYST DIVIDED BY THE
*     BULK GAS MOLE FRACTION AT THE AXIAL POSITION IN THE MEMBRANE
*     REACTOR WHERE THE EFFECTIVENESS FACTOR (ETA1) IS EVALUATED.
*     ORTHOGANAL COLLOCATION IS USED TO CONVERT THE DIFFERENTIAL
*     MATERIAL BALANCE EQUATION AND BOUNDARY CONDITIONS WRITTEN
*     ABOVE FOR NH3 INTO A SYSTEM NP1 NONLINEAR EQUATIONS AND
*     NP1 UNKNOWNS.  FOR MORE INFORMATION ON ORTHOGONAL COLLOCATION
*     PROCEDURES FOR ANALYSIS OF DIFFUSION AND REACTION CALCS,
*     SEE SECTION 4.7 OF FINLAYSON (1980).  THE SYSTEM OF NON-
*     LINEAR EQUATIONS GENERATED BY THE COLLOCATION METHOD
*     IS SOLVED USING THE NEWTON RAPHSON METHOD.  AFTER THIS
*     THE PROGRAM CALCULATES THE EFFECTIVESNESS FACTOR.
*
*    REQUIRED INPUT DATA TO THE PROGRAM ARE AS FOLLOWS:
*
*    COLLOCATION PARAMETERS:
*
*            NP1 = NUMBER OF COLLOCATION POINTS (INCLUDES POINT
*                  AT r=1.)
*     A(NP1,NP1) = A MATRIX FOR FIRST DERIVITIVE TERMS
*     B(NP1,NP1) = B MATRIX FOR SECOND DERIVITIVE TERMS
*         W(NP1) = WEIGHTING PARAMETERS FOR NUMERICAL INTEGRATION
*     XCOLL(NP1) = COLLOCATION POINTS (IE. RADIAL POSITIONS (r)
```

```
*                   IN CATALYST WHERE NORMALIZED NH3 CONCENTRATIONS
*                   ARE DETERMINED BY COLLOCATION -- NOTE: XCOLL IS
*                   NOT INCLUDED IN ANY CALCULATIONS IN THE PROGRAM.)
*
*       NOTE THAT THE COLLOCATION PARAMETERS ARE NOT CALCULATED IN
*       THE PROGRAM.  THEY ARE READ IN FROM THE DATA FILE NAMED
*       DATA.  THE SUBROUTINE IS WRITTEN TO HANDLE A MAXIMUM OF
*       SEVEN (6 INTERIOR PLUS OUTER SURFACE POINT) COLLOCATION
*       POINTS AT THE PRESENT TIME.
*
*    OTHER REQUIRED INFORMATION:
*
*             T = TEMPERATURE IN K
*             P = PRESSURE IN ATMOSPHERES
*         DPTOT = PRESSURE IN Pa
*          FLOW = GAS FLOW RATE IN SCCM
*         YNH3G = MOLE FRACTION OF NH3 IN BULK GAS
*          YH2G = MOLE FRACTION OF H2 IN BULK GAS
*          YN2G = MOLE FRACTION OF N2 IN BULK GAS
*            DR = REACTOR DIAMETER IN METERS
*            DP = DIAMETER OF CATALYST PARTICLE IN METERS
*           VIS = VISCOSITY OF GAS IN KG/M/SEC
*       BEDVOID = VOID FRACTION OF CATALYST BED
*         SURFA = SURFACE AREA OF CATALYST (M^2/KG)
*       TORTFAC = TORTUOSITY FACTOR FOR CATALYST
*       CATBDEN = DENSITY OF CATALYST PARTICLE (KG/M^3)
*         AMASS = PROPORTIONALITY CONSTANT IN CORRELATION
*                 FOR INTERPHASE MASS TRANSFER COEFFICIENTS.
*                 (THIS IS C1 IN THE TEXT OF MY THESIS).
*
*       THE KINETIC PARAMETERS USED IN THE MAIN PROGRAM AND
*       SUBROUTINES LISTED ABOVE ARE ALSO REQUIRED IN THE
*       CALCULATION OF ETA1.
*
*       THE SUBROUTINE ALSO CALCULATES VARIOUS DIFFUSION
*       COEFFICIENTS NEEDED TO DETERMINE ETA1.
*
*
      IMPLICIT DOUBLE PRECISION(A-H,O-Z)
      INTEGER ITMAX,N,NP1
      DOUBLE PRECISION ERRREL,KCNH3,KCH2,KR,KCN2
      COMMON/CRXN/ A(7,7),B(7,7),NP1,W(7),XCOLL(7)
      COMMON/FEED/YM
      COMMON/COUNT/ML
      COMMON/MASSTX/AMASS,DP,GUESS,ERRREL,BEDVOID,TORTFAC,CATVOID,
     *              SURFA,CATBDEN
      COMMON/SET1/DRKO,DE,DTEMP,DPTOT,DFAO,DEQ,
     1            DR1,DRLO,DPA,DPN,DPH,DPI,DPR
      COMMON/BET/DBETA
      COMMON/CONST/C1,C2,C3,DENH3,DEH2,DEN2,BINH3,BIH2,BIN2,
     1            YNH3G,YH2G,YN2G,YN2,YH2,C5,C6,C7,C8
      COMMON/FUGA/DFAT,DFNT,DFHT,DFIT,DFAS,DFNS,DFHS,DFIS
      DIMENSION YGUESS(7),Y(7),YH2(7),YN2(7)
      DIMENSION YM(8),YN(3),AVIS(3),AMW(3),PHEV(3,3),DMIX(4)
      DR=2.0*DR1
C
C  CALCULATE THE VISCOSITY OF THE GAS USING THE METHOD RECOMMENDED
C  BY REID ET AL. (1977) FOR LOW-PRESSURE MULTICOMPONENT GAS
C  MIXTURES.
C  SINCE AMMONIA IS VERY DILUTE, THE GAS VISCOSITY IS CALCULATED
C  ASSUMING THE MIXTURE ONLY CONTAINS N2, H2, AND HE.
C
```

```
C  NOTE THAT YM(I) IS THE DIMENSIONLESS FLOW RATE OF COMPONENT I
C  AT THE AXIAL POSITION IN THE MEMBRANE REACTOR WHERE ETA1 IS
C  BEING CALCULATED.
C
      TOT=YM(2)+YM(3)+YM(4)
      DO 130 I=1,3
      YN(I)=YM(I+1)/TOT
130   CONTINUE
      AMW(1)=28.
      AMW(2)=2.
      AMW(3)=4.
      AVIS(1)=DEXP(.640804*DLOG(DTEMP)-14.5546)
      AVIS(2)=DEXP(.67123*DLOG(DTEMP)-15.4543)
      AVIS(3)=DEXP(.67306*DLOG(DTEMP)-14.667)
      DO 140 I=1,3
      DO 135 J=1,3
        PHEV(I,J)=(1.0+DSQRT(AVIS(I)/AVIS(J))*(AMW(J)/AMW(I))**(1.0/
     *              4.0))**2/DSQRT(8.0*(1.0+AMW(I)/AMW(J)))
 135  CONTINUE
 140  CONTINUE
      VIS=0.0
      DO 150 I=1,3
       SUM2=0.0
       DO 145 J=1,3
          SUM2=SUM2+YN(J)*PHEV(I,J)
 145     CONTINUE
       VIS=VIS+YN(I)*AVIS(I)/SUM2
 150  CONTINUE
C
C  CALCULATE THE MOLE FRACTIONS IN THE BULK GAS STREAM FOR NH3, N2,
C  H2 AND HE AND THE MOLECULAR WEIGHT OF THE GAS AT THE AXIAL
C  POSITION WHERE ETA1 IS BEING EVALUATED.
C
      TOT=TOT+YM(1)
      YNH3G=YM(1)/TOT
      YN2G=YM(2)/TOT
      YH2G=YM(3)/TOT
      YIG=YM(4)/TOT
C
C   CALCULATE MW OF GAS IN KG/MOL
C
      AMWG=(17*YNH3G+28*YN2G+2*YH2G+4*YIG)/1000
C
C   THIS PART OF THE PROGRAM CALCULATES THE VALUES OF
C   BiNH3,BiH2,BiN2 (BIOT #s FOR MASS TRANSFER) AND Rep
C   FROM THE INPUT DATA OF DP,DR,DTEMP,DPTOT, DFAO,YM
C   VALUES, MOLECULAR WEIGHTS AND VISCOSITY.
C
C   CALCULATE GAS FLUX IN KG/M^2/SEC USING THE COMPONENT MOLAR FLOW
C   RATES
C
      GFLUX=((YM(1)*.017+YM(2)*.028+YM(3)*.002+YM(4)*.004)*DFAO)/
     1      (3.14/4.0*DR**2)
C
C   CALCULATE THE PARTICLE REYNOLDS NUMBER
C
      REP=GFLUX*DP/VIS
C
C   CALCULATE THE EFFECTIVE DIFFUSIVITIES FOR NH3, N2 AND H2,
C   DENH3,DEN2 AND DEH2 IN M^2/SEC.
C
```

```
C    FIRST CALCULATE MOLECULAR DIFFUSION COEFFICIENTS DMIX(I) USING
C    THE SUBROUTINE DIFFUSE
C
       CALL DIFFUSE(DTEMP,DPTOT,DMIX)
C
C    NOW CALCULATE THE KNUDSEN DIFFUSION COEFFICIENTS FOR THE
C    CATALYST PARTICLE.
C
       DKNH3=194.*CATVOID**2/TORTFAC/SURFA/CATBDEN*DSQRT(DTEMP/17.0)
       DKH2=194.*CATVOID**2/TORTFAC/SURFA/CATBDEN*DSQRT(DTEMP/2.0)
       DKN2=194.*CATVOID**2/TORTFAC/SURFA/CATBDEN*DSQRT(DTEMP/28.)
C
C    NOW CALCULATE THE EFFECTIVE DIFFUSION COEFFICIENTS
C
       DENH3=1.0/(1.0/(DMIX(1)*CATVOID/TORTFAC)+1.0/DKNH3)
       DEH2=1.0/(1.0/(DMIX(3)*CATVOID/TORTFAC)+1.0/DKH2)
       DEN2=1.0/(1.0/(DMIX(2)*CATVOID/TORTFAC)+1.0/DKN2)
C
C      CALCULATE BULK PHASE GAS CONCENTRATION IN MOL/M^3
C      ASSUMING AN IDEAL GAS AND THE THE DENSITY IN KG/M3
C
       P=DPTOT/101.325D+03
       CT=P/DTEMP/82.06D-06
       PDENG=CT*AMWG
C
C      NOW CALCULATE CONVECTIVE MASS TRANSFER COEFFICIENTS FOR
C      NH3, N2 AND H2, KC IN M/SEC ASSUMING
C      Sh=AMASS*Rep
C
       KCNH3=AMASS*REP*DMIX(1)/DP
       KCH2=KCNH3*DMIX(3)/DMIX(1)
       KCN2=KCNH3*DMIX(2)/DMIX(1)
C
C      NOW CALCULATE THE BIOT NUMBERS FOR NH3 AND H2
C
       BINH3=KCNH3*DP/2./DENH3
       BIH2=KCH2*DP/2./DEH2
       BIN2=KCN2*DP/2./DEN2
C
C      NOW CALCULATE THE REACTION RATE CONSTANT KR IN
C      MOLS/M^3 CATALYST/Pa-DBETA USING THE TEMPKIN-PYSHEV EQN.
C      THEN CALCULATE THE EQUILIBRIUM CONSTANT FOR THE
C      REACTION DDDEQ IN Pa.
C
       KR=DRKO/(1.0-BEDVOID)*DEXP(-DE/8.314/DTEMP)
       DLOGKB=2250.322/DTEMP-.8534-1.51049*DLOG10(DTEMP)-25.898D-05
      *        *DTEMP+14.8961D-08*DTEMP**2
       DDKB=10.0**DLOGKB
       DDDEQ=1.0/DDKB*1.01325D+05
C
C      NOW SET THE FUGACITY COEFFICIENTS FOR NH3, N2, AND H2
C      (VNH3, VN2, AND VH2) TO THE COEFFICIENTS CALCULATED
C      BY THE FUGACITY SUBROUTINE LISTED ABOVE.
C
       VNH3=DFAT
       VH2=DFHT
       VN2=DFNT
C
C    CALCULATE THE CONSTANTS C1, C2, C3 WHICH WILL BE USED IN
C    SUBROUTINE USRFUN.
C
       C1=((YNH3G*VNH3)**2/(VH2*YH2G)**3/DPTOT)**DBETA
```

```
      C2=VN2*PT*YN2G/DDDEQ**2*(((VH2*YH2G)**3*PT)/(VNH3*YNH3G)**2)**
     *   (1-DBETA)
      C3=KR*(DP/2.0)**2/CT/YNH3G/DENH3
      c5=0.0
      if(yn2g.gt..01)then
      C5=1.5*DENH3*YNH3G/(DEH2*YH2G)
      endif
      C6=BINH3/BIH2
      C7=0.5*DENH3*YNH3G/(DEN2*YN2G)
      C8=BINH3/BIN2
C
C     INITIAL GUESS FOR NORMALIZED NH3 MOLE FRACTIONS
C
      IF(MSET.EQ.0) THEN
      DO 30 I=1,NP1
      Y(I)=GUESS
 30   CONTINUE
      MSET=1
      ENDIF
      ITMAX=100
C
C     CALL THE SUBROUTINE MNEWT TO DETERMINE NORMALIZED YNH3
C     CONCENTRATION PROFILE.  WHEN CALLED Y IS THE ARRAY
C     CONTAINING THE GUESSES FOR THE NORMALIZE NH3 MOLE
C     FRACTIONS.  THE RETURNED Y ARRAY CONTAIN THE CALCULATED
C     NORMALIZED MOLE FRACTIONS.  ERRREL IS THE CONVERGENCE
C     CRITERIA.
C
      NP2=NP1
      CALL MNEWT (ITMAX,Y,NP2,1,NP2,ERRREL,ERRREL)
C
C     CALCULATE THE EFFECTIVENESS FACTOR ETA1 BASED ON
C     BULK STREAM CONDITIONS USING EQN 4-142 OF FINLAYSON (1980).
C
      SUM=0
      SUM1=0
      C4=C1-C2
      DO 32 J=1,NP1
       SUM=SUM+W(J)*(C1*(Y(J)**2/YH2(J)**3)**DBETA-C2*YN2(J)*
     1       (YH2(J)**3/Y(J)**2)**(1.0-DBETA))
      SUM1=SUM1+W(J)
 32   CONTINUE
      ETA1=SUM/(SUM1*C4)
C
      RETURN
      END
C-----------------------------------------------------------------
C
      SUBROUTINE USRFUN(Y,FJAC,F)
C
C  THIS SUBROUTINE CONTAINES THE SET OF NONLINEAR EQUATIONS
C  AND CORRESPONDING JACOBIAN MATRIX THAT IS SOLVED BY THE
C  NEWTON RAPHSON METHOD TO DETERMINE THE NORMALIZED AMMONIA
C  PROFILE IN THE CATALYST.
C
C  Y(I) IS THE NORMALIZED NH3 MOLE FRACTION IN THE CATALYST
C  PARTICE = YNH3(R)/YNH3G.  YH2(I) AND YN2(I) ARE THE
C  NORMALIZED MOLE FRACTIONS OF N2 AND H2 IN THE CATALYST
C  PARTICLE.
C
      IMPLICIT DOUBLE PRECISION (A-H,O-Z)
      INTEGER N,NP1
```

```
      COMMON /CRXN/ A(7,7),B(7,7),NP1,W(7),XCOLL(7)
      COMMON/BET/DBETA
      COMMON/CONST/C1,C2,C3,DENH3,DEH2,DEN2,BINH3,BIH2,BIN2,
     1            YNH3G,YH2G,YN2G,YH2,YN2,C5,C6,C7,C8
      DIMENSION Y(7),F(7),YH2(7),YN2(7),FJAC(7,7)
      N=NP1-1
C
C  FIRST CALCULATE THE NORMALIZED MOLE FRACTIONS OF H2 AND N2
C  AS A FUNCTION OF POSITION IN THE CATALYST BASED ON THE NH3
C  NORMALIZED MOLE FRACTION.
C
      DO 10 I=1,NP1
       IF(Y(I).LE.0.0) THEN
          Y(I)=1.0D-8
       ENDIF
       YH2(I)=1.0+1.5*DENH3*YNH3G/(DEH2*YH2G)*(Y(NP1)+BINH3/BIH2
     1          *(1.0-Y(NP1))-Y(I))
       yn2(i)=1.
       if(yn2g.gt..01)then
       YN2(I)=1.0+0.5*DENH3*YNH3G/(DEN2*YN2G)*(Y(NP1)+BINH3/BIN2
     1          *(1.0-Y(NP1))-Y(I))
       endif
 10   CONTINUE
C
C  NOW CALCULATE THE VALUE OF THE NONLINEAR EQUATION (F(I)
C  WRITTEN FOR EACH OF THE INTERIOR COLLOCATION POINTS.
C  THE VALUE OF EACH F(I) IS ZERO WHEN THE SOLUTION HAS BEEN
C  DETERMINED.
C
      DO 100 J=1,N
      SUM3=0.0D+00
      DO 90 J1=1,NP1
        SUM3=SUM3+B(J,J1)*Y(J1)
 90     CONTINUE
      F(J)=-(SUM3-C3*(C1*(Y(J)**2/YH2(J)**3)**DBETA-C2*YN2(J)*
     1       (YH2(J)**3/Y(J)**2)**(1.0-DBETA)))
 100  CONTINUE
C
C   NOW CALCULATE THE VALUE OF THE NONLINEAR EQUATION WRITTEN AT THE
C   EXTERIOR COLLOCATION POINT AT r=1.
C
      SUM4=0.0D+00
      DO 110 J2=1,NP1
      SUM4=SUM4+A(NP1,J2)*Y(J2)
 110  CONTINUE
      F(NP1)=-(SUM4+BINH3*(Y(NP1)-1.0))
C
C   NOW CALCULATE THE JACOBIAN MATRIX FOR THE SYSTEM
C   OF NONLINEAR EQUATIONS GENERATED BY THE COLLOCATION
C   METHOD.
C
      DO 200 I=1,N
      DO 210 J=1,NP1
        FJAC(I,J)=B(I,J)
210     CONTINUE
200   CONTINUE
      DO 220 I=1,N
      TERM1=(2.0*DBETA*YH2(I)**(3.0*DBETA)*Y(I)**(2.0*DBETA-1.0))
      TERM2=C5*3.0*DBETA*YH2(I)**(3.0*DBETA-1.0)*Y(I)**(2.0*DBETA)
      TERM3=C1*(TERM1+TERM2)/(YH2(I)**(6.0*DBETA))
      C9=3.0*(1.0-DBETA)
      C10=2.0*(1.0-DBETA)
```

```
      TERM4=C7*YH2(I)**C9+C5*C9*YH2(I)**(C9-1.0)*YN2(I)
      TERM5=C10*Y(I)**(C10-1.0)*YN2(I)*YH2(I)**C9
      TERM6=C2*(Y(I)**C10*TERM4+TERM5)/Y(I)**(2.0*C10)
      FJAC(I,I)=FJAC(I,I)-C3*(TERM3+TERM6)
220   CONTINUE
      DO 230 I=1,NP1
      FJAC(NP1,I)=A(NP1,I)
230   CONTINUE
      FJAC(NP1,NP1)=FJAC(NP1,NP1)+BINH3
C
C  RETURN TO THE MNEWT SUBROUTINE
C
      RETURN
      END
C-------------------------------------------------------------------------
C
C  THE FOLLOWING SUBROUTINES (MNEWT,INVR,SOLVE, AND FACTOR)
C  ARE PART OF THE PROGRAM CODE USED
C  TO SOLVE THE NONLINEAR SYSTEM OF EQUATIONS GENERATED BY THE
C  ORTHOGONAL COLLOCATION METHOD.  THE NEWTON RAPHSON METHOD IS
C  USED TO SOLVE THE SYSTEM OF EQUATIONS.  THE PROGRAM CODE WAS
C  ADAPTED FROM 'NUMERICAL RECIPES' BY PRESS ET AL. (1986).
C
$debug
      SUBROUTINE FACTOR(A,N,NP,INDX,D,NI,NF)

C ------------------------------
C performs LU decomposition of matrix A i.e. LU = A
C adapted from Numerical Recipes
C variables in argument list:
C       A = matrix to be factorized (input)
C       N = actual size of the matrix (input)
C       NP = physical size of the matrix (input)
C       INDX = permutation vector (output)
C       D = determinant of matrix A (output)
C       [NI-NF] = initial and final indexes in vector of unknowns
C       NI = initial row to be operated on (input)
C       NF = final row to be operated on (input)
C ------------------------------

      IMPLICIT REAL*8 (A-H,O-Z)
      PARAMETER (NMAX=100,TINY=1.0E-20)
      DIMENSION A(NP,NP),INDX(N),VV(NMAX)

      D = 1.
      DO 12 I = NI,NF
      AAMAX = 0.
      DO 11 J = NI,NF
        IF (ABS(A(I,J)).GT.AAMAX) AAMAX = ABS(A(I,J))
11      CONTINUE
      IF (AAMAX.EQ.0.) PAUSE 'Singular matrix.'
      VV(I) = 1./AAMAX
12    CONTINUE
      DO 19 J = NI,NF
      IF (J.GT.NI) THEN
        DO 14 I = NI,J-1
          SUM = A(I,J)
          IF (I.GT.NI) THEN
            DO 13 K = NI,I-1
            SUM = SUM - A(I,K)*A(K,J)
13            CONTINUE
            A(I,J) = SUM
```

```
            ENDIF
14          CONTINUE
        ENDIF
        AAMAX = 0.
        DO 16 I = J,NF
          SUM = A(I,J)
          IF (J.GT.NI) THEN
            DO 15 K = NI,J-1
              SUM = SUM - A(I,K)*A(K,J)
15            CONTINUE
            A(I,J) = SUM
          ENDIF
          DUM = VV(I)*ABS(SUM)
          IF (DUM.GE.AAMAX) THEN
            IMAX = I
            AAMAX = DUM
          ENDIF
16        CONTINUE
        IF (J.NE.IMAX) THEN
          DO 17 K = NI,NF
            DUM = A(IMAX,K)
            A(IMAX,K) = A(J,K)
            A(J,K) = DUM
17          CONTINUE
          D = -D
          VV(IMAX) = VV(J)
        ENDIF
        INDX(J) = IMAX
        IF (J.NE.NF) THEN
          IF (A(J,J).EQ.0.) A(J,J) = TINY
          DUM = 1./A(J,J)
          DO 18 I = J+1,NF
            A(I,J) = A(I,J)*DUM
18          CONTINUE
        ENDIF
19      CONTINUE
        IF (A(N,N).EQ.0.) A(N,N) = TINY
        RETURN
        END


        SUBROUTINE SOLVE(A,N,NP,INDX,B,NI,NF)

C ---------------------------
C solves LUx = b by backsubstitution
C adapted from Numerical Recipes
C
C arguments in variable list:
C       A = matrix that has been factorized by FACTOR (input)
C       N = actual size of matrices (input)
C       NP = physical size of matrices (input)
C       INDX = permuation vector defined in FACTOR (input)
C       B = vector containing the solution to the matrix problem
(output)
C       NI = initial index in vector of unknowns (input)
C       NF = final index in vector of unknowns (input)
C ---------------------------

        IMPLICIT REAL*8 (A-H,O-Z)
        DIMENSION A(NP,NP),INDX(N),B(N)

        II = 0
```

```
      DO 12 I = NI,NF
      LL = INDX(I)
      SUM = B(LL)
      B(LL) = B(I)
      IF (II.NE.0) THEN
        DO 11 J = II,I-1
          SUM = SUM - A(I,J)*B(J)
11        CONTINUE
      ELSE IF (SUM.NE.0.) THEN
        II = I
      ENDIF
      B(I) = SUM
12    CONTINUE
      DO 14 I = NF,NI,-1
      SUM = B(I)
      IF (I.LT.NF) THEN
        DO 13 J = I+1,NF
          SUM = SUM - A(I,J)*B(J)
13        CONTINUE
      ENDIF
      B(I) = SUM/A(I,I)
14    CONTINUE
      RETURN
      END


      SUBROUTINE INVR(Q,N,NP,NI,NF)

C --------------------
C  inversion of matrix Q
C
C  arguments defined as above
C --------------------

      IMPLICIT REAL*8(A-H,O-Z)
      PARAMETER(NMX=20)
      DIMENSION Q(NP,NP),INDX(NMX),YID(NMX,NMX)

      DO 100 I = 1,N
      DO 50 J = 1,N
        YID(I,J) = 0.
50      CONTINUE
      YID(I,I) = 1.
100   CONTINUE

      CALL FACTOR(Q,N,NP,INDX,D,NI,NF)

      DO 200 J = 1,N
      CALL SOLVE(Q,N,NP,INDX,YID(1,J),NI,NF)
200   CONTINUE

      DO 300 I = 1,N
      DO 300 J = 1,N
        Q(I,J) = YID(I,J)
300   CONTINUE
      RETURN
      END


      SUBROUTINE MNEWT(NTRIAL,X,N,NI,NF,TOLX,TOLF)

C ---------------------
```

```
C  solves nonlinear system of equations by Newton's Method,
C  adapted from Numerical Recipes
C
C  variables in argument list:
C       NTRIAL = maximum number of iterations to be done (input)
C       X = contains initial guess on input and solution on output
C       NI, NF = defined as in FACTOR and SOLVE
C       TOLX = desired tolerance in the solution to the problem
C       TOLF =    "         "     in absolute value of functions
C
C  additional comments:
C       user must supply subroutine USRFUN that contains the
C       jacobian matrix as well as the nonlinear functions
C       themselves
C               where:     alpha(i,j) = d(Fi)/dxj   and
C                          beta(i) = - f(i)
C ---------------------

      IMPLICIT REAL*8 (A-H,O-Z)
      PARAMETER (NP=7)
      DIMENSION X(NP),ALPHA(NP,NP),BETA(NP),INDX(NP)

      DO 13  K = 1,NTRIAL
      CALL USRFUN(X,ALPHA,BETA)
      ERRF = 0.
      DO 11 I = NI,NF
        ERRF = ERRF + ABS(BETA(I))
11      CONTINUE
      IF (ERRF.LE.TOLF) RETURN
      CALL FACTOR(ALPHA,N,NP,INDX,D,NI,NF)
      CALL SOLVE(ALPHA,N,NP,INDX,BETA,NI,NF)
      ERRX = 0.
      DO 12 I = NI,NF
        ERRX = ERRX + ABS(BETA(I))
        X(I) = X(I) + BETA(I)
12      CONTINUE
      IF (ERRX.LE.TOLX) RETURN
13    CONTINUE
      RETURN
      END
C
C-----------------------------------------------------------------
C     This subroutine calculates multicomponent bulk diffusion
C     coefficients for NH3, N2, H2, and He.
C
      SUBROUTINE DIFFUSE(DTEMP,DPTOT,DMIX)
      IMPLICIT DOUBLE PRECISION(A-H,O-Z)
      COMMON/FEED/Y
      DIMENSION DABB(4,4),DABT(4,4),PL(4),Y(8),YMF(4),YSTAR(4)
      DIMENSION DMIX(4)
C
C     *** CALCULATION OF BULK DIFFUSIVITIES
C
C
C    FIRST SET VALUES OF THE EXPERIMENTAL DIFFUSIVITIES THAT WILL BE
C    USED AS THE BASIS FOR CALCULATING THE ESTIMATED BINARY
C    DIFFUSIVITES.  IN ALL CALCULATIONS, COMPONENTS 1,2,3,4 REFER TO
C    NH3, N2, H2, AND HE, RESPECTIVELY. EXPERIMENTAL DIFFUSIVITIES
C    ARE FROM CUSSLER, PAGE 106-107.
C
       DABB(1,2)= 2.3D-05
       DABB(2,1)=DABB(1,2)
```

```
      DABB(1,3)=7.83D-05
      DABB(3,1)=DABB(1,3)
      DABB(1,4)=8.42D-05
      DABB(4,1)=DABB(1,4)
      DABB(2,3)=7.79D-05
      DABB(3,2)=DABB(2,3)
      DABB(2,4)=6.87D-05
      DABB(4,2)=DABB(2,4)
      DABB(3,4)=1.132D-04
      DABB(4,3)=DABB(3,4)
      TB=2.98D+02
      PB=101.325D+03
C
C  NOW SET THE E/K (KELVIN) VALUES USING DATA FROM CUSSLER P111.
C
      PL(1)=5.583D+02
      PL(2)=7.14D+01
      PL(3)=5.97D+01
      PL(4)=1.022D+01
C
C  DLPT AND DLPTB REFER TO VALUES OF THE COLLISION INTEGRAL.  THE
C  EQUATION USED TO CALCULATE THEM IS FROM P 550 OF PROPERTIES OF
C  GASES AND LIQUIDS(REID, ET AL., 3RD EDITION). THIS EQUATION IS
C  THE EQUATION DEVELOPED BY WILKE (WILKE, 1950).
C
      DO 10 I=1,3
      K=I+1
      DO 20 J=K,4
        EABK=DSQRT(PL(I)*PL(J))
        TSTAR1=DTEMP/EABK
        TSTAR2=TB/EABK
        DLPT=1.06036/TSTAR1**0.15610+0.193/DEXP(.47635*TSTAR1)+
     *          1.03587/DEXP(1.52996*TSTAR1)+1.76474/DEXP(3.89411*
     *          TSTAR1)
        DLPTB=1.06036/TSTAR2**0.15610+0.193/DEXP(.47635*TSTAR2)+
     *          1.03587/DEXP(1.52996*TSTAR2)+1.76474/DEXP(3.89411*
     *          TSTAR2)
        DABT(I,J)=DABB(I,J)*(DTEMP/TB)**(1.5)*DLPTB/DLPT*
     *              PB/DPTOT
        DABT(J,I)=DABT(I,J)
  20    CONTINUE
  10  CONTINUE
C
C   NOW ESTIMATE THE MULTICOMPONENT BULK DIFFUSION COEFFICIENTS
C
      YTOT=Y(1)+Y(2)+Y(3)+Y(4)
      DO 30 I=1,4
      YMF(I)=Y(I)/YTOT
 30   CONTINUE
      DO 50 I=1,4
      SUM=0.0D+00
      DO 40 J=1,4
        IF(I.EQ.J) GOTO 40
        SUM=YMF(J)+SUM
 40     CONTINUE
      DO 45 L=1,4
        IF(L.EQ.I) GOTO 45
        YSTAR(L)=YMF(L)/SUM
 45     CONTINUE
      SUM1=0.0D+00
      DO 46 L1=1,4
        IF(L1.EQ.I) GOTO 46
```

```
        SUM1=SUM1+YSTAR(L1)/DABT(I,L1)
46      CONTINUE
      DMIX(I)=1.0/SUM1
50    CONTINUE
      RETURN
      END
```